DCAF 101242

ECOLEN
SCIENTIFIC RESEARCH CENTER

FLAMELET MODEL APPLICATION FOR NON-PREMIXED TURBULENT COMBUSTION

Final Report under Cooperative Agreement NoNCCW-75
with National Aeronautics and Space Administration

Principle investigator: A.Secundov

Participants: L.Bezgin, Yu.Buriko, O.Guskov, V.Kopchenov, I.Laskin, K.Lomkov, S.Tshepin, D.Volkov, S.Zaitsev

Moscow
July 1996

PREFACE

The current Final Report contains results of the study which was performed in Scientific Research Center "ECOLEN" (Moscow, Russia) according to National Aeronautics and Space Administration Cooperative Agreement No.NCCW-75. The study was addressed to the development and verification of non-expensive approach for modeling of supersonic turbulent diffusion flames based on flamelet consideration of the chemistry/turbulence interaction (FL approach). Research work included: development of the approach and CFD tests of the flamelet model for supersonic jet flames; development of the simplified procedure for solution of the flamelet equations based on partial equilibrium chemistry assumption; study of the flame ignition/extinction predictions provided by flamelet model. The performed investigation demonstrated that FL approach allowed to describe satisfactory main features of supersonic H_2/air jet flames. Model demonstrated also high capabilities for reduction of the computational expenses in CFD modeling of the supersonic flames taking into account detailed oxidation chemistry. However, some disadvantages and restrictions of the existing version of approach were found in this study. They were: i) inaccuracy in predictions of the passive scalar statistics by our turbulence model for one of the considered test cases; ii) applicability of the available version of the flamelet model to flames without large ignition delay distance only.

Based on the results of the performed investigation, we formulated and submitted to the National Aeronautics and Space Administration our Project Proposal for the next step research directed toward further improvement of the FL approach.

CONTENT

Pages

INTRODUCTION.....4

PART I. DESCRIPTION OF THE FLAMELET MODEL APPROACH (FL).....8

I.1 Assumptions and Equations.....8

I.2 Averaging Procedure and Physical Interpretation.....13

I.3 Coupling with Compressible CFD Solvers.....16

PART II. CFD TESTS FOR SUPERSONIC JET FLAMES.....18

II.1 Beach Coaxial Experiment.....20

Description of the test case.....20
Flamelet library generation.....20
Flow field calculations.....24
Results of computations.....29

II.2 Burrows-Kurkov Experiment.....31

Description of the test case.....31
Flamelet library generation.....31
Flow field calculations.....33
Results of computations.....40

II.3 Comparative Analysis and Conclusions.....46

Computational expenses.....46
Accuracy of predictions and suggestions for model improvement.....47

PART III. SUPPLEMENTED STUDIES.....50

III.1 Simplification of the Flamelet Calculations Based on Partial Equilibrium Chemistry Assumption...50

III.2 Flamelet Predictions for Extinction/Ignition Phenomena.....58

III.3 Conclusions about Results of Supplemented Studies...62

REFERENCES.....64

APPENDIXES.....69

Appendix A. Account of the flamelet equations.....70

Appendix B. Description of the solvers used in the research work.....72

Appendix C. Detailed kinetics and thermodynamics approximations.....78

FIGURES.....81

INTRODUCTION

Accurate prediction of the turbulent combustible flows requires to utilize joint probability density function (pdf) for averaging of highly nonlinear chemical source terms in reactive scalars conservation equations. Neglecting of the turbulence/chemistry interaction effects (so-called "quasilaminar" approach) can lead to sufficient inaccuracy in predictions [1,2].

Usually, modelers utilize approach where pdf form is assumed based on some kind of intuitive consideration (Assumed PDF approach) [3-6]. Here, successful choice of the pdf form is based fully on the intuitia of modeler and it can not be unique for different reacting systems. Much more elaborate way for pdf construction is the solution of evolution equation for pdf using Monte-Carlo simulation (Evolved PDF approach) [7,8]. Significant progress has been achieved during last years due to both computers and appropriate numerical algorithms fast improvement [9-11]. However, up to now, Evolved PDF modeling requires enormous computational expenses due to large multidimensionality of pdf evolution equation [12].

One of the ways for development of the computationally non-expensive procedure for pdf construction is flamelet approach [13-16]. The simplification of the problem is achieved here based on physical assumption that chemical processes are mostly confined in the local vicinity of the near-stoichiometric surfaces (this feature is approximately valid for many classes of the turbulent flames). The assumption about small thickness of the reaction zones allows to reduce instantaneous mass conservation equations for reactive scalars to the system of the ordinary differential equations (flamelet equations). Its solution gives relations for reactive species mass fractions and temperature depending on mixture fraction z and its scalar dissipation $N=D(\nabla z)^2$ (D is molecular diffusivity) i.e. $C\alpha=C\alpha(z,N)$, $T=T(z,N)$. The later relations allows to present joint pdf for reactive scalars $p(C_1,\ldots,C_J,T)$ depending on mixture fraction and scalar dissipation pdf $p(z,N)$ and to reduce consideration of the reactive

scalars statistics to the large- and small-scale statistics of passive scalar. The passive scalar pdf is well-investigated and it can be modeled based on the first couple of the moments for mixture fraction [1,2,17].

There is additional advantage of the FL approach. In many cases, flamelet equations can be integrated before the start of hydrodynamics calculations. So, CFD modeling can be performed using tabulated solutions for reactive scalars and temperature versus mixture fraction z and scalar dissipation N (flamelet library approach). Thus, a time needed for numerical calculations of non-premixed flames could be significantly reduced. By such a manner very complex detailed kinetics schemes can be incorporated into the CFD codes without computational time increasing.

The FL approach versions varies between creators [13,18-20]. In our studies, we use flamelet model proposed by Dr.V.Kuznetsov in [19,21]. Previously, Kuznetsov's flamelet model have been tested using numerous data obtained in free- and confined subsonic jet diffusion flames (H_2/air, CH_4/air, C_3H_8/air) [1,22]. Flamelet model demonstrated quite satisfactory capabilities in predictions of temperature, stable species and radicals concentrations. It was used also for prediction of nitric oxides (NOx) emissions from diffusion flame combustors of gas turbine engines [23].

This state of art was the starting point for the current one-year investigation. Its goal was to generalize the flamelet model approach for new classes of combustible flows and to investigate its computational capabilities for CFD modeling of diffusion flames. The discussions which we were able to have with Dr. L.Povinelli (NASA Lewis Research Center) allowed to adjust the problem still further. The supersonic jet configurations were chosen for investigation. Test cases [24,25], where supersonic H_2/air jet flames were studied experimentally, were selected for model validation.

Specifically, three tasks were formulated for the current investigation:

- *Development of non-expensive approach for modeling of supersonic jet flames based on FL model. Verification of its computational efficiency and accuracy of predictions in CFD tests.*

- *Consideration of the possible simplifications in flamelet calculations based on partial equilibrium assumption for the detailed oxidation chemistry.*
- *Study of the FL predictions features for ignition/extinction phenomena in high-enthalpy flows.*

The interim results which were obtained during research work implementation were documented in our two Reports to NASA [26],[27]. The main results of the research were reported and discussed also during NASA delegation visit to Russia in March 1996. The current Final Report summarizes results of the performed study as a whole.

The Final Report is organized as follows.

Part I describes flamelet approach (Sec.I.1), its averaging procedure (Sec.I.2) and developed procedure for the flamelet model incorporation into compressible CFD solvers (Sec.I.3). Account of the flamelet model equations is given in Appendix A.

Part II is addressed to the CFD tests of the flamelet model capabilities (both computational and physical). The detailes of CFD tests for the conditions of the Beach et al. experiment [24] are presented in Sec.II.1. and for conditions of Burrows-Kurkov experiment [25] - in Sec.II.2. The additional verifications performed at the final step of the research does not change results and conclusions concerning performed CFD tests reported in interim Report [27]. So, Sec.II.1 and II.2 compiled mostly results [27]. Additional illustrations were introduced in these Sections to demonstrate accuracy of performed computations only. Brief summary of the CFD tests results, our conclusions concerning model capabilities and ways for its improvement are given in Sec.II.3. Comparative estimations of the flamelet model capabilities with Evolved and Assumed PDF modeling are presented in Sec.II.3 also. Used computational codes are described in Appendix B. Used thermochemistry approximations are presented in Appendix C.

The Part III contains results of the supplemented studies which were obtained at the final step of the research. Sec.III.1 describes semi-analytical procedure which was developed for the additional reduction of computational expenses and simplification of the flamelet calculations based on the partial equilibrium

assumption for the H_2 oxidation chemistry (two-body reactions are equilibrated). The results of the parametric flamelet model calculations of the ignition/extinction phenomena for high-enthalpy flames are presented in Sec.III.2. Conclusions concerning results of supplemented studies are given in Sec.III.3.

Research team greatly thanks to Dr. Louis Povinelli (NASA LeRC) for the formulation of the problem for current investigation and for fruitful results discussions during study implementation.

PART I. DESCRIPTION OF THE FLAMELET MODEL APPROACH (FL)

I.1 ASSUMPTIONS AND EQUATIONS

The characteristic feature of the majority of the nonpremixed combustion problems is that the maximum temperature and the highest reaction rates are observed in the local vicinity of the surfaces with the stoichiometric mixture composition. As a rule the relative role of the chemical reactions outside near-stoichiometric zones is small enough. So one can expect that thickness δ_{ch} of these near-stoichiometric reactions zones (flamelets) is small enough (see Fig.1).

In turbulent flows the stoichiometric surface is highly curved and randomly fluctuated. To characterize its location the mixture fraction z is introduced as the total mass fraction of all kinds of atoms initially been contained in fuel and then converted to other chemical species arising in the flame. The mixture fraction z equals to 0 in the flow of pure oxidizer and it equals to 1 in the flow of pure fuel. The mixture fraction z has value $z=z_s=1/(1+St)$ at the stoichiometric surface (dotted line in Fig.1), where St is the mass stoichiometric coefficient. Using the atoms conservation equations and neglecting the difference in molecular diffusivities of reactive species one has the following equation which mixture fraction obeys:

$$\rho \frac{\partial z}{\partial t} + \rho(\vec{U}\nabla) z = \nabla \rho D \nabla z \qquad (I.1)$$

where t is time; ρ is density; D is molecular diffusivity; $\vec{U}$ is flow velocity.

The reactive species conservation equations can be seriously simplified based on the assumption about small thickness of the reaction zones . The convective and unsteady terms can be dropped out and mixture fraction z can be used as an independent variable instead of space coordinate (full account is somehow length, that is why it is given in Appendix A). As the result, reactive species conservation equations are reduced to the following system of the ordinary differential equations:

$$N^s \frac{d^2 C\alpha}{dz^2} + R\alpha = 0 \qquad \alpha=1,\ldots,J \qquad (I.2)$$

where $C\alpha$ are the reactive species mass fractions; $R\alpha$ are the chemical production terms; J is total number of reactive species; parameter $N^s=D\left(\frac{\partial z}{\partial n}\right)_s^2$ is the value of instantaneous scalar dissipation $N=D(\nabla z)^2$ at the stoichiometric surface which characterize the reactive species fluxes to the reaction zones [1,2]; D is molecular diffusivity; n is coordinate normal to the surface $z=z_s$ (Fig.1).

The mixture fraction fluctuations have the turbulent integral length scaling but the scalar dissipation fluctuations have turbulent micro-length scaling [1,2]. So, it is expected that mixture fraction and scalar dissipation are non-correlated (inside the turbulent mixing layer) and parameter N^s is treated in the flamelet model equations (I.2) as some random and fluctuating number, which does not depend on z.

The same kind of reasoning can be applied to the energy conservation equation. Here the additional suggestions are:
i) Lewis number Le equal to unity; ii) the role of the unsteady pressure fluctuations, viscous dissipation and radiative heat losses terms is small enough. As the result the energy conservation equation can be reduced to the following form:

$$\frac{d^2H}{dz^2} = 0 \qquad (I.3)$$

where total enthalpy H is defined as $H = h + (\vec{U}\cdot\vec{U})/2$; $h=\sum_{\alpha=1}^{J} h_\alpha C_\alpha$ is static enthalpy; species specific enthalpies $h_\alpha = \int_{T_o}^{T} C_{P\alpha}dT + \Delta h_\alpha(T_o)$ are used taking into account species heats of formation Δh_α at reference temperature $T=T_o$.

The boundary conditions (*BC*) for the flamelet model equations (I.2)-(I.3) are posed at z=1 (pure fuel) and z=0 (pure oxidizer):

$$\begin{array}{ll} z=0 & H=H^A;\ C_\alpha=C_\alpha^A \\ z=1 & H=H^F;\ C_\alpha=C_\alpha^F \end{array} \qquad \alpha=1,\ldots,J \qquad (I.4)$$

where superscripts F and A denote composition and total enthalpies for the flows of fuel and oxidizer respectively.

The eq.(I.3) is integrated over z from 0 to 1 and the total

enthalpies of hydrogen (H^F) at z=1 and air (H^A) at z=0 is used to define the constants in the obtained linear relation. As the result the flamelet model equations (I.2),(I.3) are re-written in a form:

$$N^s \frac{d^2 C\alpha}{dz^2} + R_\alpha = 0 \qquad \alpha=1,\ldots,J$$
$$h=(H^F-H^A)z + H^A - U^2/2 \qquad (I.5)$$

The formulated flamelet model boundary problem (I.5) with the boundary conditions (I.4) gave the solution for C_α and static temperature T in the following parametric form:

$$C_\alpha=C_\alpha(z,\ N^s,\ P_s,\ \frac{U^2}{2},BC)$$
$$T=T(z,\ N^s,\ P_s,\ \frac{U^2}{2},BC) \qquad (I.6)$$

where P_s is pressure in the reaction zone and *BC* denotes boundary conditions (I.4). The solution (I.6) is considered in the flamelet approach as an instantaneous relations between the reactive species mass fractions and temperature from one hand and mixture fraction, scalar dissipation at the stoichiometric surface, local flow velocity and pressure from the other.

Additional simplifications are possible for the low-Mach number combustible flows. The role of $U^2/2$ term in (I.6) can be neglected. The pressure in the flamelet model equations can be treated as some constant. As the result one has:

$$C_\alpha=C_\alpha(z,\ N^s,BC)$$
$$T=T(z,\ N^s,BC) \qquad (I.7)$$

It is seen that flamelet model equations are splitted fully from the hydrodynamical ones in this case. This feature allows to perform the flamelet model calculations before the starting of the hydrodynamics one. The flamelet model eqs.(I.5) are solved for different values N^s. The value of N^s is considered as input parameter in these calculation. The obtained solutions (I.7) are collected in some database (flamelet library) in a parametric form on z and N^s. Further to obtain the mean values of temperature, density and reactive species mass fractions the joint probability

density function (pdf) $p(z,N^s)$ is needed. So the averaging procedure is reduced to the pdf model for passive scalar field only.

In the current study, we tried to generalize flamelet library concept for the case of compressible jet flames with relatively small pressure gradients (it is such kind of H_2/air diffusion flames [24,25] were proposed as the test cases). That is why additional simplifications were adopted: i) the role of the pressure fluctuations on the combustion chemistry was ignored; ii) correlation between flow velocity and mixture fraction distributions was applied in eq.(I.5) in a simplified form, which is approximately valid for unconfined jets [28]:

$$\frac{U - U^A}{U^F - U^A} = z^{\beta} \qquad (I.8)$$

where U^A, U^F are the mean flow velocities of the air and fuel respectively, β is some exponent which was chosen as $\beta \approx 1/Sc_t$ (Sc_t is the turbulent Schmidt number).

Such treatment allowed us to split flamelet model equations from the hydrodynamical ones and to apply flamelet library concept. The flamelet model eqs.(I.5) were solved for different values of N^s and P_s. The obtained solutions were collected in flamelet library in a parametric form on z, N^s and pressure P_s:

$$C_\alpha = C_\alpha(z,\ N^s,\ P_s,\ BC)$$
$$T = T(z,\ N^s,\ P_s,\ BC) \qquad (I.9)$$

To obtain the mean values of temperature, density and reactive species mass fractions the joint probability density function (pdf) $p(z,N^s)$ was used since the role of the pressure fluctuations on the combustion chemistry was ignored in the current calculations.

It is convenient to demonstrate chart of the possible flamelet model solutions using some particular example. Such an example is given in Fig.7a (H_2/air diffusion flame, conditions are given in Fig.3). Here water mass fraction distributions are plotted vs z for different values of scalar dissipation N^s.

It is seen that flamelet model equations give the chemically equilibrium solution in the case $N^s=0\ sec^{-1}$ (see also eq.(I.2):

$R_\alpha(C_1,...,C_J,P,T)=0 \qquad \alpha=1,...,J$

Grow of scalar dissipation N^s increases nonequilibriumness of the chemical processes (due to the increasing of the fluxes of reagents into the reaction zones). Such developing nonequilibriumness of the water mass fraction distributions is seen in Fig.7a (distributions for N^s =10, 500, 969 sec^{-1} respectively).

When value of N^s becomes too high (for the considering here example $N^s \geq 970$ sec^{-1} was found) the flame extincts and the flamelet model gave mixing solution:

$$C_\alpha=(C_\alpha^F - C_\alpha^A)z + C_\alpha^A \qquad \alpha=1,...,J \qquad (I.10)$$

accompanied by negligibly slow oxidation. This solution is obtained from the flamelet model equations when the chemical source terms are kept to zero in (I.2).

The scalar dissipation value at flame extinction is referred to as critical value of scalar dissipation N_{cr}. The burning solution exists only if $N^s < N_{cr}$. This means that the flame extincts when the mixing rate becomes too high compare to the fuel and air consumption inside the reaction zone due to the limitations of the finite chemistry*). The calculations demonstrate that N_{cr} is a pure chemical characteristic depended only on the fuel detailed oxidation chemistry and boundary conditions (I.4):

$$N_{cr}= N_{cr}(P_s, T_a, T_f, \text{kind of fuel})$$

where T_a and T_f are incoming air and fuel temperatures.

The typical values of N_{cr} for diffusion combustion of different fuels in air at room conditions (P=0.1MPa, T=300K) are summarized in Table 1.

Table 1.

Fuel	H_2	C_3H_8	CH_4
N_{cr}, sec^{-1}	121	51	17

*) Features of the FL predictions for the flame ignition/extinction regimes are discussed in Sec.III.2 in more detailes.

Value of N_{cr} increases with the increasing both incoming temperatures and pressure [22].

Due to the discussed here switch on/off property of the flamelet model solutions the range of the scalar dissipation variation in the flamelet model calculations is restricted by the range $[0, N_{cr})$. For the higher values of N^s the pure mixing solution (I.10) can be used to calculate the mixture composition and thermodynamics properties such as density and enthalpy.

I.2 AVERAGING PROCEDURE AND PHYSICAL INTERPRETATION

It is seen that flamelet model predicts dependence of the reactive scalars on only two characteristics of the scalar field i.e. mixture fraction z and scalar dissipation at the flame front N^s. The joint pdf for reactive species mass fractions C_α, temperature T, z and N^s has the form:

$$p(z,N^s,C_1,\ldots,C_J,T) = p(z,N^s)\ \delta(T-T^{fl})\ \prod_{\alpha=1}^{J} \delta(C_\alpha - C_\alpha^{fl})$$

where $T^{fl}=T(z,N^s)$ and $C_\alpha^{fl}=C_\alpha(z,N^s)$ are the solutions of the flamelet model equations (I.5). So, only $p(z,N^s)$ requires additional modeling.

To approximate the joint pdf of mixture fraction and scalar dissipation and to obtain the averaged values of the reactive species mass fractions the pdf approach [1,17] is used. Its features are as follows.

The scalar field is considered as to be divided into two intermittent parts: i) turbulent mixing layer ($0<z<1$); ii) flow outside the turbulent mixing layer ($z=0$). The role of the pure fuel flow ($z=1$) is neglected.

It is expected that scalar dissipation at the flame front N^s and mixture fraction z are statistically independent inside the turbulent mixing layer. The role of the scalar dissipation fluctuations is neglected and its value $\bar{N}_t^s$ conditionally averaged over the time moments when the turbulent mixing layer is observed in a given point is used.

The Favre joint pdf of mixture fraction z and scalar

dissipation at the stoichiometric surface N^s is considered in a following form:

$$\rho/\bar{\rho}\cdot p(z,N^s) = (1-\gamma)\delta(z)\delta(N^s) + \gamma\cdot p_t(z)\delta(N^s-\bar{N}_t^s) \qquad (I.11)$$

where γ is the intermittency factor; ρ is density; p_t is the mixture fraction probability density function in a turbulent mixing layer; δ is the Dirac function. The intermittency factor γ is calculated using approximate relation [1]:

$$\gamma = \begin{cases} 1.31/(1+\sigma^2/(\tilde{z})^2) & \text{if} \quad \sigma/\tilde{z} > 0.555; \\ 1 & \text{if} \quad \sigma/\tilde{z} < 0.555; \end{cases} \qquad (I.12)$$

where $\tilde{z}=\overline{\rho z}/\bar{\rho}$ is Favre averaged mixture fraction and $\sigma^2 = \overline{\rho z''z''}/\bar{\rho}$ is mixture fraction variance. The approximate relation (I.12) is based on the assumption that the fluctuation intensity inside the turbulent mixing layer (σ_t/z_t) is some fixed number. Its value was obtained from the consideration of eigenvalue problem for the pdf equation $(\sigma_t/z_t \approx 0.555)$. This approximation was verified in [1,29,30] using various experimental data.

There were the following reasoning to neglect scalar dissipation fluctuations in averaging procedure. The solutions of the flamelet model problem (both obtained analytically and numerically) predicts relatively weak dependence of the reactive species mass fractions on scalar dissipation at the stoichiometric surface N^s. For example, the OH mass fraction depends on N^s as $(N^s)^{1/3}$ [1],[13]. That is why, the using of this simplification does not lead to the significant errors in averaged distributions of the reactive species.

Obtained in [1] self-similar solutions of pdf equation are used to approximate the mixture fraction pdf $p_t(z)$ in the turbulent mixing layer $(0<z<1)$. It is adopted that:

i). p_t has the gaussian form in the non-intermittent $(\gamma=1)$ part of the mixing layer (deeply inside the mixing layer) :

$$p_t = \frac{1}{\sqrt{2\pi}\ \sigma} \exp\left(- \frac{(z - \tilde{z})^2}{2\ \sigma^2} \right) \qquad (I.13)$$

ii). p_t has the form of Airy function (Fig.2) in the intermittent ($\gamma<1$) regions:

$$p_t = \frac{1.404}{z_t} Ai(1.788 \frac{z}{z_t} - 2.338) \qquad (I.14)$$

where $z_t = \tilde{z}/\gamma$ is the mixture fraction value conditionally averaged over the moments when the turbulent mixing layer is observed in a given point.

The conditionally averaged value of scalar dissipation at the stoichiometric surface is approximated as:

$$\tilde{N}_t^s = \frac{\tilde{N}|\tilde{z}=z_s}{\gamma|\tilde{z}=z_s} \qquad (I.15)$$

where $\tilde{N}|\tilde{z}=z_s$ and $\gamma|\tilde{z}=z_s$ are the mean value of the scalar dissipation $\tilde{N}$ and intermittency factor γ calculated under the condition that mean value of mixture fraction $\tilde{z}=z_s$. The conventional for the turbulence modeling approximation for the mean scalar dissipation $\tilde{N}$ is used:

$$\tilde{N}=0.07 \frac{K\ \sigma^2}{\nu_t} \qquad (I.16)$$

where K is turbulence kinetic energy, ν_t is eddy viscosity. In such a treatment only turbulence kinetic energy K, eddy viscosity ν_t, mean mixture fraction $\tilde{z}=\overline{\rho z}/\bar{\rho}$ and its variance $\sigma^2 = \overline{\rho z''z''}/\bar{\rho}$ are needed to calculate the pdf in any given point of the flowfield. These turbulent mixing characteristics are calculated using conventional semi-empirical transport equations of the turbulence modeling.

The formulated here flamelet approach together with its averaging procedure has the following physical interpretation. The typical values of the mixture fraction stoichiometric values z_s are small enough ($z_s \approx 0.03$ for H_2/air flames; $z_s \approx 0.05$-0.06 for different hydrocarbons/air flames). This means that the flame front is located close to the outer boundary of the mixing layer. In this region, turbulent large-scale movement governs the mixture fraction large-scale fluctuations associated with the intermittency phenomenon. Small thickness of the reaction zone allows to consider it as to be "frozen" into this large-scale turbulent movement and to dropped out large-scale turbulence

influence on the chemical processes inside reaction zone. The role of the large-scale fluctuations is taken into account only through the pdf in the averaging procedure. At the same time the small-scale turbulence can influence the chemical process in the reaction zone. This influence is taken into account through the parameter $\bar{N}_t^s$, since N^s characterizes fluxes of substances to the reaction zone [2]. The flamelet model is based on the assumption that this is the main cause which is responsible for the influence of turbulent mixing on the local nonequilibriumness of combustion chemistry.

I.3 COUPLING WITH COMPRESSIBLE CFD SOLVERS

The following procedure was proposed for the flamelet library incorporation into the compressible flow hydrodynamics solver. The "effective" heat capacities CP_α of the reactive species are introduced in the same manner as it was done in [31]:

$$CP_\alpha = \int_{T_o}^{T} C_{P_\alpha} dT/(T-T_o) \qquad (I.17)$$

Using (I.17), the total mixture enthalpy can be written as:

$$H = CP\cdot(T-T_o) + \sum_{\alpha=1}^{J} C_\alpha \Delta h_\alpha + (\vec{U}\cdot\vec{U})/2 \qquad (I.18)$$

where $CP=\sum_{\alpha=1}^{J} CP_\alpha C_\alpha$ is the "effective" heat capacity of the mixture.

Let us introduce two additional "effective" parameters. "Effective" heat capacities ratio Γ which is defined as:

$$\Gamma=1/(1- R/(CP\cdot\mu)) \qquad (I.19)$$

and "effective" heat of mixture formation defined as:

$$Q=\sum_{\alpha=1}^{J} C_\alpha \Delta h_\alpha - CP\cdot T_o \qquad (I.20)$$

where μ is the mixture molar weight and R=8.31 J/(mol K) is universal gas constant

Using the thermal equation of state for mixture $P=\rho RT/\mu$ and

eqs.(I.19),(I.20) one can obtain from (I.18) the following "effective" form for the total enthalpy:

$$H=\Gamma/(\Gamma-1)\ P/\rho + Q + (\vec{U}\cdot\vec{U})/2 \qquad (I.21)$$

Multiplying eq.(I.21) by density and Favre-averaging one has:

$$\bar{\rho}\ \tilde{H} = \overline{[\Gamma/(\Gamma-1)]\ P} + \bar{\rho}\tilde{Q} + \bar{\rho}\tilde{U}^2/2 + \bar{\rho}K \qquad (I.22)$$

where K is turbulent kinetic energy.

Additional simplifications were adopted i.e. the correlation $\overline{(P'\Gamma')}$ and K in (I.22) were neglected. As the result one has:

$$\bar{\rho}\ \tilde{H} = \overline{[\Gamma/(\Gamma-1)]}\ \bar{P} + \bar{\rho}\ \tilde{Q} + \bar{\rho}\tilde{U}^2/2 \qquad (I.23)$$

It is seen from (I.19),(I.20) that values of $\Gamma/(\Gamma-1)$ and Q depend only on reactive species mass fractions and temperature. That is why, they can be obtained from the flamelet calculations. To obtain the mean values of $\overline{\Gamma/(\Gamma-1)}$ and $\tilde{Q}$ the averaging procedure of Sec.I.2 can be used. The value of $\tilde{H}$ is obtained from the Favre-averaged energy conservation equation in its conventional form. As the result, eq.(I.23) give the relation between mean values of density $\bar{\rho}$, pressure $\bar{P}$ and flow velocity $\tilde{U}$ where only two parameters (Γ and Q) are needed from the flamelet model calculations. Of course such a simplified procedure does not allow to calculate all the mixture thermodynamics properties (for example, the local speed of sound) however it allows significantly reduce computational expenses. If mean mixture composition is needed in some cross sections the whole flamelet library should be used.

PART II. CFD TESTS FOR SUPERSONIC JET FLAMES

CFD tests of the flamelet model capabilities were done for two test cases [24,25] where H_2 jet combustion in supersonic air flow was studied experimentally. The goals of the tests were:

- *to estimate computational expenses for FL realization in CFD;*
- *to examine accuracy of model predictions.*

The flamelet library concept of Sec.I.1 was applied (FL approach). At the first step, flamelet equations (I.5) were solved parametrically and obtained solutions were collected into the flamelet library. At the second step, flamelet library was used together with the appropriate CFD solvers for the flowfield calculations using procedure of Sec.I.3.

Additional series of calculations were done using "quasilaminar" combustion model together with the same CFD solvers (QL approach) to obtain the reference point for comparison of FL approach computational and physical capabilities. The mass, momentum and energy conservation equations, in QL approach, were solved together with the averaged conservation equations for the reactive species where the role of the reactive scalars turbulent fluctuations was neglected:

$$\frac{\partial}{\partial x_i}\bar{\rho}\tilde{U}_i\tilde{C}_\alpha = \frac{\partial}{\partial x_i}\bar{\rho}\left(\frac{\nu_t}{Sc_t} + D\right)\frac{\partial\tilde{C}\alpha}{\partial x_i} + \bar{\rho}R_\alpha(\bar{T},\bar{\rho},\tilde{C}_1,\ldots,\tilde{C}_J) \qquad \alpha=1,\ldots,J \qquad \text{(II.1)}$$

where x_i are the Cartesian coordinates; the chemical source terms R_α are postulated in Arrenius form for the mean values of species mass fractions $\tilde{C}_\alpha$, temperature $\bar{T}$ and density $\bar{\rho}$.

Both FL and QL series of calculations were done using the same initial and boundary conditions, model of turbulence and approximations for the detailed kinetics and thermodynamics properties.

The detailed hydrogen oxidation chemistry was approximated by the Miller-Bowman kinetics scheme [32]. The thermal NO formation mechanism was taken into account also. The resulting detailed kinetics model included 21 reactions between 11 species (H_2, O_2, H_2O, H, O, OH, H_2O_2, HO_2, N_2, N, NO). It is given in Appendix C. The species specific enthalpies $h_\alpha = \int_{T_o}^{T} C_{p_\alpha} dT + \Delta h_\alpha(T_o)$ were used in

a form of polynomial approximations $h_\alpha = A_{I\alpha} + \sum_{i=1}^{7} A_{i\alpha}(T/1000)^i$ taken from [33]. Here Δh_α are the species heats of formation at reference temperature $T_0 = 298.15K$. The polynomial coefficients are given in Appendix C also.

The account about details of computations and obtained results are given in Sec.II.1 and Sec.II.2. These results and their detailed analysis were presented in previous interim Reports [27]. Additional methodological tests of the computations accuracy, which were done at the final step of the research, did not change results and conclusions of [27]. So, Sec.II.1 and Sec.II.2 mostly compiled [27]. Brief summary and comparative analysis of the results are presented in Sec.II.3 together with our suggestions concerning ways for the further model improvement.

II.1 BEACH COAXIAL EXPERIMENT [24]

DESCRIPTION OF THE TEST CASE

The sketch of the Beach et al. test case [24] is given in Fig.3 together with the nozzle exit conditions (flow parameters and gas composition). The hydrogen was injected through supersonic axisymmetric nozzle with the Mach number $M_{H2}=2$. The hot air was obtained by burning of hydrogen in air, replacing the oxygen and expanding through supersonic nozzle with the Mach number $M_{air}=1.9$. The hydrogen injector tube had external diameter $d_j=0.009525$m with a lip thickness 0.0015m. The air nozzle free stream diameter D was 0.0653m.

FLAMELET LIBRARY GENERATION

The boundary conditions for the flamelet equations were adjusted according to the data presented in Fig.3. The influence of the pressure variation inside the flowfield on the combustion chemistry was neglected and flamelet model equations were calculated for a fixed value of pressure $P_s=0.1$MPa. The value of exponent β in approximation (I.8) was chosen as $\beta=1.25$ which corresponded to the value of the $Sc_t=0.8$.

The flamelet eqs.(I.5) were solved using time-relaxation code *FLSLV* (its description is given in Appendix B) for different N^s to cover whole range of the possible flamelet model solutions from $N^s=0$ up to $N^s=N_{cr}$. The obtained distributions of reactive species $C_\alpha(z,N^s)$ $(\alpha=1,...,J)$ and static temperature $T(z,N^s)$ were introduced into the flamelet library. The whole flamelet library was calculated using exponential grid consisted of I=81 points with grid points clustering near z=0 boundary.

Computational strategy and convergence

The calculations were started from lowest value of $N^s=N^{(1)}$ (it was chosen as $N^{(1)}=0.001$ sec^{-1}). The chemically equilibrium solution for reactive species and temperature was used at this step as the initial approach. Further the converged solution for the first value of $N^s=N^{(1)}$ was used as the initial approach in calculations performed for the next value of $N^s=N^{(2)}$ and so on.

The increments in time $\delta\vec{C}$ control was applied for choice of the

optimal pseudo-time step τ and to fasten the convergence to steady state solution (see detailed in Sec.B.I of Appendix B). The norm for δC was calculated at each time step as:

$$\varepsilon^j = \max_{\alpha} \max_{i} \{ \mathrm{mod}(\delta C_\alpha)_i^j / (C_\alpha)_i^{j-1} \}$$

where maxima was got through all species (α=1,...,11) and all grid points z_i (i=1,...,I). The time relaxation was stopped when the value of ε^j became lower than $\varepsilon_0=10^{-6}$. The obtained solution was considered as converged. Typical residual norm ε^j and time step τ^j behavior in course of flamelet library generation are shown in Fig.4. The required number of iterations to obtain the converged solution was 80 at the first step of the flamelet library generation and then it rapidly decreased up to the value 5. The required iterations number chart during the flamelet library generation is given in Fig.5.

Accuracy of the computations

Two tests were done to estimate the accuracy of the obtained flamelet library.

The first one was the extrapolation of the obtained numerical solution to zero-length grid step ($h \to 0$). For this purpose the additional methodological calculations for total grid point number I=41 and I=161 were performed for three selected values of scalar dissipation N^s (N^s=0.01;100;900 sec^{-1}). The obtained reactive species profiles were compared with those which were obtained at "basis" grid I=81. To avoid errors associated with the application of extrapolation procedure to the case where the numerical grid was nonuniform the fine grid cells were generates by dividing of the rough grid cells in half strictly. The results of calculations obtained for three grids ("basis" I=81; "fine" I=161 and, for the control, "rough" I=41) were used in extrapolation of the solution to the zero-length step solution $\vec{C}^{(Rch)}$. The following norm for the accuracy of solution was introduced:

$$\mathrm{ERROR}_\alpha^{(Rch)} = \max_{N^s} \max_{i} \mathrm{mod}[(C_{\alpha i}^{(81)} - C_{\alpha i}^{(Rch)}) / C_{\alpha i}^{(Rch)}]$$

where maxima was got through three control solutions corresponded to N^s=0.01, 100, 900 sec^{-1} and all grid points z_i of the "basis" grid (I=81). The reactive species mass fraction values lower than $10^{-8} C_\alpha^{max}$ were ignored in this estimation. It was found that

$ERROR_{\alpha}^{(Rch)}$ was lower 0.3% for "effective" heat capacities ratio Γ, "effective" heat of formation Q and all substances except H_2O_2. For H_2O_2 its value was 1%. However this feature can not influence the accuracy of the flamelet library as a whole since the H_2O_2 mass fraction was too small ($<10^{-6}$) and could not influence total mixture thermodynamics properties. The examples of the extrapolation procedure for maximum concentrations values of two substances (H, OH were selected) are given in Fig.6. They are plotted vs $1/I^2$ where I is the total number of grid points. The solid line in Fig.6 corresponds to the mean root square linear approximation.

The second test of the flamelet library accuracy was associated with the fact that the CFD will require to obtain the reactive species profiles at interim values of N^s. To investigate the accuracy of the interpolation the additional calculations were performed for interim values of $N^s_{r+1/2} = (N^s_r + N^s_{r+1})/2$; (r=1,...,37) where N^s_r, N^s_{r+1} are scalar dissipation values corresponded to the particular solutions which were included to the flamelet library . The results were compared with those obtained by the linear interpolation of the flamelet library data between solutions at N^s_r and at N^s_{r+1}. The accuracy of the interpolation was defined as:

$$ERROR_{\alpha}^{(int)} = \max_{N^s_{r+1/2}} \max_{i} \mathrm{mod}[(C_{\alpha i}^{(N)} - C_{\alpha i}^{(int)})/C_{\alpha i}^{(N)}]$$

where maxima was got through all interim solutions and all grid points z_i of the "basis" grid (I=81); $C_{\alpha i}^{(N)}$ denotes results of flamelet calculations at $N^s = N^s_{r+1/2}$ and $C_{\alpha i}^{(int)}$ denotes results of interpolation between solutions containing in the library. It was found that $ERROR_{\alpha}^{(int)}$ was lower than 0.5% for Γ,Q and species concentrations higher than 10^{-6}. The $ERROR_{\alpha}^{(int)}$ value was found to be about 10% for radicals H_2O_2 and HO_2 but the concentration of these radicals was small ($<10^{-6}$) and can not influence total mixture properties.

Obtained results and computational expenses for flamelet library generation.

Total flamelet library included 38 particular solutions in the range of N^s variation from 0.001 sec^{-1} up to N_{cr} = 970 sec^{-1}. Additional time was required (8 particular solutions) to adjust

the value of N_{cr} with the accuracy 0.1%. Pure mixing solution (I.10) was postulated for $N^s \geq N_{cr}$. Examples of the obtained distributions in parametric form on N^s are given in Fig.7a-c for stable species (H_2O, H_2, O_2), in Figs.8a-c for main radicals (OH, H, O) and in Figs.9a,b for "effective" parameters Γ,Q.

The flamelet library generation was done using conventional PC AT 486DX2/66MHz computer. The computational expenses required for the generation of the flamelet library are summarized in Table 2.

Table 2

Number of species	11
Grid in z direction	81 points
CPU time per iteration per grid point	0.0092sec
Total time for flamelet library generation	607sec
Total number of calculated particular solutions	46
Number of particular solutions included into the library	38
Required memory for library storing	0.8Mb

Tests of results sensitivity

The methodological tests were done to investigate the sensitivity of the flamelet model calculations to the choice of the detailed kinetics scheme for conditions of the Beach test case. The solution of the flamelet model equations for three selected values of scalar dissipation N^s (N^s=1,100,800 sec^{-1}) was obtained using detailed kinetics for H_2 oxidation proposed by Warnatz in [34] (it is presented in Appendix C) and compared with the results obtained by Miller-Bowman scheme. The examples of obtained results are given in Fig.10 for two substances (H_2O and OH). We have not found any significant influence of the detailed kinetics approximation on the results of calculations for main reactive species. For example, the difference for H_2O concentrations was about 2% and for maximum OH concentrations it was about 15%.

The additional methodological test was done to investigate the sensitivity of the results to the exponent β in the adopted

correlation (I.8). The parameter β was varied in the range β=0.5-2.0. The water and hydroxil radical mass fractions (C_{H_2O},C_{OH}) distributions obtained at scalar dissipation value N^s=50 sec^{-1} and different values of β are presented in Figs.11a,b. It was found that the sensitivity of the results to the β variation is relatively small (less then 1% for main stable species and less than 12% for radicals). It is compatible with the sensitivity to the adopted detailed chemistry approximation.

FLOW FIELD CALCULATIONS

Adopted simplifications and system of equations

The assumption about H_2 jet in co-flowing infinite air stream for flow hydrodynamics was adopted. The role of the air flow mixing with the ambient air was neglected. The features of the flowfield in the vicinity of the hydrogen nozzle exit lip were taken into account only through the initial conditions in the initial cross section of the computational domain in cross-section x/d_j=0.33 downstream the injector. It was expected that the flowfield can be described by the parabolized approximation (PNS) of the 2-D Favre-averaged conservation equations.

A special approach concerning governing system of equations was adopted in current study to provide the stable marching calculations of PNS equations in slightly subsonic regions which can arise inside the mixing layer for the conditions of Beach test case [24]. For this purpose the procedure of PNS equations regularization proposed in [35-37] was applied. The term with longitudinal pressure gradient in x-momentum equation was multiplied by the parameter ω, which was expected to be function of the local Mach number M_x estimated on the longitudinal velocity component U. The Cauchy problem with initial data for PNS equations in subsonic regions (M_x<1) is well posed at the condition [37]:

$$\omega < M_x^2$$

In the pure supersonic regions (M_x>1) parameter ω was equal to 1. The influence of the rejected part of the longitudinal pressure gradient $(1-\omega)\ \frac{\partial p}{\partial x}$ on the solution was neglected since the pressure gradients are small for the conditions of Beach test

case. So only downstream marching without global pressure iterations was applied.*)

The system of the regularized PNS equations had the form:

continuity equation:

$$\frac{\partial(\bar{\rho}\tilde{U})}{\partial x} + \frac{\partial(\bar{\rho}\tilde{V})}{\partial y} + \frac{\bar{\rho}\tilde{V}}{y} = 0 \qquad \text{(II.2)}$$

X-momentum equation:

$$\frac{\partial(\bar{\rho}\tilde{U}\tilde{U})}{\partial x} + \frac{\partial(\bar{\rho}\tilde{V}\tilde{U})}{\partial y} + \frac{\bar{\rho}\tilde{U}\tilde{V}}{y} = \frac{\partial}{\partial y}\left(\bar{\rho}\nu_t\frac{\partial\tilde{U}}{\partial y}\right) + \frac{\bar{\rho}\nu_t}{y}\frac{\partial\tilde{U}}{\partial y} - \omega\frac{\partial\bar{p}}{\partial x} \qquad \text{(II.3)}$$

Y-momentum equation:

$$\frac{\partial(\bar{\rho}\tilde{U}\tilde{V})}{\partial x} + \frac{\partial(\bar{\rho}\tilde{V}\tilde{V}+\bar{p})}{\partial y} + \frac{\bar{\rho}\tilde{V}\tilde{V}}{y} =$$

$$= \frac{\partial}{\partial y}\left(\frac{2}{3}\bar{\rho}\nu_t\left(2\frac{\partial\tilde{V}}{\partial y} - \frac{\tilde{V}}{y}\right)\right) + \frac{2\bar{\rho}\nu_t}{y}\left(\frac{\partial\tilde{V}}{\partial y} - \frac{\tilde{V}}{y}\right) \qquad \text{(II.4)}$$

Energy conservation equation:

$$\frac{\partial\bar{\rho}\tilde{U}\tilde{H}}{\partial x} + \frac{\partial\bar{\rho}\tilde{V}\tilde{H}}{\partial y} + \frac{\bar{\rho}\tilde{V}\tilde{H}}{y} = \frac{\partial}{\partial y}\left(\frac{\bar{\rho}\nu_t}{Pr_t}\frac{\partial\tilde{h}}{\partial y}\right) + \frac{1}{y}\frac{\bar{\rho}\nu_t}{Pr_t}\frac{\partial\tilde{h}}{\partial y} +$$

$$+ \frac{\partial}{\partial y}\bar{\rho}\nu_t\left(\tilde{U}\frac{\partial\tilde{U}}{\partial y} + \frac{2}{3}\tilde{V}\left(2\frac{\partial\tilde{V}}{\partial y} - \frac{\tilde{V}}{y}\right)\right) \qquad \text{(II.5)}$$

Here x,y are the longitudinal and transverse axe of the coordinate system; $\tilde{U},\tilde{V}$ are the components of the velocity vector; $\bar{\rho}$ is density; $\bar{P}$ is pressure; $\tilde{h}$ is static enthalpy of the mixture taking into account formation enthalpies of the mixture components; $\tilde{H}$ is the total enthalpy which is defined as $\tilde{H}=\tilde{h}+(\tilde{U}^2+\tilde{V}^2)/2$; ν_t is the eddy viscosity; Pr_t is the turbulent Prandtl number (Pr_t=0.8); the upper symbols ($\tilde{}$) and ($\bar{}$) denote Favre and time averaging respectively; ω is regularization factor.

The Secundov's one-equation turbulence model "ν_t- 90" was used to calculate the eddy viscosity ν_t. Here its general form was reduced to the following parabolic equation:

$$\frac{\partial\bar{\rho}\tilde{U}\nu_t}{\partial x} + \frac{\partial\bar{\rho}\tilde{V}\nu_t}{\partial y} + \frac{\bar{\rho}\tilde{V}\nu_t}{y} = \frac{\partial}{\partial y}\left(\bar{\rho}(c_1\nu_t + \nu)\frac{\partial\nu_t}{\partial y}\right) +$$

$$\frac{\bar{\rho}(c_1\nu_t + \nu)}{y}\frac{\partial\nu_t}{\partial y} + c_2\bar{\rho}\nu_t G + c_3\nu_t\left(\tilde{U}\frac{\partial\bar{\rho}}{\partial x} + \tilde{V}\frac{\partial\bar{\rho}}{\partial y}\right) - c_4\bar{\rho}\nu_t^2\frac{G^2}{a^2} \qquad \text{(II.6)}$$

---

*)The validity of the marching PNS calculations for the test case [24] was checked at the final step of the study. The full NS solver FNAS2D (see Sec.B.3 of Appendix B) was used for calculations of the Beach test case. The minor difference in results was found.

where $G=\left|\frac{\partial\tilde{U}}{\partial y}\right|$; a is local speed of sound; $c_1=2$; $c_3=0.7$; $c_4=5$;

$c_2 = 0.2\ \frac{y^4G^2}{(30\ \nu t)^2+y^4G^2}$; ν is kinematic viscosity.

To obtain values of the mean $\tilde{z}$ and variance σ^2 mixture fraction values and mean scalar dissipation $\tilde{N}$ the following equations were solved:

mixture fraction $\tilde{z}=\overline{\rho z}/\bar{\rho}$ transport equation

$$\frac{\partial}{\partial x}\bar{\rho}\tilde{U}\tilde{z} + \frac{\partial}{\partial y}\bar{\rho}\tilde{V}\tilde{z} + \frac{\bar{\rho}\tilde{V}\tilde{z}}{y} = \frac{\partial}{\partial y}\left(\frac{\bar{\rho}\nu t}{Sc_t}\frac{\partial\tilde{z}}{\partial y}\right) + \frac{1}{y}\frac{\bar{\rho}\nu t}{Sc_t}\frac{\partial\tilde{z}}{\partial y};$$

mixture fraction variance $\sigma^2=\overline{\rho z''z''}/\bar{\rho}$ transport equation

$$\frac{\partial\bar{\rho}\tilde{U}\sigma^2}{\partial x} + \frac{\partial\bar{\rho}\tilde{V}\sigma^2}{\partial y} + \frac{\bar{\rho}\tilde{V}\sigma^2}{y} = \frac{\partial}{\partial y}\left(\frac{\bar{\rho}\nu t}{Sc_t}\frac{\partial\sigma^2}{\partial y}\right) + \frac{1}{y}\frac{\bar{\rho}\nu t}{Sc_t}\frac{\partial\sigma^2}{\partial y} +$$

$$+ 2\frac{\bar{\rho}\nu t}{Sc_t}\left(\frac{\partial\tilde{z}}{\partial y}\right)^2 - \beta_1\frac{\bar{\rho}K\sigma^2}{\nu t};$$

the turbulent kinetic energy K balance equation

$$\frac{\partial\bar{\rho}\tilde{U}K}{\partial x} + \frac{\partial\bar{\rho}\tilde{V}K}{\partial y} + \frac{\bar{\rho}\tilde{V}K}{y} = \frac{\partial}{\partial y}\left(\bar{\rho}k_2\nu t\frac{\partial K}{\partial y}\right) + \frac{1}{y}\bar{\rho}k_2\nu t\frac{\partial K}{\partial y} + \bar{\rho}\nu t\left(\frac{\partial\tilde{U}}{\partial y}\right)^2 - \beta_2\frac{\bar{\rho}K^2}{\nu t}$$

where $k_2=1.4$; $\beta_1=0.14$; $\beta_2=0.1$; $Sc_t=0.8$.

The values of $\tilde{z}$, σ^2 were used to calculate the mixture fraction pdf p(z) using formula (I.11)-(I.14) of Sec I.2.

The conditionally averaged value of scalar dissipation at the flame front $\bar{N}_t^s$ was calculated by approximation (I.15) using the mean scalar dissipation $\tilde{N}=0.07\frac{K\ \sigma^2}{\nu t}$ and intermittency factor γ distributions.

The particular solution of the flamelet model problem at $N^s=\bar{N}_t^s$ was obtained from the flamelet library by the linear interpolation between neighboring solutions for $N^{(k)}$ and $N^{(k+1)}$, where $N^{(k)}\le N_t^s\le N^{(k+1)}$ and linear interpolation on z. The obtained solution for the "effective" heat capacities ratio Γ and effective heat of "formation" Q were averaged using calculated p(z). The averaged values of $\overline{\Gamma/(\Gamma-1)}$ and $\tilde{Q}$ were used for the closure of the governing system of conservation equations (II.2)-(II.6) using procedure outlined in Sec I.3.

Boundary and initial conditions

The computations were done for the rectangular domain presented in Fig.12. The calculations were started in the cross section $x/d_j=0.33$ and they were stopped in the cross section $x/d_j=30$. The upper boundary of computational domain was at $y/d_j=2$ position. The no-reflection conditions were posed at the upper boundary of the computational domain. The symmetry conditions were posed at the axis of symmetry.

The parameters profiles adopted as the initial conditions at cross section $x/d_j=0.33$ are presented in Fig.13. The initial profiles for the longitudinal velocity and turbulent characteristics were chosen based on estimations of the boundary layers thickness on the external and internal sides of hydrogen injector and additional turbulence production in the wake downstream nozzle lip. The non-dimensional initial distributions of the longitudinal component of the flow velocity $U^{(o)}=\tilde{U}/U_{H2}$; eddy viscosity $\nu_t^{(o)}=\nu_t/(U_{H2}d_j)$; turbulent kinetic energy $K^{(o)}=K/U_{H2}^2$ as well as initial distributions of $\tilde{z}$, σ^2 are given in Fig.13. The transverse component of the velocity $\tilde{V}$ was expected to be zero. The species mass fractions (H_2, O_2, H_2O, N_2) were expected to be constants in the inner and outer flows and their values were chosen in accordance with data of Beach [24]. In the intermediate region they were postulated as linear functions of mixture fraction $\tilde{z}$. All other species concentrations were equaled to zero.

The total enthalpy distribution was expected to be uniform for pure H_2 and pure air flows. In the intermediate region it was expected to be linear dependent on $\tilde{z}$.

Minimum information concerning nozzle configuration and initial distributions was given in the original paper of Beach et al. [24]. However we have tried to make an indirect estimation of adopted distributions for U, H, and z validity. For this purpose we calculated the pitot pressure distribution in the initial cross section using the adopted initial distributions and compared it with the experimental data of Beach (Fig.14a). The validity of the adopted profile for eddy viscosity was approximately estimated from the correspondence of the centerline H_2 mass fraction distribution obtained in FL approach calculations with the experimentally measured by Beach (Fig.14b). It is seen that basis

features of the experimentally measured distributions were reproduced correctly.

CFD solver and numerical grid

The regularized PNS equations were solved using modified version of the marching code SUPNEF. The code SUPNEF is based on explicit finite difference method which is the generalization of the well-known steady analogy of Godunov method [38] for the steady supersonic flows. The code description is given in Sec.B.2 of Appendix B.

Code modifications were connected with the incorporation of the regularization procedure for slightly subsonic regions in accordance with [39]. For this purpose the characteristic relations for the inviscid part of the regularized PNS equations were used for the solution of two flows interaction problem based on the assumption that intensity of main discontinuities is small. The obtained solutions were used to approximate the convective fluxes on the cell boundaries in subsonic regions (regularization factor $\omega<1$). In supersonic region ($\omega=1$) these relations coincide with usual relations for steady supersonic flows interaction problem. The following relation for the regularization factor ω was used in real calculations:

$$\omega=\min\left(1,\left(\frac{M_x}{1.1}\right)^2\right)$$

The calculations were done using adaptive grid. The grid adaptation was realized in accordance with spring analogy [40]. In each cross-section all grid nodes were supposed to be connected by springs with the stiffness proportional to the gradient of Mach number. The nodes positions were determined in accordance with springs system equilibrium conditions.

Methodological tests and computational expenses

The methodological calculations were performed using 50, 100 and 200 computational cells in cross sections for both FL and QL approaches. The role of the grid nodes number variation on the calculated distributions of reactive species mass fractions and turbulent mixing characteristics is given for both FL and QL approaches in Fig.15a,b respectively for $x/d_j=8.26$ cross section.

All the final FL and QL computations were performed using adaptive grids containing 100 computational cells in each cross section. They are given for both approaches in Fig.12.

The computations were performed using workstation HP 9000/735. The CPU time requirements are given in Table 3.

Table 3. Computational expences for flowfield calculations

	QL approach (21 reactions, 11 species)	FL approach (21 reactions, 11 species)
Number of grid cells	100	100
CPU time per grid cell	0.00162sec	0.00097sec*)
Total CPU time of computation	424sec	260sec

*)CPU requirements connected with flamelet library interpolation, calculations of p(z) and averaging were 0.00017sec/cell

RESULTS OF COMPUTATIONS

The obtained H_2O mass fraction contours are given in Fig.16 for both FL and QL approaches. It is seen that flamelet model predicted transition from mixing to burning regime in the vicinity of $x/d_j=3$ cross section. Here the conditionally averaged value of the scalar dissipation at the flame front $\bar{N}_t^s$ became lower its critical value N_{cr} (Fig.17).

The obtained Mach number contours are given in Fig.18 for both FL and QL approaches. It is seen that mixture ignition in the flamelet model calculations is accompanied by the sharp increasing of the released heat and generation of the weak compression wave and slightly subsonic region. It is seen that QL approach predicts more smooth heat release increasing in the mixing/burning transition region.

The cause of such difference between FL and QL predictions is seen from the consideration of Fig.19, where the O_2 mass fraction profiles obtained slightly upstream and downstream ignition point are presented for both FL and QL approaches. Flamelet model generates solution which corresponds to the approach where all the fuel, which initially penetrated fuel-lean part of the mixing layer, reacts with the oxygen in narrow vicinity of the ignition point. The QL approach generates solution where fuel and oxygen consumption is much more weak. It is observed only in the regions

with near-stoichiometric mixture composition, which is more realistic in nature. Fortunately, the ignition distance for the conditions of Beach test case was small enough and the amount of the H_2 penetrated the fuel-lean part of the mixing layer was about 1.6% of its total mass flow rate. That is why the disturbance of the flow field was small also. Such flamelet model behavior is not important for the flames with the short ignition delay length or stabilized in the vicinity of the fuel injectors. However it can be serious disadvantage of the model in the case of flames having large ignition delay.

The obtained in FL approach contours of the turbulent mixing characteristics (mean and variance mixture fraction, turbulent kinetic energy) are given in Fig.20.

The obtained in FL approach distributions of the averaged mass fractions of H_2O, H_2, O_2 and N_2 are given in Figs.21a-d by solid lines together with the data of Beach for four cross sections (x/d_j= 8.26,15.5, 21.7 and 27.9). Good correlation between FL predictions and experimental data is seen. As a rule, FL predictions of species distributions were possible with accuracy better than 20%. Much discrepancy (≈25%) was observed only in predictions of H_2O peak value and for only one test section (x/d_j=8.26). Such discrepancy can be explained taking into account that the estimated error of measurements was higher than 15% (due to mentioned in [24] possible mixture reacting inside the sampling probe). It can be attributed also to the kind of averaged values (Reynolds or Favre) measured by sampling technique.

Results of the QL predictions are given in Fig.21a-d by dotted lines. It is seen that the FL predictions are closer to the experimental data as a whole compare to the QL ones. The QL approach gave significant overprediction of O_2 mass fraction in fuel-rich regions and displacement of the H_2O peak location in comparison with experimental data.

It was concluded that FL approach gave satisfactory result for Beach test case [24].

II.2 BURROWS-KURKOV EXPERIMENT [25]

DESCRIPTION OF THE TEST CASE

Fig.22 shows scheme of setup and test conditions of Burrows-Kurkov experiment [25]. The test section was rectangular duct having the constant width (0.051m). The air supply duct had 0.089m height. Hydrogen was injected parallel to the vitiated air flow. It was injected with a sonic speed through the two-dimensional slot located at the backward step in the initial cross section. Slot height was h=0.004m. Lip thickness at the top of the step was $0.76 \cdot 10^{-3}$m. Test section total height expanded linearly from 0.0938m in the initial cross section to 0.105m at the exit cross section. Composition measurements were done at the exit plane of the test section located at x=0.356m downstream the injector location.

FLAMELET LIBRARY GENERATION

The procedure of the flamelet library generation was basically the same as that used for the Beach test case. The boundary conditions for the flamelet equations were adjusted according to the data presented in Fig.22. The thermochemistry approximation of Appendix C was used for species enthalpies and detailed chemistry model (21 reactions between J=11 species). Only one additional feature was taken into account. It was the influence of the pressure variation inside the flowfield on the combustion chemistry. The range of the pressure variation was adjusted based on the presented in [25] static pressure distributions along the duct wall (≈0.08-0.12MPa). The flamelet model calculations were done for the pressure values in the reaction zone $P=P_s=0.08, 0.1, 0.12$ MPa. The obtained solutions were united into the total flamelet library.

The value of exponent β in approximation (I.8) was chosen as $\beta=1$ which corresponded to the value of the $Sc_t=1$.

The whole flamelet library was calculated using the same as for Beach test case exponential grid consisted of I=81 points.

Total flamelet library included 171 particular solutions in

the range of N^s variation from 0.001 sec^{-1} up to $N_{cr} = N_{cr}(P_s)$ where the later quantity was calculated for three values of P_s=0.08, 0.1 and 0.12 MPa. The $N_{cr}(P_s)$ dependence was approximated as $N_{cr}=777.43\cdot(P_s/0.1MPa)-135.419$ sec^{-1} with the accuracy 0.4%.

Examples of the obtained distributions of temperature T, H_2O, OH radical, and "effective" parameters Q and Γ are given in Fig.23a-e in parametric form on N^s. The influence of the pressure variation on the results of flamelet model calculations is illustrated by Fig.24a-c.

The computational expenses required for the generation of the flamelet library at PC AT 486DX2/66MHz are summarized in Table 4.

Table 4.

Number of species	11
Grid in z direction	81 points
CPU time per iteration per grid point	0.0092sec
Total time for flamelet library generation	2368sec
Total number of calculated particular solutions	185
Number of particular solutions included into the library	171
Required memory for library storing	3.21Mb

The same, as for the Beach test case, norms of the flamelet library accuracy were estimated:

i) relative error $ERROR^{(Rch)}$ associated with the Richardson extrapolation of the obtained numerical solutions to zero-length grid step;

ii) relative error $ERROR^{(int)}$ associated with the accuracy of the interpolation for the interim values of scalar dissipation N^s and pressure P_s using solutions contained in the flamelet library.

It was found that $ERROR_\alpha^{(Rch)} < 0.3\%$ and $ERROR_\alpha^{(int)} < 0.5\%$ for "effective" heat capacities ratio Γ, "effective" heat of formation Q and for all the reactive species mass fractions having the maximum values higher than 10^{-6}.

Tests of results sensitivity to the detailed chemistry model

and adopted U=U(z) correlation were done.

The Miller-Bowman detailed chemistry approximation was substituted by the Warnatz one [34]. The calculations of the flamelet model were repeated with the new detailed chemistry approximation for three different values of scalar dissipation N^s (N^s=1,30,250 sec^{-1}) and were compared with the results obtained by Miller-Bowman scheme. The examples of obtained results are given in Fig.25 for two substances (H_2O and OH). We have found minor influence of the detailed kinetics approximation on the results of calculations for main reactive species and "effective" parameters Q and Γ.

The parameter β in U=U(z) correlation (I.8) was varied in the range β=0.5-2.5. The temperature, water and effective parameters Q and Γ distributions obtained for scalar dissipation value N^s=30 sec^{-1} and different values of β are presented in Figs.26a-d. It was found that the sensitivity of the results to the β variation is relatively small and compatible with the sensitivity of the results to the adopted detailed chemistry approximation (about 1% for main stable species, about 2% for temperature and less than 20% for radicals).

FLOW FIELD CALCULATIONS

Adopted simplifications

The flow field was expected 2-D. The role of the boundary layer at the upper duct wall was neglected since it was difficult to have satisfactory resolution for the boundary layers on the both walls of the duct due to limitations in operational memory of the available HP workstation (64Mb). However the adopted approximation seems to be justified because the height of the test section was much greater than the slot for hydrogen injection. It is possible to assume that the boundary layer on the upper wall does not perturb the mixing and boundary layers near the lower wall.

The simplest molecular transport model was applied i.e. the mixture molecular viscosity and diffusivity were estimated based on H_2 molecular diffusivity and fixed laminar Prandtl and Schmidt numbers Pr=Sc=0.72.

System of equations

The following 2-D approximation of steady, averaged Navier-Stokes (NS) equations was used for the flowfield calculations:

$$\frac{\partial \vec{F}}{\partial x} + \frac{\partial \vec{G}}{\partial y} = 0; \qquad \text{(II.7)}$$

where vectors of fluxes $\vec{F}, \vec{G}$ were as follows:

$$\vec{F} = \begin{pmatrix} \bar{\rho}\tilde{U} \\ \bar{\rho}\tilde{U}^2 + \bar{P} - \bar{\tau}_{xx} \\ \bar{\rho}\tilde{U}\tilde{V} - \bar{\tau}_{xy} \\ \bar{\rho}\tilde{U}\tilde{H} - \tilde{U}\bar{\tau}_{xx} - \tilde{V}\bar{\tau}_{xy} + \bar{q}_x \end{pmatrix}; \quad \vec{G} = \begin{pmatrix} \bar{\rho}\tilde{V} \\ \bar{\rho}\tilde{U}\tilde{V} - \bar{\tau}_{yx} \\ \bar{\rho}\tilde{V}^2 + \bar{P} - \bar{\tau}_{yy} \\ \bar{\rho}\tilde{V}\tilde{H} - \tilde{U}\bar{\tau}_{yx} - \tilde{V}\bar{\tau}_{yy} + \bar{q}_y \end{pmatrix}.$$

Here: x,y are the longitudinal and transverse coordinates; $\tilde{U}, \tilde{V}$ are the components of the velocity vector; $\bar{\rho}$ is density; $\bar{P}$ is pressure; $\tilde{H}$ is the total enthalpy.

The stress terms were defined as:

$$\bar{\tau}_{xx} = \bar{\rho}(\nu+\nu_t)\left(2\frac{\partial\tilde{U}}{\partial x} - \frac{2}{3}\left(\frac{\partial\tilde{U}}{\partial x} + \frac{\partial\tilde{V}}{\partial y}\right)\right); \bar{\tau}_{yy} = \bar{\rho}(\nu+\nu_t)\left(2\frac{\partial\tilde{V}}{\partial y} - \frac{2}{3}\left(\frac{\partial\tilde{U}}{\partial x} + \frac{\partial\tilde{V}}{\partial y}\right)\right);$$

$$\bar{\tau}_{xy} = \tau_{yx} = \bar{\rho}(\nu+\nu_t)\left(\frac{\partial\tilde{U}}{\partial y} + \frac{\partial\tilde{V}}{\partial x}\right);$$

and the heat fluxes as: $\bar{q}_x = -\bar{\rho}\left(\frac{\nu}{Pr} + \frac{\nu_t}{Pr_t}\right)\frac{\partial\tilde{h}}{\partial x}$; $\bar{q}_y = -\bar{\rho}\left(\frac{\nu}{Pr} + \frac{\nu_t}{Pr_t}\right)\frac{\partial\tilde{h}}{\partial y}$;
where ν is kinematic viscosity; ν_t is the eddy viscosity; Pr_t is turbulent Prandtl number (Pr_t=1).

The Secundov's one-equation turbulence model "ν_t- 90" was used to calculate the eddy viscosity ν_t:

$$\frac{\partial\bar{\rho}\tilde{U}\nu_t}{\partial x} + \frac{\partial\bar{\rho}\tilde{V}\nu_t}{\partial y} = \frac{\partial}{\partial x}\left(\bar{\rho}(c_1\nu_t + \nu)\frac{\partial\nu_t}{\partial x}\right) + \frac{\partial}{\partial y}\left(\bar{\rho}(c_1\nu_t + \nu)\frac{\partial\nu_t}{\partial y}\right)$$

$$+ c_2\bar{\rho}\nu_t|G| + c_3\nu_t\left(\tilde{U}\frac{\partial\bar{\rho}}{\partial x} + \tilde{V}\frac{\partial\bar{\rho}}{\partial y}\right) - c_4\bar{\rho}\nu_t^2\frac{G^2}{a^2} - \bar{\rho}\frac{c_5\nu_t^2 + c_6\nu_t\nu}{S^2}; \qquad \text{(II.8)}$$

where:

$$c_2 = c_2'\frac{\nu_t^2 + 11.2\,\nu_t\nu + 12.8\,\nu^2}{\nu_t^2 - 11.2\,\nu_t\nu + 64\,\nu^2};$$

$$G^2 = 2\left(\frac{\partial\tilde{U}}{\partial x}\right)^2 + 2\left(\frac{\partial\tilde{V}}{\partial y}\right)^2 + \left(\frac{\partial\tilde{U}}{\partial y}\right)^2 + \left(\frac{\partial\tilde{V}}{\partial x}\right)^2 + 2\frac{\partial\tilde{V}}{\partial x}\frac{\partial\tilde{U}}{\partial y};$$

c_1	c_2'	c_3	c_4	c_5	c_6
2	0.2	0.7	5	3	50

Here a is local speed of sound; S is minimum distance from the wall.

To obtain values of mean mixture fraction $\tilde{z}$ and its variance σ^2 values and mean scalar dissipation $\tilde{N}$ the following transport equations were solved:

$$\frac{\partial\bar{\rho}\tilde{U}\tilde{z}}{\partial x} + \frac{\partial\bar{\rho}\tilde{U}\tilde{z}}{\partial y} = \frac{\partial}{\partial x}\left(\bar{\rho}\left(\frac{\nu_t}{Sc_t} + \frac{\nu}{Sc}\right)\frac{\partial\tilde{z}}{\partial x}\right) + \frac{\partial}{\partial y}\left(\bar{\rho}\left(\frac{\nu_t}{Sc_t} + \frac{\nu}{Sc}\right)\frac{\partial\tilde{z}}{\partial y}\right); \qquad \text{(II.9)}$$

$$\frac{\partial\bar{\rho}\tilde{U}\sigma^2}{\partial x} + \frac{\partial\bar{\rho}\tilde{V}\sigma^2}{\partial y} = \frac{\partial}{\partial x}\left(\bar{\rho}\left(\frac{\nu_t}{Sc_t} + \frac{\nu}{Sc}\right)\frac{\partial\sigma^2}{\partial x}\right) + \frac{\partial}{\partial y}\left(\bar{\rho}\left(\frac{\nu_t}{Sc_t} + \frac{\nu}{Sc}\right)\frac{\partial\sigma^2}{\partial y}\right)$$
$$+2\frac{\bar{\rho}\nu_t}{Sc_t}\left[\left(\frac{\partial z}{\partial x}\right)^2 + \left(\frac{\partial z}{\partial y}\right)^2\right] - \beta_1\frac{\bar{\rho}K\sigma^2}{\nu_t}; \qquad \text{(II.10)}$$

$$\frac{\partial\bar{\rho}\tilde{U}K}{\partial x} + \frac{\partial\bar{\rho}\tilde{V}K}{\partial y} = \frac{\partial}{\partial x}\left(\bar{\rho}(k_2\nu_t + \nu)\frac{\partial K}{\partial x}\right)$$
$$+\frac{\partial}{\partial y}\left(\bar{\rho}(k_2\nu_t + \nu)\frac{\partial K}{\partial y}\right) + \bar{\rho}\nu_t G^2 - \beta_2\frac{\rho K^2}{\nu_t}; \qquad \text{(II.11)}$$

where $k_2 = 1.4$; $\beta_1 = 0.14$; $\beta_2 = 0.1$; $Sc_t = 1$.

The values of $\tilde{z}$, σ^2 were used to calculate the mixture fraction pdf p(z) using formula (I.11)-(I.14) of Sec I.2.

The conditionally averaged value of scalar dissipation at the flame front $\bar{N}_t^s$ was calculated by approximation (I.15) using the mean scalar dissipation $\tilde{N} = 0.07\frac{K\ \sigma^2}{\nu t}$ and intermittency factor γ distributions.

The following procedure was adopted to adjust the value of the pressure P_s for the selection of instantaneous flamelet model solution. The location of the closest to the mean stoichiometric surface $\tilde{z} = z_s$ computational cell in each cross section of the duct was emphasized. The value of mean static pressure $\bar{P}$ in this cell was used as the reference pressure P_s inside the reaction zones for the cross section.

The particular solution of the flamelet model problem at $N^s=\bar{N}_t^s$ and $P_s=\bar{P}(\tilde{z}=z_s)$ was obtained from the flamelet library by the linear interpolation between neighboring solutions for scalar dissipation, pressure and mixture fraction. The obtained solution for the "effective" heat capacities ratio Γ and "effective" heat of formation Q were averaged using calculated p(z). The averaged values of $\overline{\Gamma/(\Gamma-1)}$ and $\tilde{Q}$ were used for the closure of the governing system of conservation equations using procedure outlined in Sec.I.3.

In the case of QL approach calculations the system (II.7),(II.8) was solved together with the averaged reactive species mass conservation equations (II.1).

Computational domain and boundary conditions

The computational domain is given in Fig.27. The left boundary was located in the hydrogen injection cross-section where all parameters distributions were supposed to be known in all opened parts of cross-section excluding the slot lip. No-slip velocity conditions were posed on the lip wall and on the lower wall of the duct . It was expected also that the lip temperature was fixed (T_w=300K). The lower wall was expected to be adiabatic with zero temperature gradient. The turbulent kinetic energy and turbulent viscosity were equal to zero at the lower wall and lip. The mean mixture fraction and mixture fraction variance normal derivatives were equal zero at the lower wall and lip.

The upper wall was considered as inviscid with zero transversal velocity component. All normal derivatives, which were needed to estimate viscous stresses and corresponding diffusion fluxes on the wall, were equal to zero.

In the exit plane of computational domain (located at x=0.356m cross section downstream the injector) the so-called drift boundary conditions with normal derivatives of all parameters determination from computational domain were posed.

In the case of QL approach calculations all walls were supposed to be noncatalitic and species concentrations normal derivatives were set to be equal to zero.

The parameters distributions at the inlet boundary were obtained by the following manner. The longitudinal velocity and

eddy viscosity distributions in the incoming air flow were derived from the experimental data of [25] on boundary layer thickness ($\delta \approx 0.012$m). The eddy viscosity distribution inside the boundary layer was approximated using formula:

$$\nu_t = 0.41\ y\ U_\tau (1-\exp(-\frac{yU_\tau}{26\nu})(1-y/\delta)\ \exp(-y/\delta);$$

where dynamic velocity U_τ was calculated using correlation for local skin friction factor C_f for compressible turbulent boundary layer at flat plate:

$$2U_\tau^2/U_e^2 \equiv C_f = 0.023\ (\frac{U_e\delta}{\nu})^{-0.2}\ (1+0.7(k-1)M_e^2/2)^{-0.5}(2/(1+\bar{T}_w)^{0.5}.$$

Here subscript "e" denotes parameters in core flow, $\bar{T}_w$ is the temperature factor, k is heat capacities ratio.

The longitudinal velocity distribution in the boundary layer was obtained by integrating of the equation for the shear stress:

$$\frac{\bar{\tau}_{xy}}{\bar{\rho}} = (\nu_t+\nu)\frac{\partial\tilde{U}}{\partial y};$$

where the distribution for the shear stress inside the boundary layer was approximated according to [41] as:

$$\frac{\bar{\tau}_{xy}}{\bar{\rho}} = U_\tau^2\ (1-3(y/\delta)^2+2(y/\delta)^3)$$

The turbulence kinetic energy distribution in the boundary layer was calculated from the approximate "equilibrium turbulence" relation:

$$\frac{\nu_t}{K}\ |\partial\tilde{U}/\partial y| = 0.3.$$

The same procedure was used for $\tilde{U}$, ν_t and K distributions calculations in the exit plane of the hydrogen injection slot. The boundary layers on the walls were expected to be fully developed with the thickness equal to a half of the slot height ($\delta = 1/2h = 0.002$m). The hydrogen velocity profile maximum value was adjusted to provide the same total H_2 mass flow rate as that obtained in experiment.

The 2% velocity fluctuations were expected in free stream outside the boundary layers.

The obtained non-dimensional initial distributions of the longitudinal component of the flow velocity $U^{(o)} = \tilde{U}/U_a$; eddy viscosity $\nu_t^{(o)} = \nu_t/(U_a h)$; turbulent kinetic energy $K^{(o)} = K/U_a^2$ and

total enthalpy $H^{(0)}=H/U_a^2$ are given in Fig.28 where U_a is the air flow velocity in the core flow and h is hydrogen injector slot height.

The uniform step initial profile was expected for mixture fraction $\tilde{z}$. The transverse component of the velocity $\tilde{V}$ and mixture fraction variance σ^2 were expected to be zero at the entry boundary.

To estimate the reliability of the adopted initial distributions we have calculated pure mixing regime of Burrows-Kurkov experiment. No additional oxygen was introduced into the air flow in this test run and there was no combustion as the result. The distributions of the averaged mole fractions of N_2,H_2 and H_2O obtained for cross section x=0.356m are given in Fig.29 together with the experimental data. The satisfactory agreement is seen.

CFD solver, numerical grid, convergence and computational expenses

The system of equations was solved numerically using modified version of FNAS2D code developed at CIAM [42] (description of the code is given in Sec.B.3 of Appendix B).

Details of calculations were basically the same as those reported in [27]. Only one additional modification was applied. The fully coupled solution procedure was used to increase convergence rate of the QL approach calculations compared to that reported in [27] (see detailed in Sec.B.3 of Appendix B). It allowed, by order, decrease required number of iterations and increase Courant number for QL calculations compare to the calculations reported in [27].

Main serie of calculations was done using nonuniform grid with 90 cells in transversal direction and 100 cells in longitudinal direction (Fig.27). Grid was clustered to the lower wall and to backward - facing step in accordance with geometrical progressions. The progression factors were chosen automatically to provide the given sum of progression but they were lower than 1.1. In initial cross-section, minimal cell dimension near the lower wall was $\Delta hmin_y=10^{-5}$m ($\Delta hmin_y/h=2.5\cdot10^{-2}$). For the exit cross-section, minimal cell dimension in vertical direction was chosen to be equal to $2\cdot10^{-5}$m. This provided value $y^+=yU_\tau/\nu_w\approx3.2$

for the nearest to the lower wall computational point (see Fig.30). More detailed description of the grid generation procedure was given in [27].

The calculations were done with Courant number up to 400 for the FL approach and 1500 for the QL one. The convergence was estimated by the L_2 norm for the residual of continuity equation. The L_2 norm behavior vs iteration number is given in Fig.31. In the case of FL approach calculations, this norm decreased 3.5 orders during 600 iterations. In the case of QL approach calculations the L_2 norm dropped ≈3 orders after 200 iterations.

The computations were performed using workstation HP 9000/735. The CPU time requirements are given in Table 5.

Table 5. Computational expences for flowfield calculations

	QL approach (21 reactions, 11 species)	FL approach (21 reactions, 11 species)
Grid	90x100	90x100
CPU time per grid cell per iteration	0.007sec	0.0013sec
Total number of iterations	200	600
Total CPU time of computation	≈3.5 hours	≈2 hours

Accuracy of computations

We were not able to control accuracy of computations by simple increasing of the computational cells number due to limitations in operational memory of our HP work station. So, to provide such analysis the following series of calculations was performed.

The computational domain was divided by subregions and calculations with the patched grids were performed to estimate influence of the discretization in longitudinal direction. The final grid with 90x300 points was designed to provide very fine grid near the injector lip (100 points in the longitudinal direction). Two another regions were joined with this first region in such a manner to provide the total number of grid points in longitudinal direction to be equal to 300.

Additional calculations were performed also to estimate the sensitivity of the results to the grid accuracy in the lateral

direction. For this purpose, grid was adapted in such manner to increase the number of grid points in the mixing layer with something more rough grid in the near wall region. The grid adaptation to the stoichiometric line was realized.

The obtained influence of the grid on the species mole fractions in cross-section x=0.356m is illustrated by Fig.32a for FL approach, and, by Fig.32b - for QL approach . It is seen that discretization influence on the results of calculations is ≈5%. There is no any qualitative difference between "main" (90x100) and "fine" (90x300) grid calculations. The mostly significant influence is confined in some shift of the QL predictions to the air-side of the mixing layer. It should be mentioned also that the main grid influence is connected with discretization in x-direction (especially for QL approach).

Of course, these estimations are slightly ambiguous. However, they provide to feel the influence of the grid accuracy on the results.

RESULTS OF COMPUTATIONS

The obtained H_2O mass fraction contours are given in Fig.33 for both FL and QL approaches. It is seen that the flamelet model predicted self-ignition point location 0.08m downstream hydrogen injector. The self-ignition point predicted by the QL approach is located 0.12m downstream the injector which is more close to its location in experiments (x≈0.18m). The significant difference in H_2O mass fraction distributions predicted by the QL and FL approaches downstream the ignition point is seen also. It is necessary to note that the peak water concentration value predicted by FL approach is 17% lower than that predicted by QL approach.

The comparison of the obtained reactive species mole fraction distributions with the experimental data is given in Fig.34 for test section x=0.356m where the composition measurements were done by Burrows and Kurkov. Unsatisfactory correlation between FL approach predictions and experimental data for H_2O and O_2 mole fractions is seen. For example, the ≈35% underprediction of the H_2O peak value is observed. The results of the QL approach

predictions correlates with the experimental data reasonably well. The difference between measured and predicted by QL approach H_2O concentration peak values is lower than 20%.

The significant underprediction of the water origin in the flame by FL approach leads to approximately the same (≈35%) underprediction of the mean static temperature peak value as it is shown in Fig.35 (solid line). It is seen that QL approach calculations gave satisfactory result again (denoted by dashed line in Fig.35).

Unfortunately, one can conclude that the flamelet approach gave unsatisfactory results for the Burrows-Kurkov test case.

Roots of the obtained discrepancy were analyzed in [27]. It was found that the mostly probable cause of discrepancy was too high level of the mixture fraction variance σ^2 predicted by eq.(II.10), which was resulted in overprediction of the turbulent fluctuations intensity $INT=\sigma/\tilde{z}$ level inside mixing layer for the considering wall-jet configuration. The main reasons leading to such conclusion are presented below.

Let us start consideration from the discussion of the chemistry/pdf relative role in total FL approach predictions budget for the Burrows-Kurkov test case. It is given in Fig.36. Here the dashed line denotes the equilibrium chemistry solution for water mole fraction $\chi_{H2O}^{(eq)}$ plotted vs mixture fraction z. It was obtained based on the assumption that both chemical nonequilibriumness and scalar field fluctuations are absent in the flow so it is the upper limit for possible water concentration distributions. The obtained in cross section x=0.356m instantaneous flamelet model solution for water mole fraction $\chi_{H2O}^{(FL)}(z,N^s,P_s)$ is plotted vs mixture fraction z by fine solid line. The averaged distribution of water mole fraction:

$$\bar{\chi}_{H2O}^{(FL)} = \int_0^1 \chi_{H2O}^{(FL)} p(z)\,dz$$

is plotted in Fig.36 by fat solid lines.

It is seen approximately 50%÷50% input of both chemistry nonequilibriumness and averaging procedure into the resulting averaged water mole fraction distribution $\bar{\chi}_{H2O}^{(FL)}$ predicted by the FL approach. Here averaged concentration peak value is 35% lower

than the peak value for $\chi_{H2O}^{(eq)}$ distribution. Such a prediction contradicts to experimental data of Burrows and Kurkov denoted in Fig.36 by crosses.*) It is seen that experimentally measured H_2O mole fraction distribution is very close to the equilibrium limit $\chi_{H2O}^{(eq)}$. This means that the role of both chemistry nonequilibriumness and scalar field fluctuations is very low for the considering test section of Burrow-Kurkov experiment. At the same time the flamelet approach overpredicted role of both effects. So one could expect that the flamelet model failure was due to failure of the used detailed kinetics model and/or due to failure of the averaging procedure.

The additional tests demonstrated that version concerning detailed chemistry approximation failure for considering test conditions is improbable. The reasons here are as follows. The results of the flamelet model calculations varied very weakly when the Miller-Bowman chemistry approximation [32] was substituted by the Warnatz [34] one. At the same time the averaging of the equilibrium chemistry distribution $\chi_{H2O}^{(eq)}$ (using obtained in calculations distributions of $\tilde{z}$ and σ^2) gave the mean

---

*) This was done as follows. The measured in Burrows-Kurkov experiment distributions of N_2 mole fraction was used to re-plot reactive species mean mole fractions vs mean mixture fraction $\tilde{z}$ instead of space coordinate y. It was expected that the molecular nitrogen N_2 does not react with other species. Hence its mass fraction C_{N2} has to be approximately linear depending on mixture fraction: $C_{N2}=C_{N2}^{A}(1-z)$ if difference in molecular diffusivities is neglected. Here C_{N2}^{A} is the molecular nitrogen mass fraction in the air flow. The fluctuations can not change this dependence due to its linearity and it remains valid for mean values $\tilde{C}_{N2}=C_{N2}^{A}(1-\tilde{z})$. We used this relation to obtain the mean mixture fraction distributions $\tilde{z}(y)$ in the test sections. We re-plotted experimental data of Burrows-Kurkov in a form of $\tilde{\chi}_{\alpha}$ on $\tilde{z}$, using the experimentally measured distributions of the reactive species mole fractions $\tilde{\chi}_{\alpha}(y)$ and the obtained relation $\tilde{z}(y)$. Such a re-plotted H_2O mole fraction distribution (denoted by crosses) is given in Fig.36. The experimental N_2 mole fraction distribution had non-monotonic part (three measured points) at the fuel-lean edge of the mixing layer (please see Fig.34) which can be referred to instrumental errors. That is why these 3 points were rejected from the analysis.

distribution $\bar{\chi}_{H2O}^{(eq)}$ which was very close to the averaged flamelet model solution $\bar{\chi}_{H2O}^{(FL)}$.

One could expect improper thermochemistry model operation due to using of the simplified correlation U=U(z) which could introduce some errors in enthalpy distribution. However we controlled results sensitivity to U=U(z) correlation influence. This influence was very weak (please see Figs.26a-d).

So one can expect that the roots of the failure are connected with the averaging procedure.

First of all we have verified role of the shape of our pdf model. For this purpose we have performed averaging of the instantaneous solution using two another approximations for p(z). The first one was widely used β-distribution [43]. As the second approximation for pdf we have used analytical solution of the mixture fraction pdf equation obtained in [44] for variable density homogeneous turbulent flows. The obtained averaged distributions were slightly different but minor difference for the peak values of averaged water concentration was found (Fig.37).

The "smoothing" of the species and temperature instantaneous distributions by probability density function is governed by the parameter INT=$\sigma/\tilde{z}$. The results of averaging are mostly sensitive to INT level in near-stoichiometric regions ($z \approx z_s$) where significantly non-linear variation of the instantaneous reactive species distributions and temperature vs mixture fraction is observed. At the same time the main discrepancy between FL approach averaged distributions and experimental data was observed in near-stoichiometric regions also (see Fig.36). This feature sent us to analyze obtained in calculations INT distribution. This distribution vs mean mixture fraction $\tilde{z}$ is given in Fig.38 for test section x=0.356m. It is seen that the eqs.(II.9),(II.10) generated INT distribution with a level of about 150-200% in the near-stoichiometric regions ($\tilde{z} \approx z_s$). This prediction of "concentration subsystem" (II.9),(II.10) of the turbulence model is quite questionable for the considering planar wall jet configuration. Results of presented analysis of Burrows-Kurkov experimental data allows to expect that INT level in their experiments was sufficiently lower. The reasons here are as follows. It is known that approximately the same INT level

(≈200%), as it was predicted by eqs.(II.9),(II.10), is typical for unconfined flames in still air where it provides significant difference between instantaneous and averaged distributions of parameters [1]. For example, it provides ≈400K (≈20-25%) difference between instantaneous and averaged peak temperature values in laboratory H_2/air round jet diffusion flames which was approved both by experiments and calculations [45].

The possible overprediction of INT level explains also why the instantaneous flamelet solution differed so significantly from equilibrium limit (see Fig.36). The nonequilibriumness for FL approach is governed by approximation (I.15) for conditionally averaged value of scalar dissipation at the stoichiometric surface:

$$\bar{N}_t^s = \frac{\tilde{N}|_{\tilde{Z}=Z_s}}{\gamma|_{\tilde{Z}=Z_s}} .$$

The value of $\bar{N}_t^s \sim INT^B$ where exponent B is varied in the range 2-4 i.e. $\bar{N}_t^s$ value is very sensitive to the overprediction of fluctuations intensity level. So the overprediction of the fluctuations intensity leads to overprediction of the $\bar{N}_t^s$ value and as a result to overprediction of chemical nonequilibriumness role by flamelet model equations (I.5).

We estimated possible range of the intensity reduction which can improve the results of the FL approach predictions. The $INT^0=INT(\tilde{z})$ distribution obtained in FL approach calculations was diminished "by hand" by a factor ψ = 0.5 and 0.25 sequentially ($INT=\psi \cdot INT^0$). The influence of INT decreasing on the predictions of water mole fraction values is illustrated by Fig.39. It is seen that improvement can be obtained if intensity of fluctuations would be ≈3-4 times lower than that obtained in current FL approach calculations.

Based on the results of the presented here analysis, we expect that the fluctuations intensity in the conditions of Burrows-Kurkov experiment was low enough (especially in near-stoichiometric and fuel-lean regions) and subsystem (II.9),(II.10) failed to predict it accurately. We expect also that the low level of mixture fraction fluctuations provided relative success of the QL approach obtained not only in our but in many other QL approach calculations for the conditions of

Burrows-Kurkov test case (for example [4,5,46]).

We expect that the overprediction of the INT level in our calculations was mostly due to overprediction of mixture fraction variance σ^2 level by semi-empirical eq.(II.10). Previously, this equation was verified mostly for round jet configurations and for low Mach numbers. We expect that performed tests demonstrated that this equation requires additional verification and improvement for complex flow configurations (compressible flows, wall jets, etc.). We expect also that adopted approach for the calculation of the intermittency factor γ requires additional re-examination and (may be) improvement. The intermittency factor γ was calculated from the simplified relation $\gamma=\min\{1;A/(1+INT^2)\}$ (see eq.(1.12)) which was previously obtained and verified in [1,29,30] for incompressible flows only. At the same time some of the available experimental studies performed for compressible flows demonstrated decreasing of the intermittency effects role with the increasing of the Mach number due to the role of compressibility [47,48]. We hope that such improvement of the "passive scalar statistics" block in our turbulence model will allow to improve accuracy and reliability of FL approach predictions for reactive scalars and temperature without modification of flamelet equations (I.5).

However we have doubts concerning possibility to improve predictions of self-ignition point location by the *existing* FL approach version. This conclusion is based on the fact that existing FL approach considers only one possible cause responsible for ignition delay i.e. too high rate of reagents mixing in the vicinity of the injection point which limited rate of chemical reactions (due to reaction zone cooling). At the same time there is another possible cause responsible for ignition time delay i.e. pure chemical kinetics limitations. Both experimental data and results of QL approach calculations demonstrate that such kind of self-ignition was observed in Burrows-Kurkov experiment. So the improvement of the flamelet approach for proper prediction of self-ignition point location in such situations requires further upgrading of the flamelet equations (see Sec.II.3).

II.3 COMPARATIVE ANALYSIS AND CONCLUSIONS

Current Section summarizes our conclusions concerning performed CFD tests of the model. Computational efficiency of the FL approach, accuracy of its predictions, roots of discrepancy and our suggestions for the model improvement are discussed. We presented also estimations of the flamelet model capabilities in comparison with the another turbulent combustion models (Evolved PDF and Assumed PDF approaches). The necessary data for comparative estimations were taken from study [12] where Evolved and Assumed PDF approaches were applied for calculations of the same test case [24].

COMPUTATIONAL EXPENSES

The summary of computational expenses required for FL approach calculations is presented in Fig.40. Data were taken from Tables 2-5 of Sec.II.1,II.2. Additionally it was taken into account that PC AT 486DX2/66MHz productivity is ≈1/10 of HP 9000/735 work station.

It is seen that application of the flamelet model in CFD does not require any significant computational resources. For example, we found that generation of the sufficiently accurate (accuracy is about 0.3-0.5%) flamelet library for the detailed H_2 oxidation chemistry (11 species, 21 reactions) required ≈20% of the total CPU time necessary for the flowfield calculations if PNS marching solver is used. The relative CPU time expenses for FL library productions decreased to the value ≈4% if full NS solver is used for flowfield calculations.

The calculations of the test cases [24,25] demonstrated also that the FL approach usage allows to decrease the computational time per cell in ≈1.5 times for the PNS solver and in ≈5 times for the NS solver in comparison with QL approach.

The flamelet libraries does not require any significant memory for storing (≈1-3Mb).

The rough comparative estimation of CPU expenses for FL, Evolved PDF and Assumed PDF modeling is given in Fig.41. Here the expenses for Evolved PDF are adopted as 100% and y-axis is logarithmically scaled. The Cray-YMP CPU requirements for Evolved

and Assumed PDF calculations of Beach test case were reported in study [12]. The CPU expenses for FL approach (600sec of HP 9000/735 CPU; 50x200 grid) were obtained in FL calculations based on full NS solver FNAS2D (described in Sec.B.2 of Appendix B) of the Beach test case also. The minimal realistic assumption that productivity of Cray-YMP is only 10 times higher than productivity of our HP work station was adopted in comparative estimations. It is seen that computational expenses for FL approach *by orders lower* both Evolved and Assumed PDF modeling.

Based on the reported results, one can conclude that performed tests demonstrated high computational efficiency of the FL approach.

ACCURACY OF PREDICTIONS and SUGGESTIONS FOR MODEL IMPROVEMENT

Unfortunately, results of the performed tests does not allow to make so definite conclusion concerning accuracy of the model predictions as it was made about its computational efficiency. Moreover, these tests demonstrated that model requires further improvement.

The mostly important results of the tests are summarized in Fig.42. Here results of our FL approach water concentration predictions (taken from Figs.21 and 34) are plotted for both considered test cases. The QL approach (current), Evolved PDF modeling [10,12] and Assumed PDF modeling [12] predictions are plotted also.

It is seen that correlation between the FL approach and the experimental data was quite different for the considered test cases.

The FL approach gave satisfactory results for the Beach test case (Fig.42a). As a rule, predictions of species distributions were possible with accuracy better than ≈20%. Here FL approach predictions looks quite well compare to those obtained for Beach test case by another approaches.

However FL approach predictions were unsatisfactory for the Burrows-Kurkov test case (Fig.42b). The serious discrepancy between experimental data and results of calculations was found i.e. the ≈35% underprediction of the H_2O and temperature values;

large "smoothing" of O_2 distribution, etc. It is seen that Evolved PDF modeling for the considering test case provided best result. The QL approach predictions were satisfactory.

The analysis of the discrepancy roots was done in [27] and it was repeated in Sec.II.2. Based on its results, we can conclude that the cause of discrepancy was not directly connected with the flamelet equations. We expect that it was due to overprediction of the mixture fraction intensity level by our turbulence model. The main doubts are addressed here to the accuracy of semi-empirical eq.(II.10) for mixture fraction variance. We hope that even current version of FL approach can get satisfactory results for the predictions of the reactive species and temperature distributions after improvement of the "passive scalar statistics" block in our turbulence model. To obtain this goal, we intend to re-examine accuracy of closure approximations and role of neglected terms in (II.10) using available experimental data on turbulent mixing for flows with and without burning. Based on this analysis, we expect to propose modifications of the model equations for mixture fraction variance and intermittency factor which will allow to increase reliability and accuracy of predictions for complex flow configurations like that which was considered in current study (compressible wall-jet duct flow).

The performed tests demonstrated also that existing version of the flamelet model does not allow to predict accurately combustible flows with large ignition delay distance. This is mostly due to improper model operation in the vicinity of self-ignition point since convective terms in the flamelet model equations were dropped out. This approach is approximately valid in the mixing region upstream ignition zone and in the "well-developed" combustion region downstream this zone. But it is violated in the "self-ignition" region, where reaction zone is thick and basic assumptions of the approach can violate. We expect that this disadvantage can be overcome by introducing of convective terms into the flamelet equations based on the same kind of reasoning as it was done in Condition Moment Closure (CMC) approach proposed by R.Bilger (Sydney University, Australia) [49] and A.Klimenko (CIAM, Russia) [50]. We expect to investigate capabilities of such model upgrading for predictions of flames

with significant ignition length delay. The role of the scalar dissipation fluctuations is additional important effect which can significantly influence flamelet model predictions in the vicinity of the ignition point. The role of this effect was neglected in current study. So we expect to introduce pdf model for scalar dissipation into our averaging procedure and to investigate influence of the scalar dissipation fluctuations on the predictions of the ignition point location and averaged distributions of reactive species in vicinity of this point.

The discussed here two directions (improvement of the passive scalar statistics modeling and upgrading of the FL approach for flames with large ignition delay) were proposed to National Aeronautics and Space Administration as main tasks for the next step research directed toward further improvement of the FL approach.

PART III. SUPPLEMENTED STUDIES

III.1 SIMPLIFICATION OF THE FLAMELET CALCULATIONS BASED ON PARTIAL EQUILIBRIUM CHEMISTRY ASSUMPTION

Detailed kinetics of hydrogen oxidation consists of two main subsystems. The first one couples relatively fast two-body chain branching and chain-propagation reactions of radicals production:

$$\left.\begin{array}{l} H_2 + OH = H_2O + H \\ OH + OH = H_2O + O \\ \cdots\cdots\cdots\cdots\cdots\cdots \end{array}\right\} \quad \textit{two-body reactions} \qquad \text{(III.1)}$$

The second subsystem couples three-body radical recombination reactions which determine reaching of the chemical equilibrium by the reacting system :

$$\left.\begin{array}{l} H + OH + M = H_2O + M \\ H + O + M = OH + M \\ \cdots\cdots\cdots\cdots\cdots\cdots \end{array}\right\} \quad \textit{three-body reactions} \qquad \text{(III.2)}$$

Here third body M is required to carry out away liberated energy.

In many classes of high-enthalpy reacting flows, induction times for radicals production via two-body reactions are short compare to their consumption in three-body recombination reactions [59,60]. This feature of combustion chemistry was used previously to develop Partial Equilibrium approach (PEq) for simplification of the detailed kinetics approximation [61,62].

PEq is based on the assumption that two-body subsystem (III.1) is equilibrated while all departure from the chemical equilibrium is governed by three-body subsystem (III.2). The equilibrium conditions for two-body reactions allows to reduce number of required scalars for description of combustion chemistry to only two. Usually, mixture fraction z and primary kinetic variable C^* are used as such variables [63].

Range of PEq applicability is limited by the moderate deviations from the equilibrium. Significant increasing of the chemical nonequilibriumness leads to PEq violation due to increasing of the induction times of two-body reactions. However, benefits of PEq two-variables formalism were used successfully for the simplification of chemistry calculations in conventional

turbulence modeling of both sub- [43,63] and supersonic [64] jet flames.

In current study, we tried to apply PEq two-variables formalism for simplification of the flamelet calculations. It was possible to propose simplified semi-analytical method for approximate solution of the flamelet equations at moderate deviations from the chemical equilibrium. Description of the simplified method and account about its accuracy are presented below.

Simplified procedure for FL equations solution

Followed by [61,63], it is assumed that thermochemical system for H_2 oxidation can be approximated using six reactive species (H_2, O_2, H_2O, O, H, OH) consisted of two elements (H,O). The molecular nitrogen N_2 is considered as passive contaminant.

The PEq assumption about equilibrium of two-body reactions is used. Due to O and H atoms conservation laws, it is possible to select only three independent stoichiometric equations between six reactive scalars from the two-body reactions subsystem. The following set was selected:

$$\begin{aligned} H + O_2 &= OH + O \\ H_2 + OH &= H_2O + H \\ OH + OH &= H_2O + O \end{aligned} \qquad \text{(III.3)}$$

It is expected that all deviations from chemical equilibrium are governed by the three-body recombination reactions:

$$\begin{aligned} H + OH + M &= H_2O + M \\ H + O + M &= OH + M \\ H + H + M &= H_2 + M \end{aligned} \qquad \text{(III.4)}$$

For further consideration, let us denote H_2, O_2, H_2O, O, H, OH mass fractions as $C_1,\ldots,C_6$ respectively.

Let us introduce primary kinetic variable C^* as linear combination of reactive species so as it to be changed only by the slow recombination reactions (III.4). The choice of C^* is based on method proposed in [62]. It is as follows.

Flamelet equation for α-th specie from system (I.5):

$$N^s \frac{d^2 C\alpha}{dz^2} + R_\alpha(\rho, T, C_1, \ldots, C_J) = 0 \qquad \alpha=1,\ldots,J=6 \qquad \text{(III.5)}$$

is multiplied by arbitrary value A_α and the resulting relations are added. As a result one has:

$$N^s \frac{d^2}{dz^2}\left(\sum_{\alpha=1}^{J} A_\alpha \cdot C_\alpha\right) = -\sum_{\alpha=1}^{J} A_\alpha \cdot R_\alpha \qquad \text{(III.6)}$$

Using the relation:

$$R_\alpha = \mu_\alpha \sum_{m=1}^{M} (\nu^b_{\alpha m} - \nu^f_{\alpha m}) \cdot RR_m$$

it is possible to transform right hand side of eq. (III.6) as follows:

$$\sum_{\alpha=1}^{J} A_\alpha \cdot R_\alpha = \sum_{m=1}^{M} RR_m \sum_{\alpha=1}^{J} ((\nu^b_{\alpha m} - \nu^f_{\alpha m}) \cdot \mu_\alpha A_\alpha) \qquad \text{(III.7)}$$

where RR_m is the total rate (difference between forward and backward rates) of m-th elementary reaction from set of (III.3), (III.4); $\nu^f_{\alpha m}, \nu^b_{\alpha m}$- stoichiometric coefficients for α-th species in m-th elementary reaction; μ_α is molecular weight of α-th specie.

If the coefficients at the bimolecular reaction rates in (III.7) to equate with zero, one can obtain three linearly independent equations:

$$\sum_{\alpha=1}^{J} ((\nu^b_{\alpha m} - \nu^f_{\alpha m}) \cdot \mu_\alpha A_\alpha = 0 \qquad \text{(III.8)}$$

with regard to value of A_α. It is convenient to assume that coefficient A_1 at C_1 (H_2 concentration) is equal to unity and coefficients A_2, A_3 at C_2, C_3 (O_2 and H_2O concentrations) are equal to zero. Then from solution of the equations (III.8) it follows:

$$C^* = C_1 + \frac{\mu_1}{\mu_4} C_4 + \frac{3}{2} \cdot \frac{\mu_1}{\mu_5} C_5 + \frac{1}{2} \cdot \frac{\mu_1}{\mu_6} C_6 \qquad \text{(III.9)}$$

By the definition (III.9), primary kinetic variable C^* obeys equation:

$$N^s \frac{d^2 C^*}{dz^2} + R^*(\rho, T, C_1, \ldots, C_J) = 0 \qquad \text{(III.10)}$$

Here, effective oxidation rate R^* has the form:

$$R^* = -2\mu_1 (RR_1 + RR_2 + RR_3) \qquad \text{(III.11)}$$

where RR_1, RR_2, RR_3- total rates of three-molecular reactions (III.4); subscripts 1-3 in the values of RR_m correspond to the ordinal number of the reaction in (III.4).

Generally speaking value of the effective oxidation rate R^* is expressed through $C_1,\ldots,C_6$, ρ and T using Arrenius approximation of rates for reactions (III.4). So, the following set of equations should be used together with eq.(III.10) to obtain solution:

i) atoms conservation laws in a form:

$$\begin{aligned} &(\text{H atoms}) \Rightarrow \quad (ZH^F - ZH^A)\cdot z + ZH^A = C_1 + \frac{1}{9}\cdot C_3 + C_5 + \frac{1}{17}\cdot C_6 \\ &(\text{O atoms}) \Rightarrow \quad (ZO^F - ZO^A)\cdot z + ZO^A = C_2 + \frac{8}{9}\cdot C_3 + C_4 + \frac{16}{17}\cdot C_6 \end{aligned} \qquad \text{(III.12)}$$

ii) flamelet form (I.5) of energy conservation equation:

$$H = (H^F - H^A)\,z + H^A \qquad \text{(III.13)}$$

iii) equilibrium conditions for two-body reactions (III.3):

$$\prod_{\alpha=1}^{J} \left(\frac{\rho\, C_\alpha}{\mu_\alpha}\right)^{(\nu^b_{\alpha m} - \nu^f_{\alpha m})} = K_m^{eq} \qquad \text{(III.14)}$$

iv) thermal equation of state:

$$P = \rho RT \sum_{\alpha=1}^{J} C_\alpha/\mu_\alpha \qquad \text{(III.15)}$$

v) definition of the primary kinetic variable C^*:

$$C^* = C_1 + \frac{\mu_1}{\mu_4}\, C_4 + \frac{3}{2}\cdot\frac{\mu_1}{\mu_5}\, C_5 + \frac{1}{2}\cdot\frac{\mu_1}{\mu_6}\, C_6 \qquad \text{(III.16)}$$

Here: ZH^F, ZO^F are hydrogen and oxygen atoms mass fractions in the fuel flow (z=1); ZH^A, ZO^A are hydrogen and oxygen atoms mass fractions in the oxidizer flow (z=0); H is total enthalpy; K_m^{eq} - equilibrium constant; R is universal gas constant. Additionally, similarity between mixture fraction conservation equation and atoms conservation equations is taken into account in (III.12).

Necessity to solve large subsystem of additional algebraic equations together with differential eq.(III.10) decreases computational benefits of the PEq approach. So, based on results of [20], the following simplified procedure was used.

The effective oxidation rate R^* is approximated by a simple formula:

$$R^* = -\,k\cdot(C^* - C_e^*)^n\,, \qquad \text{(III.17)}$$

where k and n are some constants, C_e^* is equilibrium value of C^*.

The factor k and exponent n for approximation (III.17) can be found from the algebraic subsystem (III.12)-(III.16). This

subsystem is solved parametrically for various (and given) values of $\Delta C^*=C^*-C_e^*$. As the result, reactive species, temperature and density are found as the function of mixture fraction z, increment of the primary kinetic variable ΔC^*, and pressure in the reaction zone P_s:

$$C_\alpha=C_\alpha(z,\ \Delta C^*, P_s)$$
$$T=T(z,\ \Delta C^*, P_s) \qquad \text{(III.18)}$$

The obtained relations are substituted into the relation (III.11) for the effective oxidation rate R^*. As the result, one has:

$$R^*=R^*(z,\ \Delta C^*, P_s) \qquad \text{(III.19)}$$

Further k and n are obtained by approximation of (III.19).

Using approximation (III.17), equation (III.10) for primary kinetic variable is written as:

$$N^s \frac{d^2C^*}{dz^2} - k(C^* - C_e^*)^n = 0 \qquad \text{(III.20)}$$

It is seen that this equation can be solved independently on algebraic subsystem (III.12)-(III.16) in parametric form on N^s.

Two approaches were formulated previously for approximate analytical solution of eq.(III.20). The first one was reported in study [20]. It is based on the expansion over small parameter $\varepsilon=N^s/k<<1$ which is contained in eq.(III.20). Here, for the first approximation, solution has the form:

$$C^* = C_e^* + \left(\frac{N^s}{k}\frac{d^2C_e^*}{dz^2}\right)^{1/n} + \bar{o}(\varepsilon^{1/n}) \qquad \text{(III.21)}$$

The second analytical approach for solution of (III.20) was proposed previously in our group [1]. Here, the equilibrium value of primary kinetic variable C_e^* is approximated by formula:

$$C_e^* = k_0(z-z_s)\theta(z-z_s)$$

where $k_0=(1-z_s)^{-1}$ and θ is Heaviside step function. This approximation allows to obtain the following analytical solution in the vicinity of the stoichiometric surface:

$$C^*=k_0\left((z-z_s)\theta(z-z_s) + \Omega\cdot Da^{\frac{1}{1+n}}\left(\frac{n-1}{2}\left(\frac{abs(z-z_s)}{Da^{1/(1+n)}}+\Psi\right)\right)^{\frac{2}{1-n}}\right) \qquad \text{(III.22)}$$

where Damkohler number is defined as $Da= N^s k_0^{(1-n)}/k$; Ω and Ψ are some constants depended on n.

Unfortunately, tests, performed in the course of the current study, demonstrated that both solutions have very limiting range of applicability restricted by extra-low departure from chemical equilibrium ($N^s<0.01sec^{-1}$). So, they are useless for practical calculations.

Keeping in mind this finding, we used approach where boundary problem for equation (III.20) was solved numerically. Further, substituting solutions for C^*, we re-calculated reactive species concentrations and temperature vs z and N^s using solutions (III.18) of the algebraic subsystem (III.12)-(III.16).

So, simplified PEq method consisted of three particular steps:

i) At the first step, algebraic subsystem (III.12)-(III.16) was solved parametrically for different values of primary kinetic variable increment $\Delta C^*=C^*-C^*_e$. The concentrations and temperature were obtained in a form (III.18):

$C_\alpha=C_\alpha(z,\ \Delta C^*, P_s)$

$T=T(z,\ \Delta C^*, P_s)$

These dependencies were used to obtain factor k and exponent n for approximation (III.17).

ii) At the second step, single differential equation (III.20) was solved numerically for various values of scalar dissipation N^s. Scalar sweeping was used for solution of the finite difference equation. As the result, increment of primary kinetic variable $\Delta C^*=C^*-C^*_e$ was obtained in parametric form on mixture fraction z and N^s:

$$\Delta C^*= \Delta C^*(z,\ N^s,\ P_s,\ BC) \qquad \text{(III.23)}$$

where *BC* denotes boundary conditions at z=0 and z=1 ends.

iii) At the third step, results of parametric calculations (III.18) for algebraic subsystem which were obtained at the first step and solution (III.23) were used together to re-calculate dependencies for reactive species and temperature vs z and N^s in conventional for flamelet approach form (I.9):

$C_\alpha=C_\alpha(z,\ N^s,\ P_s,\ BC)$

$T=T(z,\ N^s,\ P_s,\ BC)$

So, single ordinary differential equation was needed to solve

in simplified PEq method instead of full system of flamelet model equations (I.5) and without internal stiffness in the source term.

Examples of calculations and accuracy

We obtained flamelet solutions using simplified PEq method for conditions of Beach and Burrows-Kurkov test cases [24,25] considered in Part II of the Report. The kinetics constants for recombination reactions (III.4) were taken as those in original Miller-Bowman detailed kinetics scheme presented in Appendix C. The equilibrium constants for two-body reactions (III.3) were taken in accordance with [33].

The calculated by PEq method best fit approximations for effective oxidation rate R^* were close one to another for both considered test cases. It provided approximation for R^* as:

$$R^* = -5.5\cdot 10^5\cdot (C^*-C_e^*)^2$$

Using obtained approximation for R^*, we calculated reactive species and temperature distributions vs z for different values of scalar dissipation N^s in the range $0<N^s\leq 100 sec^{-1}$.

The accuracy and range of applicability for PEq method were controlled by comparison with "accurate" flamelet solutions obtained based on detailed kinetics model. The accurate solutions of the flamelet equations were obtained using Miller-Bowman detailed chemistry model [32] (see Appendix C) without assumptions concerning equilibria of the two-body reactions*). These solutions were used to calculate effective oxidation rate R^* and primary kinetic variable C^* directly from the definitions (III.9), (III.11) and without any assumptions adopted in PEq method.

The accuracy of the simplified PEq method for calculation of the effective oxidation rate R^* is illustrated by Fig.43. Here, both approximation for R^* provided by simplified PEq method (blue line) and results of accurate flamelet calculations based on detailed kinetics and definition (III.11) (black points in the rose area) are presented for the whole range of z and N^s variation. It is seen that approximation (III.17) allows to calculate R^* with the accuracy about 10% in the range of N^s

---

*) In reality, these accurate solutions were taken from the flamelet libraries generated for FL approach CFD tests reported in Part II.

variation $0<N^s\leq 100sec^{-1}$. Further increasing of N^s leads to rapid loosing of accuracy by approximation (III.17).

The primary kinetic variable increment ΔC^* can be calculated using PEq method with the accuracy within 6% in comparison with accurate flamelet solutions in the range $0<N^s\leq 100sec^{-1}$ as it is shown in Fig.44. The aforementioned range of N^s variation corresponds to ΔC^* variation in the range $0<\Delta C^*\leq 0.02$

The comparison of the simplified PEq method predictions for species mass fractions and temperature with those provided by accurate solution of the flamelet equations based on full detailed kinetics scheme are presented in Figs.45a-d (Beach test case) and 46a-c (Burrows-Kurkov case). The results of calculations provided by simplified PEq method are plotted by dashed lines. The results of accurate flamelet calculations are presented by solid lines. It is seen that simplified PEq method allows to calculate with good accuracy reactive species mass fractions and temperature at moderate deviation from equilibrium. The accuracy of PEq method was better than 1.5% for stable substances, better that 3% for temperature, and better than 10% for main radicals. The obtained inaccuracy of PEq method is small enough. It is close to scattering of results obtained based on different detailed kinetics schemes as it was reported in Part II. It was possible to obtained flamelet solutions by simplified PEq method with such accuracy in the range of scalar dissipation variation $0<N^s\leq 100sec^{-1}$. The accuracy provided by the PEq method decreased for higher values of N^s. Of course it can not be used for calculations at highest values of N^s in extinction/ignition region where PEq approximation became worth. However, performed calculations shows that more than 50-60% of the FL libraries can be generated based on outlined simplified PEq method. Its range of applicability by four orders higher than that provided by analytical solutions (III.21),(III.22). It is interesting to note that approximation (III.17) for effective oxidation rate has sufficiently wide range of applicability (in current calculations - up to $N^s/N_{cr}\approx 0.15$, where N_{cr} is critical value of scalar dissipation). So, may be, such kind of analytical approximations could be useful for simplification of the terms contained derivatives over reactive scalars in Evolved PDF modeling.

III.2 FLAMELET PREDICTIONS FOR EXTINCTION/IGNITION PHENOMENA

As a rule, combustion chambers and burners operate at moderate values of the incoming flow temperature ($T_a \approx 450-800K$). It is well-known [65], that it is impossible to provide stable combustion regimes without implementation of flameholding systems at such conditions. Induction times for reaction chemistry are too high and reactions acceleration requires increasing of incoming flow temperature by special devices. Flameholders (bluff bodies, flow swirling, etc.) are used to transfer some heat from zones with "well-developed" combustion back to the fresh mixture. Loosely speaking such a transfer helps to change the "state of mixing" to the "state of burning".

The increasing of the incoming flow temperature decreases rapidly induction times of chemical reactions. There are some boundary conditions of operation where flameholding became useless. The combustion wave can self-develop at such conditions without additional backward heat transfer and there is no need to use flameholders. For example, such regimes could be expected in scramjet combustors due to high value of the incoming static temperatures.

We tried to estimate location of the boundary between aforementioned combustion regimes using flamelet model. For this purpose we considered features of the flamelet model ignition/extinction predictions for H_2/air flames in different ranges of operational conditions. Flamelet model calculations were performed based on Miller-Bowman detailed kinetics model for H_2 oxidation and thermodynamics approximations for species enthalpies presented in Appendix C.

Typical dependencies of the maximum temperature value in H_2/air diffusion flame T_m vs scalar dissipation N^s, which were obtained from the flamelet model calculations, are presented in Fig.47 together with the regime conditions.

It is seen (CASE A in Fig.47), that flamelet eqs.(I.5) have two solutions at moderate values of the incoming temperatures of reactants. The first one corresponds to the burning regime (red line). The second solution corresponds to the mixing of reactants accompanied by the very slow oxidation (blue line). It is seen

also that there are three different regions which are separated one from another by parameters $N_{cr}^{(1)}$ and $N_{cr}^{(2)}$. We will refer to these parameters as critical values of scalar dissipation at flame extinction ($N_{cr}^{(1)}$) and flame ignition ($N_{cr}^{(2)}$)*). Only mixing solution exists at very high values of scalar dissipation in the reaction zone N^s (region $N^s>N_{cr}^{(1)}$) due to too high rate of reagents mixing compare to their consumption in chemical reactions. Both burning and mixing solutions can be found if value of N^s obeys condition $N_{cr}^{(2)}<N^s<N_{cr}^{(1)}$. Only burning solution exists if $N<N_{cr}^{(2)}$. So, for this combustion regimes, transition from the mixing to the burning requires flameholders "to jump" from mixing solution to the burning one and to overcome finite chemistry limitations in fresh mixture. We denoted such combustion mode as CASE A.

Qualitatively another results were found at high values of the incoming reagents temperatures (CASE B in Fig.47). It is seen that flamelet solution is unique for such conditions at any values of the scalar dissipation in the reaction zone N^s. So, transition from mixing to the burning regime occur continuously and it does not require flameholders since chemistry is rapid enough to provide self-ignition. We denoted such combustion mode as CASE B.

It is seen that boundary which separates CASE A from CASE B combustion regimes can be introduced by the condition:

$$N_{cr}^{(2)}=N_{cr}^{(1)} \qquad \text{(III.24)}$$

Both critical values of the scalar dissipation depend on incoming fuel and air temperatures (T_f,T_a), pressure in reaction zone P_s and detailed chemistry of fuel oxidation (kind of fuel). These dependencies can be found from the flamelet model calculations as:

$$\begin{aligned} N_{cr}^{(1)}&=N_{cr}^{(1)}(P_s,T_f,T_a,\text{ kind of fuel}) \\ N_{cr}^{(2)}&=N_{cr}^{(2)}(P_s,T_f,T_a,\text{ kind of fuel}) \end{aligned} \qquad \text{(III.25)}$$

Substituting solutions (III.25) into condition (III.24) one has relation between thermodynamics parameters at the boundary which separates CASE A combustion mode from CASE B one in a form:

$$T_a^{(b)}=\varphi(T_f^{(b)},P_s^{(b)}) \qquad \text{(III.26)}$$

---

*) We used single value of N_{cr} in CFD tests of the flamelet model reported in Part II. It corresponded to $N_{cr}^{(1)}$ value.

We estimated location of this boundary for the H_2/air diffusion flames. Parametric flamelet calculations were done in the range of conditions summarized in Table 6 to cover possible range of parameters variation in scramjet combustors at different flight conditions. The air composition was taken as: O_2 mass fraction 0.231 and N_2 mass fraction 0.769.

Table 6. Initial data for FL calculations

P_s,MPa	T_a,K	T_f,K
0.05-0.2	300-2600	300-1000

We calculated dependencies (III.25) for both critical values of scalar dissipation. The regimes, where values of $N_{cr}^{(2)}$ and $N_{cr}^{(1)}$ differed one from another less than 1%, were adopted to adjust location of the boundary between CASE A and CASE B combustion modes.

Examples of the obtained parametric dependencies of $N_{cr}^{(1)}$ and $N_{cr}^{(2)}$ are given in Fig.48a,b. It is seen (Fig.48a) that the mostly important parameters governed transition from CASE A to CASE B regimes are the air and fuel incoming temperatures T_a,T_f. Their increasing rapidly decreases difference between $N_{cr}^{(1)}$(red lines) and $N_{cr}^{(2)}$(blue lines). More weak influence of the pressure P_s on the transition boundary was found in calculations (Fig.48b) for the considered range of P_s variation (P_s=0.05-0.2MPa).

Summary of the obtained results is presented in Fig.49. Here the obtained incoming air boundary temperature $T_a^{(b)}$which corresponds to the transition between combustion modes is plotted vs fuel temperature $T_f^{(b)}$ for different pressures in the reaction zone.

We compared obtained results with some typical scramjet combustor operational conditions at different flight Mach numbers to estimate, roughly, their possible practical significance. The summary of used scramjet operational conditions is presented in Table 7. They correspond to "hypothetical" constant dynamic pressure scramjet trajectory q_∞=const≈50-75KPa, where q_∞ is dynamic pressure of free air stream.

Table 7. Expected scramjet operational conditions

(flight trajectory $q_\infty \approx 50-75$KPa)

M_∞	8	10	12	15
M_{air}	~3-3.5	~4	~4.5	~5-5.5
T_{air}, K	900-1000	1100-1200	~1500	~1900
P_{air}, MPa	0.08-0.12	0.1-0.07	0.08-0.06	0.06-0.05
M_{H2}	~3-3.5			
T^*_{H2}, K	~1000			
P_{H2}, MPa	~0.09	~0.11	~0.15	~0.18

Here: M_∞ is flight Mach number; M_{air}, T_{air}, P_{air} are the Mach number, static temperature and static pressure for the air flow at the entrance of combustor; M_{H2}, T^*_{H2}, P_{H2} are the Mach number, total temperature and static pressure for the entering hydrogen flow.

Results of comparative estimations are presented in Fig.50. It is seen that they does not give hope. Flamelet model predicts that the CASE A combustion mode dominates up to the very high flight Mach numbers ($M_\infty \approx 14$). Transition from CASE A to CASE B combustion regimes can be expected at near-orbital vehicle velocities ($M_\infty \approx 15-16$ and higher).

Of course, presented estimations are rough enough. They does not take into account accurately many important flow features (shocks, induction delay of the chemistry, etc.). Thus, this finding demonstrates that, now, performed calculations have mostly academic interest for the study of the flamelet solutions features for flame critical regimes rather than any practical application.

III.3 CONCLUSIONS ABOUT RESULTS OF SUPPLEMENTED STUDIES

Two supplemented studies, related with the investigation of the flamelet model capabilities were done in the course of current research work. They were:

- *Consideration of the possible simplifications in flamelet calculations based on partial equilibrium assumption for the detailed oxidation chemistry.*
- *Study of the FL predictions features for ignition/extinction phenomena in high-enthalpy flows.*

Performed investigation demonstrated that:

1. It was possible to formulate simplified procedure for solution of the flamelet model equations at moderate ($N^s/N_{cr} \leq 0.1-0.15$) deviations from chemical equilibrium using Partial Equilibrium (PEq) assumption for the H_2 combustion chemistry. The simplified PEq method is based on numerical solution of single flamelet equation for primary kinetic variable C^* where effective oxidation rate is analytically approximated using equilibrium conditions for two-body reactions, energy and atoms conservations laws [20]. Tests of its accuracy were done. It was found that accuracy of PEq method was better than 1.5% for stable substances, better that 3% for temperature, and better than 10% for main radicals in the aforementioned range of N^s/N_{cr} variation. This finding allows to apply simplified PEq method for calculations of about 50-60% of the total FL libraries. We expect that this results are encouraging and it would be useful to test capabilities of PEq method in more wide range of regime parameters and for another fuels than that considered in current study.

2. Feature of flamelet solutions in the vicinity of the flame ignition/extinction regimes of H_2/air diffusion flames were studied . It was found two different combustion modes depending on the range of regime parameters. The first combustion mode (CASE A mode) corresponded to the regimes where flameholding is needed for stabilization of the flame. The second combustion mode (CASE B mode) corresponded to the regimes where flameholding became useless and burning can self-develop. The parametric calculations

were done to find location of the boundary which separates operational conditions corresponded to different combustion modes. Results demonstrated that transition boundary located at very high level of the incoming air static temperature (T_a=2200-2500K). Its decreasing to the air temperature level which could be of any practical interest (T_a=1700-1900K) required significant increasing of the H_2 temperature ($T_f \approx$ 900 - 1000K). Even for scramjet operational conditions, estimations demonstrated that transition from CASE A to CASE B combustion mode could be expected at very high flight Mach numbers ($M_\infty \approx$14-16). Thus, this finding demonstrates that, now, performed calculations have mostly academic interest for the study of the flamelet solutions features in near-critical regimes rather than any practical applicability.

REFERENCES

1.Kuznetsov,V.R.,Sabel'nikov,V.A.,"Turbulence and Combustion", (P.A.Libby ed.), Hemisphere Publ., 1990.

2.Bilger,R.W.,"Turbulent Flows with Non-premixed Reactants", Turbulent Reacting Flows, Springer-Verlag, Berlin, 1980, p.65.

3.Spiegler,E.,Wolfshtein,M.,Manheimer-Timnat,Y.,"A Model of Unmixedness for Turbulent Reacting Flows", Acta Astronautica, v.3, p.265, 1976.

4.Evans,J.S.,Schexnayder,C.J.,"Influence of Chemical Kinetics and Unmixedness on Burning in Supersonic Hydrogen Flames", AIAA Journal, v.18, N 7, 1980.

5.Kolesnikov,O.M.,"Concentrations Fluctuations Influence on Ignition of Wall Hydrogen Jet in Supersonic Flow", Fizika Gorenia i Vzriva(russian), v.21, N1, p.53, 1981.

6.Baurle,R.A.,Alexopoulos,G.A.,Hassan,H.A.,Drummond,J.P., "An Assumed Joint-Beta PDF Approach for Supersonic Turbulent Combustion",AIAA Paper 92-3844, 1992.

7.O'Brien,E.E.,"The Probability Density Function Approach to Reacting Turbulent Flows",Turbulent Reacting Flows, Springer-Verlag, Berlin, 1980, p.185.

8.Pope,S.B.,"A Monte-Carlo Method for the PDF Equations of Turbulent Reactive Flows", Combustion Science and Technology, v.25,N5, 1981, p.159.

9.Hsu,A.T.,"A Study of Hydrogen Diffusion Flames Using PDF Turbulence Model", AIAA Paper 91-1780, 1991.

10.Hsu,A.T.,Tsai,Y.-L.P.,Raji,M.S.,"A PDF Approach for Compressible Turbulent Reacting Flows", AIAA Paper 93-0087, 1993.

11.Hsu,A.T.,Raji,M.S.,Norris,A.T.,"Application of a PDF Method to Compressible Turbulent Reacting Flows", AIAA Paper 94-0781, 1994.

12.Baurle,R.A.,Hsu,A.T.,Hassan,H.A., "Comparison of Assumed and Evolution PDF's in Supersonic Turbulent Combustion Calculations", AIAA Paper 94-3180, 1994.

13.Peters,N.,"Laminar Diffusion Flamelet Models in Non-premixed Combustion", Progr.Energy Combust.Sci., 1984, 10, p. 319.

14.Liew,S.K.,Bray,K.N.C.,Moss,J.B., Combustion and Flame, v.56,p.199, 1984.

15.Buriko,Yu.Ya.,Kuznetsov,V.R.,"Nitric Oxides Formation in

Turbulent Duffusion Flames of Hydrogen and Propane", Proc. of the 7-th World Hydrogen Energy Conf., Moscow, USSR, v.3, p.2025, 1988.

16.Zheng,I.I.,Bray,K.N.C., "An Application of New Combustion and Turbulence Models to H_2-Air Nonpremixed Supersonic Combustion", Combustion and Flame, v.99, p.440, 1994.

17.Kuznetsov,V.R.,"Probability of passive scalar in turbulent shear flows",Izv.AN SSSR, Mekhanika Zhitkosti i Gaza (russian),N5, 1972,p.86.

18.Williams,F.A.,"Turbulent Mixing in Non-Reactive and Reactive Flows",(S.N.B. Murthy ed.),p.189, Plenum, 1975.

19.Kuznetsov,V.R.,"Mixing up to a Molecular Level and the Development of a Chemical Reaction in a Turbulent Flow", Fluid Dynamics, v.12, No. 3, 1977, p.369.

20.Bilger,R.W.,"Perturbation analysis of turbulent non-premixed combustion", Comb.Sci. and Technology, v.22, N3,p.251,1980.

21.Kuznetsov,V.R.,"Influence of Turbulence on the Formation of High Nonequilibrium Concentrations of Atoms and Free Radicals in Diffusion Flames", Fluid Dynamics, v.17, N 6, 1982, p.815.

22.Buriko,Yu.Ya.,Kuznetsov,V.R.,Uryvsky,A.F.,Volkov,D.V., Zaitsev,S.A.,"A Test of a Flamelet Model for Turbulent Non-premixed Combustion",Combustion and Flame,v.96,p.104, 1994.

23. Buriko Yu.Ya., Gorbatko A.A., Tchepin S.A., Zaitsev S.A., Volkov D.V.,"NO_x predictions for aerocombustors and gas turbine engines based on flamelet model for turbulent diffusion combustion", 1995 Yokohama International Gas Turbine Congress, Japan, v.II, p.291,1995.

24.Evans,J.S.,Schexnayder,C.J.,Beach,H.L.,"Application of Two-Dimentional Parabolic Computer Program to Prediction of Turbulent Reacting Flows",NASA TP-1169,1978.

25.Burrows,M.C.,Kurkov,A.P.,"Analytical and Experimental Study of Supersonic Combustion of Hydrogen in a Vitiated Air Stream" ,NASA TM X-2828,1973.

26."Preliminary Study of the Flamelet Model Capabilities for Supersonic Non-Premixed Turbulent Combustion", First interim Report under Cooperative Agreement No.NCCW-75 with National Aeronautics and Space Administration, Scientific Research Center "ECOLEN",1995.

27."Tests of the Flamelet Approach for Supersonic Jet Flames" ,

Second interim Report under Cooperative Agreement No.NCCW-75 with National Aeronautics and Space Administration, Scientific Research Center "ECOLEN",1995.

28.Abramovich,G.N.,et.al.,"Theory of Turbulent Jets", Russian Ed., Moscow, Nauka, 1984.

29.Kuznetsov,V.R.,Rashchupkin,V.I.,"Probability Distribution (PDF) and Conditional Averaging in Turbulent Flows",Izv.AN SSSR, Mekhanika Zhitkosti i Gaza (russian), N 8, p.31, 1977.

30.Kuznetsov,V.R.,Sabelnikov,V.I.,"Intermittency and Probability Distribution of Concentration in Turbulent Flows", Uspekhi Mechaniki(Russian Ed.), v.4, Part 2, p.123, 1981.

31.Gaffney,R.L.,White,J.A.,Girimaji,S.S.,Drummond,J.P., "Modeling Turbulent Chemistry Interactions Using Assumed PDF Method", AIAA Paper 92-3638, 1992.

32.Miller,J.A.,Bowman,C.I.,"Mechanism and modeling of nitrogen chemistry in combustion", Progress in Energy Combust. Sci.,v.15, p.287, 1989.

33.Alemasov,V.E.,Dregalin,A.F.,Tishin,V.P.,Hudyakov,V.A., "Thermodynamics and Thermophysics Properties of Combustion Products", Russian ed. by Gluhko,V.P., v.1, Moscow, 1971.

34.Warnatz,J.,In: "Combustion Chemistry", ed. by W.C.Gardner, New-York, Springer Verlag, 1984.

35.Kovenja,V.M.,Janenko,N.N.,"Splitting Method in Gasdynamic Problems", Nauka, Novosibirsk, 1981.

36.Vigneron,Y.C.,Rakich,J.V.,Tannehill,J.C.,"Calculation of Supersonic Viscous Flow over Delta Wings with Sharp Supersonic Leading Edges", AIAA-Paper, 78-1137, 1978.

37.Kovenja,V.M.,Tcherny,S.G.,"The Solution Method of Simplified Steady Equations for Viscous Gas", ITAM Report, Novosibirsk, 42-1981, 1981.

38.Godunov,S.K.,Zabrodin,A.V.,Ivanov,M.Ya.,Kraiko,A.N., Prokopov,G.P.,"Numerical Solution of Multi-Dimensional Gasdynamics Problems",Rus.Ed.,Moscow, Nauka, 1976.

39.Kopchenov,V.I., Laskin,I.N., "About Finite Difference Scheme for Numerical Solution of PNS Equations", Journal of Comput. Mathem. and Mathem. Physics (Russian),v.36,N2,1996.

40.Baruzzi,G.,"Structured Mesh Grid Adapting Based on a Spring Analogy", Conference of the CFD Society of Canada, Proceedings,

Montreal, June 14-15, 1993.
41.Schlichting,H.,"Boundary-Layer Theory", 6-th ed., McGraw-Hill Book Company,New York,1968.
42.Gouskov,O.V.,Kopchenov,V.I.,Nikiforov,D.A.,"Flow Numerical Simulation in the Propulsion Elements of Aviation Space System within Full Navier-Stokes Equations", International Conference on the Methods of Aerophysical Research", Proceedings, Part 1, Novosibirsk, 1994, P.104 - 109.
43.Janicka,J."The Application of Partial Equilibruim Assumptions for the Prediction of Diffusion Flames", J. Non-Equilib. Thermodyn., v.6, p.367-386, 1981.
44.Kuznetsov,V.R.,Lebedev,A.B.,Secundov,A.N.,Smirnova,I.P., "Study of Quasihomogeneous Unpremixed Turbulent Combustion Using Equation for Probability Density Function of Passive Scalar", Izv.AN SSSR, Mekhanika Zhitkosti i Gaza (russian), N4, 1981.
45.Kent,J.H.,Bilger,R.W.,"The Prediction of Turbulent Diffusion Flame Fields and Nitric Oxide Formation", Sixteenth Symposium (Int.) on Combustion, p.1643, The Combustion Institute, 1977.
46.Ebrahimi,H.B.,"CFD Validation for Scramjet Combustor and Nozzle Flows", Part I, AIAA Paper 93-1840, 1993.
47.Sandborn,V.A.,"A Review of Turbulence Measurements in Compressible Flow",NASA TM X-62337,1974.
48.Laderman,A.J.,Demetriades,A.,"Mean and Fluctuating Flow Measurements in the Hypersonic Boundary Layer over a Cooled Wall",J.Fluid Mech.,v.63,part 1,pp.121-144.
49.Bilger R.W.,"Conditional moment closure for turbulent reacting flow", Phys. Fluids A 5(2), pp.436-444, 1993.
50.Klimenko A.Yu.,"Multicomponent diffusion of various scalars in turbulent flows", Fluid Dynamics, 25, pp.327-334, 1990.
51.Bezgin,L.V.,Ganjhelo,A.N.,Gouskov,O.V.,Kopchenov,V.I., Laskin,I.N.,Lomkov,K.E.,"Development of Numerical Methods for Viscous Reacting Gas", CIAM Technical Report N 012-1879 (rus.),1994.
52.Kopchenov,V.I., Kraiko,A.N.,"Monotone Finite Difference Scheme of Second Order Accuracy for Hyperbolic Systems with Two Independent Variables", Journ. of Comput. Mathem. and Mathem. Phys. (russian), V.23, N4, p.848, 1983.
53.Ganjhelo,A.N.,"Numerical Solution of 2-D and Axisymmetric Inviscid Supersonic Flows with the Shock Capturing Method of

Second Order Accuracy",TSAGI Sc. Journ.(russian),v.17,N2,p.27,1986.
54.Rodionov,A.V.,"Monotone Scheme of Second Order Accuracy for Shock Capturing Calculations of Nonequilibrium Flow". Journ. of Comput. Mathem. and Mathem. Physics.(russian),v.27, N4,p.585,1984.
55.Kolgan,V.P.,"Using of Minimal Derivatives Principle at Finite Difference Schemes Developing for Calculation of Discontinuous Gasdynamics Solutions", TSAGI Scientific Journ.(russian), v.3, N6, p.68, 1977.
56.Van Leer,B.,"Towards the Ultimate Conservative Difference Scheme, V.A Second Order Sequel to Godunov's Methods", Journ. of Comput.Phys., v.32, N1, p.101, 1987.
57.Tillaeva N.I.,"Generalization of Modified S.K.Godunov Scheme on Space Nonregular Grids", Uchenie Zapiski TSAGI (russian), V.17, No. 2, 1986.
58.Godunov S.K.,"Finite Difference Method for the Numerical Calculations of Discontinuous Solutions of Hydrodynamics Equations", Math. Transactions,V.47, No.3, 1959.
59.Momtchiloff,I.N.,Taback,E.D.,and Buswell,R.F.,"Kinetics in Hydrogen-Air Flow Systems I.Calculations of Ignition Delays for Hypersonic Ramjets", Ninth Symposium (International) on Combustion, The Combustion Inst.,Pittsburg,PA,1963,p.220.
60.Westenberg,A.A.,Favin,S.,"Complex Chemical Kinetics in Sypersonic Nozzle Flow", Ninth Symposium (International) on Combustion, The Combustion Inst.,Pittsburg,PA,1963,p.785.
61.Kaskan,W.E.,"The Concentration of Hydroxyl and of Oxygen Atoms in Gases from Lean Hydrogen-Air Flames", Comb&Flame, v.3, N2, p.286, 1958.
62.Kaskan,W.E.,Scott,G.L.,"Requirements Imposed by Stoichiometry in Dissociation-Recombination Reactions", Comb&Flame, v.6, N1, p.73, 1962.
63.Janicka J.,Kollman,W.,"A Two-Variable Formalism for the Treatment of Chemical Reactions in Turbulent H_2-Air Diffusion Flames", Seventinth Symposium (International) on Combustion, The Combustion Inst., Pittsburg, PA ,1979, p.421.
64.Correa,S.M.,"Non-equilibrium Step-Stabilized Combustion of Hydrogen in Supersonic Air", AIAA Paper 88-3223,1988.
65.Lefebvre,A.H.,"Gas Turbine Combustion", (Russian Ed.), Moscow, Mir, 1986, p.566.

APPENDIXES

ACCOUNT OF THE FLAMELET EQUATIONS (I.2)

The outlined account of the flamelet model equations was proposed by V.Kuznetsov in [21].

Let us consider the instantaneous mass conservation equation for the reactive specie

$$\rho \frac{\partial C\alpha}{\partial t} + \rho (\vec{U}\nabla) C\alpha = \nabla\rho D\nabla C\alpha + \rho R\alpha \qquad (A.1)$$

where ρ is density , $\vec{U}$ is flow velocity in the laboratory frame; $C\alpha$ is the reactive specie mass fraction; D is its diffusivity; $R\alpha$ is chemical production term.

Let us introduce the mixture fraction conservation equation as

$$\rho \frac{\partial z}{\partial t} + \rho (\vec{U}\nabla) z = \nabla\rho D\nabla z \qquad (A.2)$$

Consider the stoichiometric surface $z=z_s=1/(1+St)$ where St is the stoichiometric coefficient. The velocity of this surface $\vec{V}$ in the laboratory frame is given by the relation:

$$\vec{V} = (\partial z/\partial t \cdot \nabla z)/(\nabla z \nabla z)$$

Using eq.(A.2) one obtains:

$$\vec{V} = (\vec{U}\cdot\nabla z)\nabla z/(\nabla z\nabla z) - \frac{1}{\rho}(\nabla\rho D\nabla z)\nabla z/(\nabla z\nabla z)$$

Let us define quantity:

$$W = ((\vec{V}-\vec{U})\nabla z)/(\nabla z\nabla z)^{1/2}$$

which is normal to the surface $z=z_s$ component of the vector $\vec{V}$ in the frame moving with a media. It is given by equation:

$$W = \frac{1}{\rho}(\nabla\rho D\nabla z)/(\nabla z\nabla z)^{1/2}$$

The quantity W has the Kolmogorov scaling since it depends only on gradients of the scalar field. Therefore one has estimate:

$$W \sim (\varepsilon\nu)^{1/4}$$

where ε is the mean dissipation, ν is the kinematic viscosity.

Let us choose some point $x=x_0$ on the surface $z=z_s$ and some time instant $t=t_0$ and adopt new frame moving with the velocity

$$W=((\vec{V}-\vec{U})\nabla z)/(\nabla z\nabla z)^{1/2}$$

The eqs. (A.1) could be written as

$$\rho\frac{\partial C\alpha}{\partial t}+\rho(\vec{W}\nabla)C\alpha=\nabla\rho D\nabla C\alpha+\rho R\alpha$$

Let us make now some estimates assuming the reaction zone thickness δ to be small. One has

$$\nabla\rho D\nabla C\alpha \approx \frac{\partial}{\partial n}\rho D\frac{\partial C\alpha}{\partial n} \sim \frac{\rho DC\alpha}{\delta^2}$$

where n is normal direction to the surface $z=z_s$. One has also

$$\rho W\nabla C\alpha \sim \frac{\rho WC\alpha}{\delta} \sim \frac{\rho C\alpha(\varepsilon\nu)^{1/4}}{\delta}$$

Since $D\sim\nu$ one can conclude that the molecular diffusion term $\nabla\rho D\nabla C\alpha$ is much larger than the convective term $\rho W\nabla C\alpha$ if

$$\delta << \eta=(\nu^3/\varepsilon)^{1/4}$$

where η is the Kolmogorov scale.

The same kind of reasoning could be applied to the non-stationary term $\rho\frac{\partial C\alpha}{\partial t}$. Hence eqs. (A.1) can be reduced to a form:

$$\nabla\rho D\nabla C\alpha + \rho R\alpha = 0 \qquad \alpha=1,\ldots,J \qquad (A.3)$$

Small thickness of the reaction zone allows to apply two additional simplifications: i) neglect the variation of ρD inside this zone; ii) consider zone as locally planar and to neglect the derivatives along the stoichiometric surface. Therefore eqs. (A.3) are simplified still further:

$$D\frac{d^2C\alpha}{dn^2}+R\alpha = 0 \qquad \alpha=1,\ldots,J$$

where n is coordinate which is normal to the surface $z=z_s$.

Finally the mixture fraction is introduced as an independent variable instead of n using the relation $z=z_s+\left(\frac{dz}{dn}\right)_s n$. As the result one has the flamelet model equations in a form (I.2) of Sec.I.1:

$$N^s\frac{d^2C\alpha}{dz^2} + R\alpha = 0 \qquad \alpha=1,\ldots J$$

DESCRIPTION OF THE SOLVERS USED IN THE RESEARCH WORK

B.I. FLAMELET EQUATIONS SOLVER *FLSLV*

The numerical solution of the flamelet model equations (I.5) was based on time relaxation method. The finite difference approximation was based on the central difference approximation for the second derivatives and the linearization of the chemical production term over reaction species mass fractions. As the result the finite difference system of equations in delta form was as follows (afterwards subscripts denote grid points along z and superscripts denote levels along t):

$$\frac{\delta\vec{C}_i^j}{\tau^j} - N^s\left(\frac{2\delta\vec{C}_{i-1}^j}{(\Delta z_{i+1}+\Delta z_i)\Delta z_i} - \frac{2\delta\vec{C}_i^j}{\Delta z_{i+1}\Delta z_i} + \frac{2\delta\vec{C}_{i+1}^j}{(\Delta z_i+\Delta z_{i+1})\Delta z_{i+1}}\right) =$$

$$= N^s\left(\frac{2\vec{C}_{i-1}^{j-1}}{(\Delta z_{i+1}+\Delta z_i)\Delta z_i} - \frac{2\vec{C}_i^{j-1}}{\Delta z_{i+1}\Delta z_i} + \frac{2\vec{C}_{i+1}^{j-1}}{(\Delta z_i+\Delta z_{i+1})\Delta z_{i+1}}\right) + \qquad \text{(B.1)}$$

$$+ \vec{W}_i^{j-1} + \left(\frac{\partial\vec{W}}{\partial\vec{C}}\right)_i^{j-1}\delta\vec{C}_i^j$$

where $\tau^j=(t^j-t^{j-1})$ is pseudotime step; $\Delta z_i=(z_i-z_{i-1})$ is grid step in z-direction; $\delta\vec{C}^j=(\vec{C}^j-\vec{C}^{j-1})$ is vector of the dependent variable increment; $(\partial\vec{W}/\partial\vec{C})$ is Jacoby matrix.

The obtained system of the finite difference equations was block-tridiagonal. At each pseudo-time step system (B.1) was solved using matrix sweep method where the elementary block matrixes were inverted using Gauss reduction. When the reactive species mass fractions were obtained at j-th pseudotime level, the energy conservation equation was used to calculate temperature distribution. The nonlinear algebraic equation for temperature was solved using simple iterations. The iterations were controlled by the relative error $ER=\max_i \mathrm{mod}\,[(h^j_{calc_i} - hz^j_i)/hz^j_i]$ where maxima was got through all grid points z_i $(i=1,\ldots,I)$.

Static enthalpy $h^j_{calc_i}$ was calculated using obtained at the current time level values of reactive species mass fractions and the static temperature obtained in the current iteration on temperature. Static enthalpy value hz^j_i was calculated directly as function of z_i from the dependence between enthalpy and mixture fraction of (I.5). The iterations were stopped when $ER<10^{-3}$.

The increments $\delta\vec{C}$ control was applied for choice of the optimal pseudo-time step τ and to fasten the convergence to steady state solution. The algorithm was as follows. The norm for δC was calculated at each time step as $\varepsilon^j = \max_\alpha \max_i \{mod(\delta C_\alpha)^j_i/(C_\alpha)^{j-1}_i\}$ where maxima was got through all the species (α=1,...,11) and all grid points z_i (i=1,...,I). Two bounds ε_l=0.5 and ε_u=1.0 were fixed. If ε^j was greater than ε_u then time step was diminished by a factor of 2.2 and calculations were repeated for the same time level again. If $\varepsilon_l < \varepsilon^j < \varepsilon_u$ then time step remained the same and calculations of the next time level was performed with the same time step. If ε^j was smaller than ε_l then time step was increased by a factor of 2 and calculations for the next time level were performed. Maximum value of time step was restricted by τ_{max}=10. The time relaxation was stopped when the value of ε^j became lower then $\varepsilon_0=10^{-6}$. The obtained solution was considered as converged.

B.2. 2D PARABOLIZED NAVIER-STOKES EQUATIONS SOLVER *SUPNEF*

The governing PNS equations were solved by marching method using numerical code SUPNEF, which was previously developed in CIAM for the steady supersonic chemically reacting flows [51]. The code is based on the explicit finite difference method which is the generalization of the well known steady analogy of Godunov scheme [38] for the steady supersonic flows. The method is based on the conservation laws for the elementary computational cell. The modification [52],[53] of Godunov scheme providing for Euler equations the higher order accuracy both in lateral and longitudinal directions is realized. In current case the predictor-corrector version [54] is used. The finite difference scheme is of the second order accuracy on regular

uniform grids and retains approximation on arbitrary nonuniform grids. The higher order accuracy scheme is monotone due to using principle of minimal increments of functions in the cell [55]. This principle is analogy to well-known minmod limitator [56]. The solution of two supersonic flows interaction problem generalized to the multispecies flow case is used at the corrector step to approximate the convective fluxes on the cell boundaries. The viscous tenses are approximated explicitly by the values in the previous cross-section using central differences modified to include nonuniform grids. Formally such viscous terms approximation decreases the order of approximation up to the first one. However this scheme allows to exclude the main approximation errors associated with the convective inviscid terms. The explicit scheme has the limitations on step of integration in longitudinal direction. However it is not a serious limitation for the pure supersonic jet-like flow.

The implicit approximation was used for the chemical source terms in species mass conservation equations. The value of $W_\alpha(C,\rho,T)$ in conservation equation for α-specie was represented in a following form:

$$W_\alpha(C,\rho,T)=-f_\alpha^+(C,\rho,T)C_\alpha+f^-(C,\rho,T)$$

so, that f_α^+ and f_α^- were positive functions. This expansion provides the solution monotonicity of the model equation

$$\frac{dc}{dt}= -f^+c + f^- .$$

The implicit approximation of the chemical source terms required to use the iterative method for the solution of the finite difference equations system for each cell. The iterative procedure included two loops: the global iterations which were necessary to find the gasdynamics parameters at known concentrations (at the finish of internal iterations) and the internal iterations for concentrations calculations to take into account the influence of temperature and density variations obtained in the previous global iteration. In the global iteration step the gasdynamics subsystem is solved at the known mass fractions. Internal iterations are carried out to define the mass

fractions from the species concentrations subsystem for the known (from previous global iteration) corrected temperature and density. The internal iterations for mass fractions were performed using Gauss-Seidel iterations. Internal iterations on concentrations are performed up to the maximum absolute accuracy less than 10^{-5}. Then the new correction of gasdynamics parameters is provided (the following global iteration) and so on up to the convergence of iterations both for thermodynamics parameters and mass fractions. The iterations convergence for gasdynamics parameters is controlled by the relative increment of temperature. This value is chosen to be less than 10^{-5}. If the number of iterations becomes too large the longitudinal step of integration is twice decreased.

B.3. 2D STEADY NAVIER-STOKES EQUATIONS SOLVER *FNAS2D*

The system of averaged NS equations was solved numerically using modified version of FNAS2D code developed at CIAM [42]. It is based on the time relaxation procedure for the modified version of Godunov's scheme providing second order accuracy of the steady state solution on regular near-uniform grid and approximation on arbitrary nonuniform grid. The method is realized on the grid constructed in physical plane without transformation to the computational plane.

The system of conservation equations is written for each cell with implicit approximation of convective and viscous fluxes through boundaries using time increments of main dependent variables vector $\vec{\zeta}$, where $\vec{\zeta}$ was $\vec{\zeta}^T=(\rho,U,V,P,\nu_t,K,z,\sigma^2)$ for FL approach calculations and $\vec{\zeta}^T=(\rho,U,V,P,\nu_t,\{C_\alpha,\alpha=1,...,J\})$ for QL approach calculations.

The arbitrary discontinuity breakdown problem (which is used in original Godunov scheme for convective fluxes approximation on the cell boundaries using parameters in cell centers) is used in modified form to include them into implicit scheme. The Riemann problem solution for the new time level is considered in linear approach. It is supposed that the configuration of main discontinuities realized after breakdown on the new time level is

identical to this one on the old time level. Therefore the identical relations exist between the parameters on the cell boundaries with the parameters in the cells centers before breakdown on the old time level from one side and between parameters increments in time on the boundaries and in the cells centers from the other. If the pressures ratio on the main shock and/or on the expansion wave is higher than 1.2 the iterative procedure is used to obtain the accurate solution of the nonlinear Riemann problem on the old time level. These corrected values are used for the convective fluxes approximation on the cell boundaries on the old time level without correction for the new time level.

To provide the higher order accuracy for the steady state solutions the piecewise linear parameters distributions within cell are assumed and the parameters in the middle point of each cell boundary edge are estimated for adjacent cells on the old time level to provide the initial data for the Riemann problem. These parameters are evaluated with the aid of minimal derivatives principle [55] modified to arbitrary nonregular grids in [57]. The minimal derivatives or minimal space increments principle provides the monotonicity condition [58] of the higher order accuracy scheme. As to the parameters increments in time, their values from the cell centers are used as the initial data for the Riemann problem (it is acceptable for time relaxation procedure without steady state solution accuracy loosing).

The viscous tenses and diffusion fluxes on the cell boundaries on the old time level are approximated with the aid of central differences generalization for arbitrary grids. The contribution of viscous terms into finite difference operator on the new time level is taken into account approximately because the contribution of some grid points is dropped out to provide the five diagonal structure of the algebraic system of equations for time increments of the dependent variables $\delta\vec{\zeta}$.

The implicit approximation is used for the chemical sources in reactive species conservation equations (for QL calculations only).

The resulting system of algebraic equations for the main

parameters increments had the following structure:

$$A_{i,j}\delta\vec{\zeta}_{i-1,j}+B_{i,j}\delta\vec{\zeta}_{i+1,j}+C_{i,j}\delta\vec{\zeta}_{i,j}+D_{i,j}\delta\vec{\zeta}_{i,j-1}+E_{i,j}\delta\vec{\zeta}_{i,j+1}=\vec{R}_{i,j} \qquad (B.2)$$

here i and j are indexes for the current grid cell center; A, B, C, D, E are matrices with size (8,8) in the case of FL approach and (5+J,5+J) in the case of QL approach, J is total number of reactive species; R is the residual of the steady state equations.

The system (B.2) was solved in the following manner:

i. *In the case of FL approach calculations* - First the equations for ν_t, $\tilde{z}$, σ^2 and K (turbulence subsystem) were solved independently one from another on new time level. Further the effective heat capacities ratio Γ and effective heat of formation Q on the new time level were approximated using flamelet library and were averaged. Then the gasdynamics subsystem (II.7) was solved taking into account the increment of the enthalpy in time estimated with the aid of known increments in time of $\bar{\Gamma}$ and $\tilde{Q}$.

ii. *In the case of QL approach calculations* - The full coupling in the implicit part of the difference operator between gasdynamics, concentrations and turbulence model subsystems was realized. This techniques provided much more better convergence characteristics of the implicit scheme than the sequential solution of the aforementioned subsystems reported in our interim Report [27].

Algebraic systems of finite difference equiations were solved using point Gauss-Seidel method. Sequential downstream and upstream sweeping in Gauss-Seidel method were performed for each time level. The number of internal iterations (in Gauss-Seidel method) on each global iteration in time was chosen depending on the global residual level and Courant number.

Appendix C.

Table C.1.

Reaction rates constants for hydrogen oxidation chemistry based on data by Miller and Bowman [32].

Reaction rate constant is presented in the form $K = AT^{B} \exp(-\frac{E}{RT})$.

Units used are Kelvins, seconds, mols and centimeters.

	Reaction	Forward rate		
		lg A	B	-E/R
1	H2 + O2 = OH + OH	13.23	0.00	-24044.0
2	OH + H2 = H2O + H	9.07	1.30	-1824.7
3	O + OH = O2 + H	14.60	-0.50	0.0
4	O + H2 = OH + H	4.70	2.67	-3165.3
5	H + O2 + M = HO2 + M	17.56	-0.72	0.0
6	OH + HO2 = H2O + O2	12.88	0.00	0.0
7	H + HO2 = OH + OH	14.15	0.00	-540.0
8	O + HO2 = O2 + OH	14.15	0.00	-540.0
9	OH + OH = O + H2O	8.78	1.30	0.0
10	H + H + M = H2 + M	18.00	-1.00	0.0
11	H + OH + M = H2O + M	22.20	-2.00	0.0
12	H + O + M = OH + M	16.79	-0.60	0.0
13	O + O + M = O2 + M	13.28	0.00	899.8
14	H + HO2 = H2 + O2	13.10	0.00	0.0
15	HO2 + HO2 = H2O2 + O2	12.30	0.00	0.0
16	H2O2 + M = OH + OH + M	17.11	0.00	-22896.7
17	H2O2 + H = HO2 + H2	12.20	0.00	-1912.2
18	H2O2 + OH = H2O + HO2	13.00	0.00	-905.8
19	N + NO = N2 + O	12.51	0.30	0.0
20	N + O2 = NO + O	9.81	1.00	-3160.2
21	N + OH = NO + H	13.58	0.00	0.0

Table C.2.

Reaction rates constants for hydrogen oxidation chemistry based on data by Warnatz [34].

Reaction rate constant is presented in the form $K = AT^B \exp(-\frac{E}{RT})$.
Units used are Kelvins, seconds, mols and centimeters.

	Reaction	Forward rate		
		lg A	B	-E/R
1	HO2 + H = OH + OH	14.18	0.00	-505.1
2	HO2 + H = H2 + O2	13.40	0.00	-348.8
3	HO2 + O = OH + O2	13.30	0.00	0.0
4	HO2 + OH = H2O + O2	13.30	0.00	0.0
5	HO2 + HO2 = H2O2 + O2	12.30	0.00	0.0
6	OH + OH + M = H2O2 + M	22.11	-2.00	0.0
7	H + H2O2 = H2 + HO2	12.23	0.00	-1888.3
8	H + H2O2 = H2O + OH	13.00	0.00	-1804.0
9	O + H2O2 = OH + HO2	13.45	0.00	-3223.4
10	OH + H2O2 = H2O + HO2	12.85	0.00	-721.6
11	H + O2 = O + OH	17.08	-0.91	-8311.0
12	H + H + M = H2 + M	17.81	-1.00	0.0
13	H + OH + M = H2O + M	22.93	-2.00	0.0
14	H + O2 + M = HO2 + M	17.85	-0.80	0.0
15	OH + H2 = H2O + H	8.00	1.60	-1659.8
16	OH + OH = O + H2O	9.18	1.14	0.0
17	O2 + H2 = OH + OH	13.74	0.00	-29106.5
18	O2 + M = O + O + M	18.26	-1.00	-59415.5
19	O + H2 = H + OH	7.18	2.00	-3800.7
20	N2 + O = NO + N	14.04	0.00	-37496.7
21	N + O2 = NO + O	9.81	1.00	-3160.2
22	N + OH = NO + H	13.58	0.00	0.0

Table C.3

Polynomial coefficients for thermodynamical properties approximation [33].

Enthalphy $H = A_I + \sum_{i=1}^{7} A_i x^i$ (J/mol), entropy $S = A_S + 10^{-3} A_1 \ln x + \sum_{i=2}^{7} \frac{i}{i-1} A_i x^{i-1}$ $(\frac{J}{mol \cdot K})$, $x = \frac{T}{1000}$

T is temperature in Kelvins, μ is molar weight in kg/mol.

	μ	A_S	A_I	A_1	A_2	A_3	A_4	A_5	A_6	A_7
O	0.016	1.8908422E+02	2.4275916E+05	2.2410764E+04	-1.7265002E+03	1.0305618E+03	-3.6058405E+02	7.2900697E+01	-7.6554363E+00	3.2357642E-01
O_2	0.032	2.2737469E+02	-7.8338353E+03	2.3363288E+04	1.1344190E+04	-5.6862959E+03	1.8430891E+03	-3.4538653E+02	3.4370091E+01	-1.4099905E+00
H	0.001	1.3986962E+02	2.1190009E+05	2.0818472E+04	-2.9523678E+01	1.9433405E+01	-6.8227195E+00	1.3074247E+00	-1.2887342E-01	5.1061121E-03
H_2	0.002	1.7071521E+02	-9.0186617E+03	3.1295524E+04	-4.7428008E+03	4.4791623E+03	-1.5709183E+03	2.9222022E+02	-2.8095988E+01	1.0976161E+00
OH	0.017	2.2486857E+02	3.0253603E+04	3.1781619E+04	-5.5713986E+03	5.5738683E+03	-2.1234197E+03	4.2335948E+02	-4.3227566E+01	1.7813063E+00
HO_2	0.033	2.4864170E+02	-6.9643738E+03	2.5088917E+04	1.9809408E+04	-8.3743023E+03	2.5338444E+03	-4.7406450E+02	4.7873608E+01	-1.9867593E+00
H_2O	0.018	2.2449392E+02	-2.5140681E+05	3.0849677E+04	2.1103526E+03	4.2017770E+03	-2.0165908E+03	4.2895533E+02	-4.4758303E+01	1.8616812E+00
H_2O_2	0.034	2.5037094E+02	-1.4648530E+05	2.7103555E+04	3.0929810E+04	-1.2428987E+04	3.4142397E+03	-5.8455816E+02	5.5567894E+01	-2.2223348E+00
N	0.014	1.7885623E+02	4.6670509E+05	2.0996093E+04	-3.8634725E+02	3.4972979E+02	-1.6133129E+02	3.7320547E+01	-3.8260814E+00	1.4528543E-01
N_2	0.028	2.2372830E+02	-8.3007961E+03	2.7351826E+04	1.3058227E+03	2.1442408E+03	-1.2906443E+03	3.1852362E+02	-3.7324427E+01	1.7050206E+00
NO	0.030	2.3850112E+02	8.3177913E+04	2.5678096E+04	6.0005054E+03	-1.3533171E+03	2.6666536E+01	4.9234895E+01	-8.8796781E+00	4.9125222E-01

FIGURES

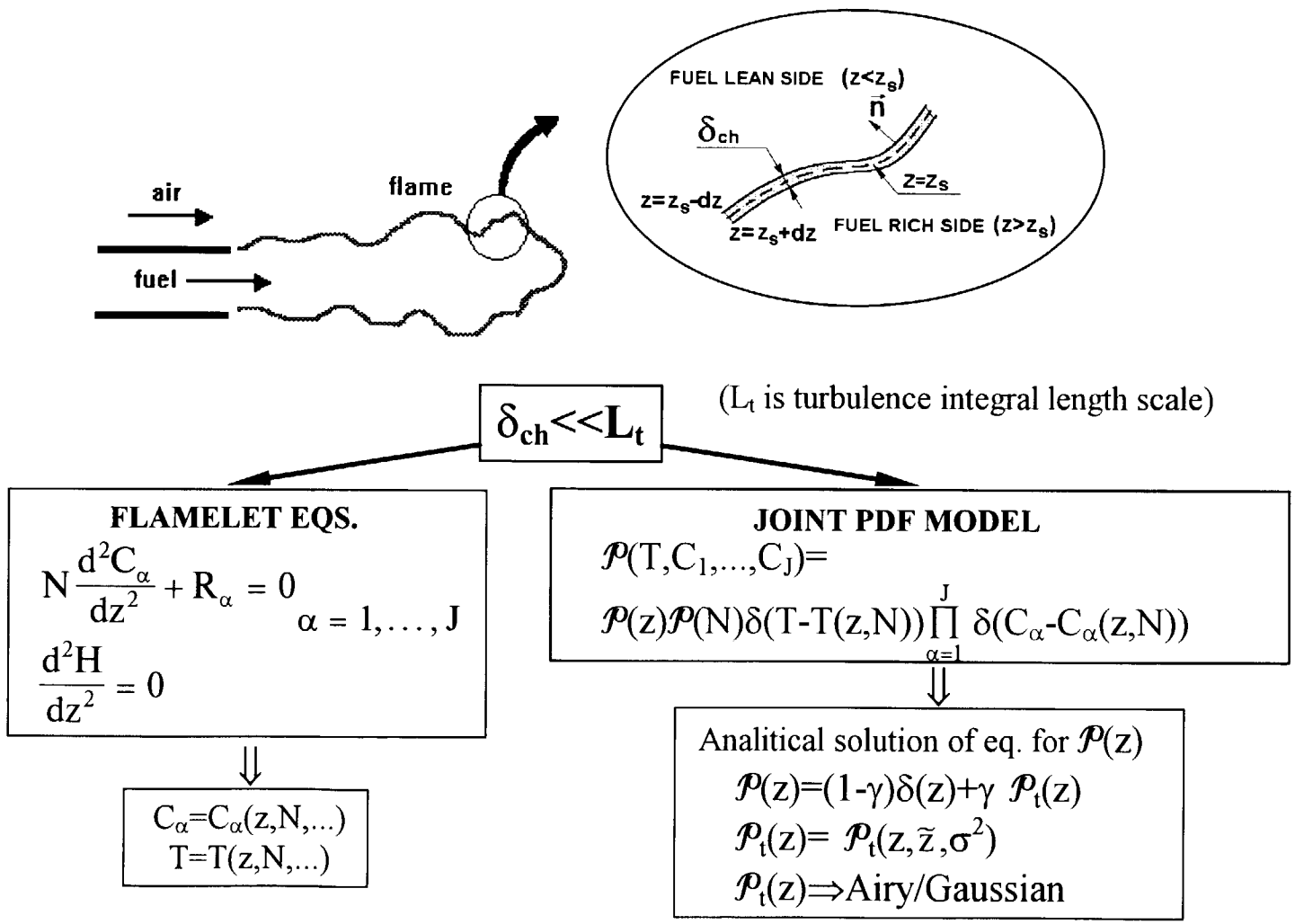

Fig.1. Schematic of the flamelet approach.

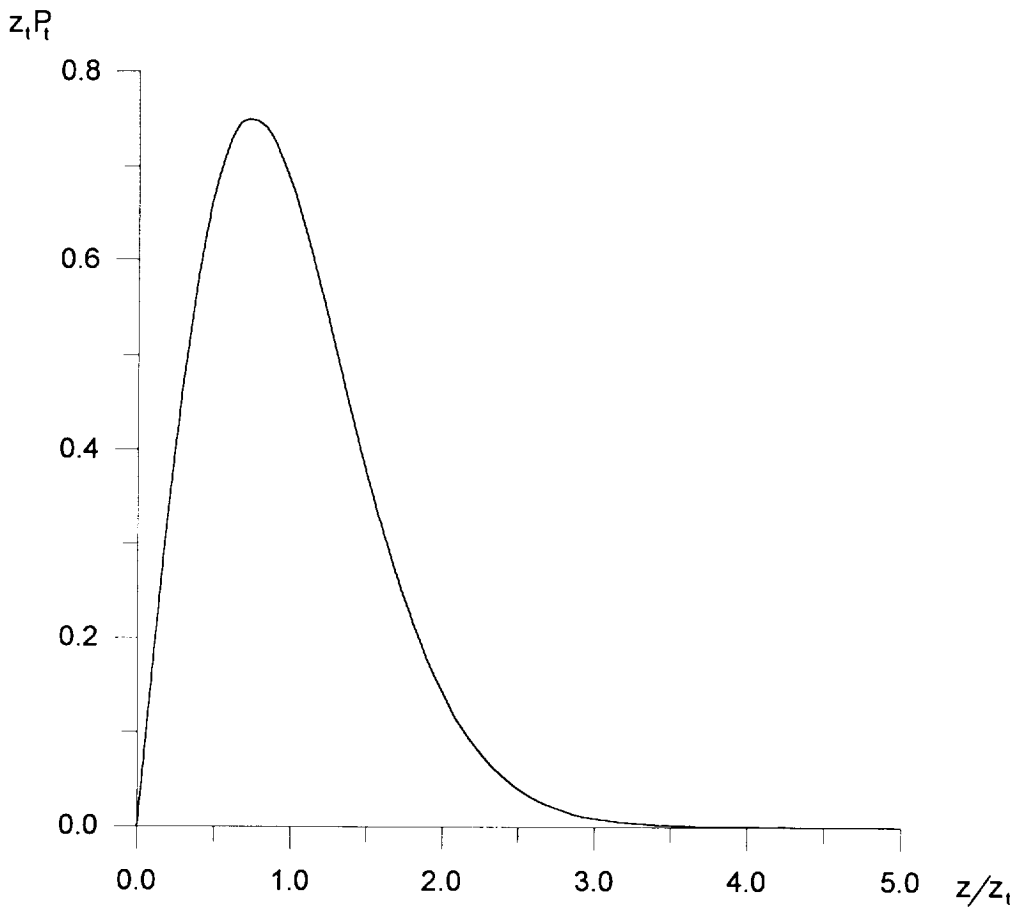

Fig.2. P_t form for intermittent region ($\gamma<1$).

$$P_t = \frac{1.404}{z_t} \mathrm{Ai}(1.778 \frac{z}{z_t} - 2.338)$$

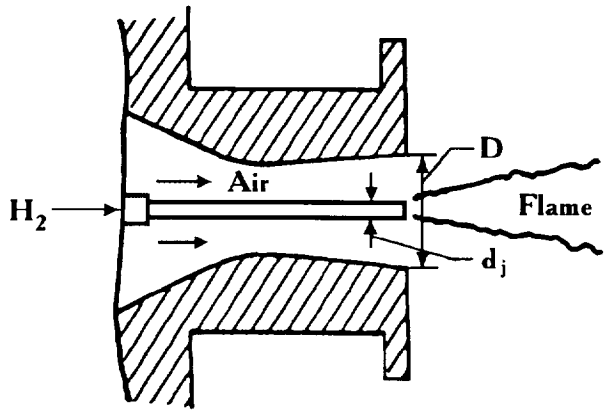

D = 0.0653 m
d_j = 0.009525 m
Injector lip thickness = 0.0015 m

	Hydrogen jet	Free stream
Mach number, M	2.00	1.90
Temperature, T, K	251	1495
Velocity, U, m/s	2432	1510
Pressure, P, MPa	0.1	0.1
Mass fractions:		
C_{H2}	1.000	0
C_{O2}	0	0.241
C_{N2}	0	0.478
C_{H2O}	0	0.281

Fig.3. Scheme and conditions of Beach et.al. coaxial experiment.

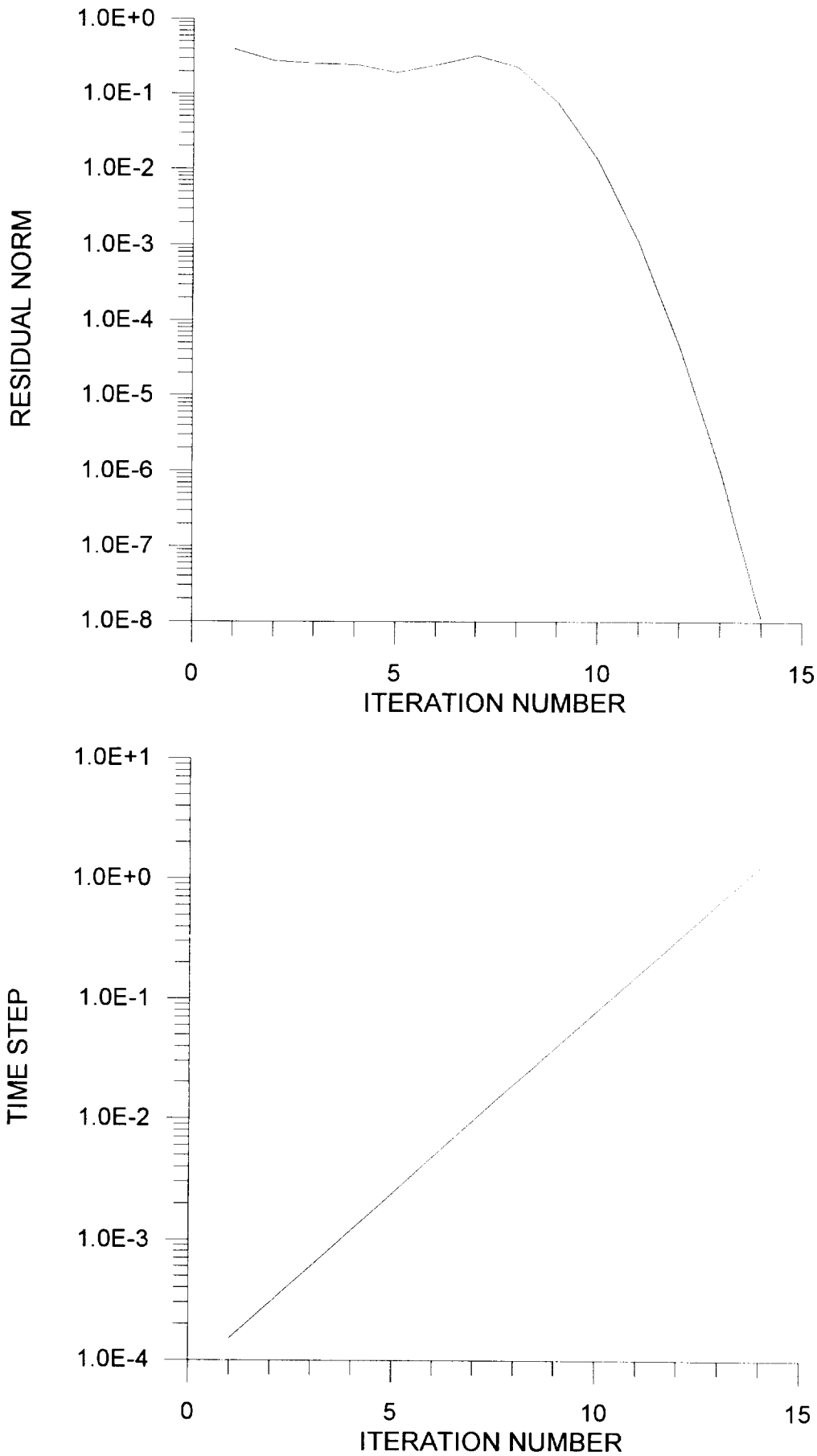

Fig.4. Flamelet library generation.
Residual norm ε and time step behaviour. $N^s = 15\ sec^{-1}$.
Solution for $N^s = 10\ sec^{-1}$ is used as initial conditions
for time relaxation.

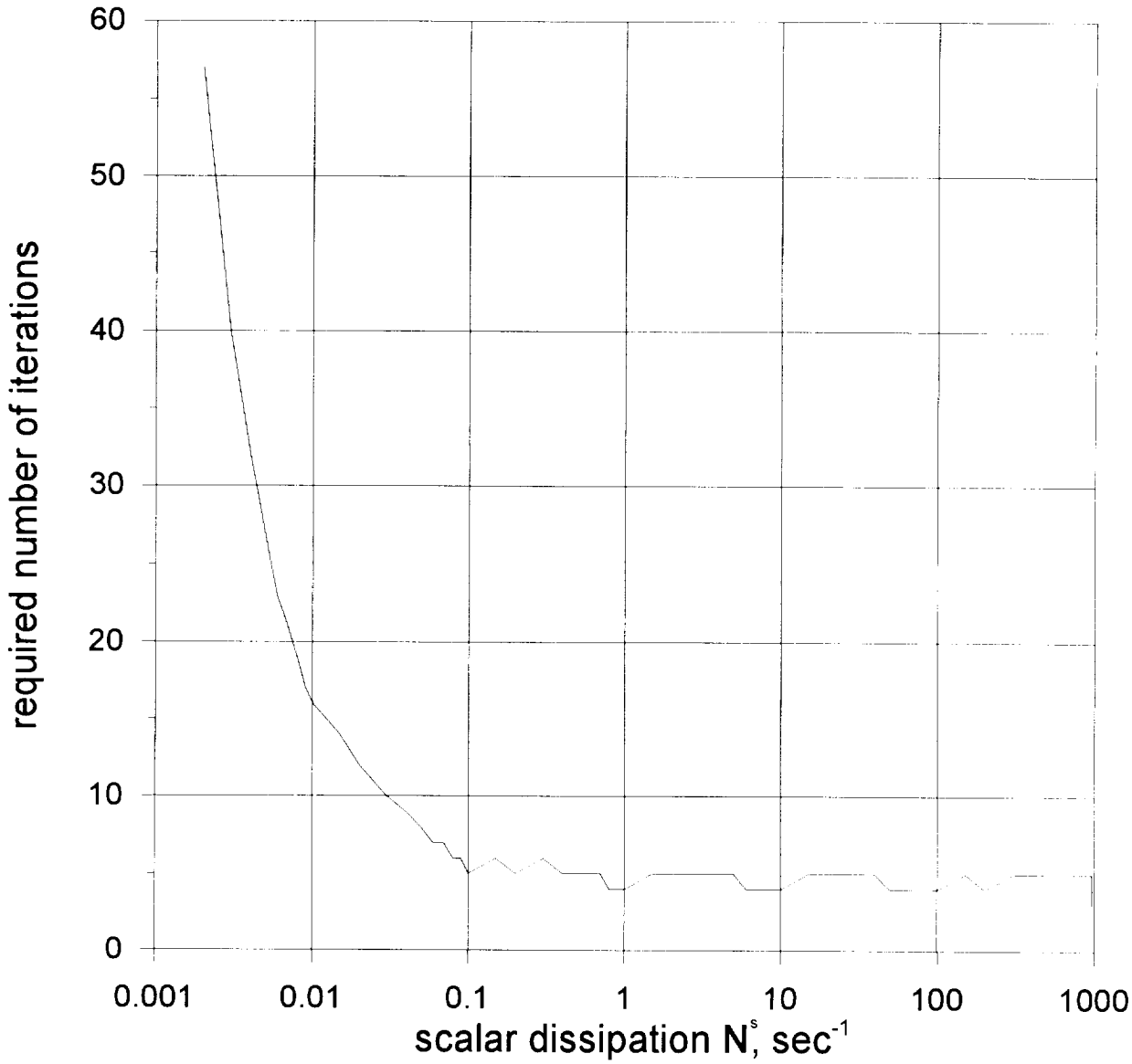

Fig.5. Required number of iterations during flamelet library generation. Beach test case.

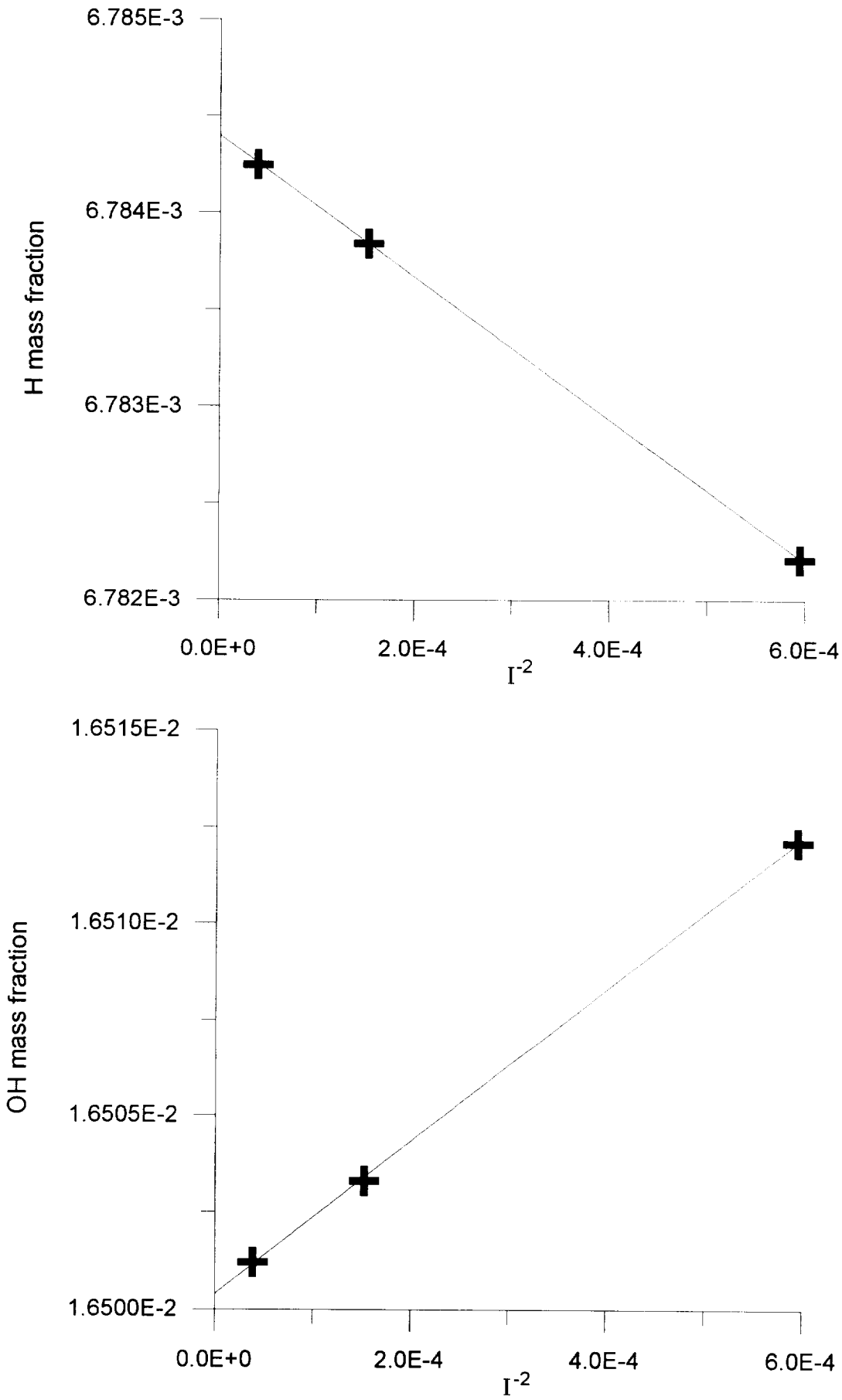

Fig.6. Estimation of calculations accuracy for H and OH mass fractions based on 'three grids' extrapolation. Calculations for the case $N^s = 100\ sec^{-1}$. I is the number of grid points.

——— mean root square interpolation.

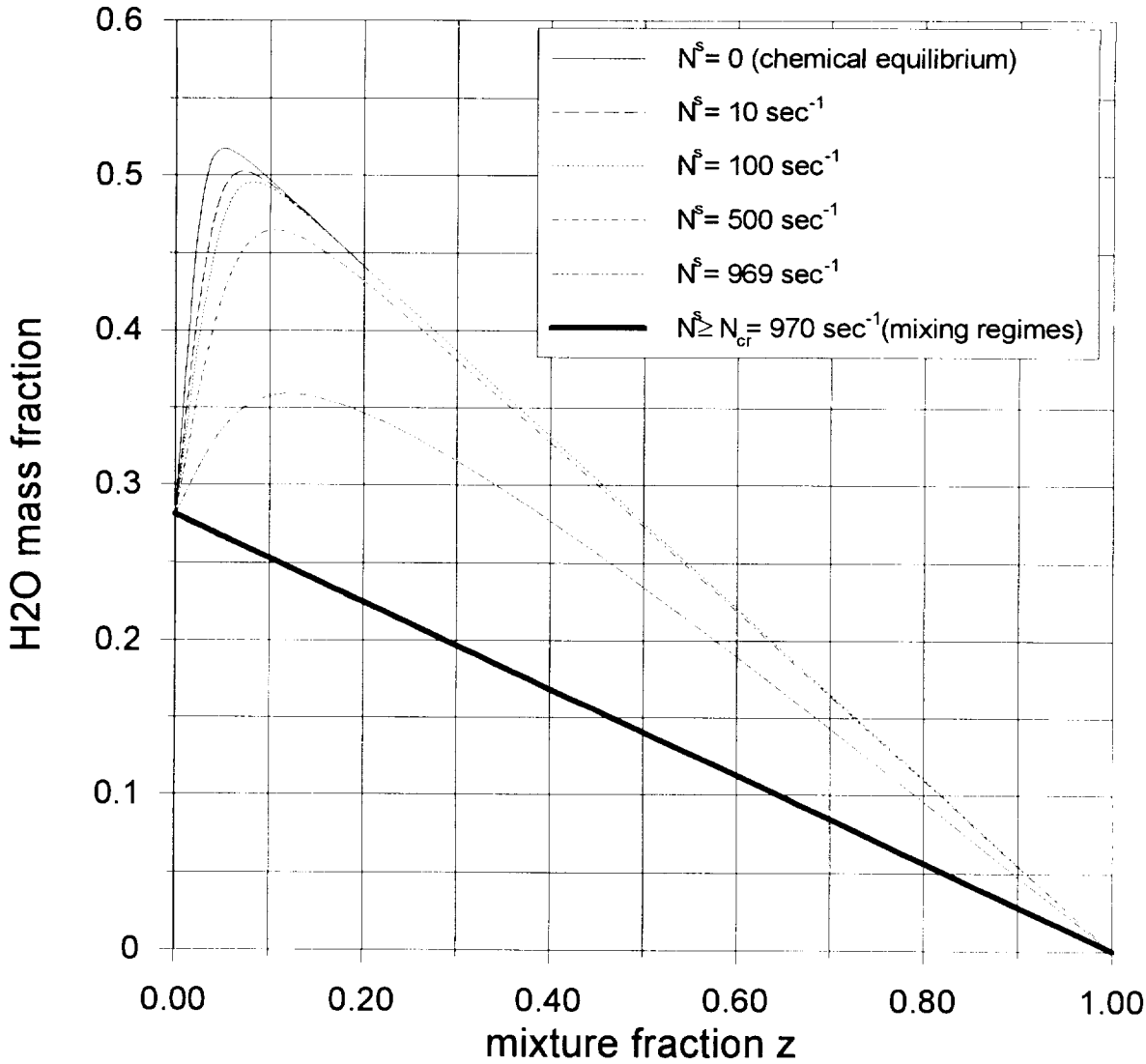

Fig.7a. Flamelet library. H2O mass fraction.
Beach test case.

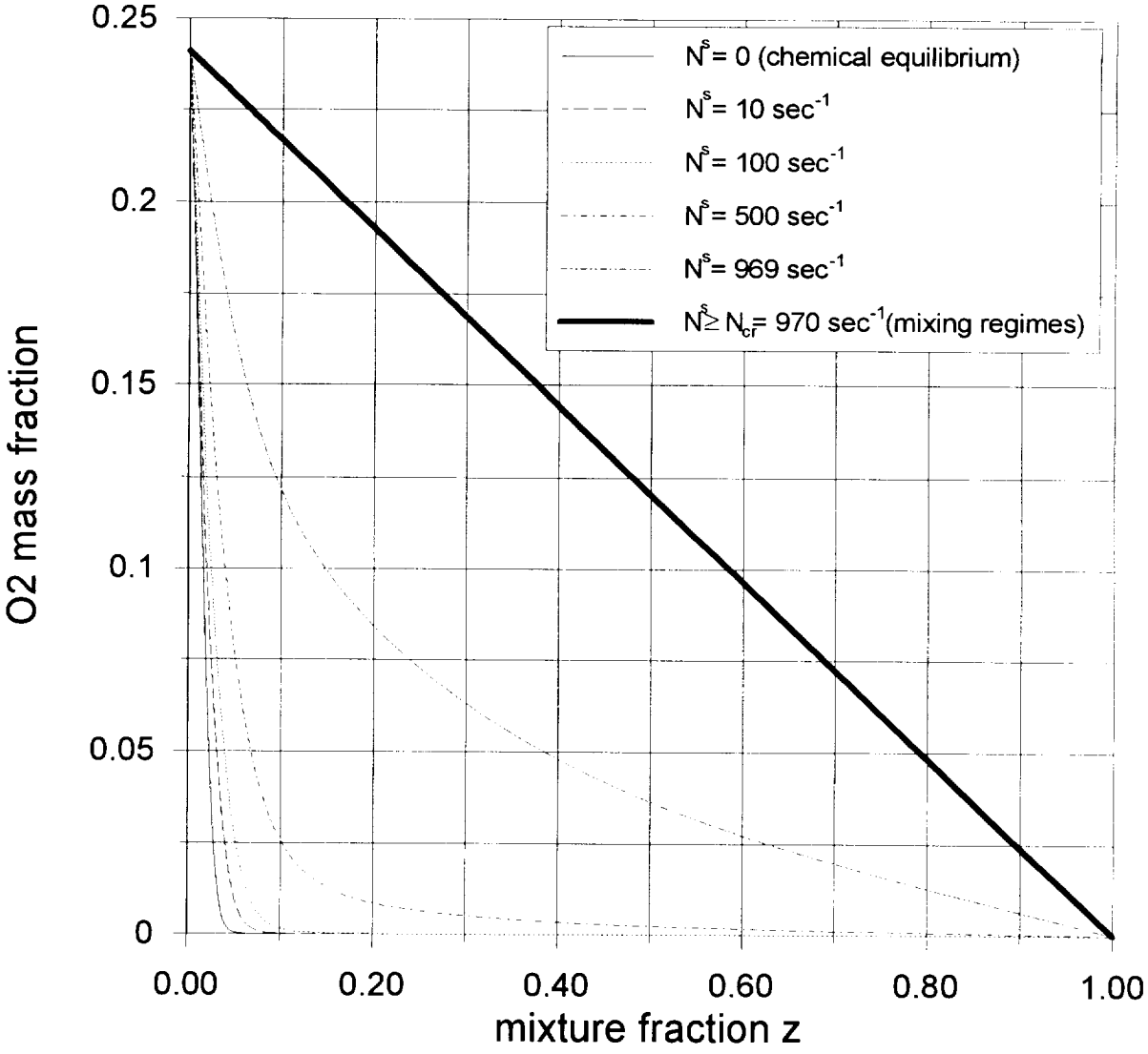

Fig.7b. Flamelet library. O2 mass fraction.
Beach test case.

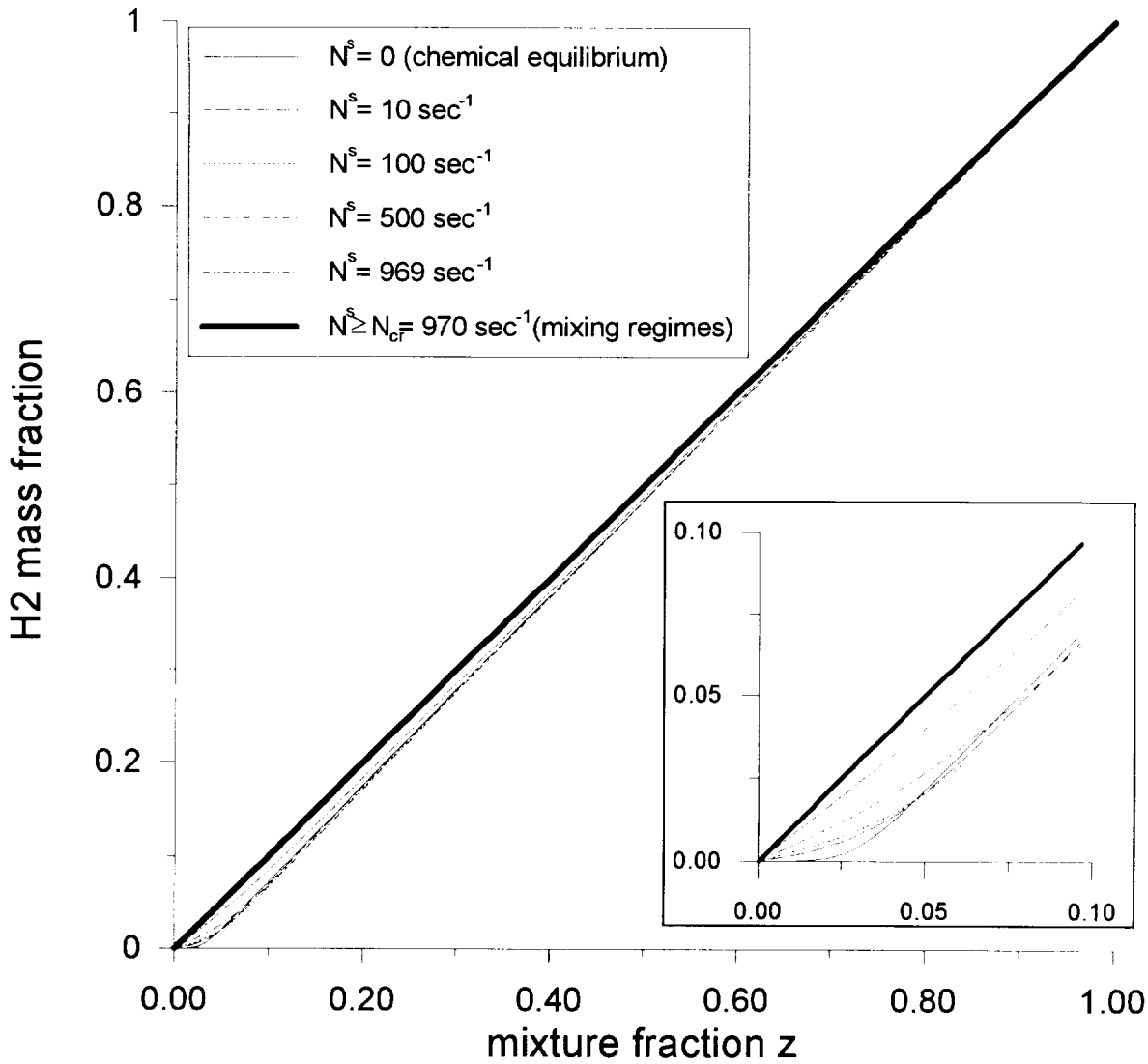

Fig.7c. Flamelet library. H2 mass fraction.
Beach test case.

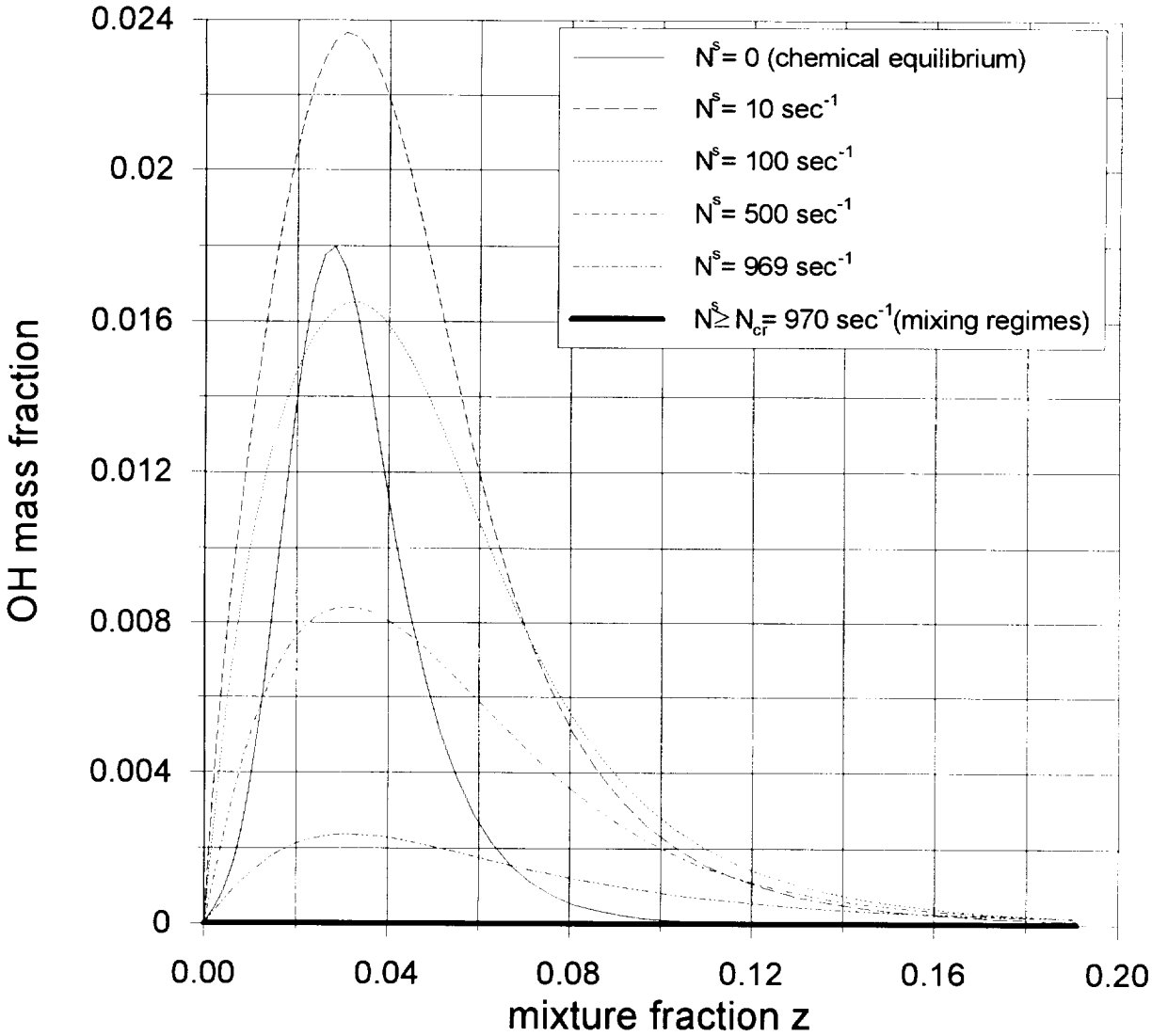

Fig.8a. Flamelet library. OH mass fraction.
Beach test case.

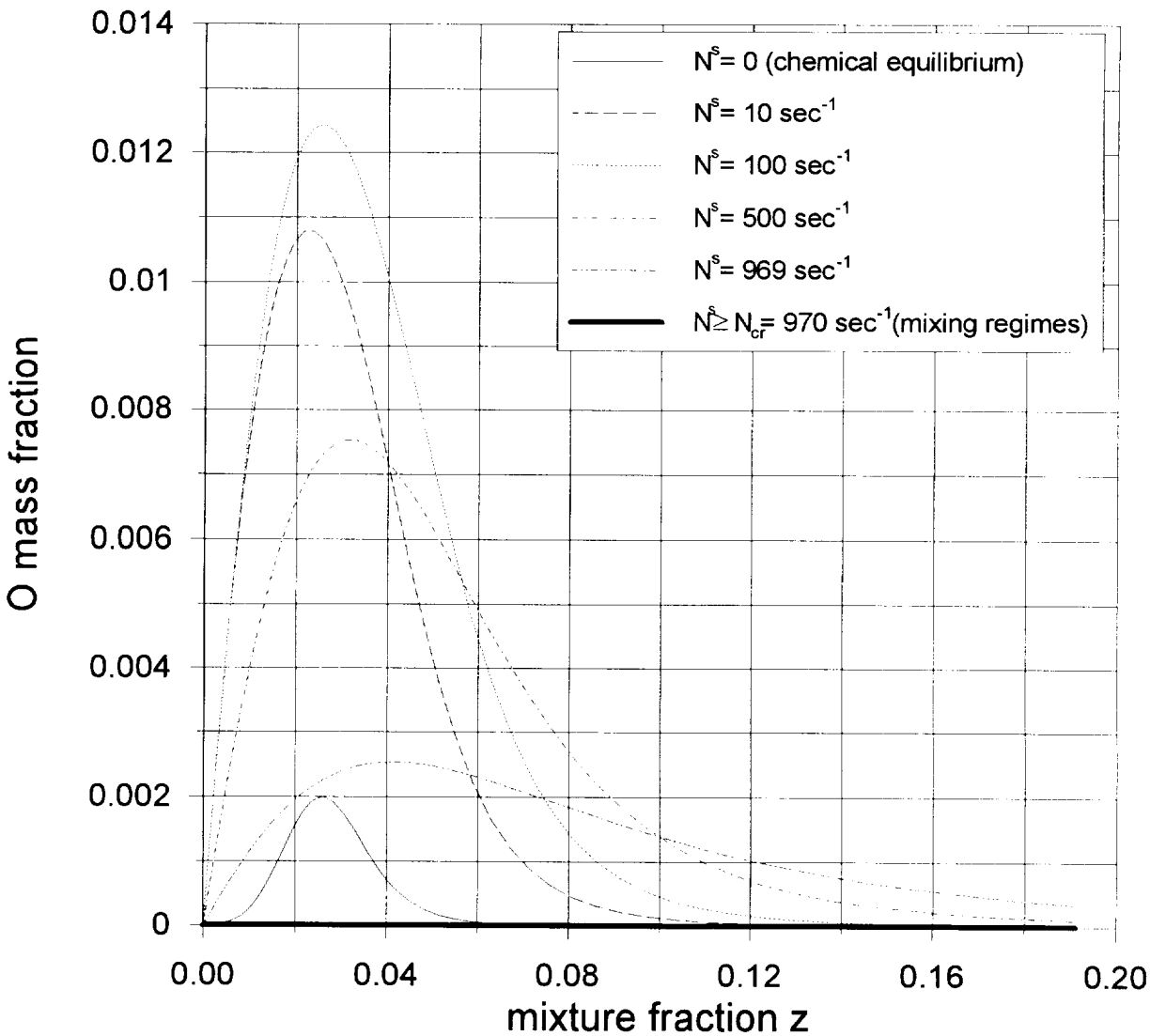

Fig.8b. Flamelet library. O mass fraction.
Beach test case.

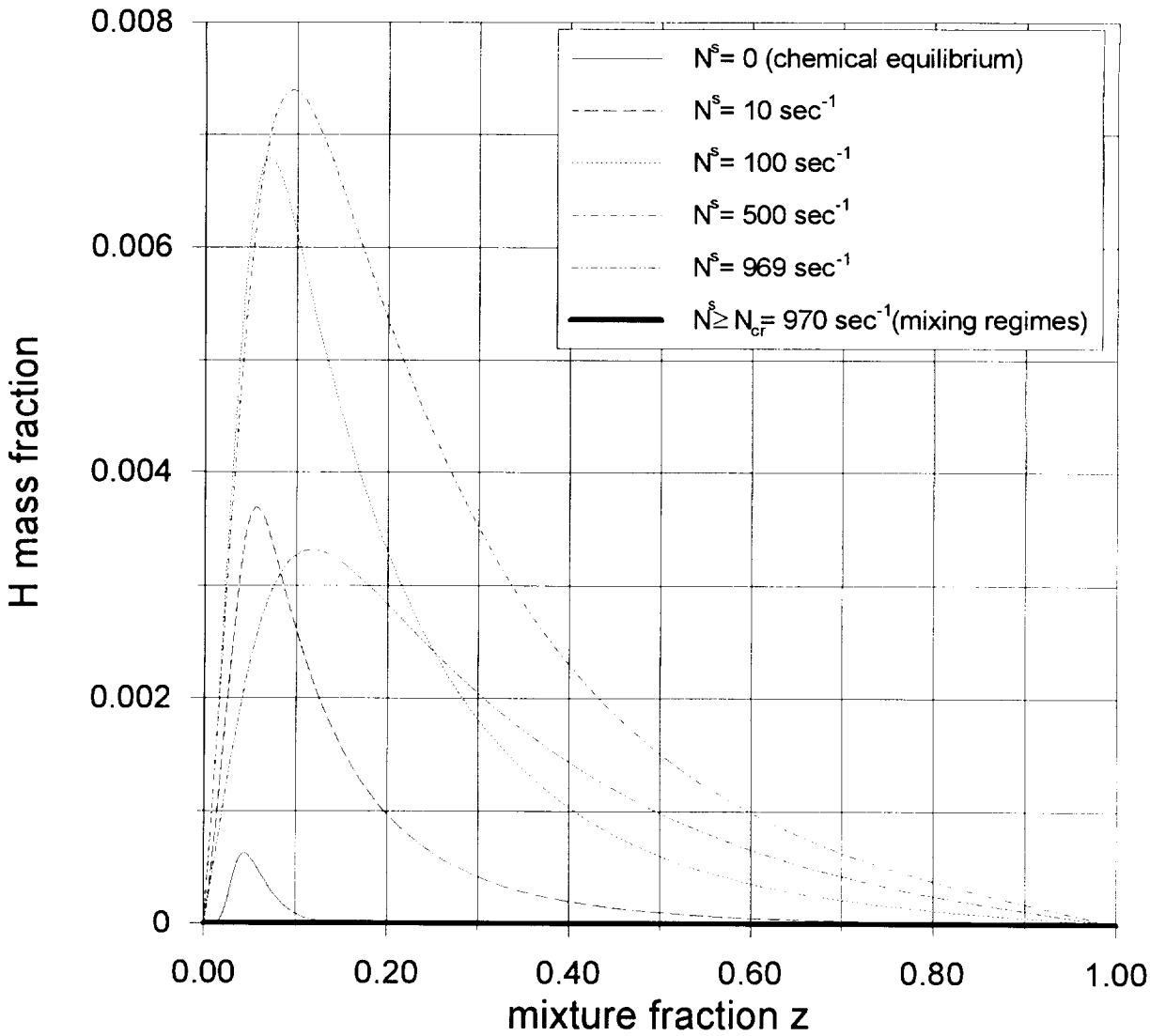

Fig.8c. Flamelet library. H mass fraction.
Beach test case.

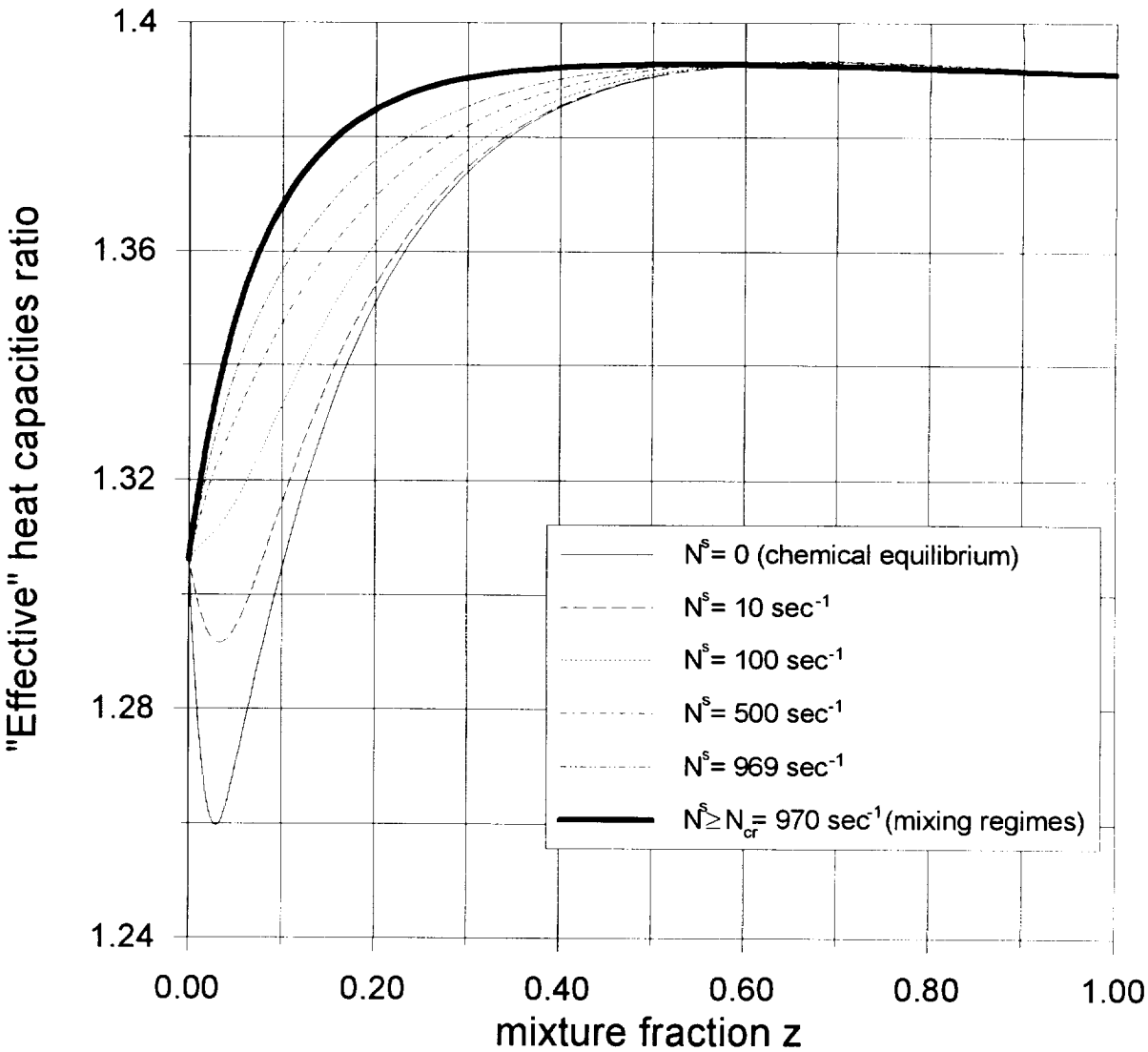

Fig.9a. Flamelet library.
"Effective" heat capacities ratio Γ.
Beach test case.

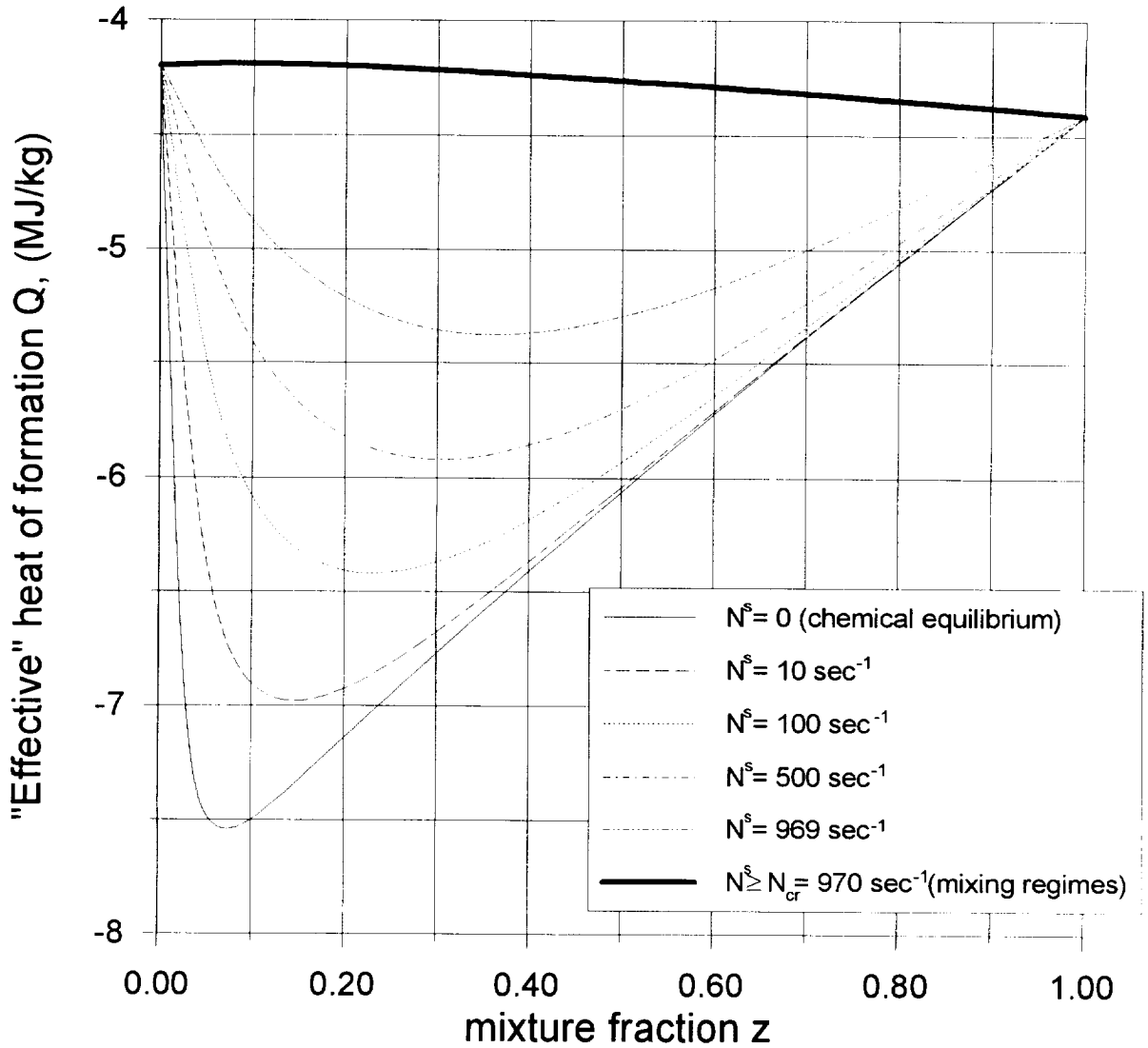

Fig.9b. Flamelet library.
Mixture "effective" heat of formation Q.
Beach test case.

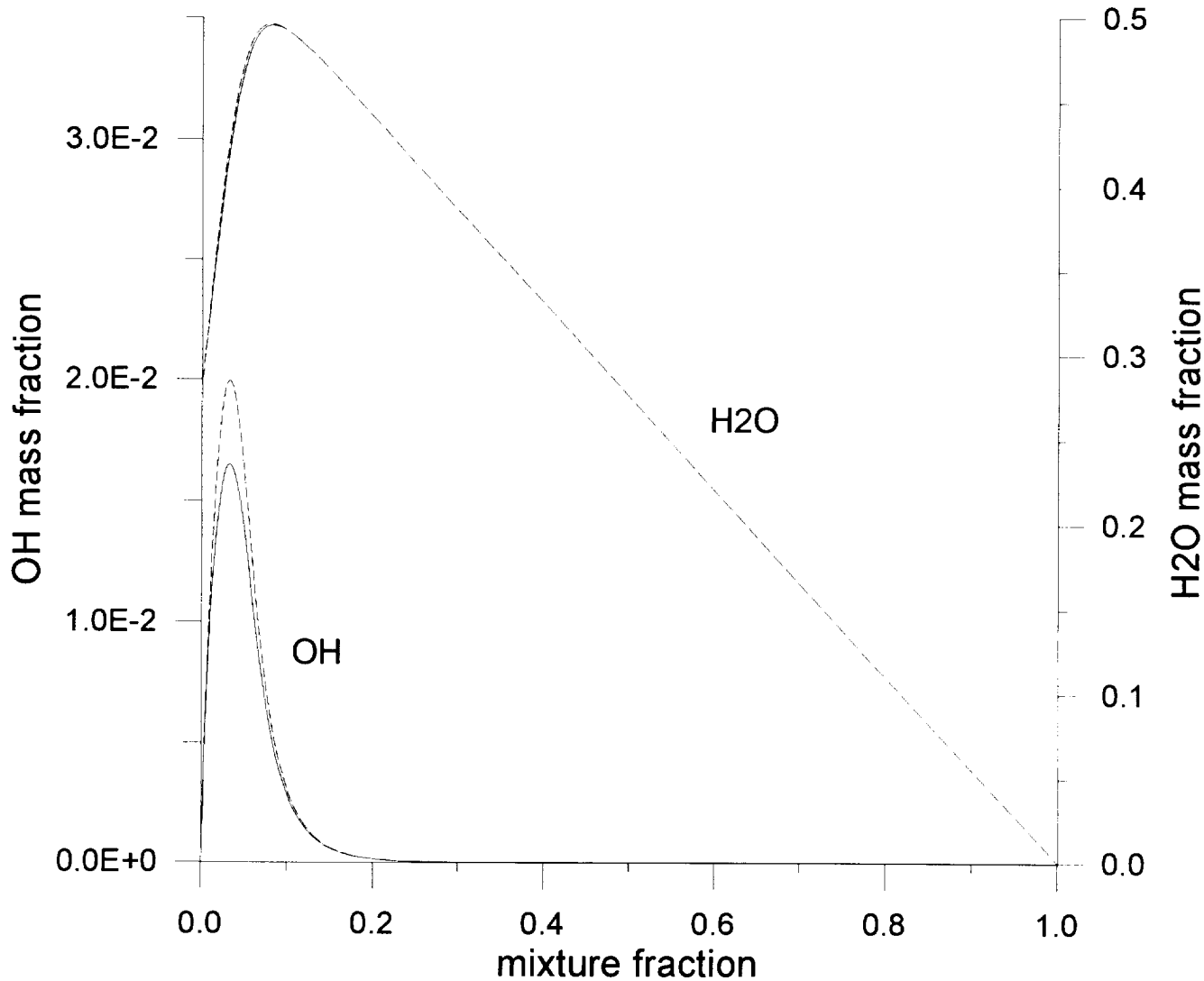

Fig.10. Flamelet model calculations based on:

——— Miller – Bowman detailed kinetics;

- - - - - - Warnatz detailed kinetics.

$N^s = 100\ sec^{-1}$; Beach test case.

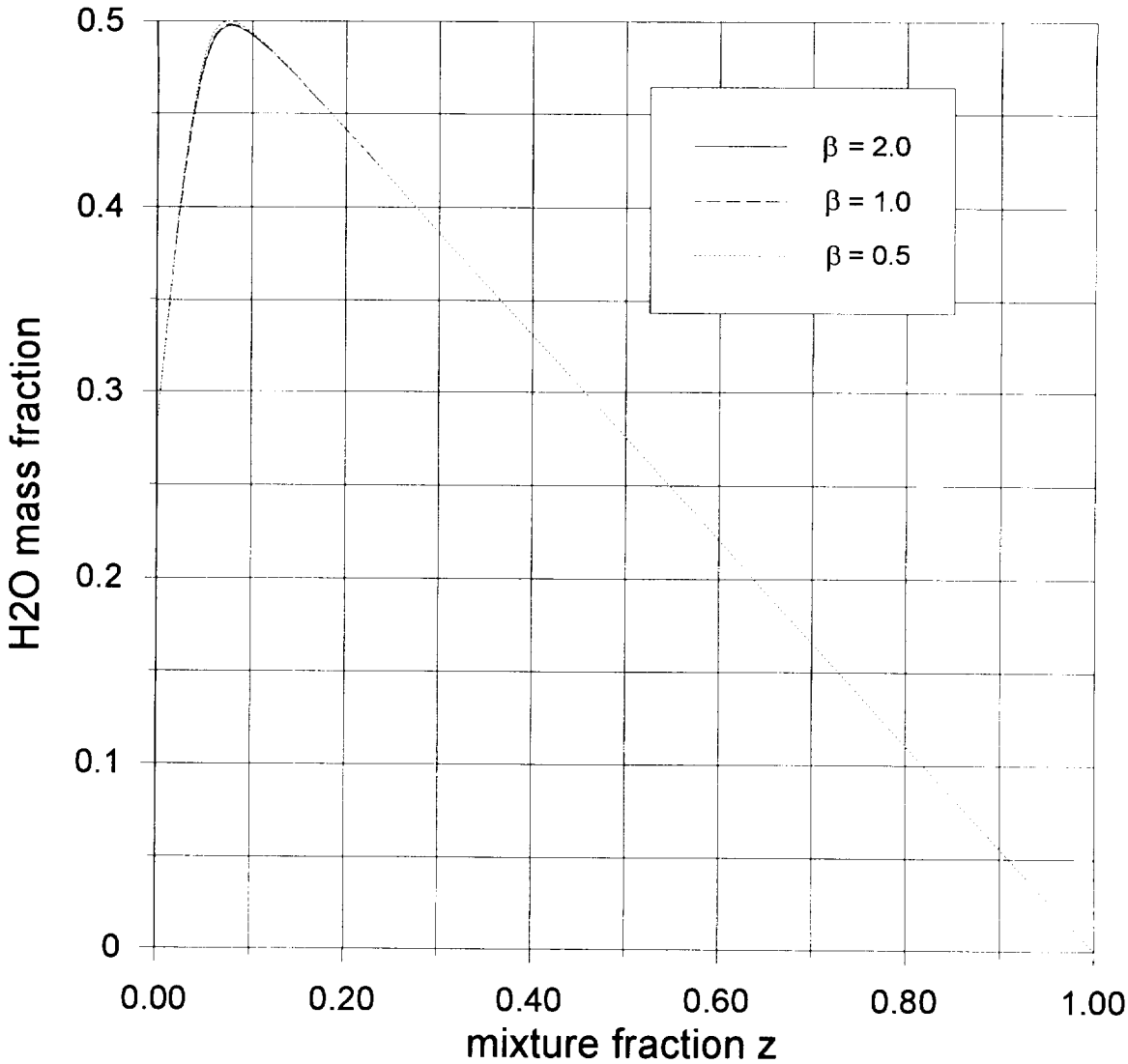

Fig.11a. Sensitivity of flamelet solution to the exponent β value in correlation (I.8). Water mass fraction.
$N^s = 50\ sec^{-1}$. Beach test case.

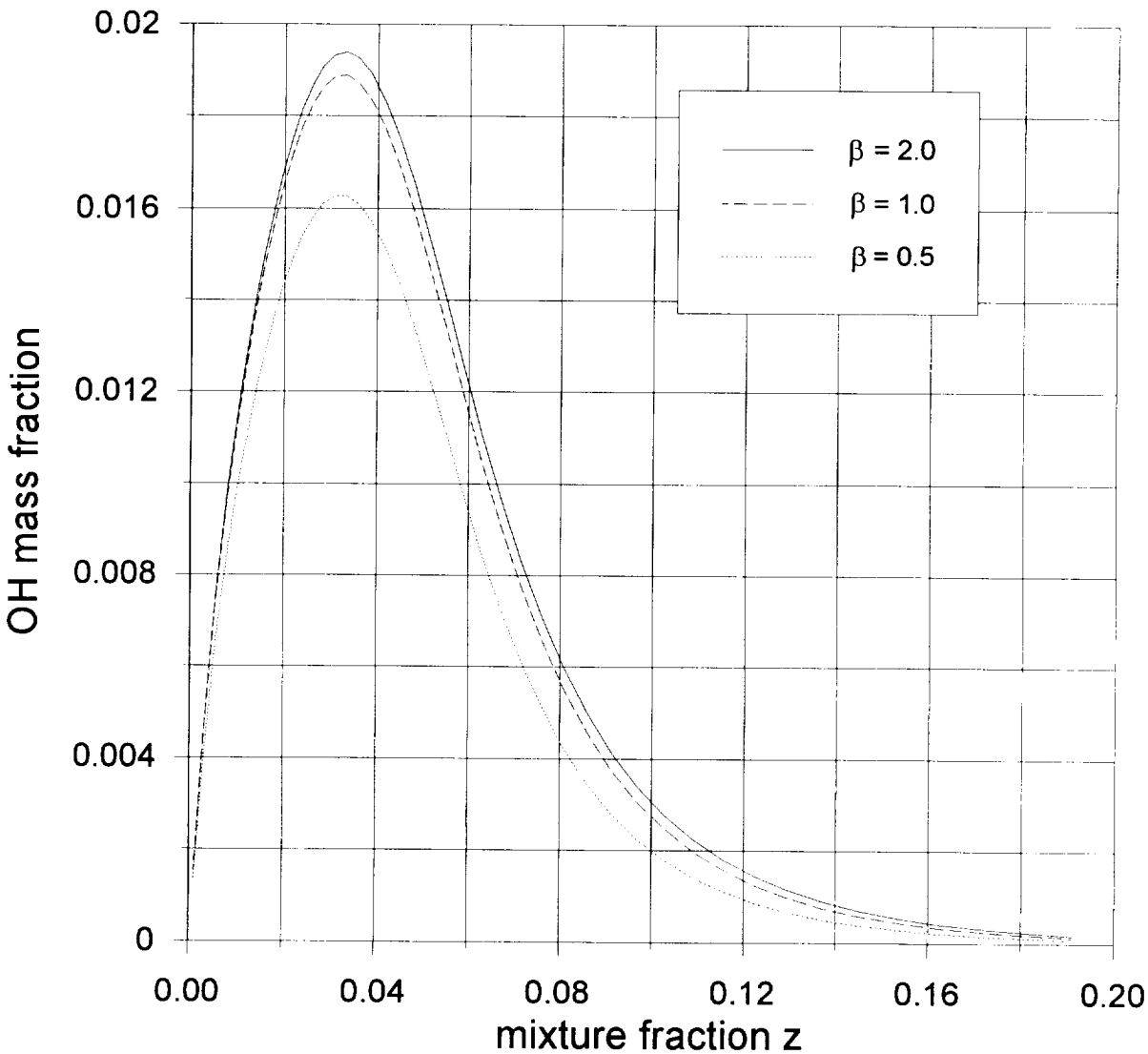

Fig.11b. Sensitivity of flamelet solution to the exponent β value in correlation (I.8). OH mass fraction.
$N^s = 50\ sec^{-1}$. Beach test case.

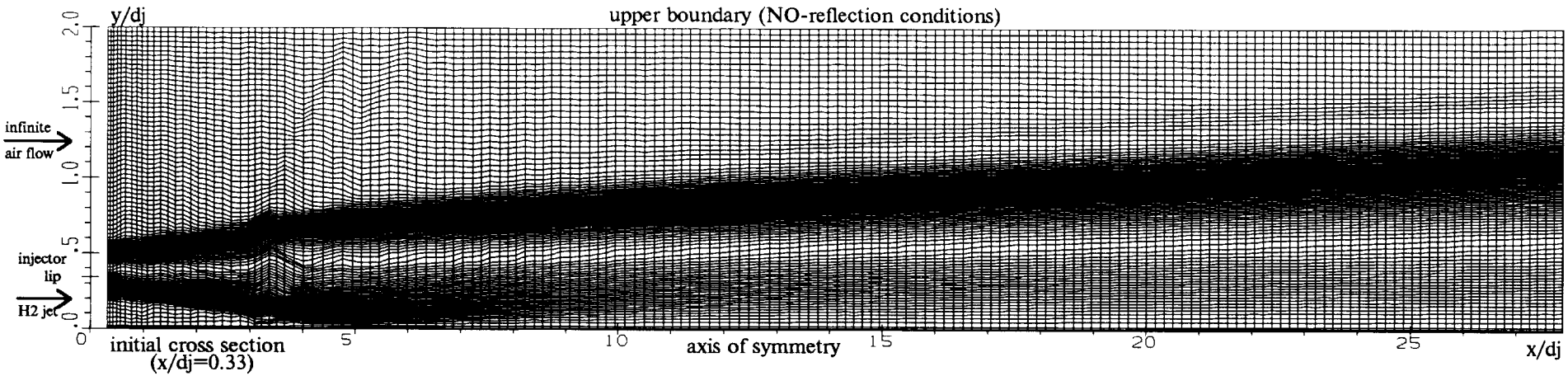

FL approach

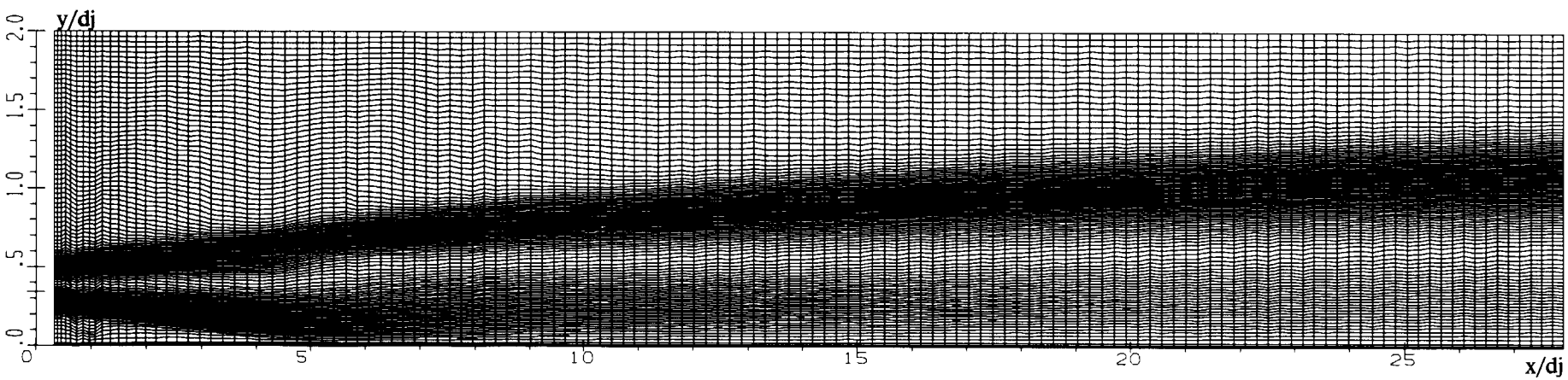

QL approach

Fig.12. Computational domain together with the adaptive grids used in calculations
(100 cells in y-direction)

Beach Test Case

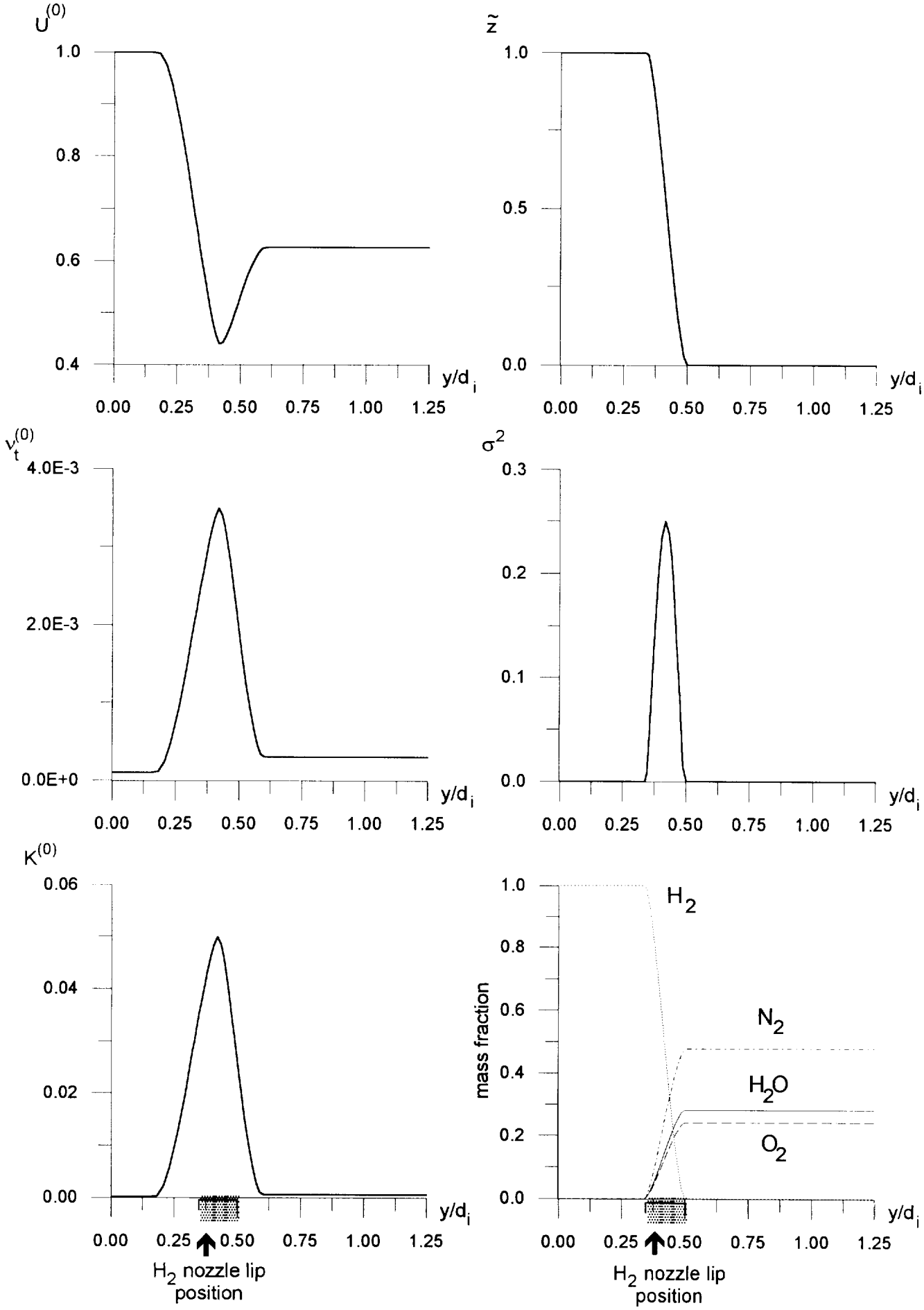

Fig.13. Initial profiles adopted in CFD calculations.
Beach test case.

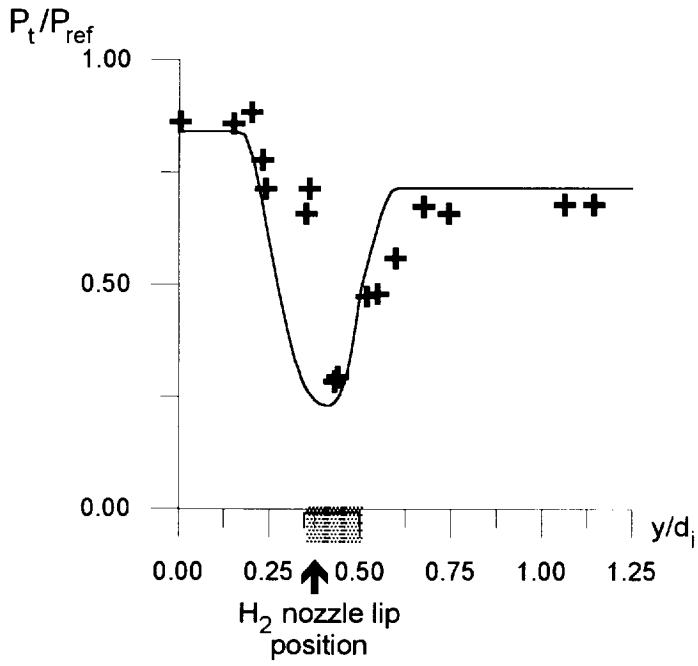

Fig.14a. Pitot pressure P_t profile in the initial cross section ($x/d_j = 0.33$).

——— calculations

✚ experimental data

$P_{ref} = 0.676$MPa

Beach test case.

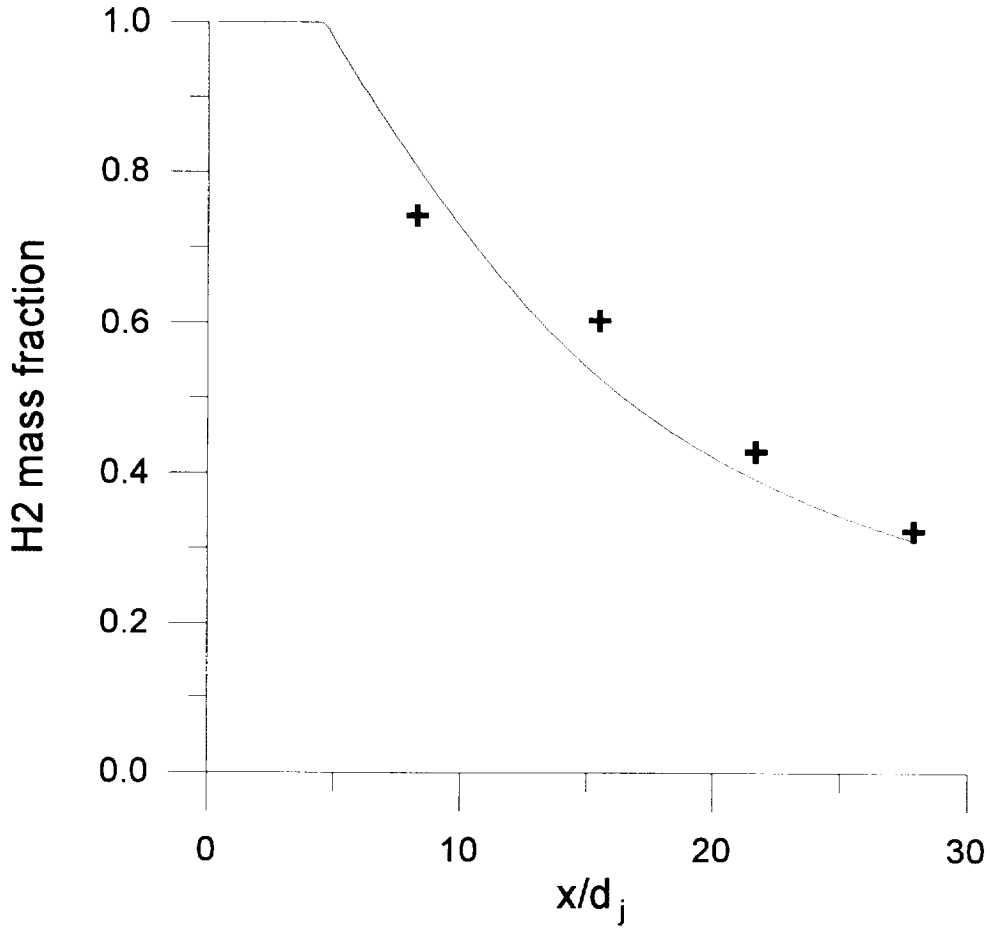

Fig.14b. Centerline distribution of the hydrogen mean mass fraction.

FL approach calculations

experimental data

Beach test case.

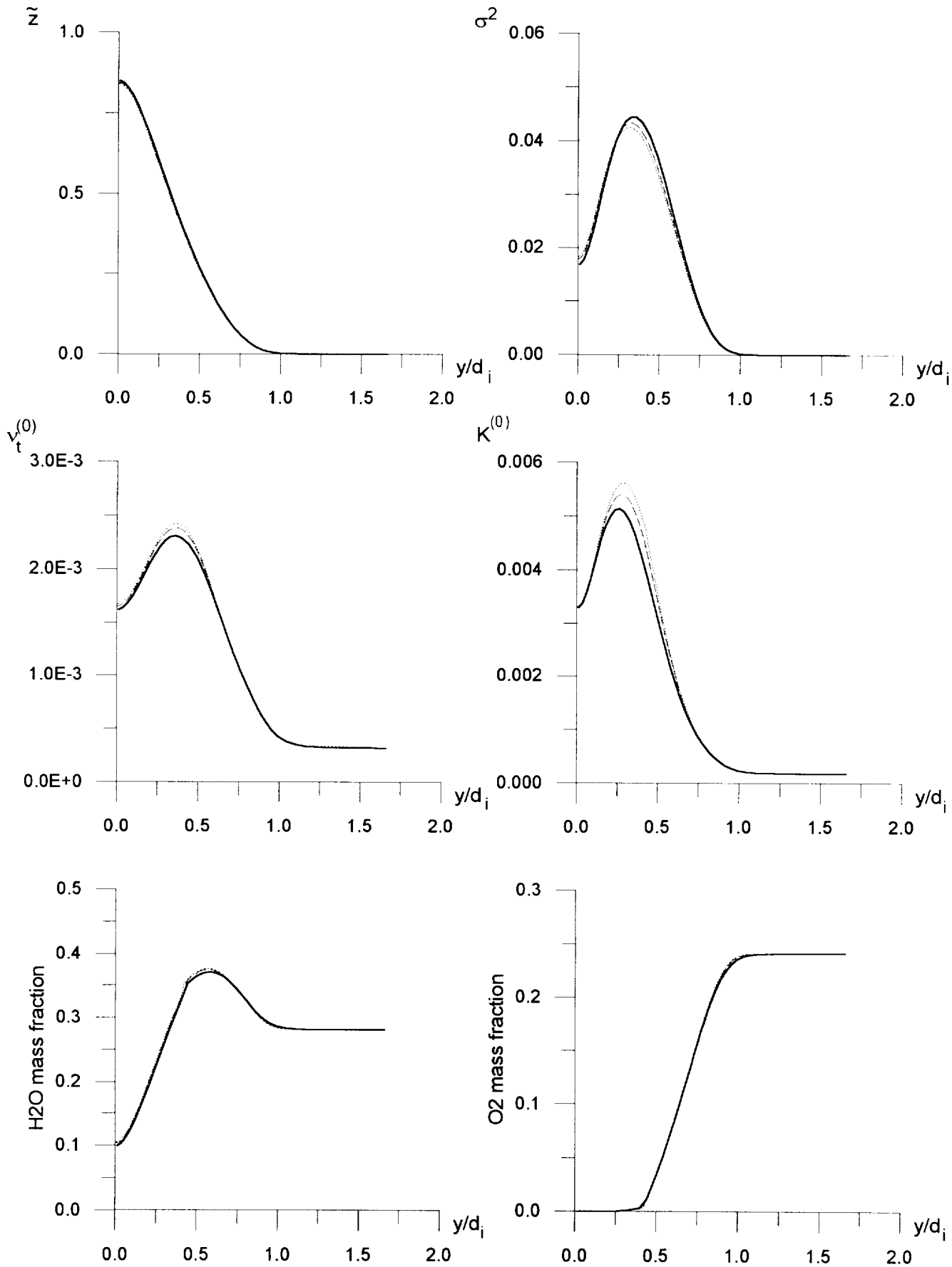

Fig.15a. Influence of the cells number on the results of FL computations.
Beach test case. $x/d_i = 8.26$

——— 50 cells

- - - - 100 cells

····· 200 cells

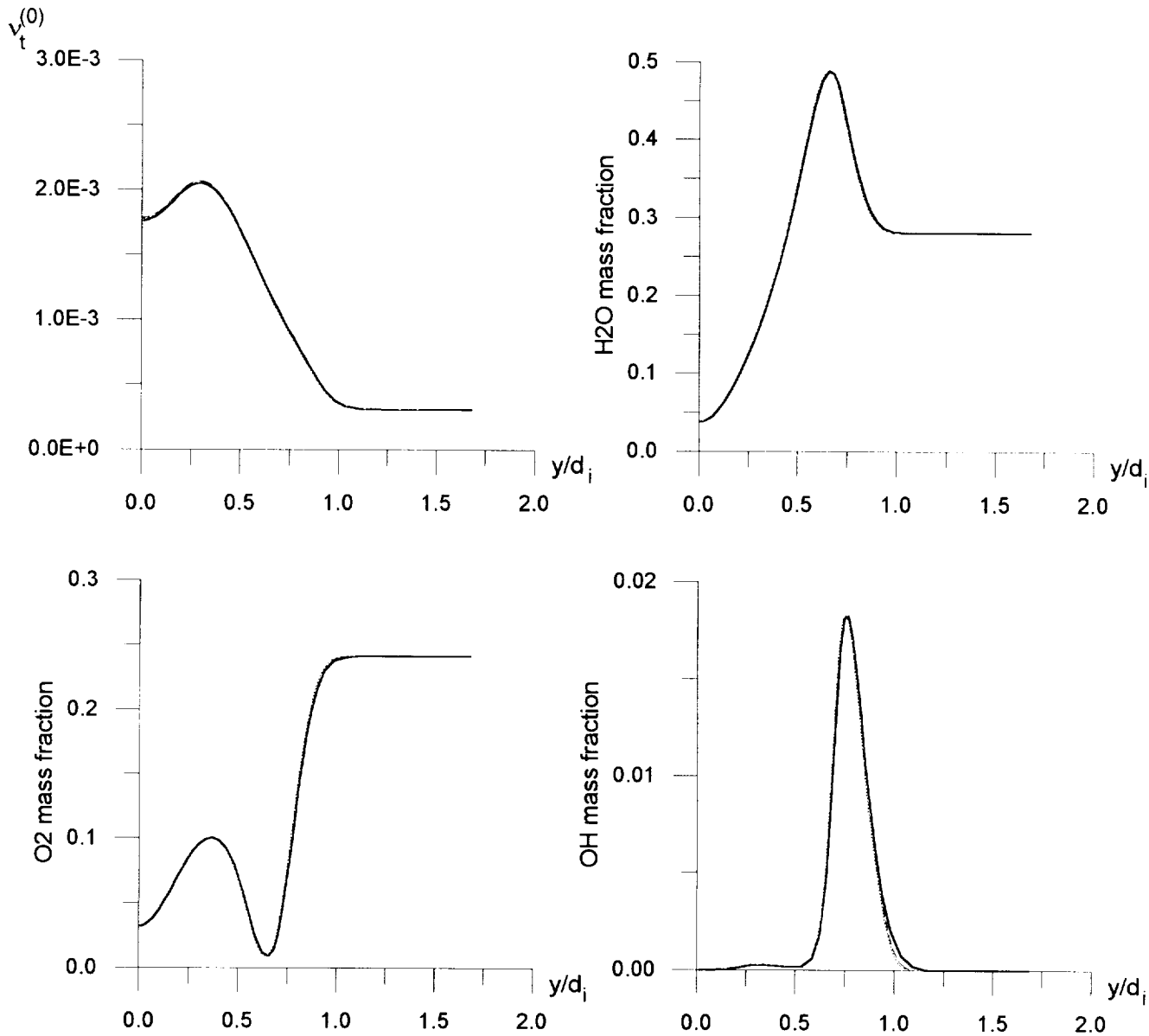

Fig.15b. Influence of the cells number on the results of QL computations.
Beach test case. $x/d_i = 8.26$

——— 50 cells

- - - - 100 cells

····· 200 cells

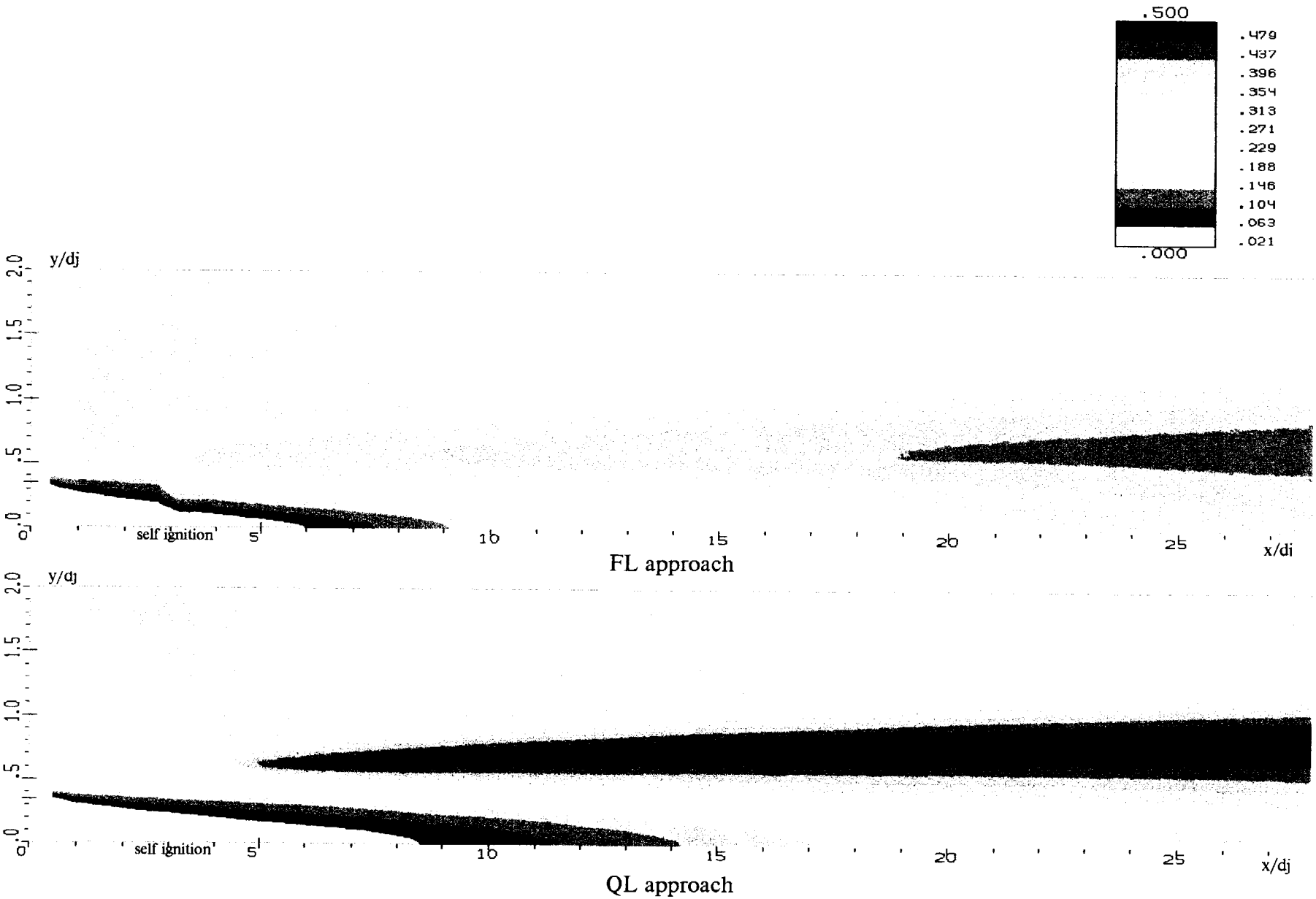

Fig.16. H_2O mass fraction contours
Beach Test Case

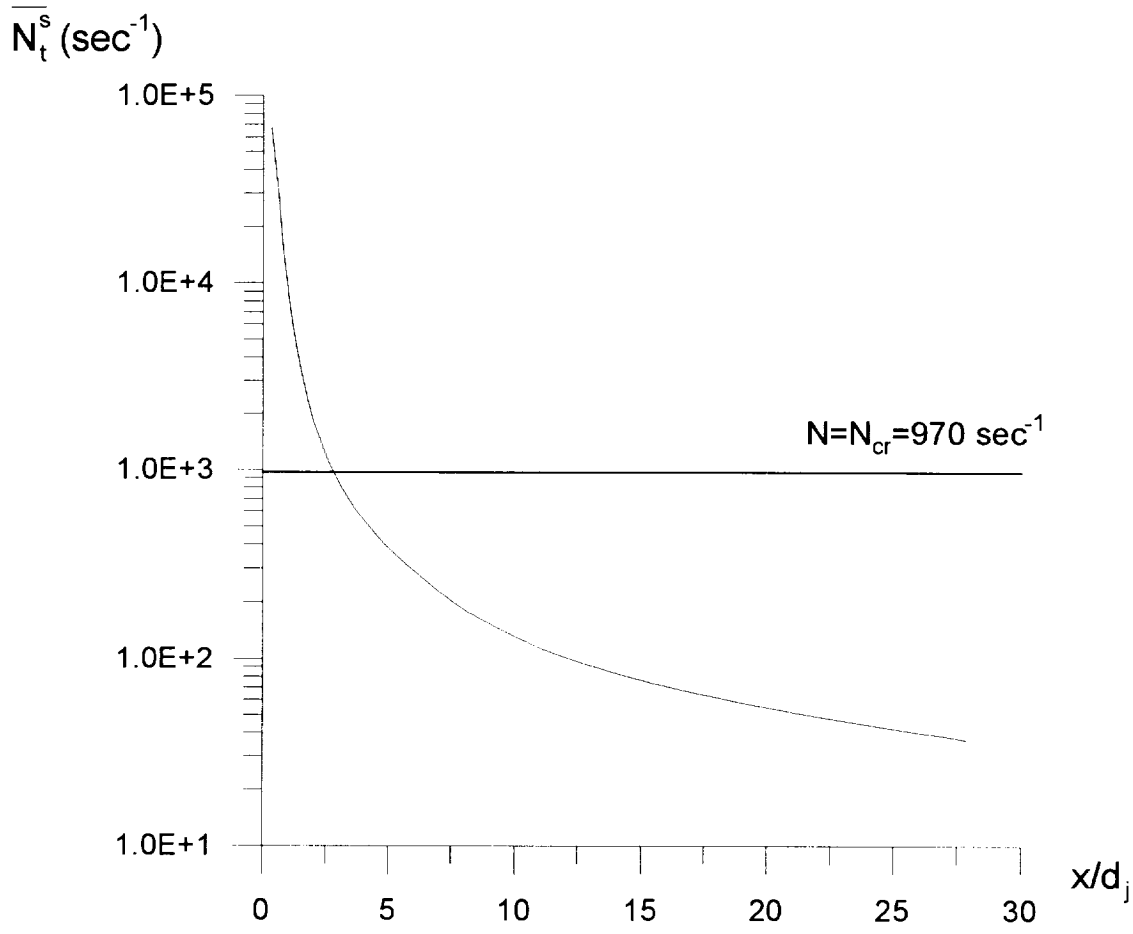

Fig.17. Calculated distribution of $\overline{N_t^s}$ vs distance from the nozzle. Beach test case.

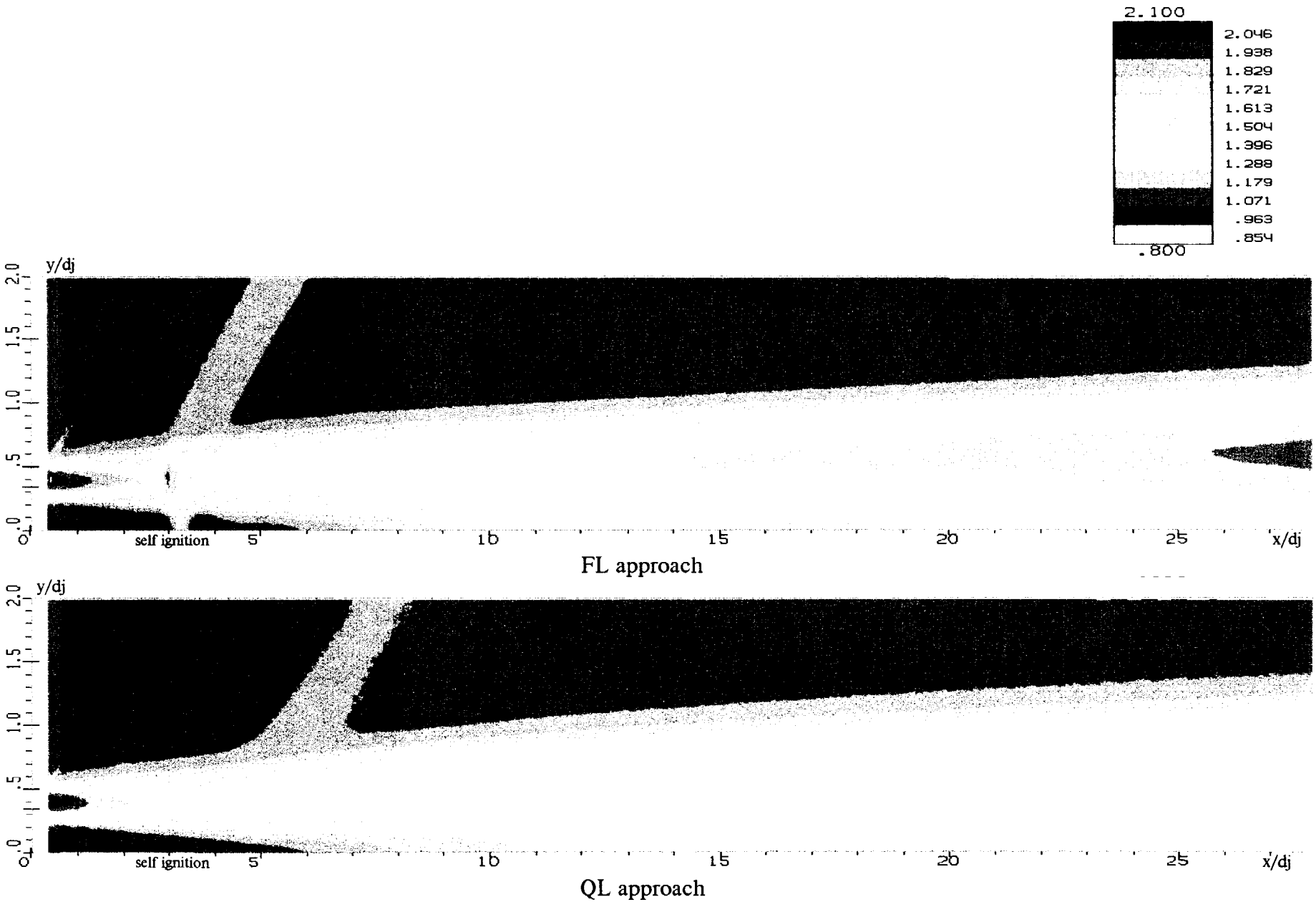

Fig.18. Mach number contours
Beach Test Case

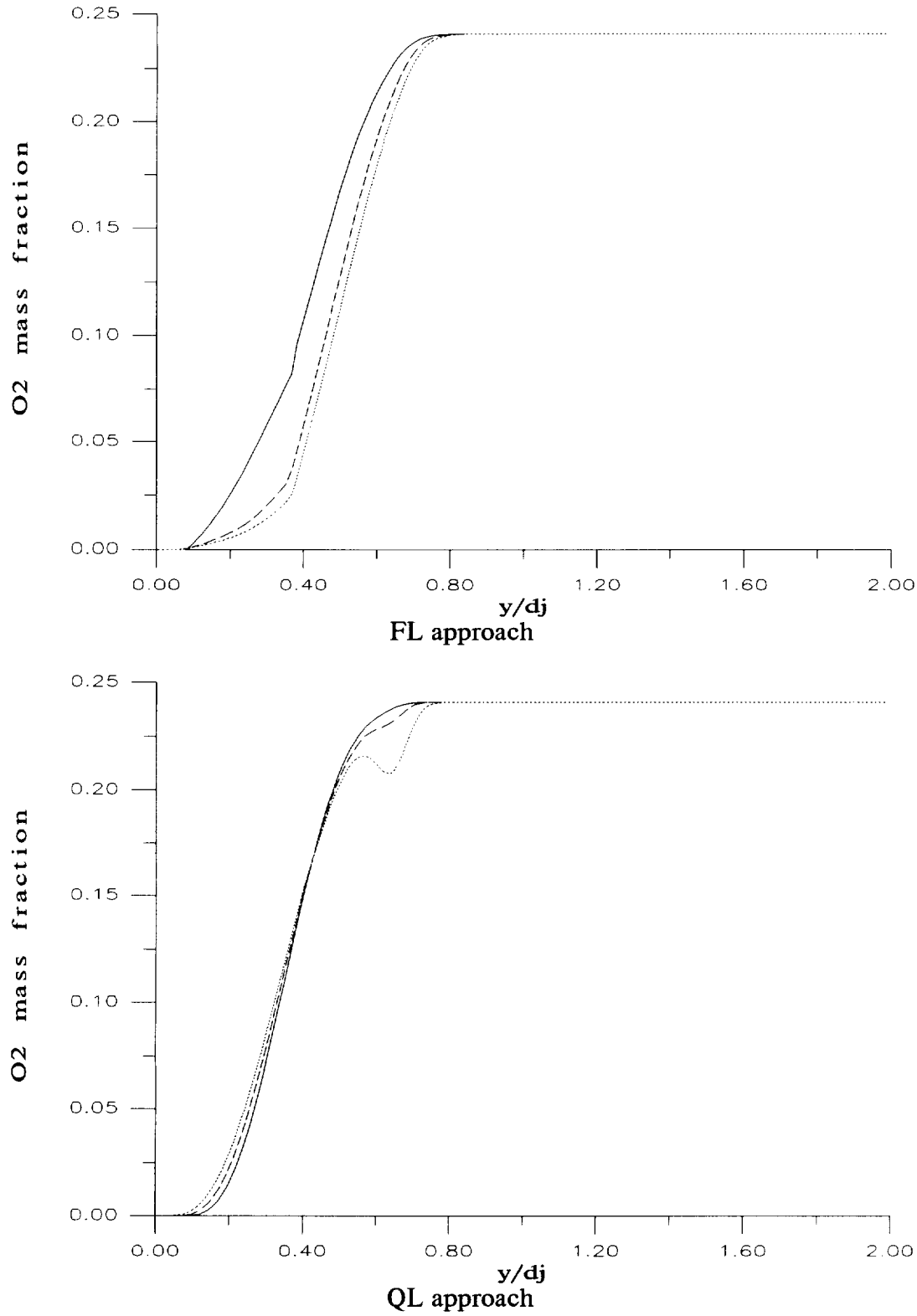

Fig.19. O_2 mass fraction behavior in the vicinity of the self-ignition point

_____ upstream ignition point
_ _ _ _ _ _ _ downstream ignition point
..... downstream ignition point (next crossection)

Beach Test Case

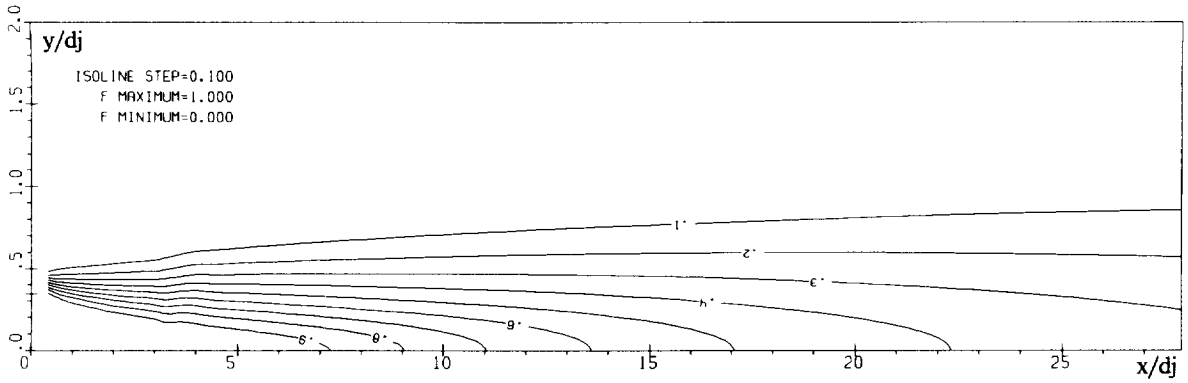

$\tilde{Z}$-contours

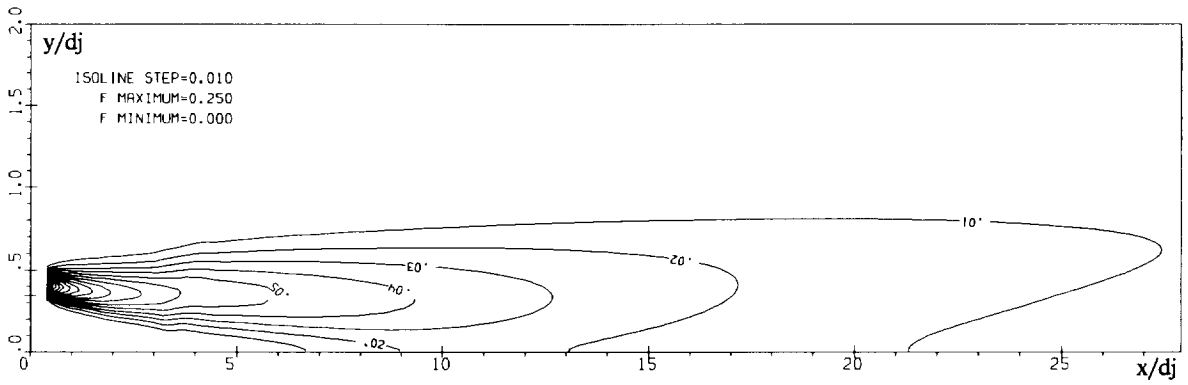

σ^2-contours

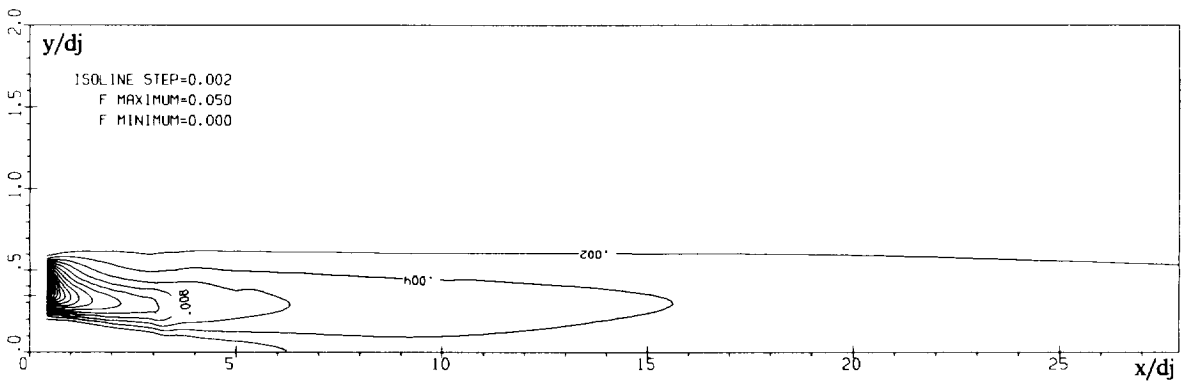

$K^{(0)}$-contours

Fig.20. Turbulent mixing characteristics contours
FL approach

Beach Test Case

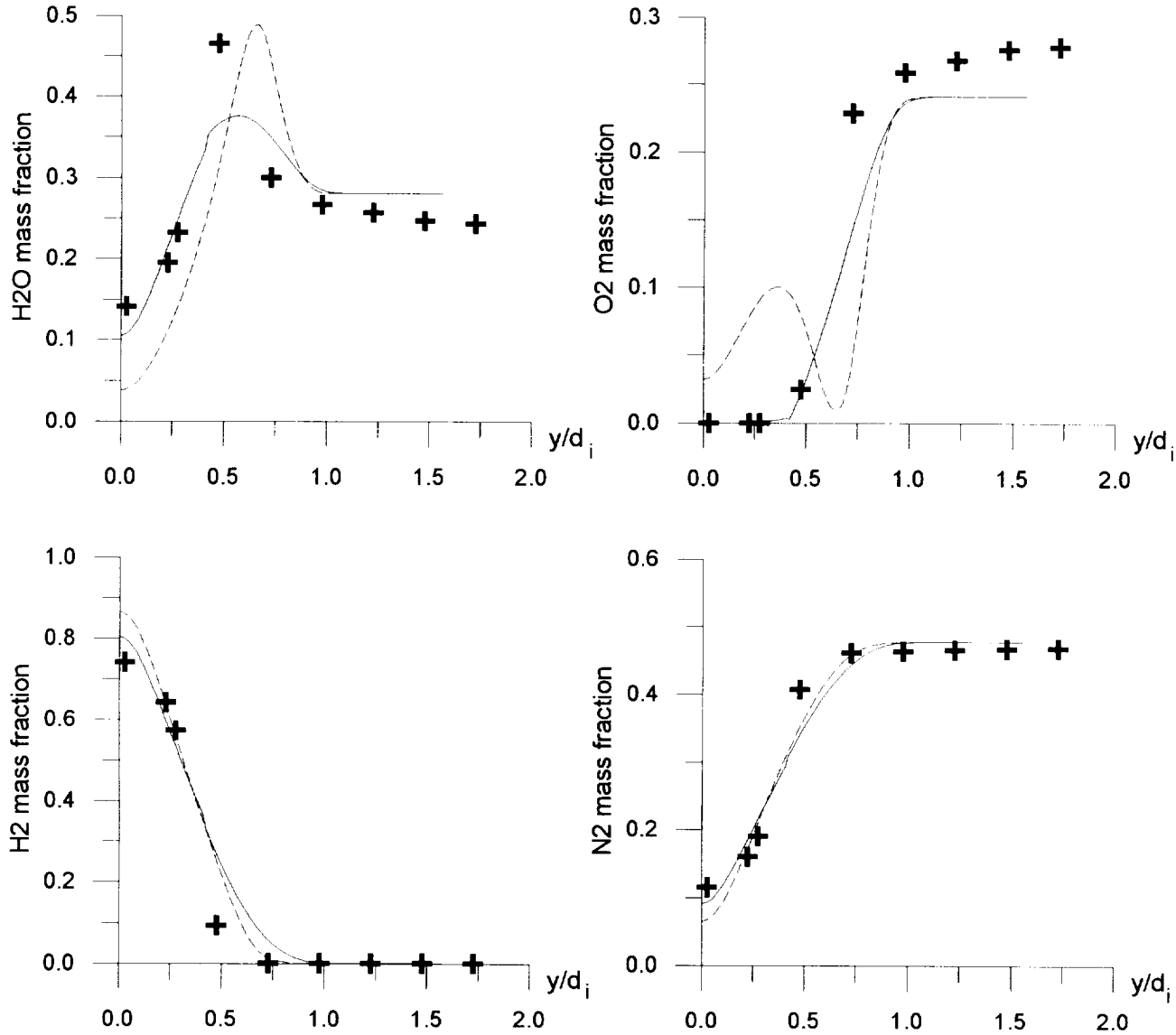

Fig.21a. Comparison of FL and QL predictions together with experimental data.

——— FL approach;

- - - - QL approach;

✚ experimental data of Beach et al.

$x/d_i = 8.26$

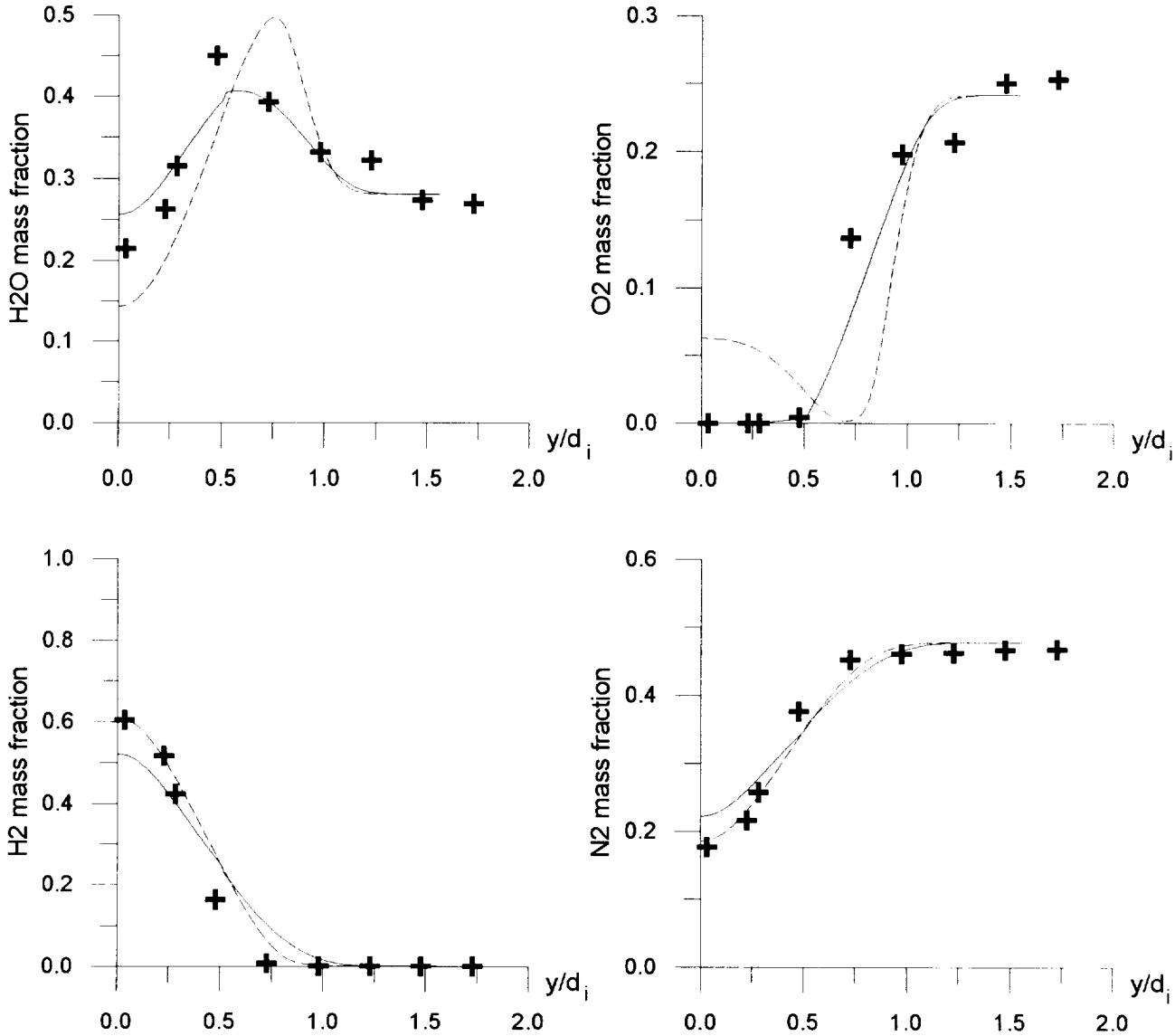

Fig.21b. Comparison of FL and QL predictions together with experimental data.

——— FL approach;

- - - - QL approach;

✚ experimental data of Beach et al.

$x/d_i = 15.5$

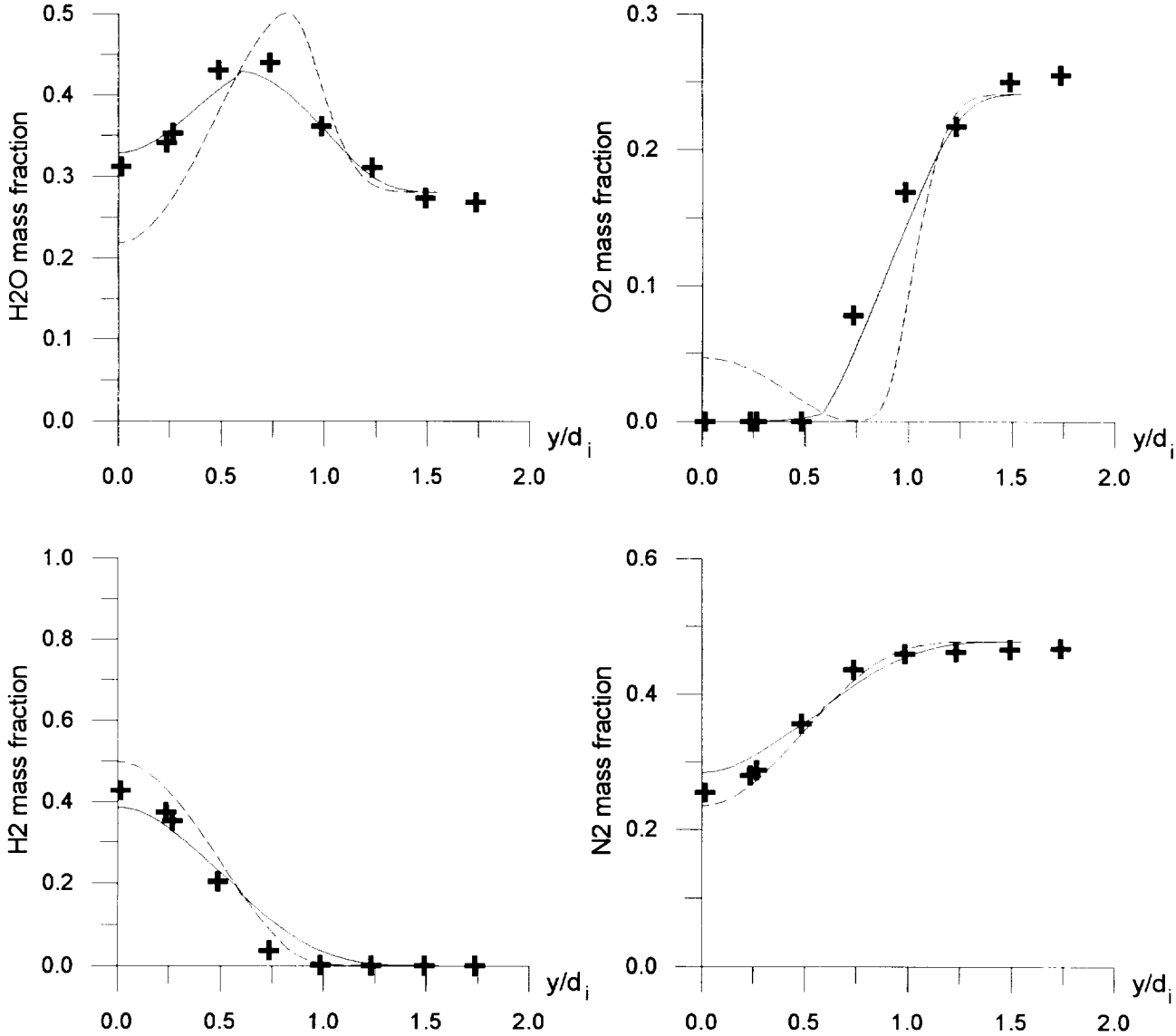

Fig.21c. Comparison of FL and QL predictions together with experimental data.

FL approach;

QL approach;

experimental data of Beach et al.

$x/d_i = 21.7$

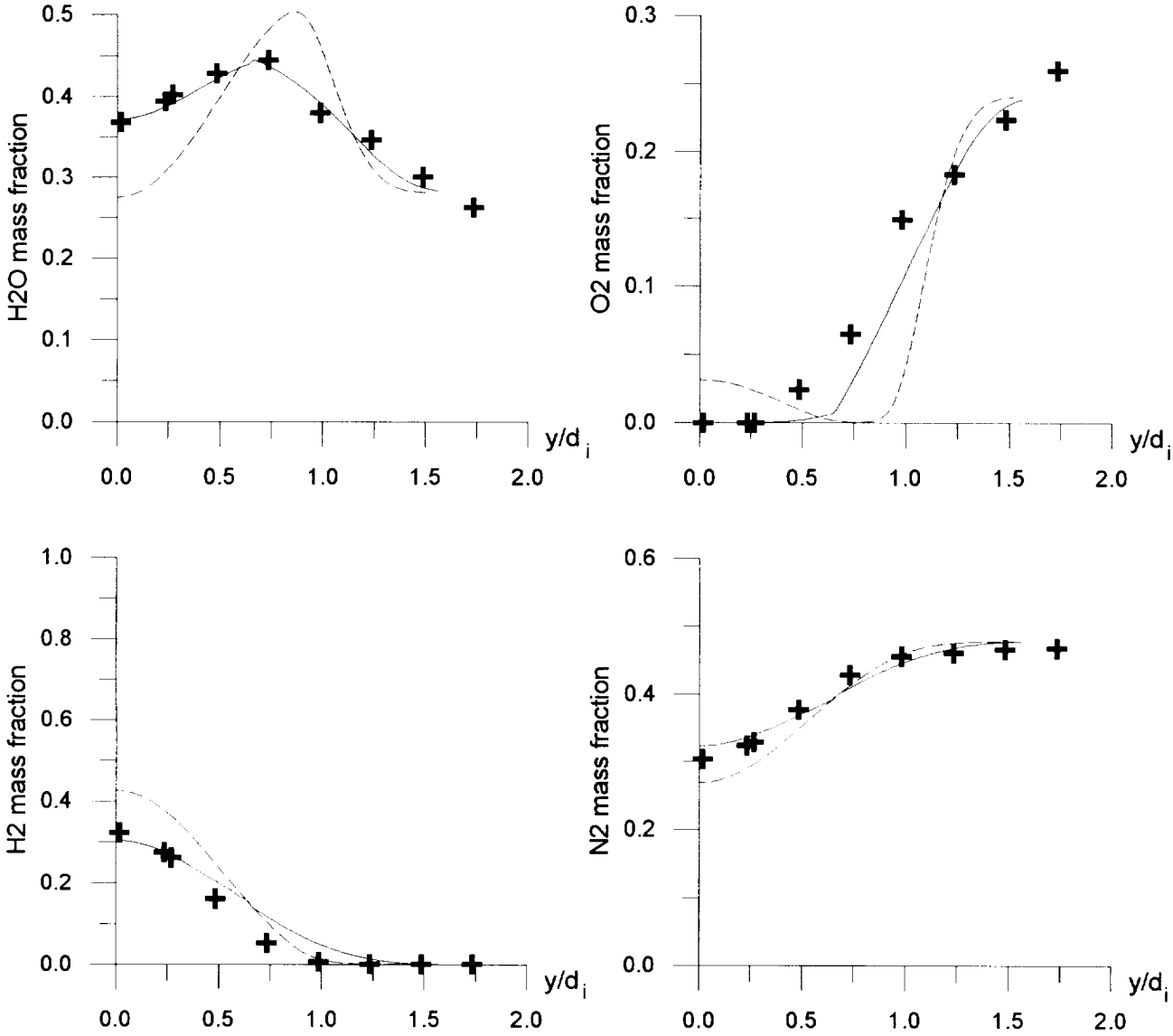

Fig.21d. Comparison of FL and QL predictions together with experimental data.

FL approach;

QL approach;

experimental data of Beach et al.

$x/d_i = 27.9$

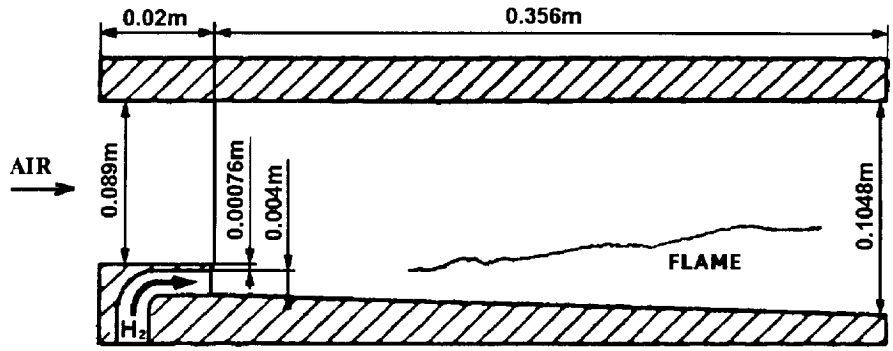

	Hydrogen jet	Air stream
Mach number, M	1.00	2.44
Temperature, T, K	254	1270
Velocity, U, m/s	1216	1764
Pressure, P, MPa	0.1	0.1
Mass fractions:		
C_{H2}	1.000	0
C_{O2}	0	0.258
C_{N2}	0	0.486
C_{H2O}	0	0.256

Fig.22. Scheme and conditions of Burrows and Kurkov experiment.

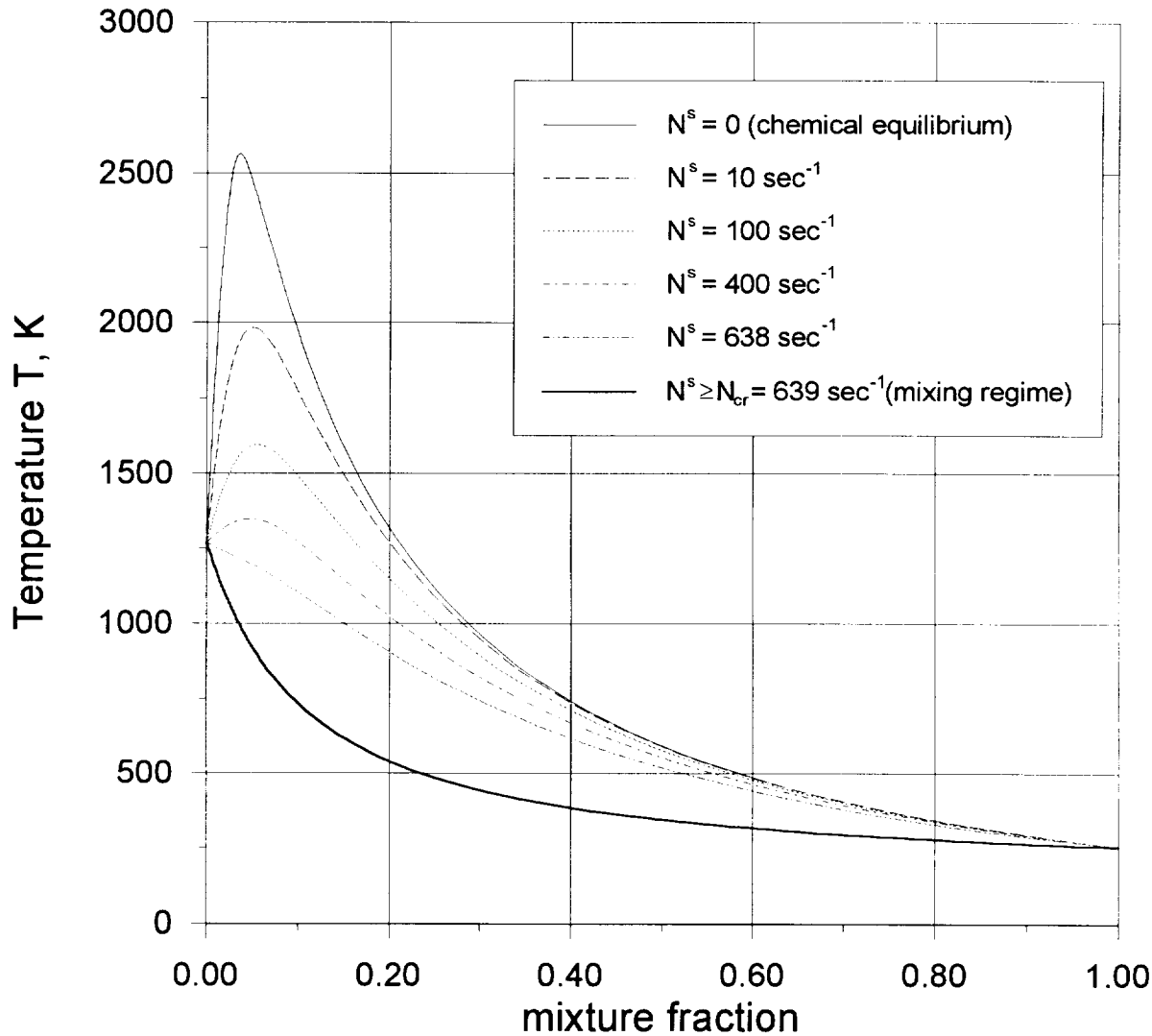

Fig.23a. Flamelet library.
Temperature T.
$P_s = 0.1$ MPa
Burros-Kurkov test case.

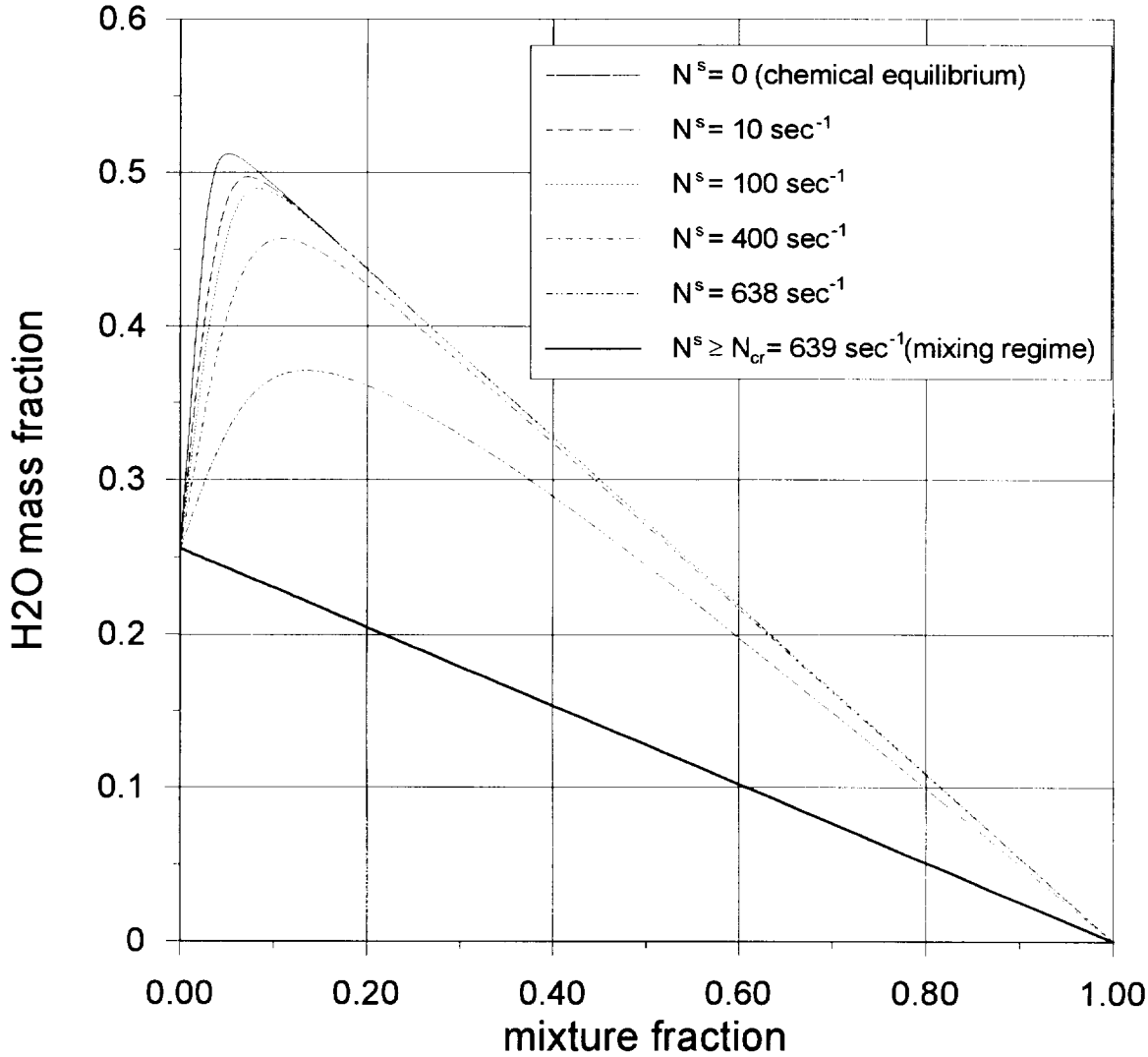

Fig.23b. Flamelet library.
H2O mass fraction.
$P_s = 0.1$ MPa
Burrows-Kurkov test case.

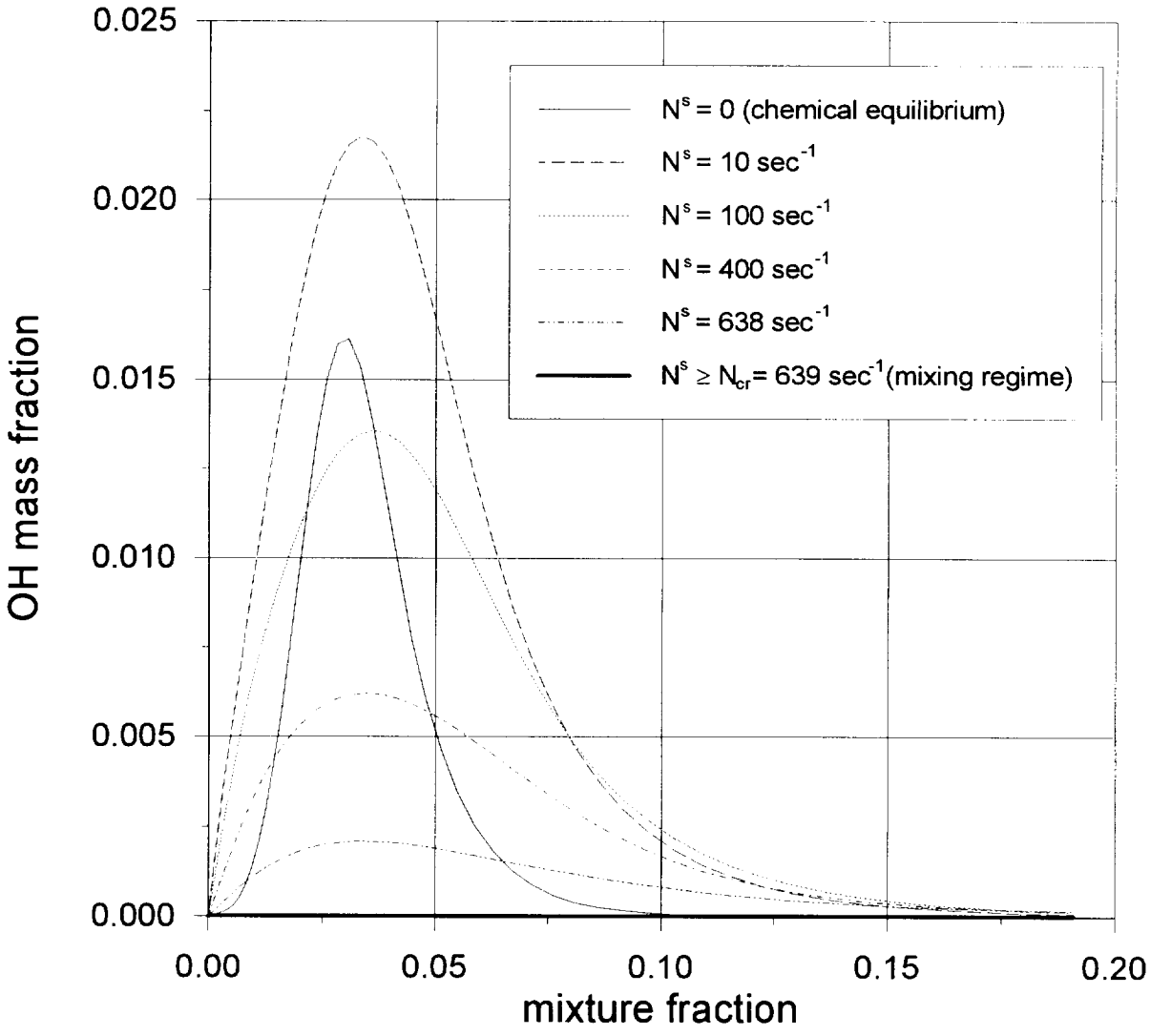

Fig.23c. Flamelet library.
OH mass fraction.
$P_s = 0.1$ MPa.
Burrows-Kurkov test case.

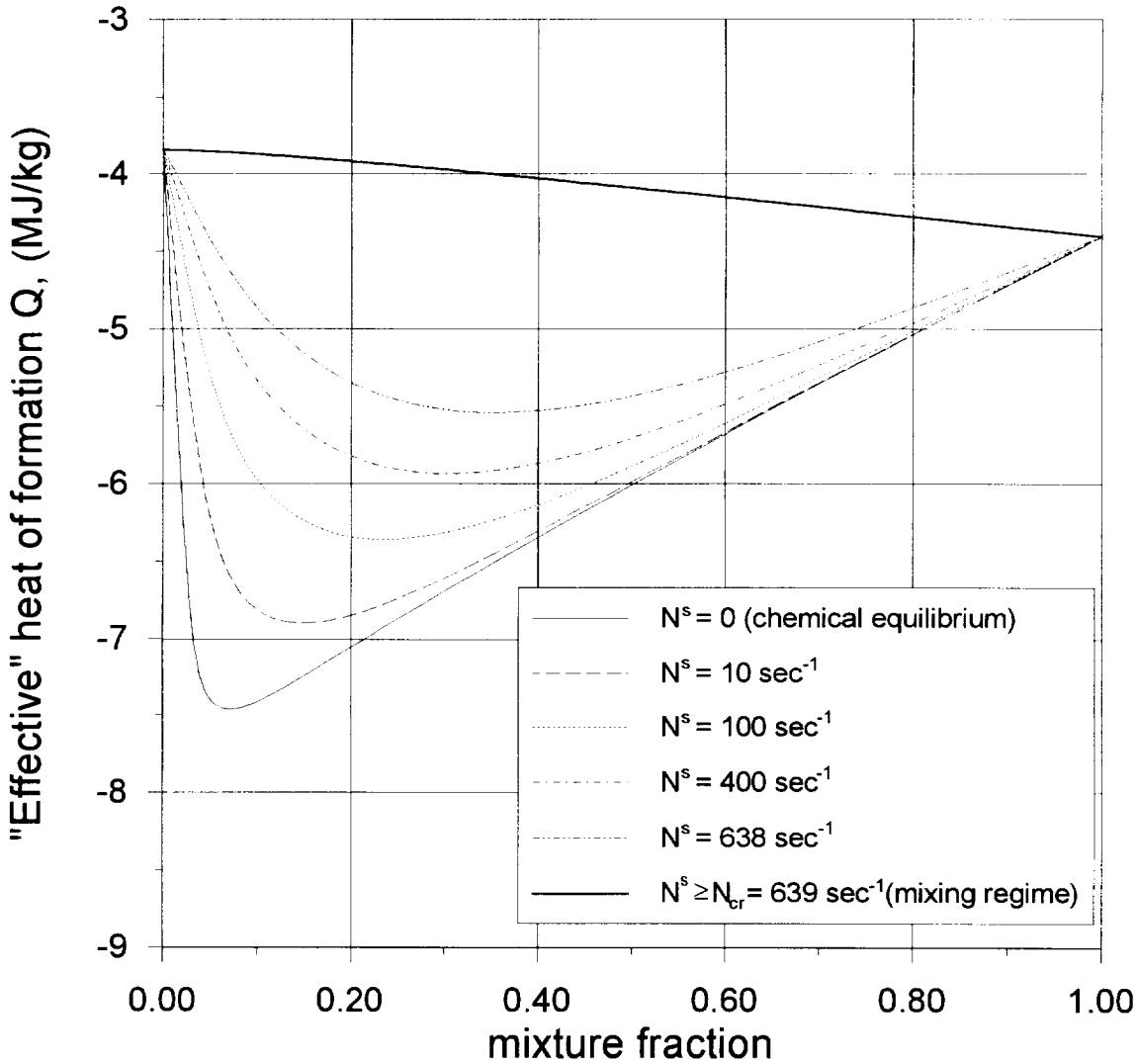

Fig.23d. Flamelet library.
"Effective" heat of formation Q.
$P_s = 0.1$ MPa.
Burrows-Kurkov test case.

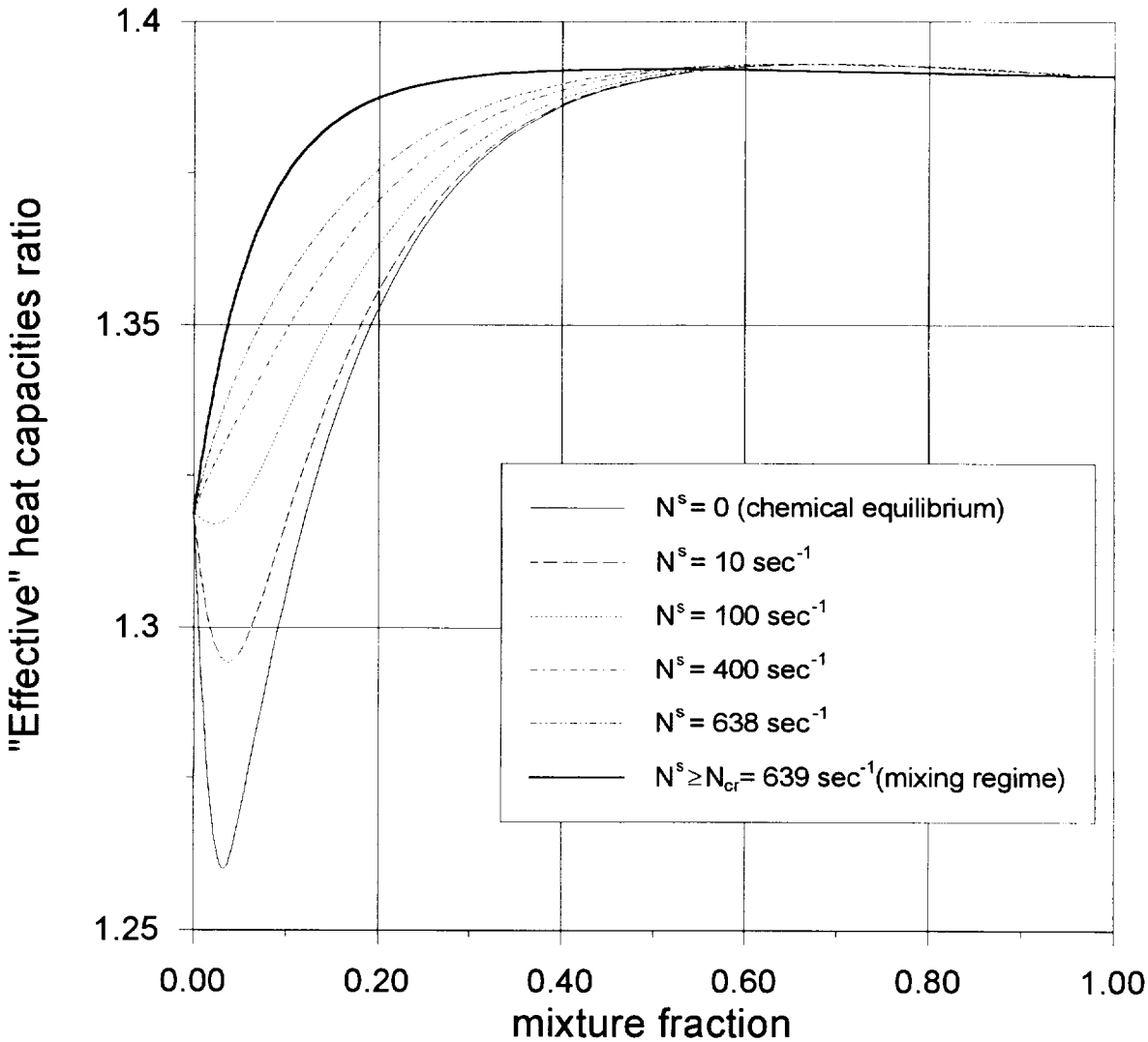

Fig.23e. Flamelet library.
"Effective" heat capacities ratio Γ.
$P_s = 0.1$ MPa.
Burrows-Kurkov test case.

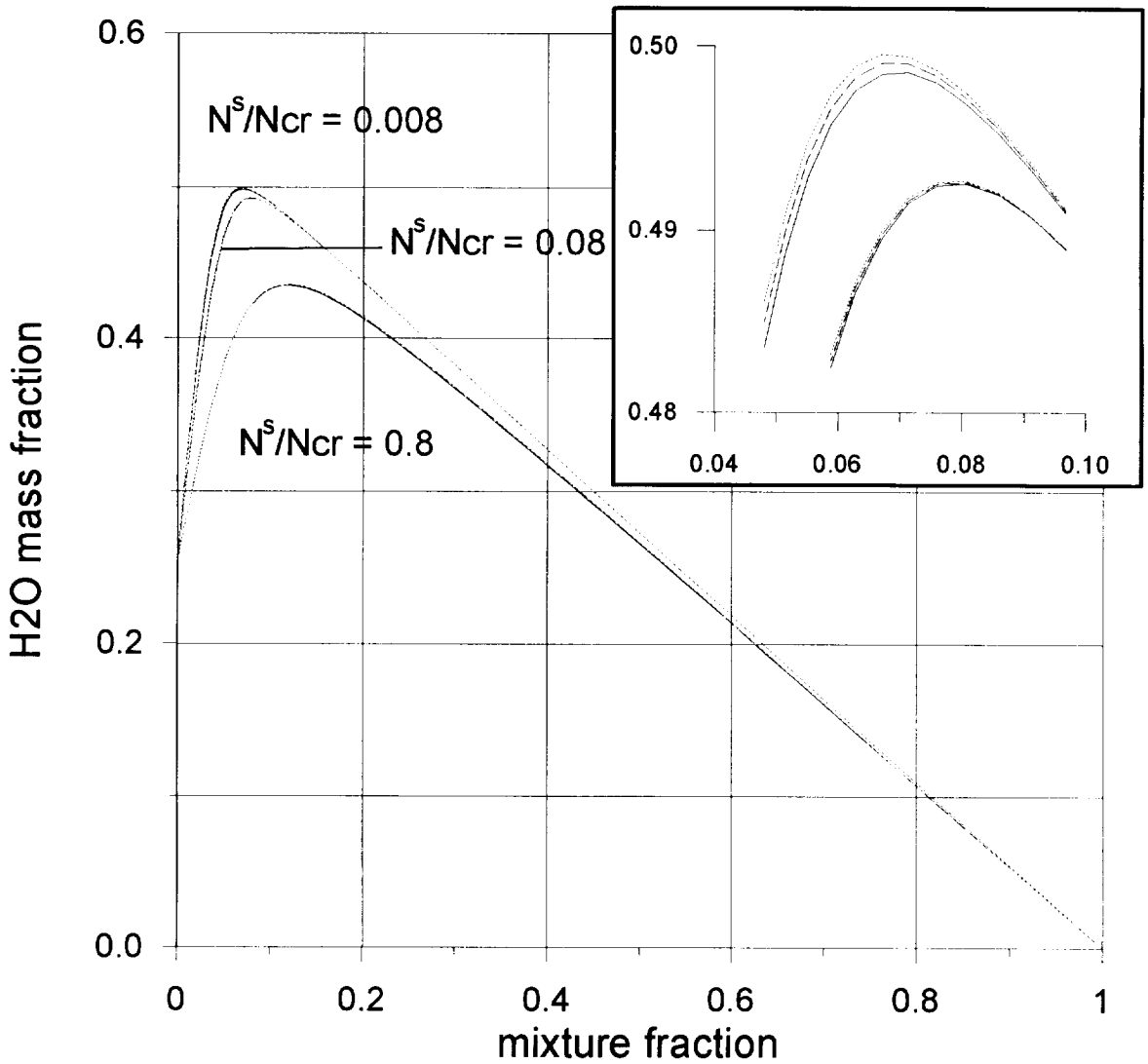

Fig.24a. Flamelet library. Role of pressure variation.
Water mass fraction.

——— $P_s = 0.08$ MPa

- - - - - $P_s = 0.10$ MPa

..... $P_s = 0.12$ MPa

Burrows-Kurkov test case.

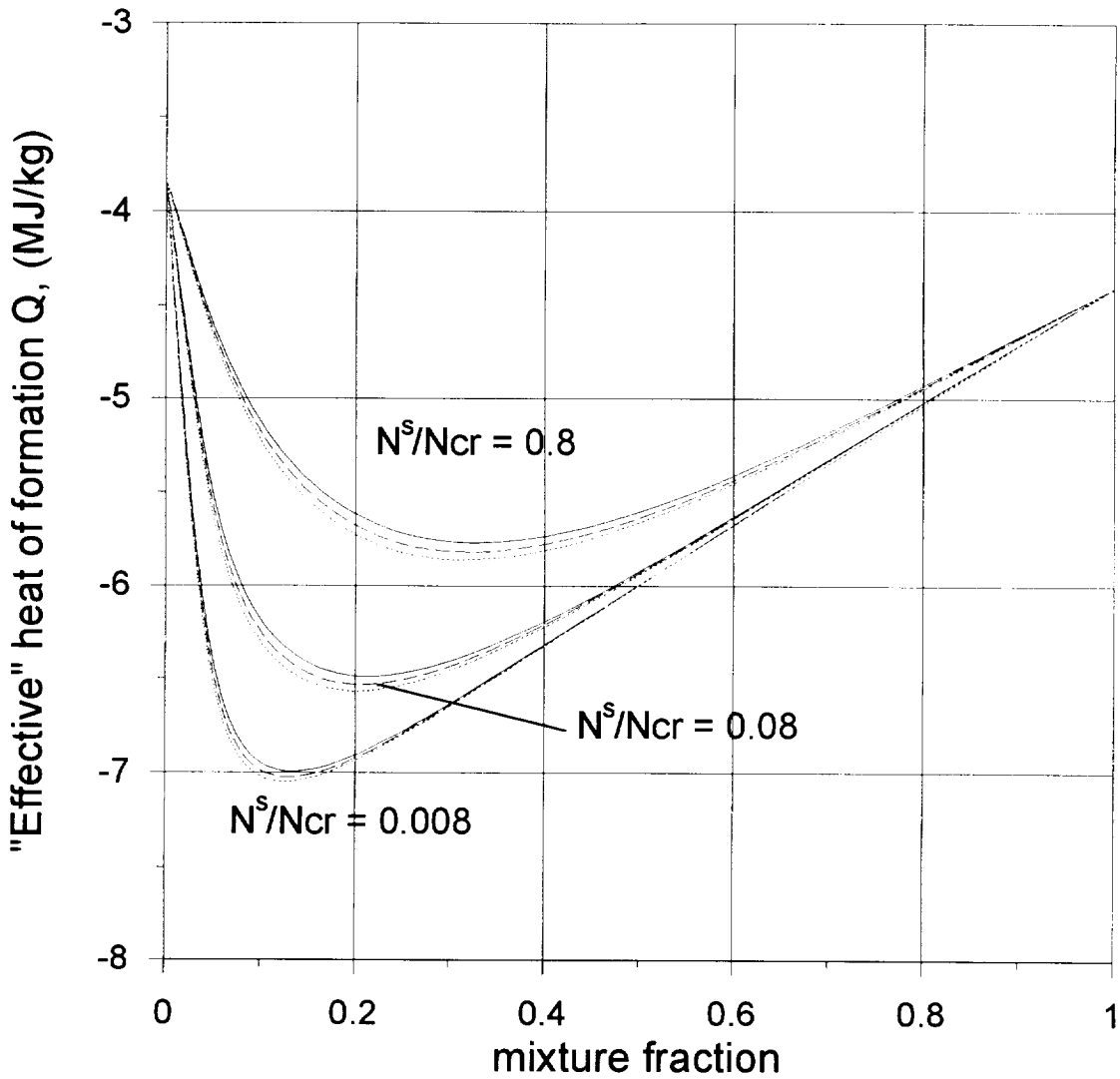

Fig.24b. Flamelet library. Role of pressure variation.
"Effective" heat of formation.

——— $P_s = 0.08$ MPa

- - - - - - $P_s = 0.10$ MPa

..... $P_s = 0.12$ MPa

Burrows-Kurkov test case.

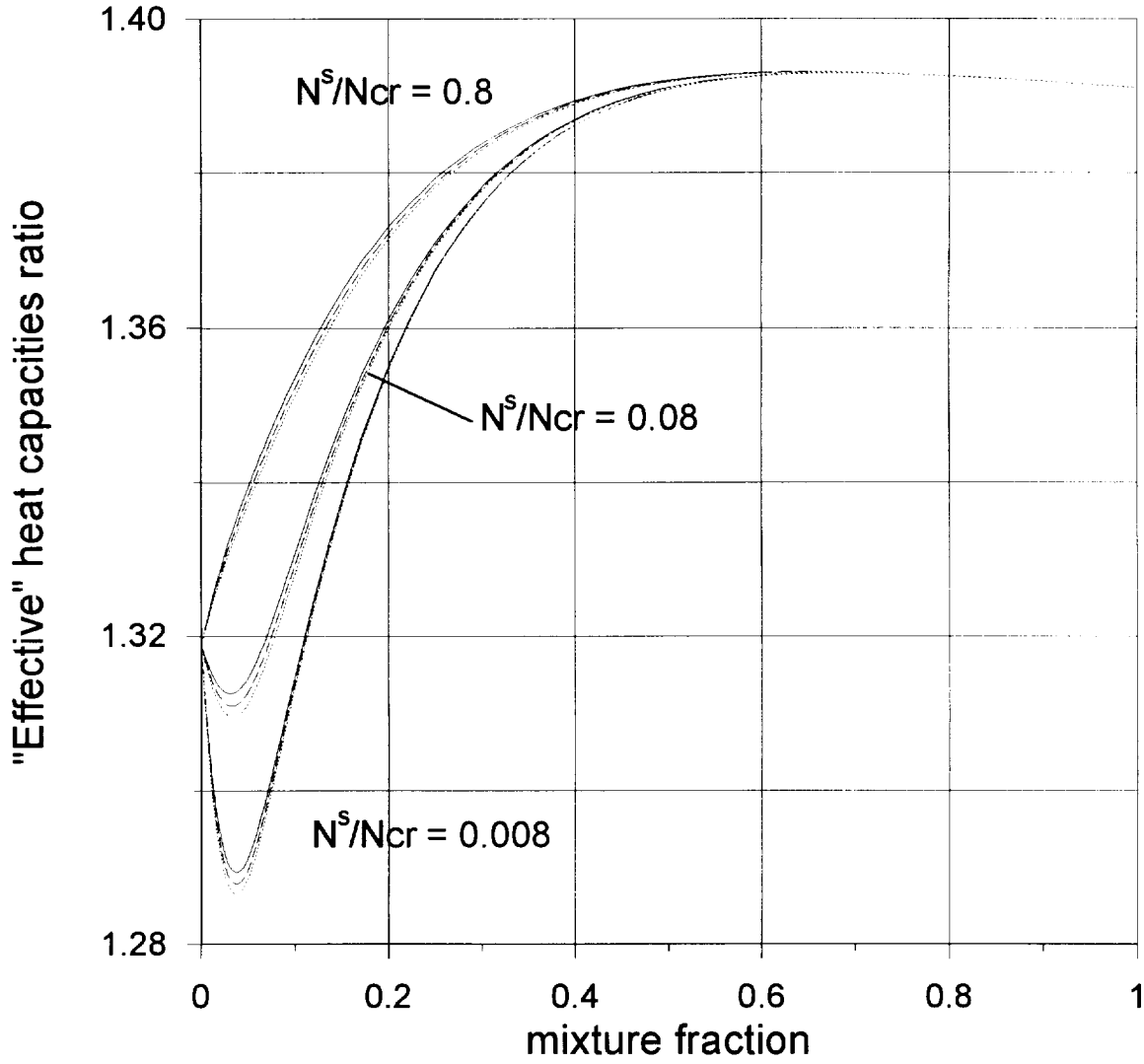

Fig.24c. Flamelet library. Role of pressure variation.
"Effective" heat capacities ratio.

———— $P_s = 0.08$ MPa

- - - - - - $P_s = 0.10$ MPa

..... $P_s = 0.12$ MPa

Burrows-Kurkov test case.

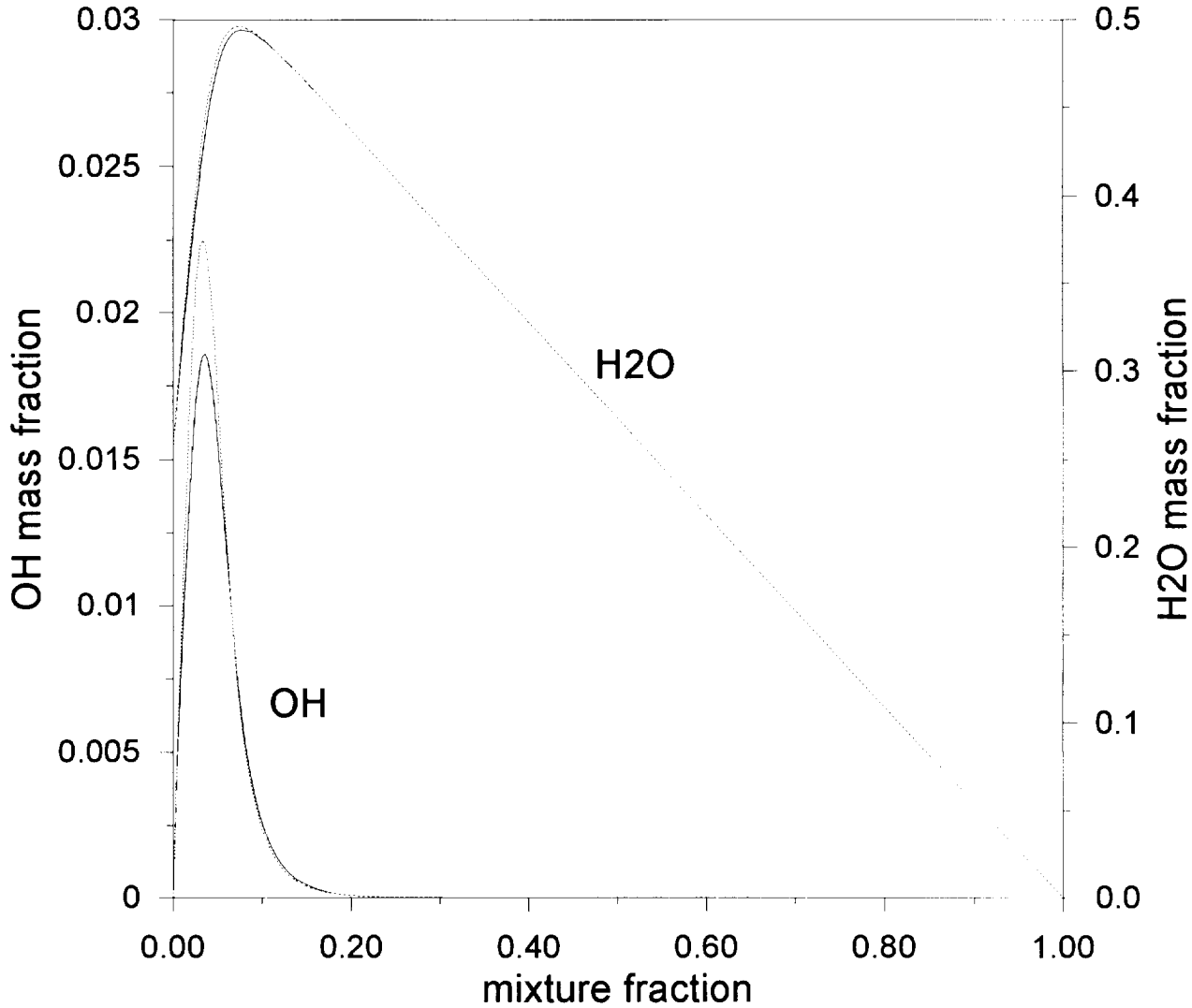

Fig.25. Sensitivity of flamelet solution to detailed chemistry model.
Flamelet model calculations based on:

——— Miller - Bowman detailed kinetics

..... Warnatz detailed kinetics

$N^s = 30\ sec^{-1}$. $P_s = 0.1$ MPa.
Burrows-Kurkov test case.

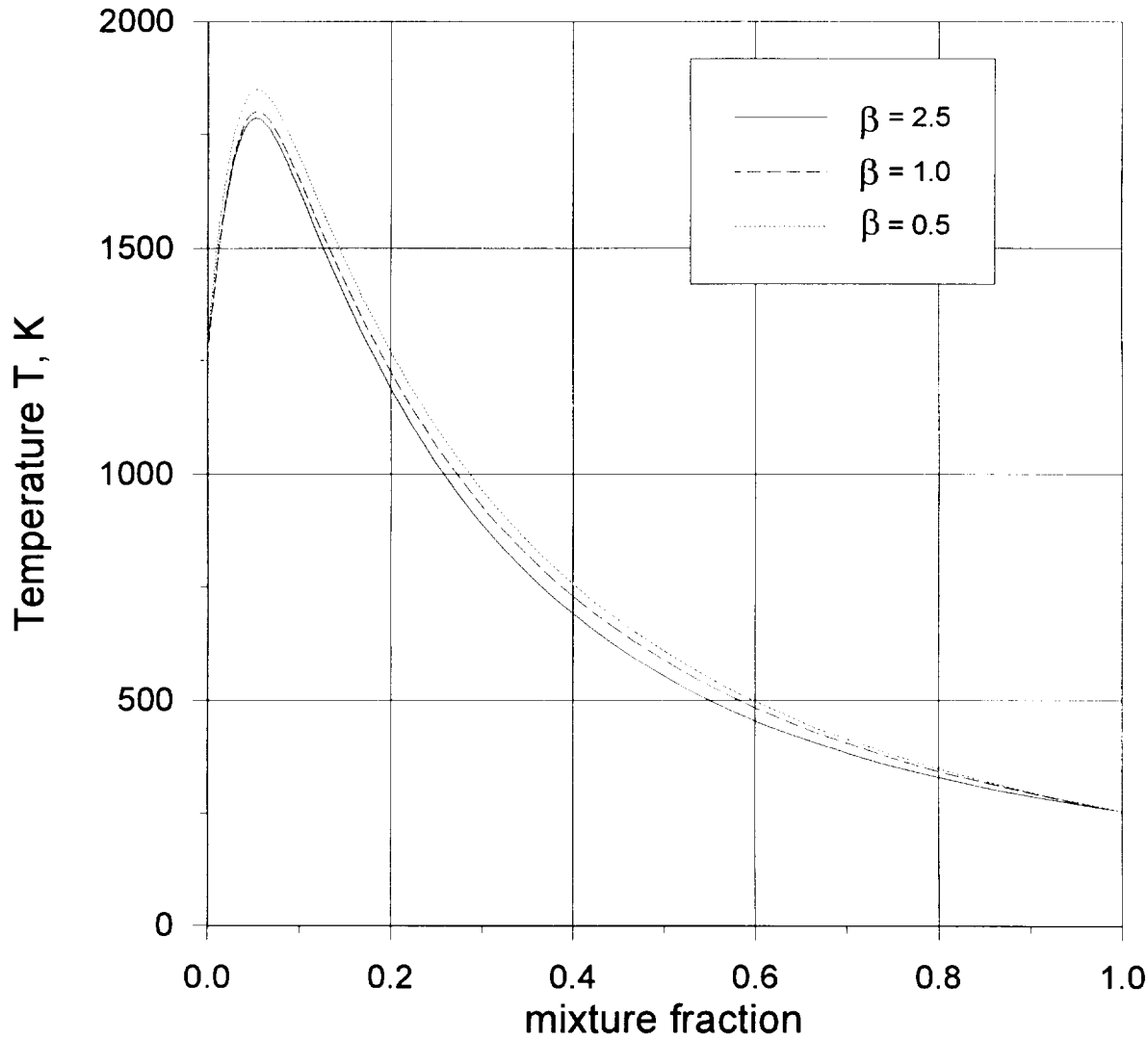

Fig.26a. Sensitivity of flamelet solution to the exponent β variation.
Temperature T.
$N^s = 30\ sec^{-1}$. $P_s = 0.1$ MPa.
Burrows-Kurkov test case.

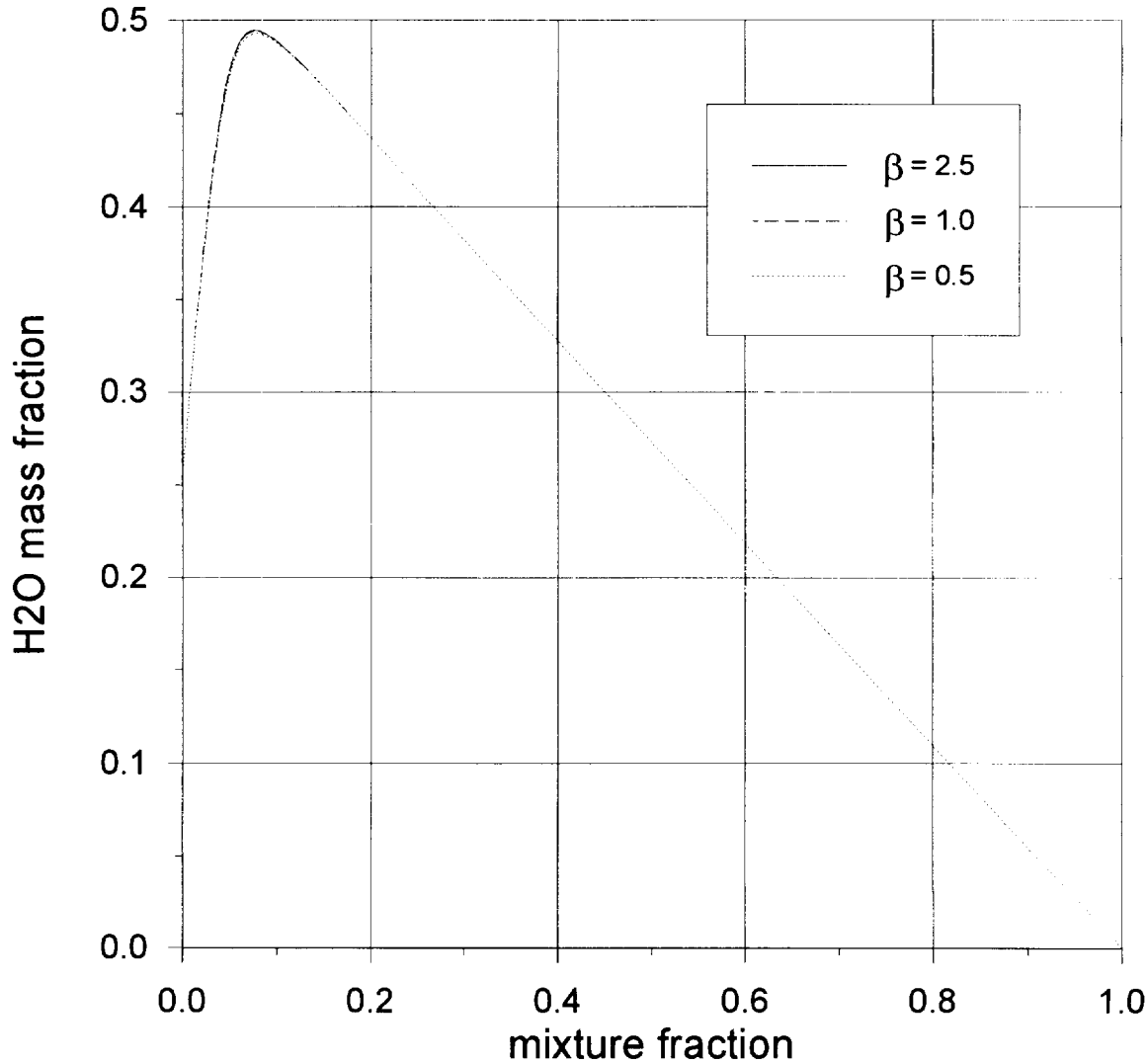

Fig.26b. Sensitivity of flamelet solution to the exponent β variation.
Water mass fraction.
$N^s = 30\ sec^{-1}$. $P_s = 0.1$ MPa.
Burrows-Kurkov test case.

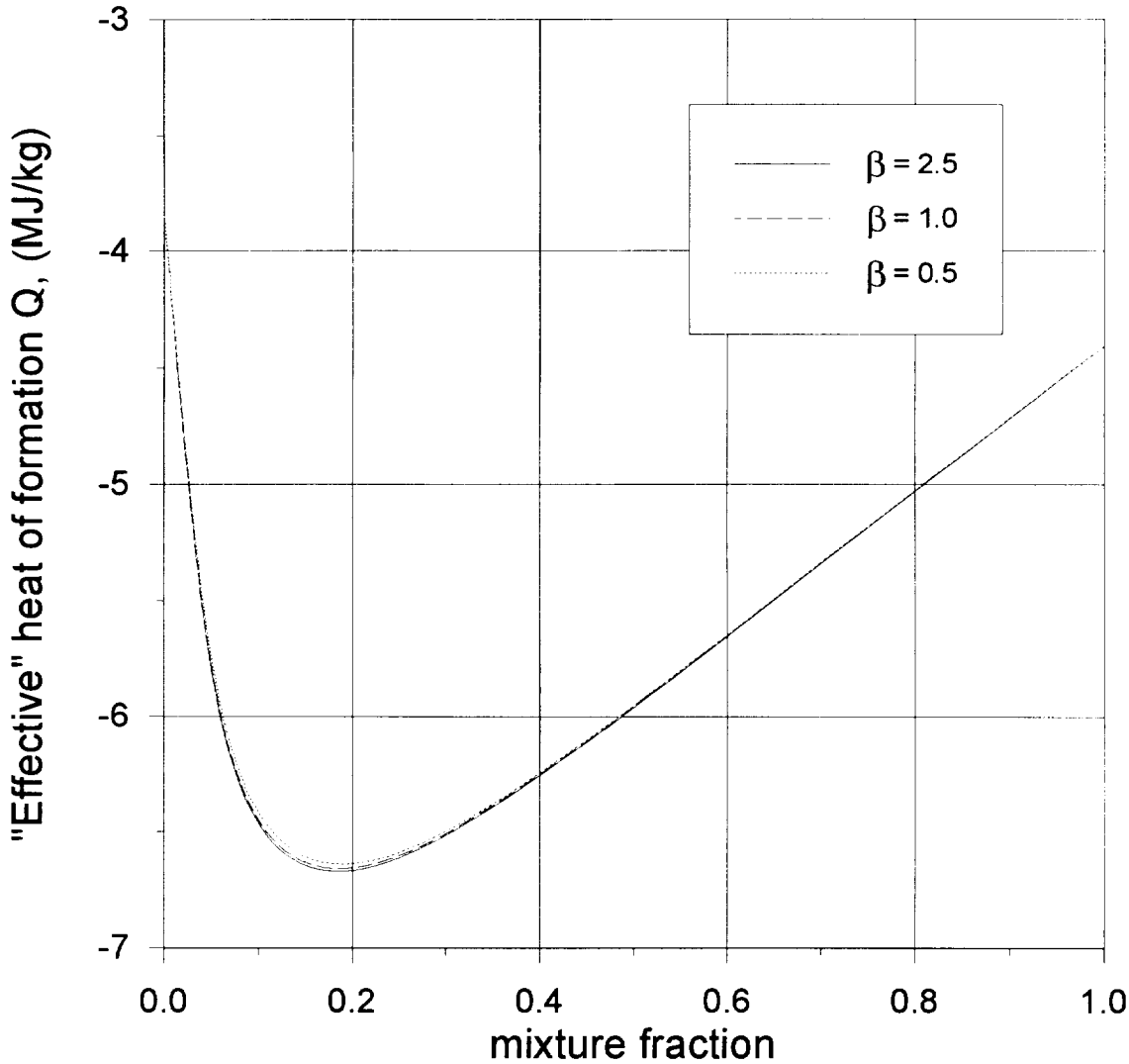

Fig.26c. Sensitivity of flamelet solution to the exponent β variation.
"Effective" heat of formation Q.
$N^s = 30\ sec^{-1}$. $P_s = 0.1$ MPa.
Burrows-Kurkov test case.

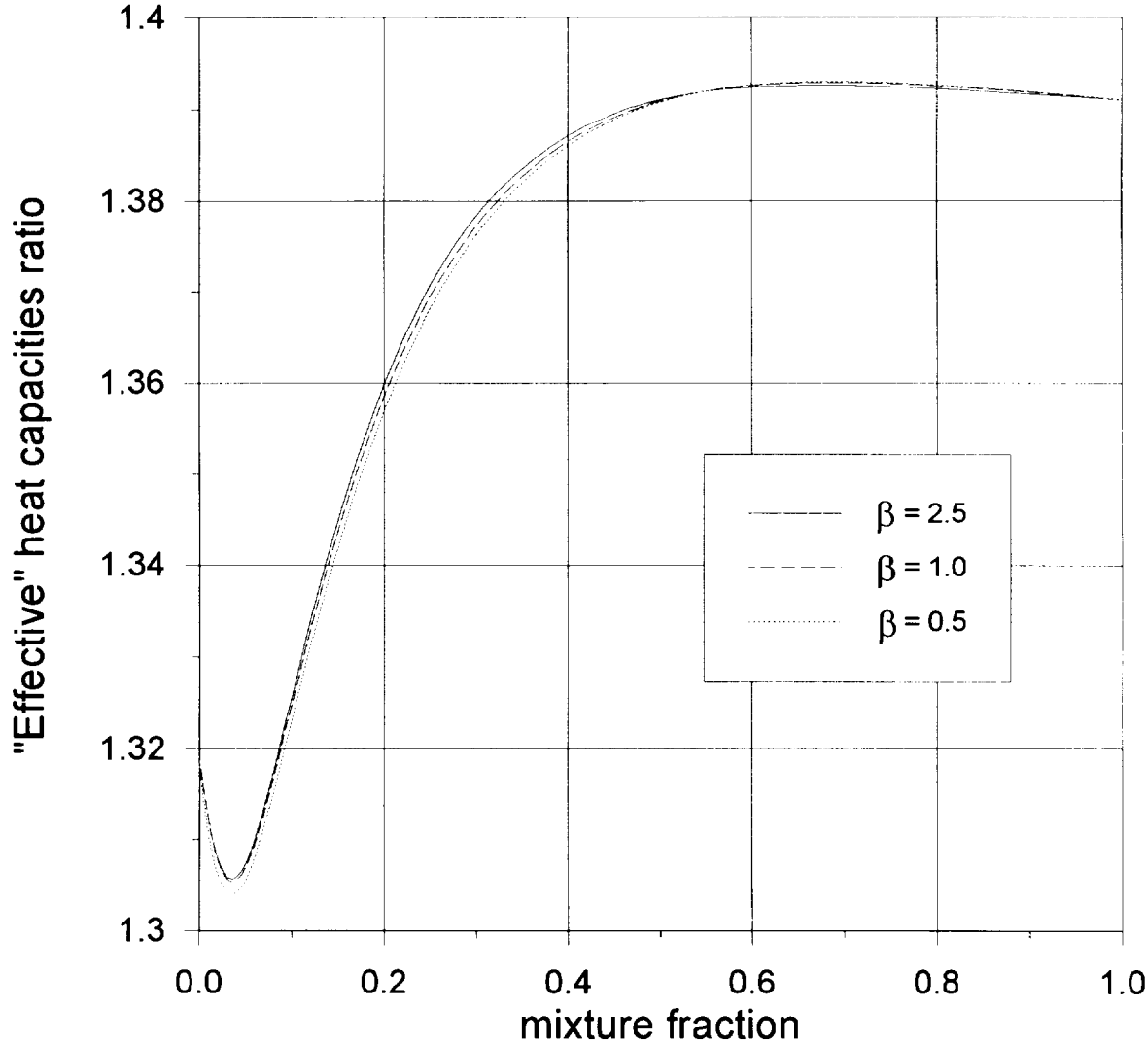

Fig.26d. Sensitivity of flamelet solution to the exponent β variation.
"Effective" heat capacities ratio Γ.
$N^s = 30\ sec^{-1}$. $P_s = 0.1$ MPa.
Burrows-Kurkov test case.

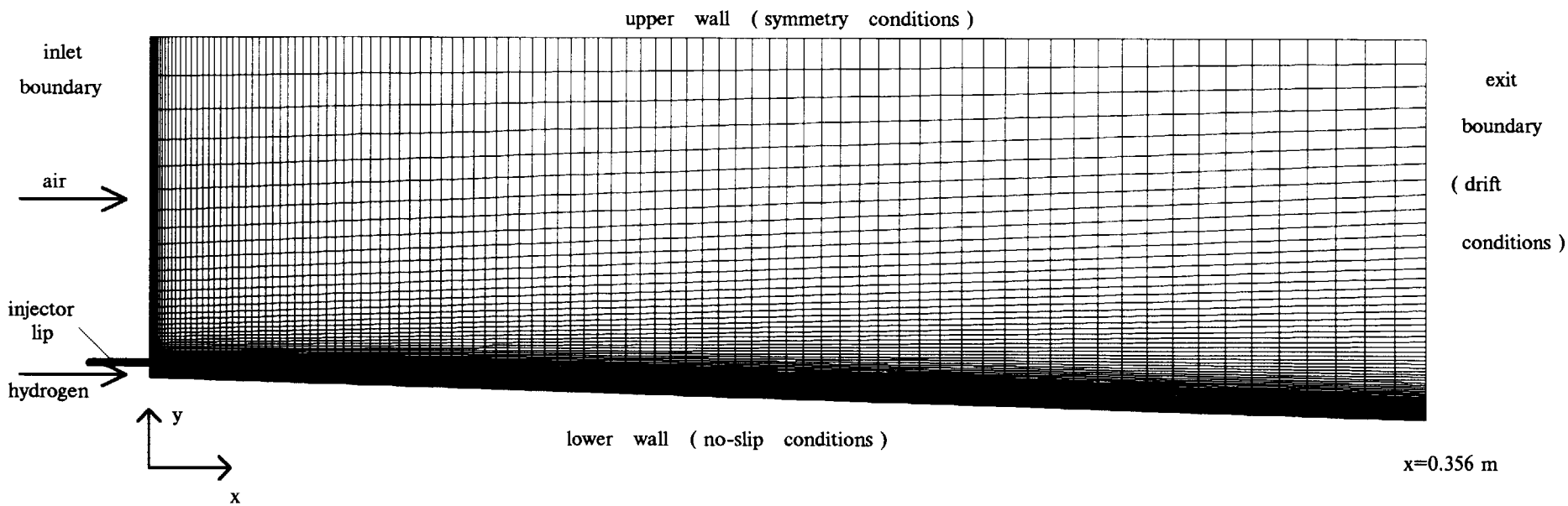

Fig.27. Computational domain together with grid (90x100 cells)

Burrows - Kurkov Test Case

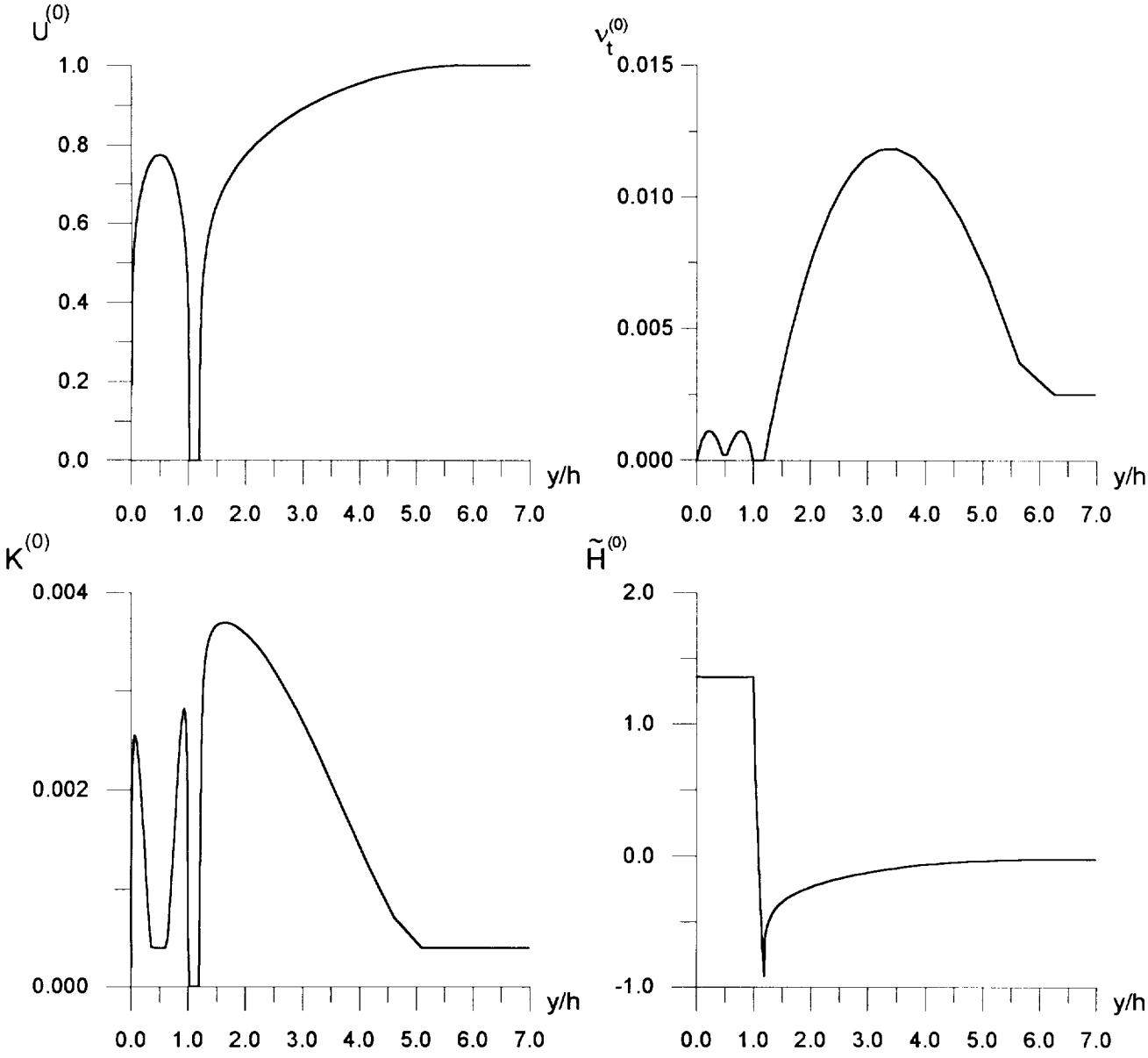

Fig.28. Profiles at the inlet boundary.
Burrows – Kurkov test case.

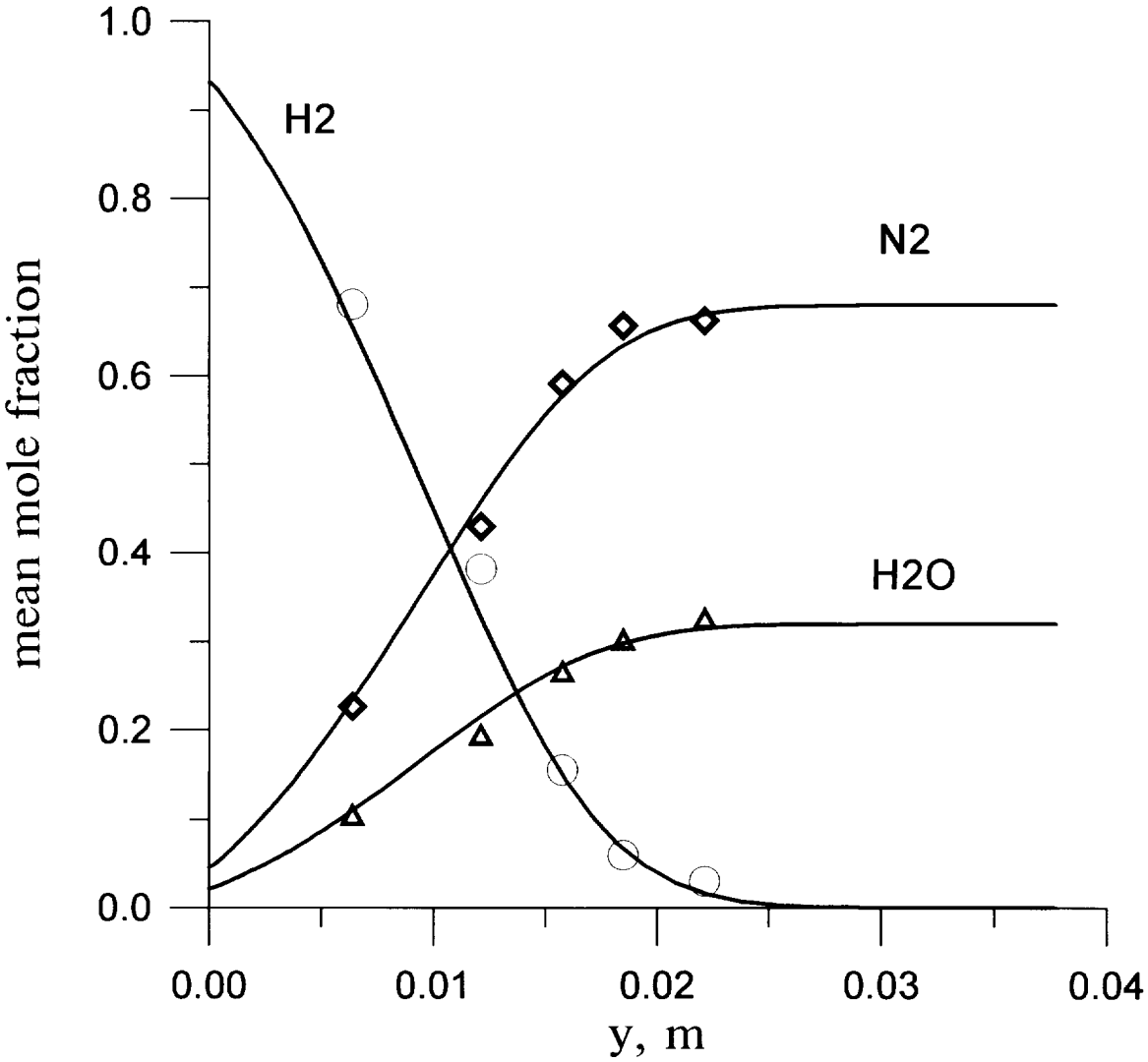

Fig.29. Composition profiles for pure mixing regime (hydrogen/inert gas). x=0.356 m.

FL calculations

H_2

N_2

H_2O

experimental data

Burrows-Kurkov test case.

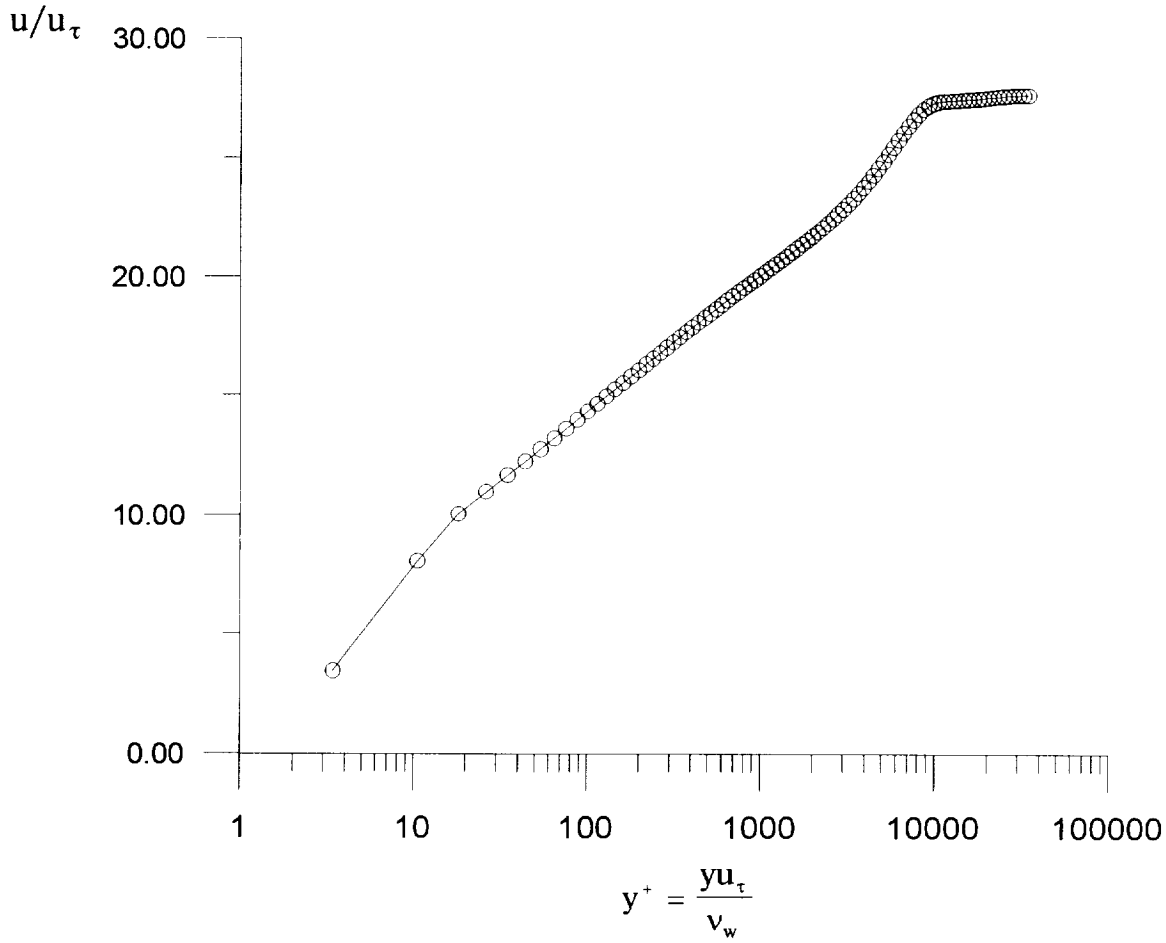

Fig.30. Velocity profile resolution in the vicinity of the lower duct wall.
Exit cross section (x=0.356m).
FL approach.
O - cell centers location.
Burrows-Kurkov test case.

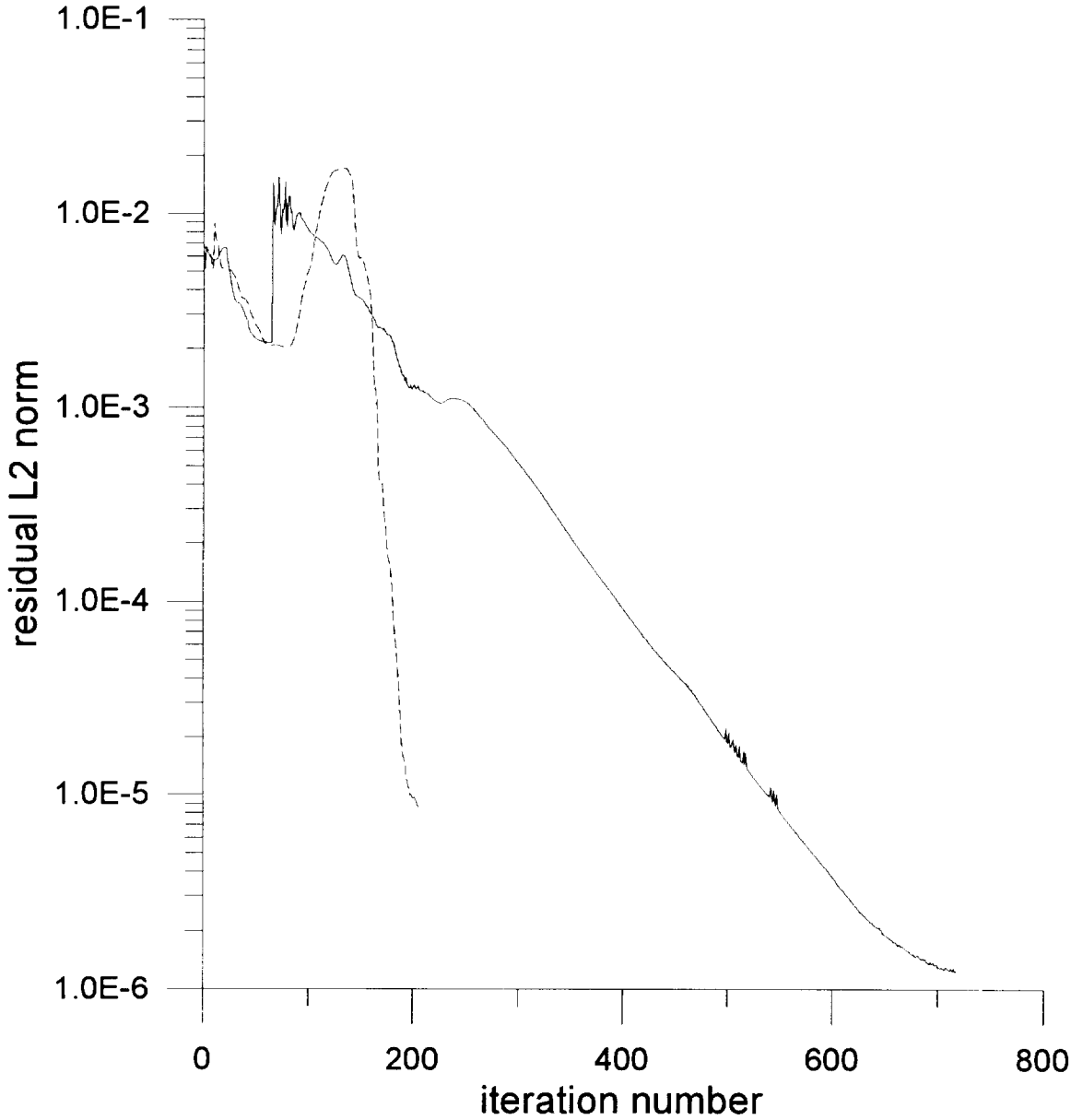

Fig.31. Convergence history.

——— FL approach

- - - - - QL approach

Burrows – Kurkov test case.

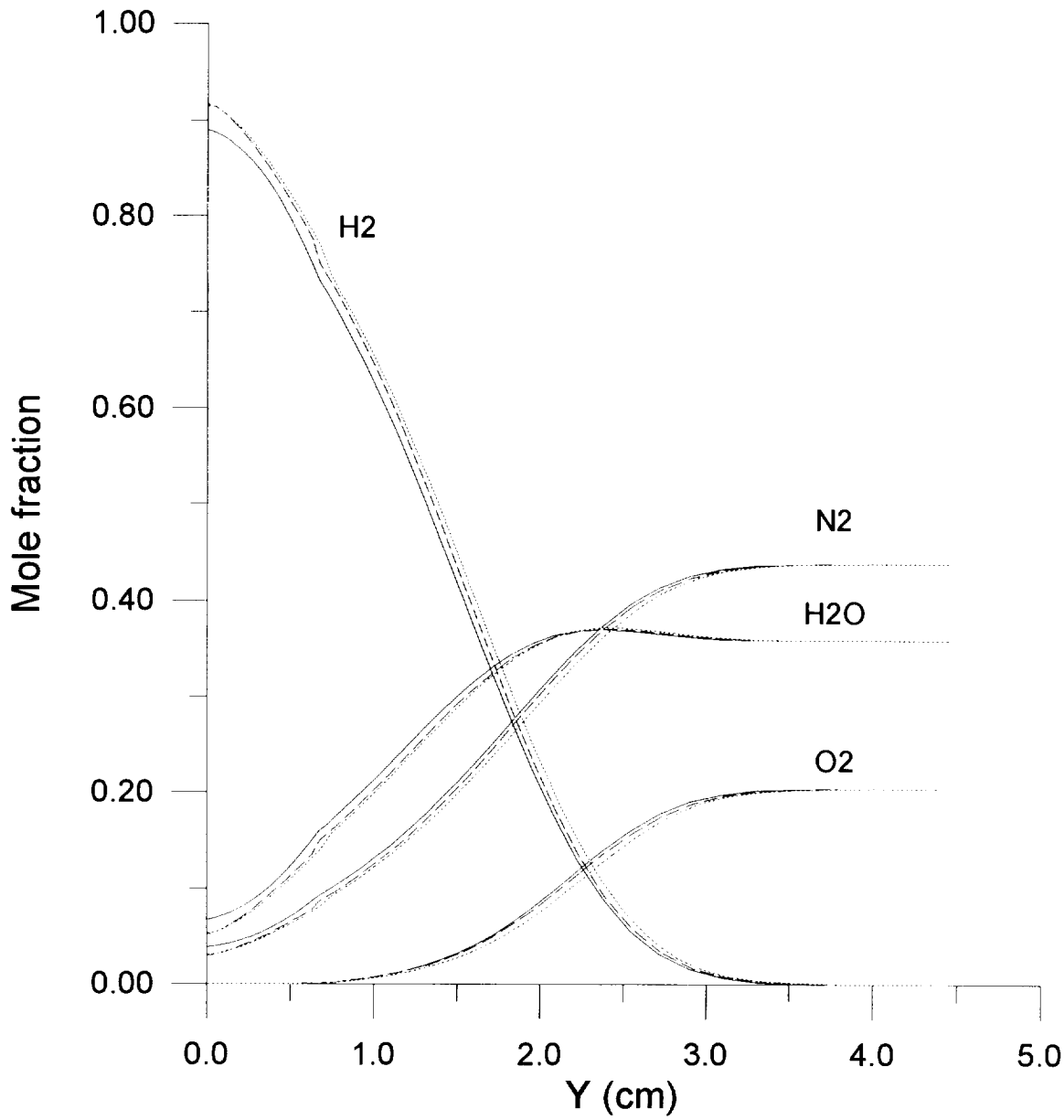

Fig.32a. Influence of discretization on result of FL predictions for species mole fractions.

——— 90x100 grid

- - - - - 90x300 grid

..... 90x300 adaptive grid

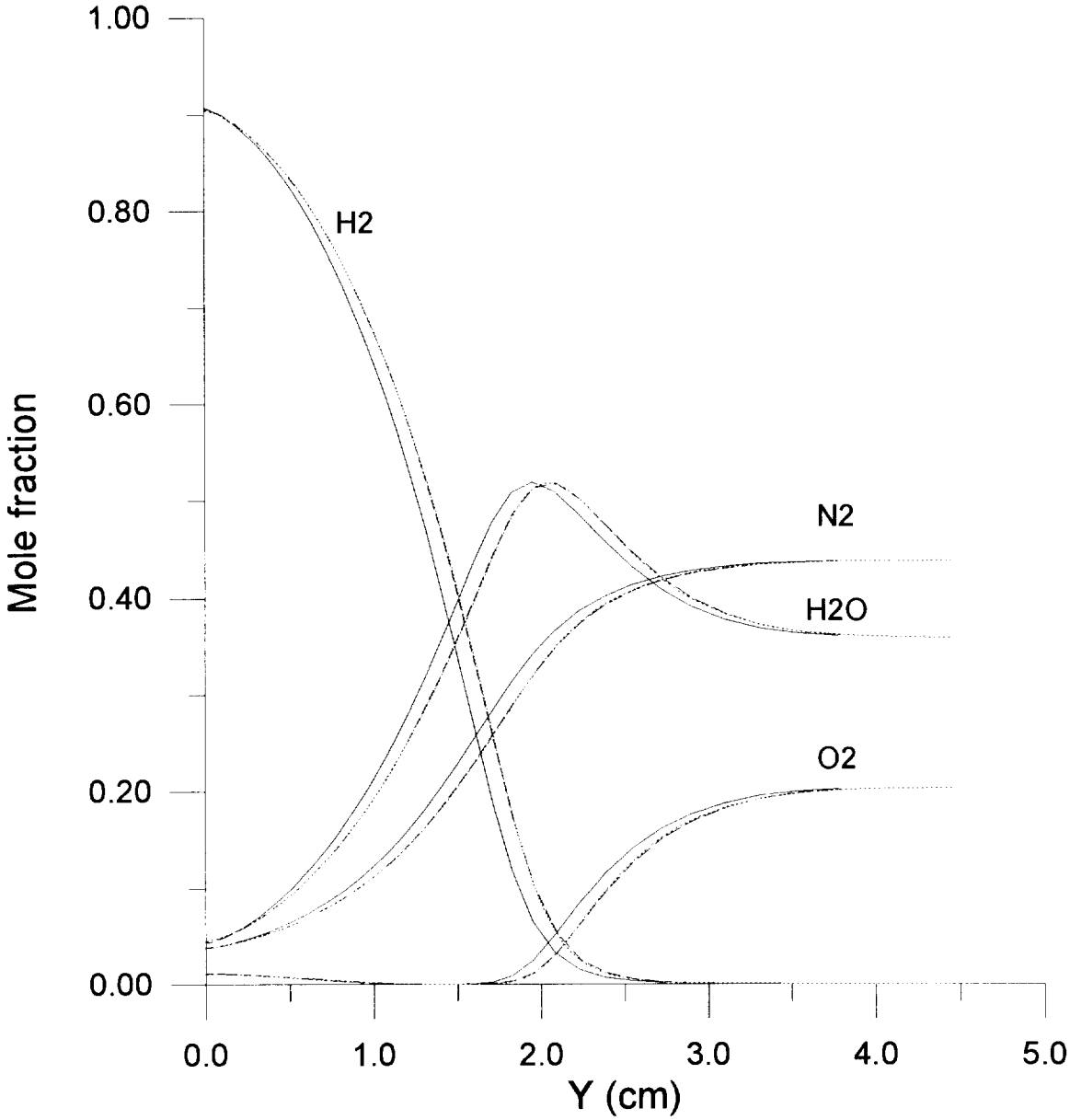

Fig.32b. Influence of discretization on result of QL predictions for species mole fractions.

——— 90x100 grid

- - - - - 90x300 grid

..... 90x300 adaptive grid

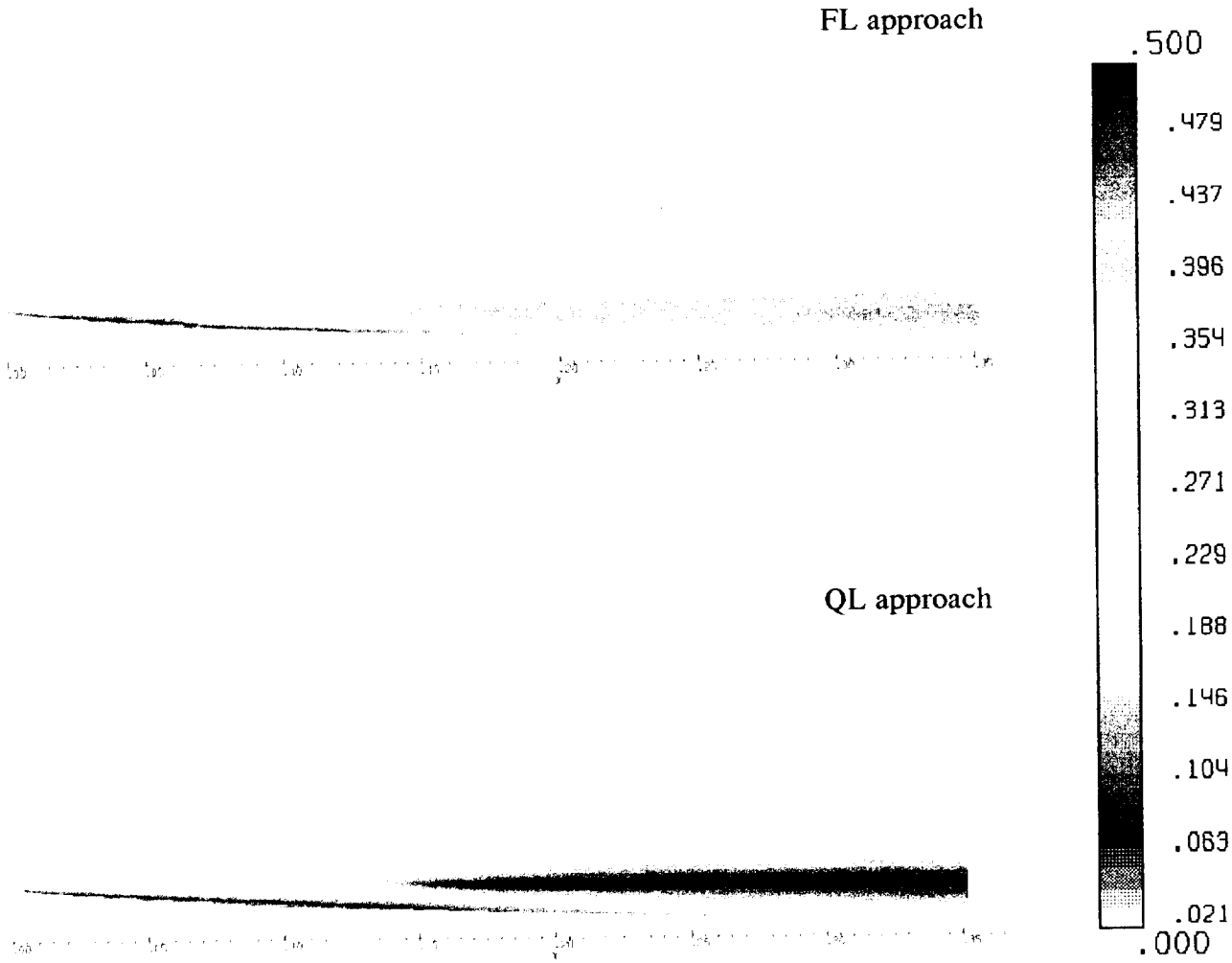

Fig.33. Water-Vapor mass fraction contours obtained in calculations

Burrows - Kurkov test case

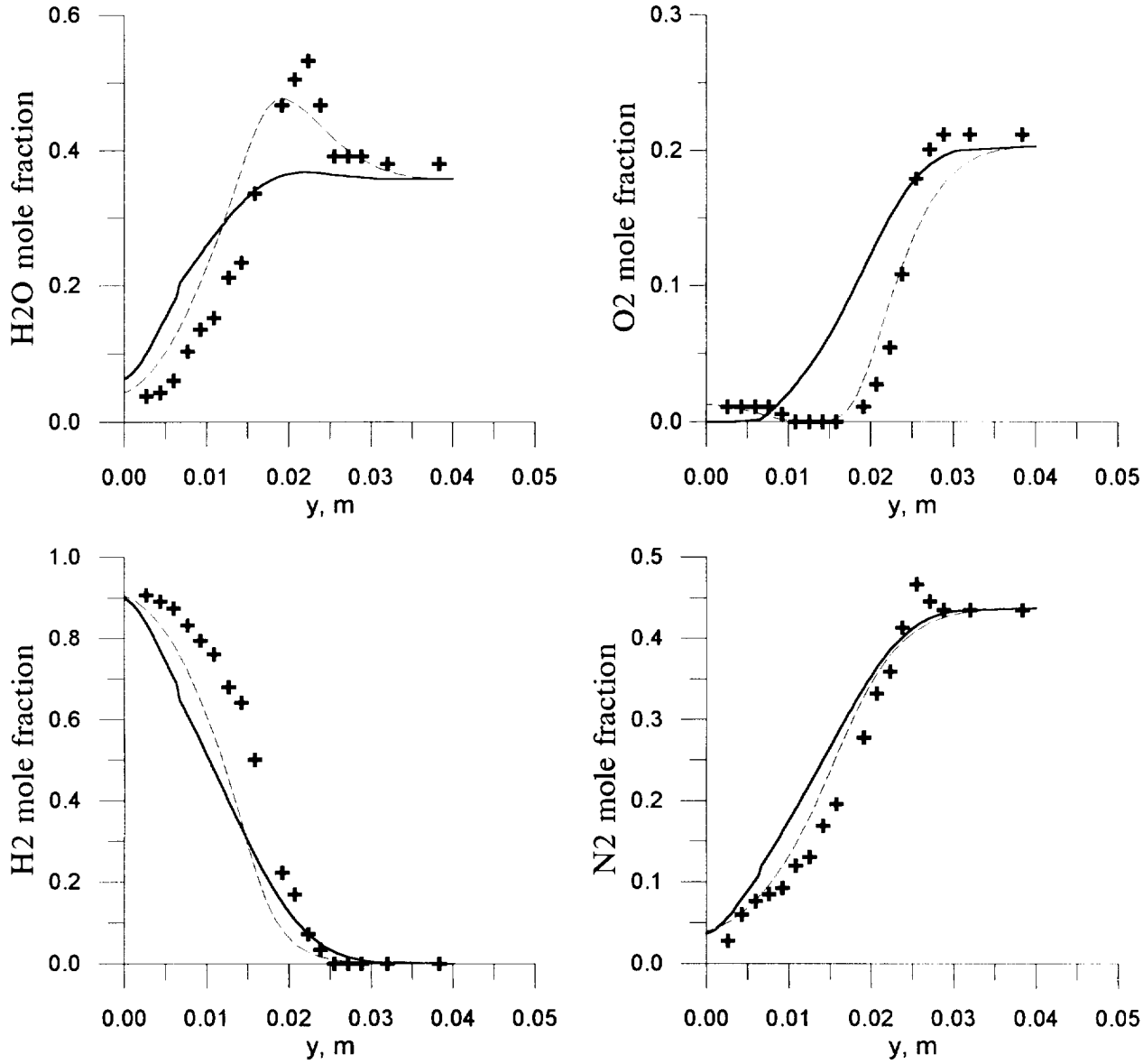

Fig.34. Comparison of FL and QL predictions together with experimental data. x=0.356 m.

——— FL approach

- - - - - QL approach

✚ experimental data

Burrows-Kurkov test case.

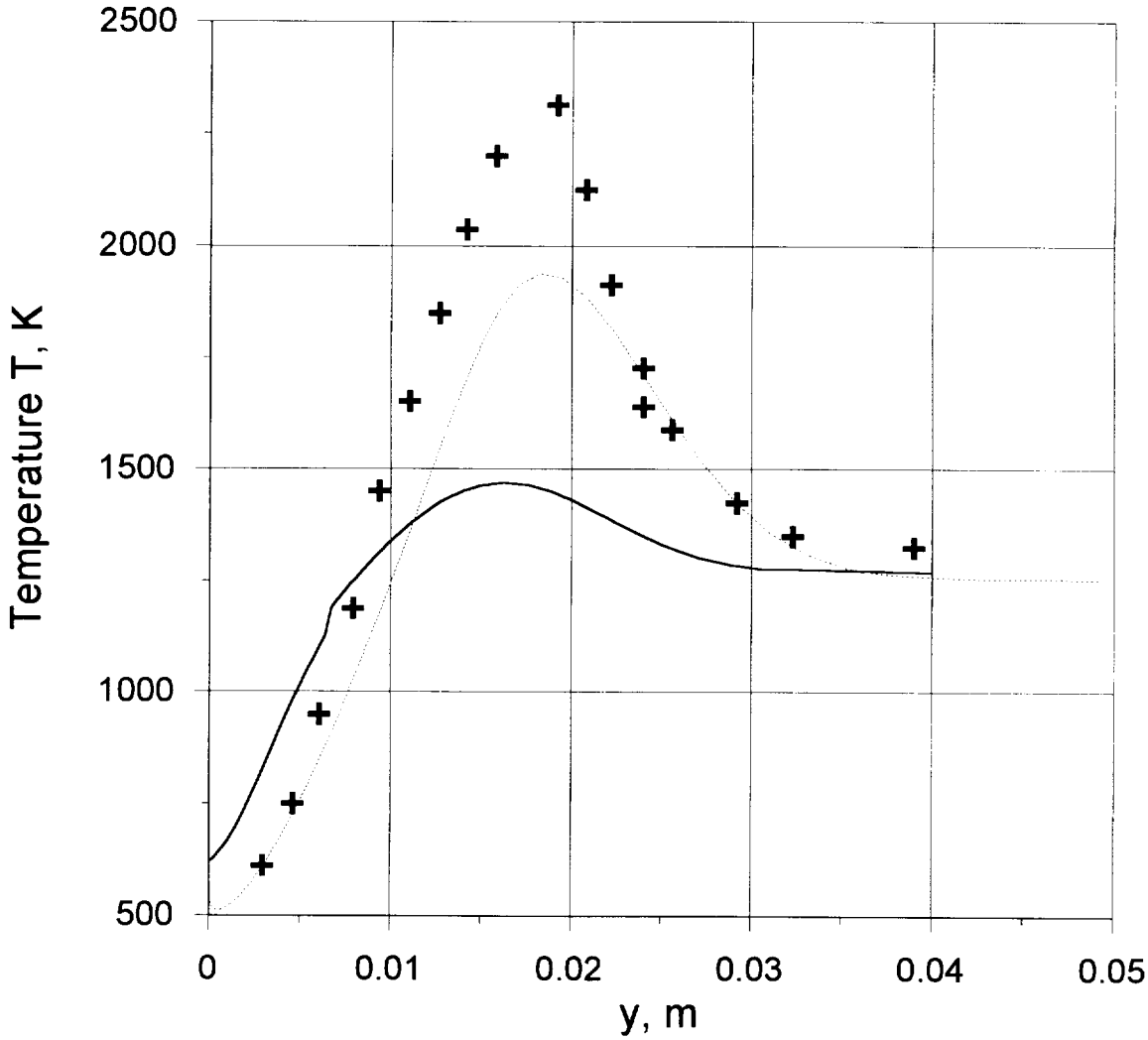

Fig.35. Comparison of FL and QL predictions together with experimental data. x=0.356 m.

FL approach

QL approach

Experimental data

Burrows-Kurkov test case.

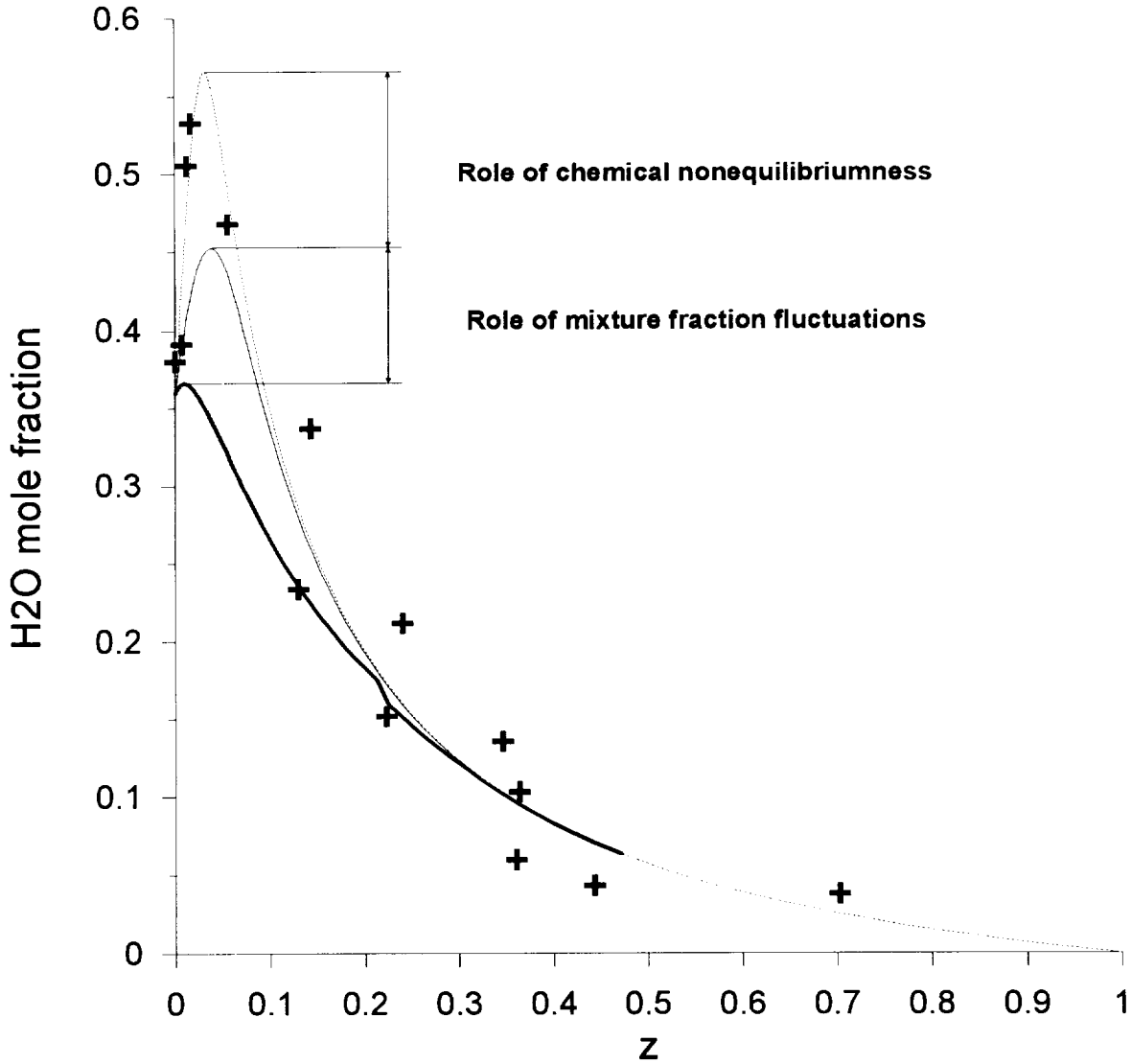

Fig.36. Relative role of the chemical nonequilibriumness/mixture fraction fluctuations in FL approach predictions budget.

Flamelet averaged solution.

Flamelet instantaneous solution.

Equilibrium chemistry limit

Experimental data

Burrows-Kurkov test case.

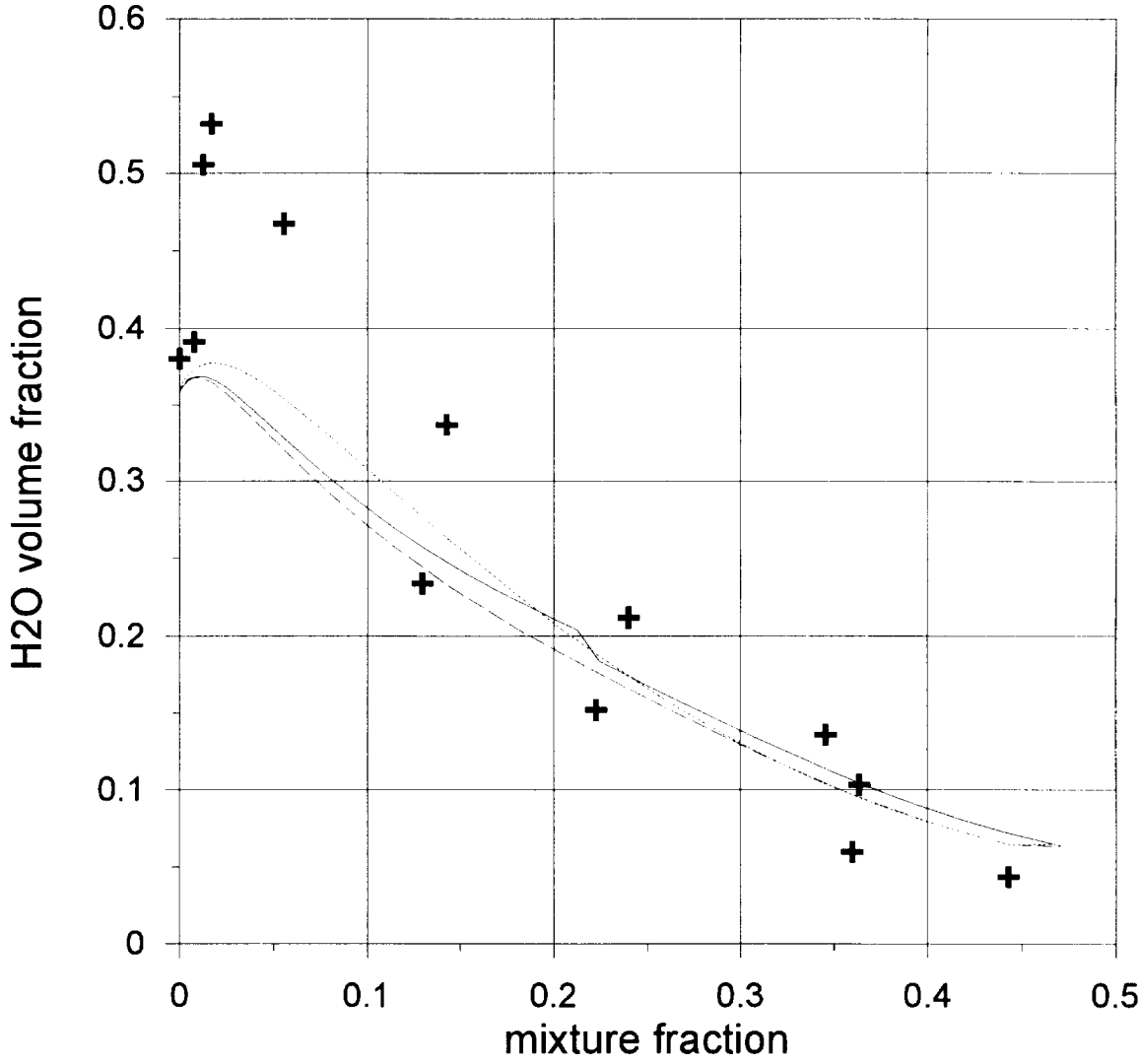

Fig.37. Results sensitivity to variation of pdf shape.

——— Airy/Gaussian P(z) model

- - - - - - "Homogeneous" P(z) model

..... β distribution

✚ Experimental data

Burrows-Kurkov test case.

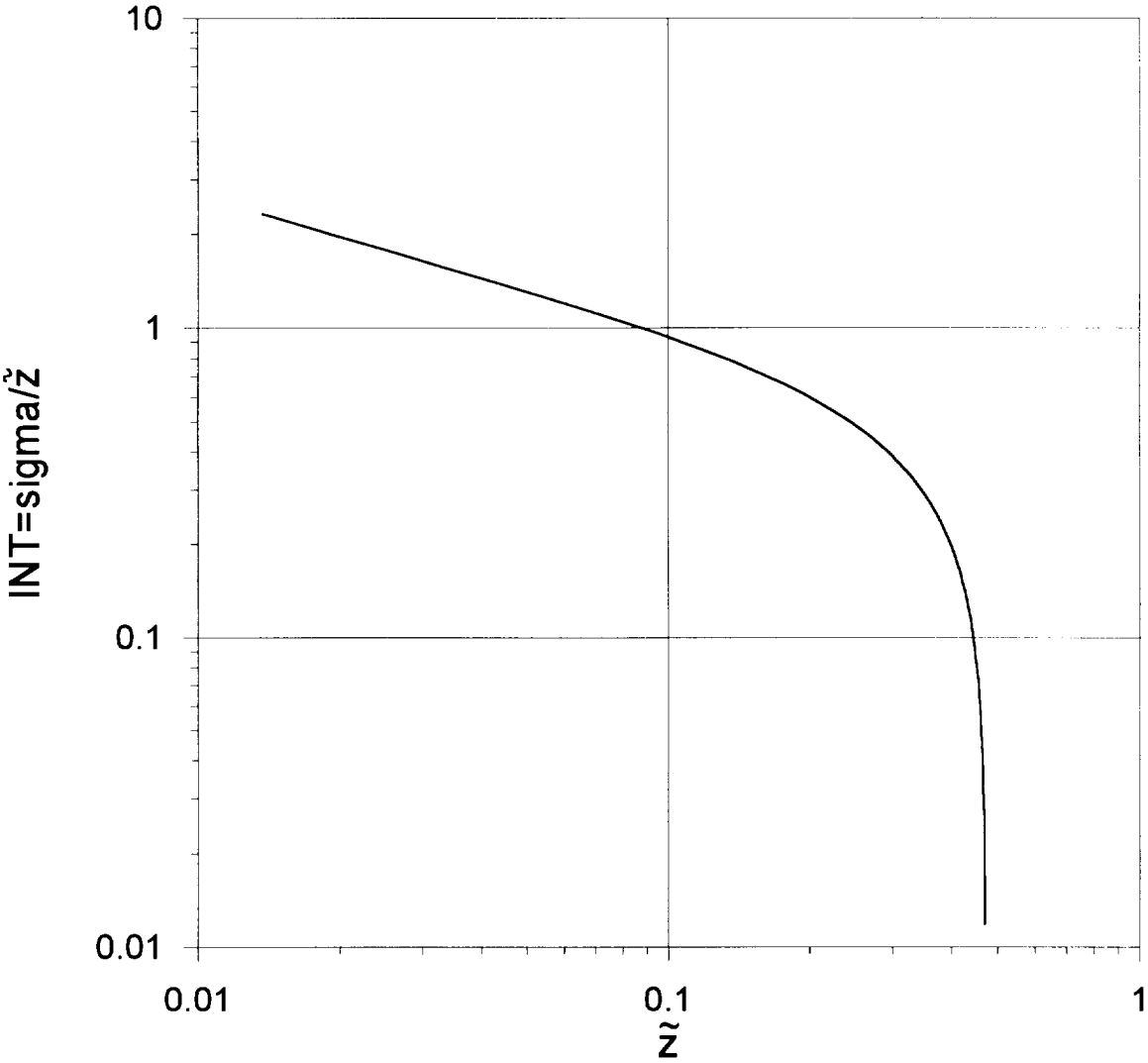

Fig.38. Mixture fraction fluctuations intensity v.s. mean mixture fraction $\tilde{z}$.
FL approach.
x=0.356 m cross section.
Burrows-Kurkov test case.

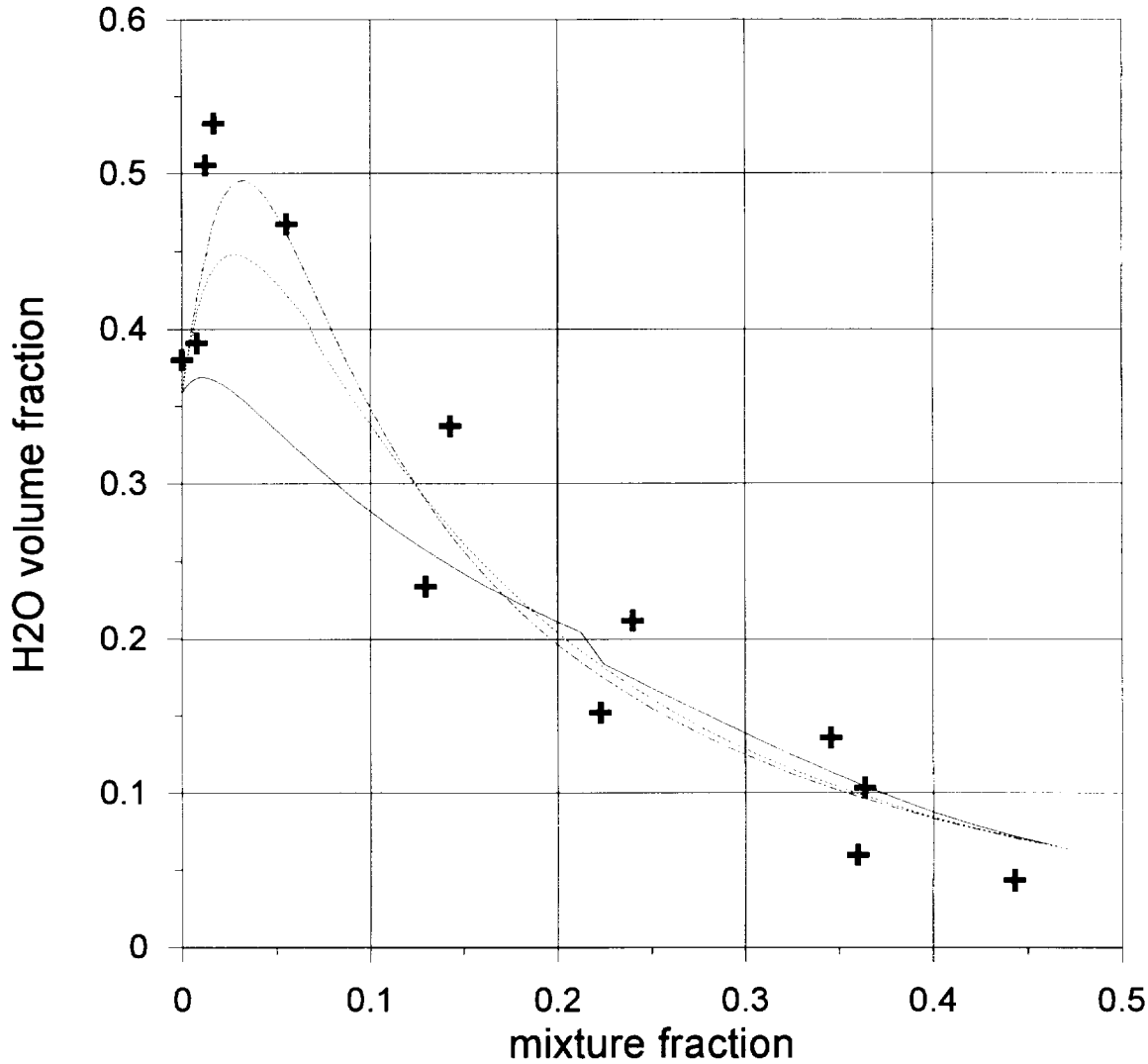

Fig.39. Results sensitivity to the turbulent fluctuations intensity level INT=$\sigma/\tilde{z}$.

$\psi = 1$

$\psi = 0.5$

$\psi = 0.25$

Experimental data

Burrows-Kurkov test case.

TOTAL CPU REQUIREMENTS

Beach Test Case
(SUPNEF PNS code at HP 9000/735)

FLAMELET APPROACH
TOTAL CPU≈5minutes

QUASILAMINAR APPROACH
TOTAL CPU≈7minutes

Burrows-Kurkow Test Case
(FNAS2D NS code with 90X100 grid at HP 9000/735)

FLAMELET APPROACH
TOTAL CPU≈2hours

QUASILAMINAR APPROACH
TOTAL CPU≈3.5hours

WEIGHT OF FL LIBRARY PRODUCTION IN TOTAL CPU REQUIREMENTS

Beach Test Case

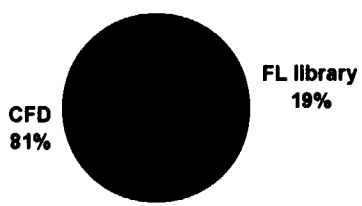

Burrows-Kurkow Test Case

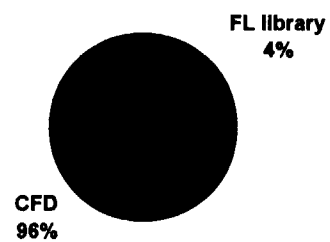

Fig.40. Computational expences.

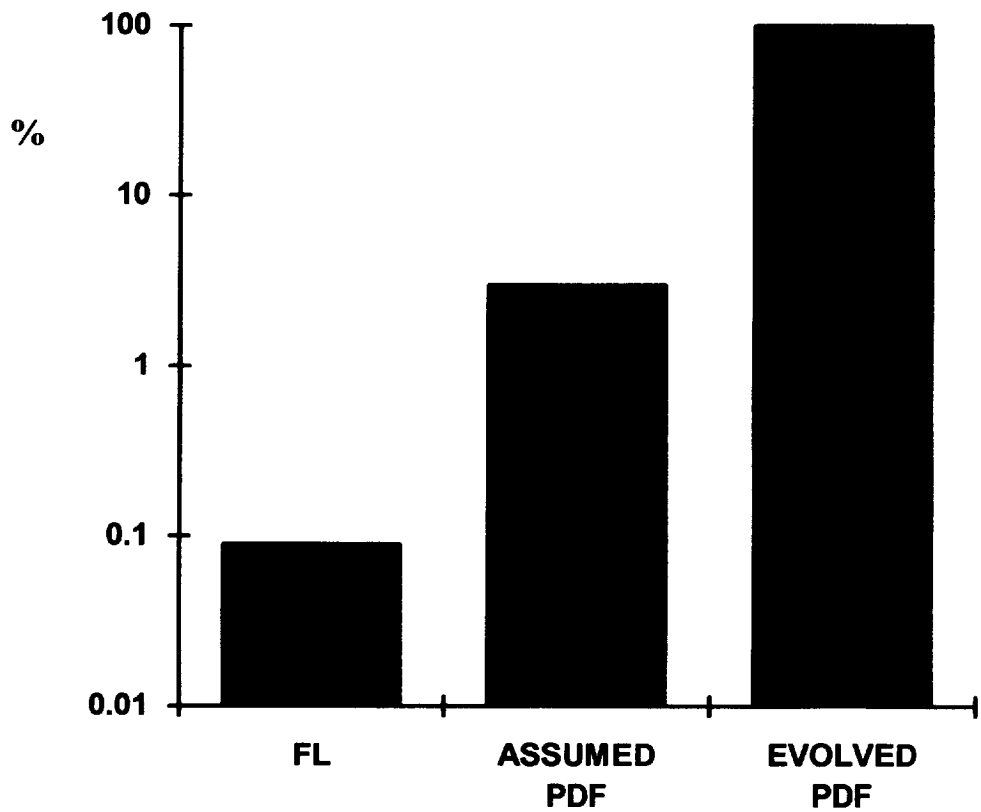

Fig.41. Comparative estimation of computational expences.
Beach test case.

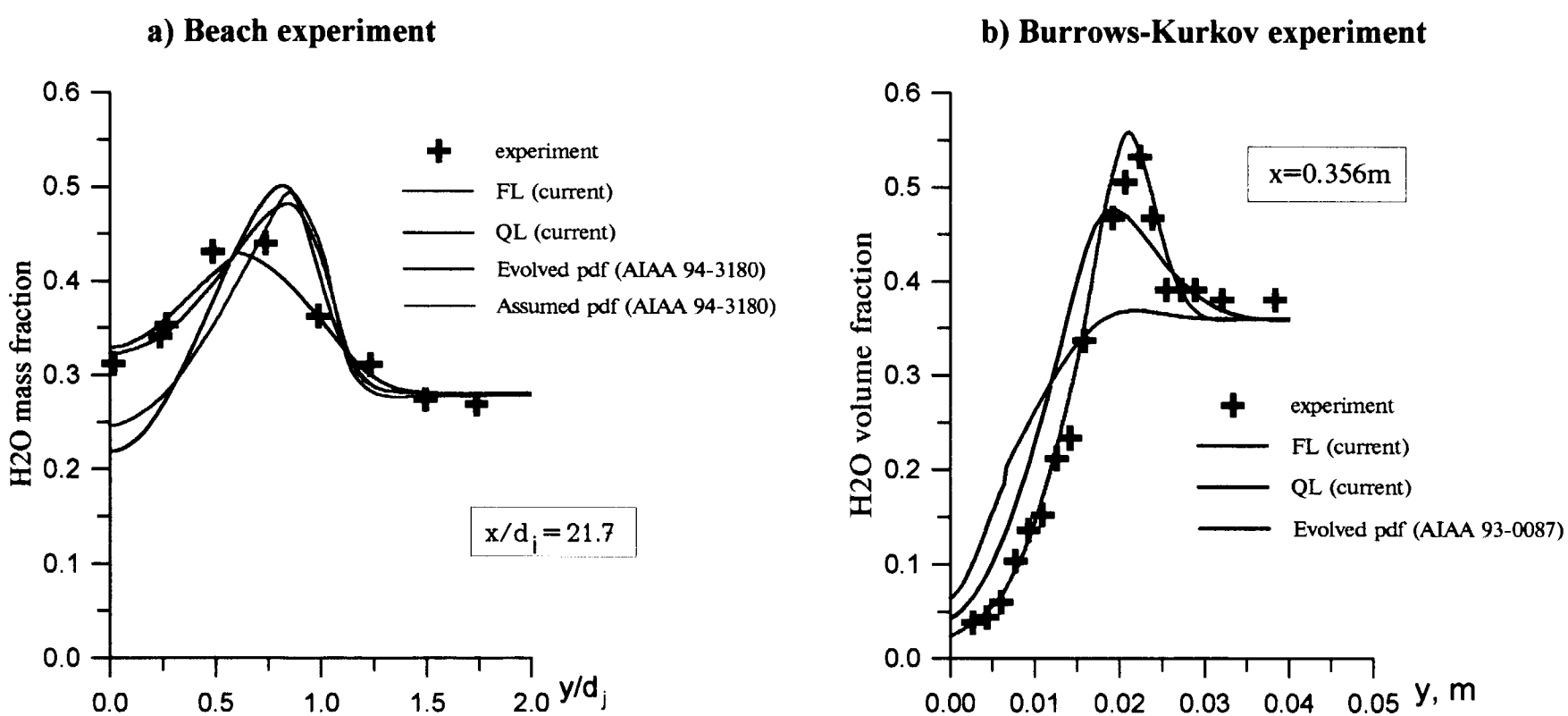

Fig.42. Accuracy of FL predictions.

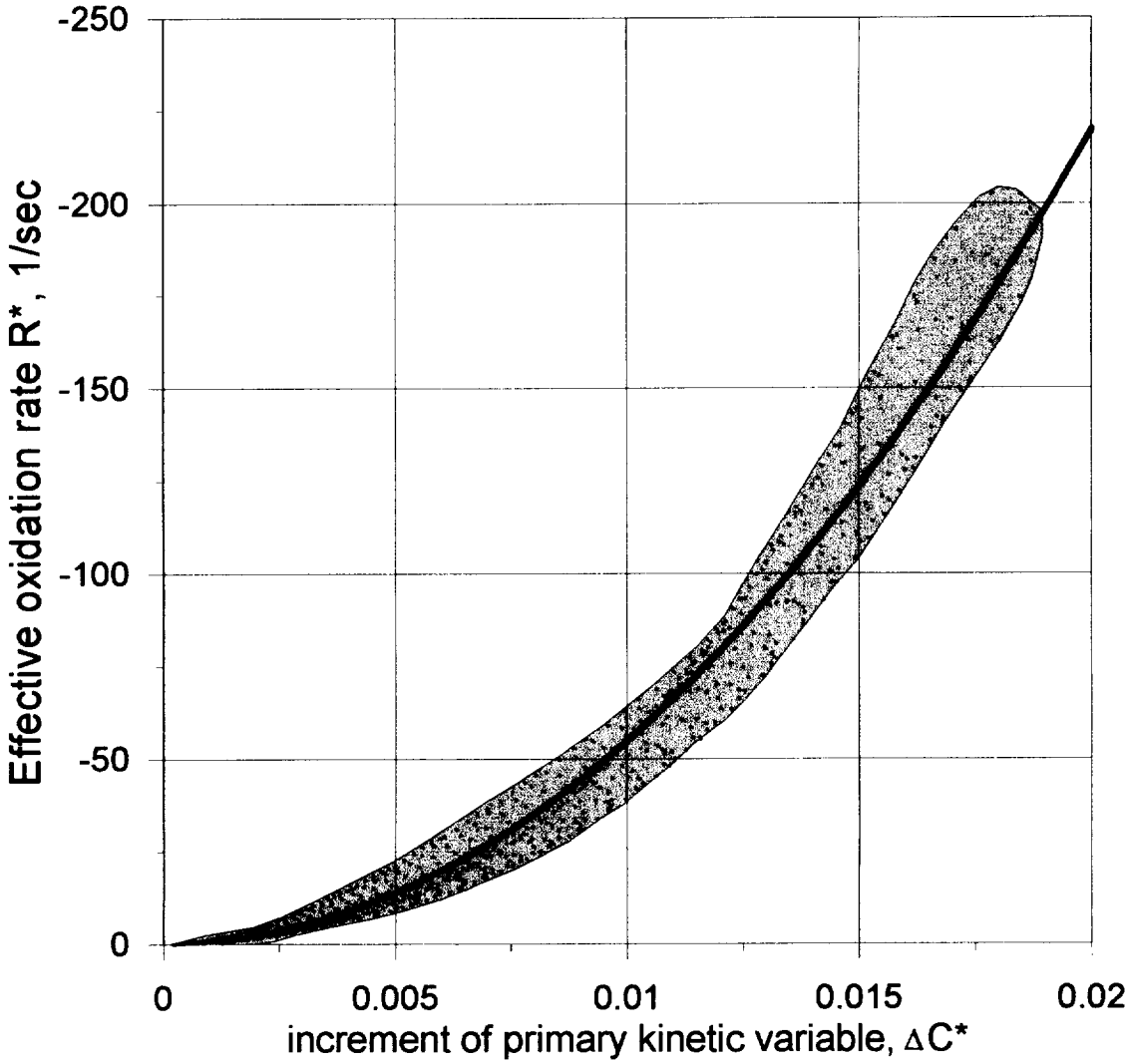

Fig.43. Accuracy of approximate relation for effective oxidation rate.
$0<N^s<100$ sec ; P=0.1 MPa

FL calculations based on detailed kinetics of Appendix C (both Beach and Burrows—Kurkov test conditions)

approximate relation (III.17)

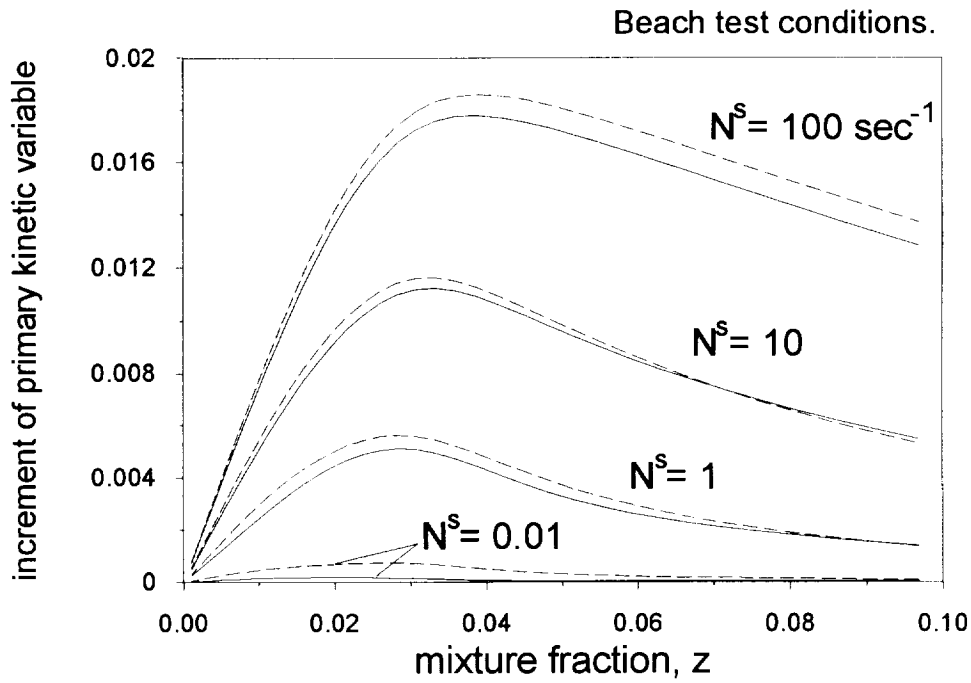

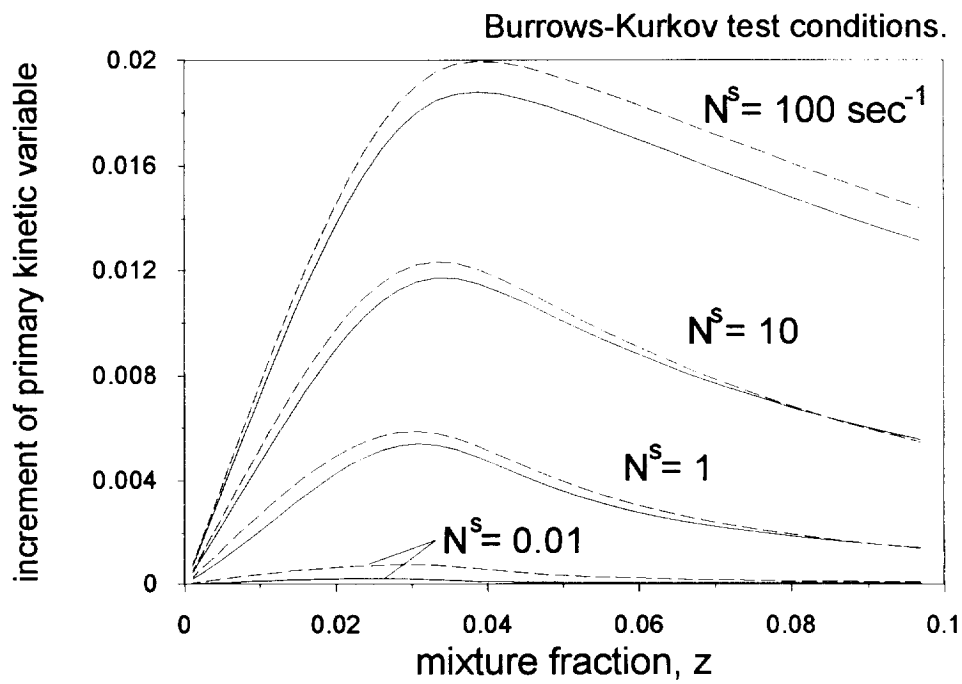

Fig.44. Accuracy of ΔC^* calculations based on approximation (III.17).

——— accurate FL solution

- - - - - simplified PEq method

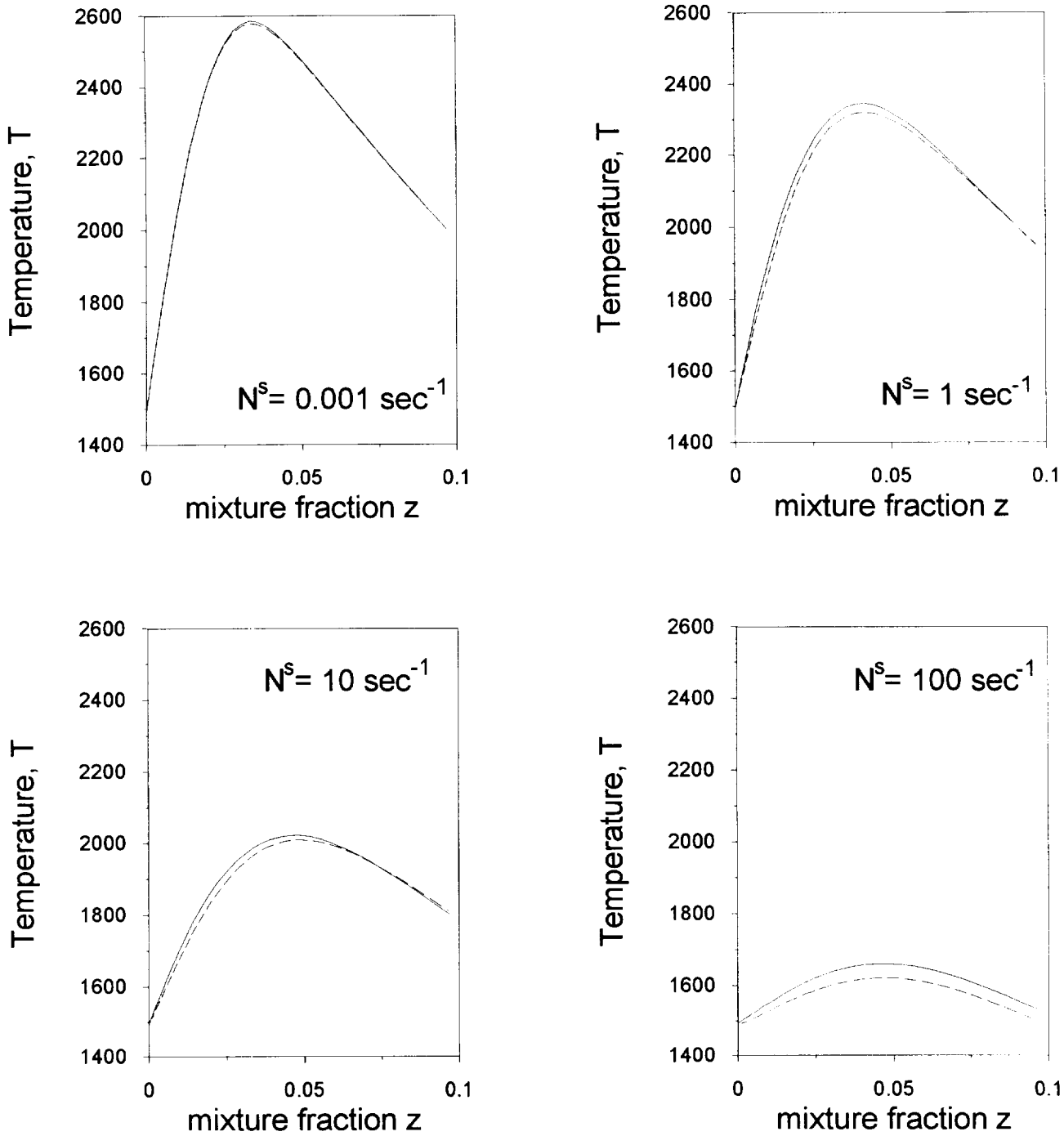

Fig.45a. Accuracy of simplified PEq method.

——— accurate FL solution

------ simplified PEq method

Beach test conditions.

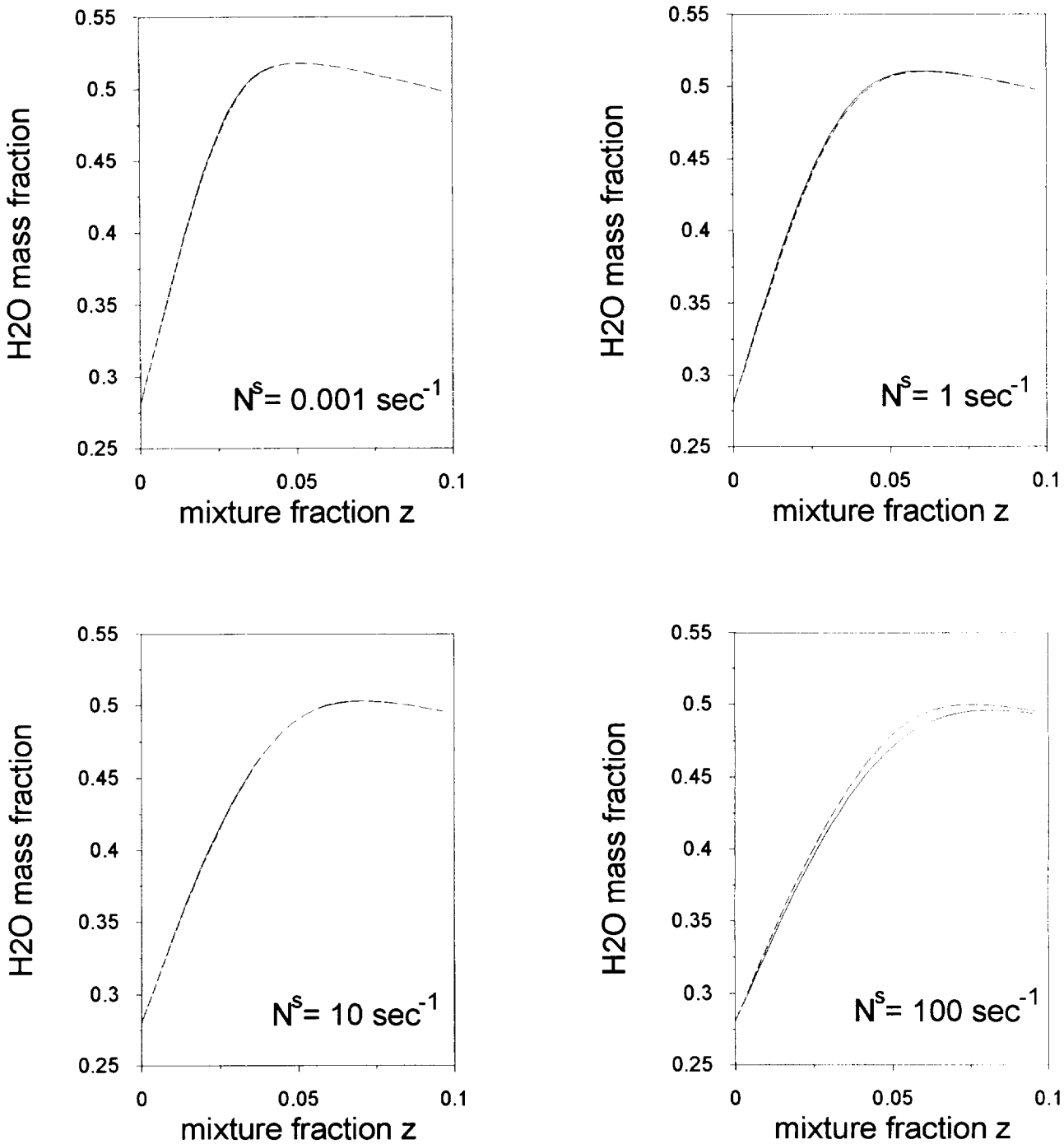

Fig.45b. Accuracy of simplified PEq method.

——— accurate FL solution

- - - - - simplified PEq method

Beach test conditions.

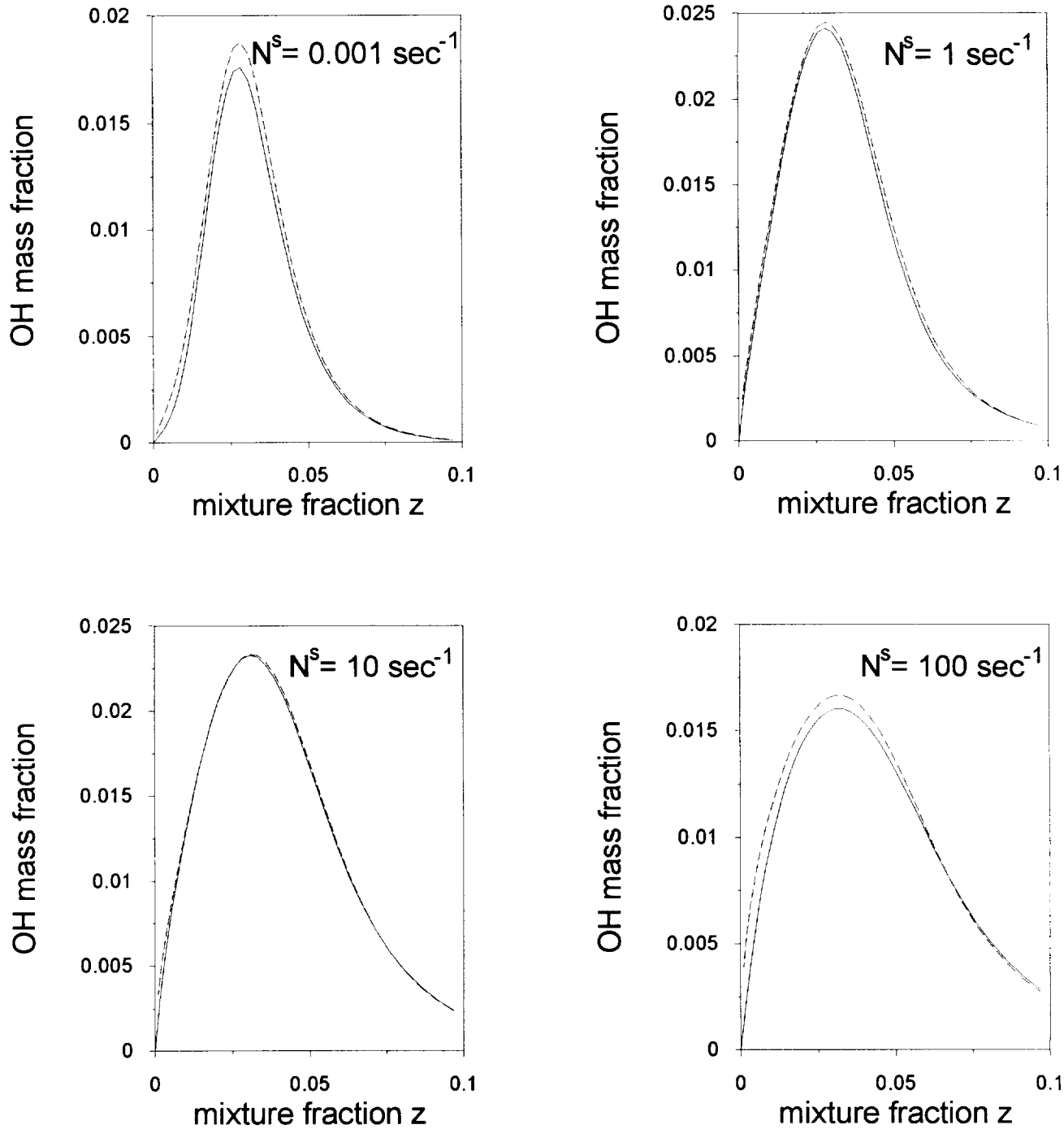

Fig.45c. Accuracy of simplified PEq method.

——— accurate FL solution

- - - - - - simplified PEq method

Beach test conditions.

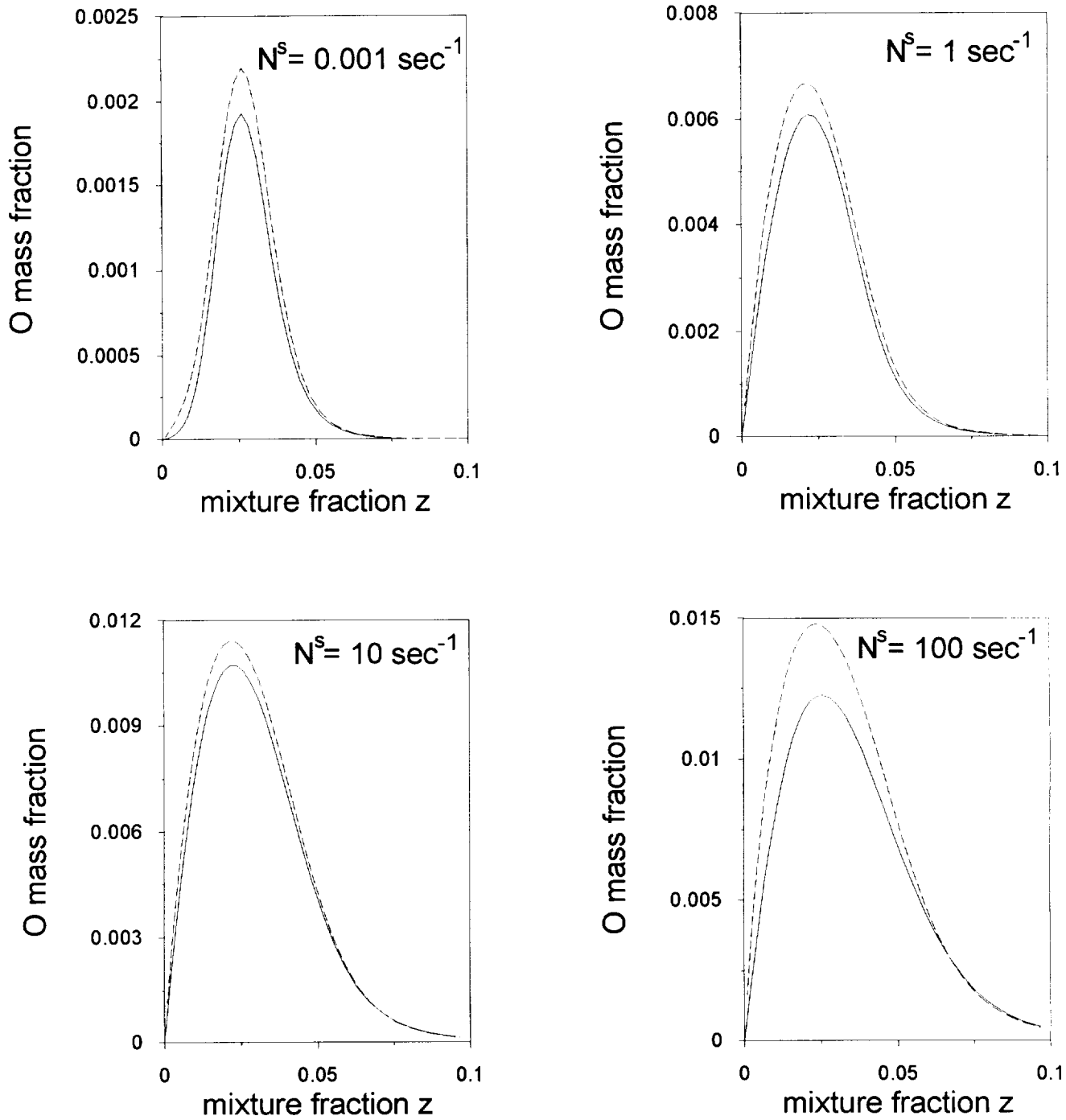

Fig.45d. Accuracy of simplified PEq method.

——— accurate FL solution

- - - - - - simplified PEq method

Beach test conditions.

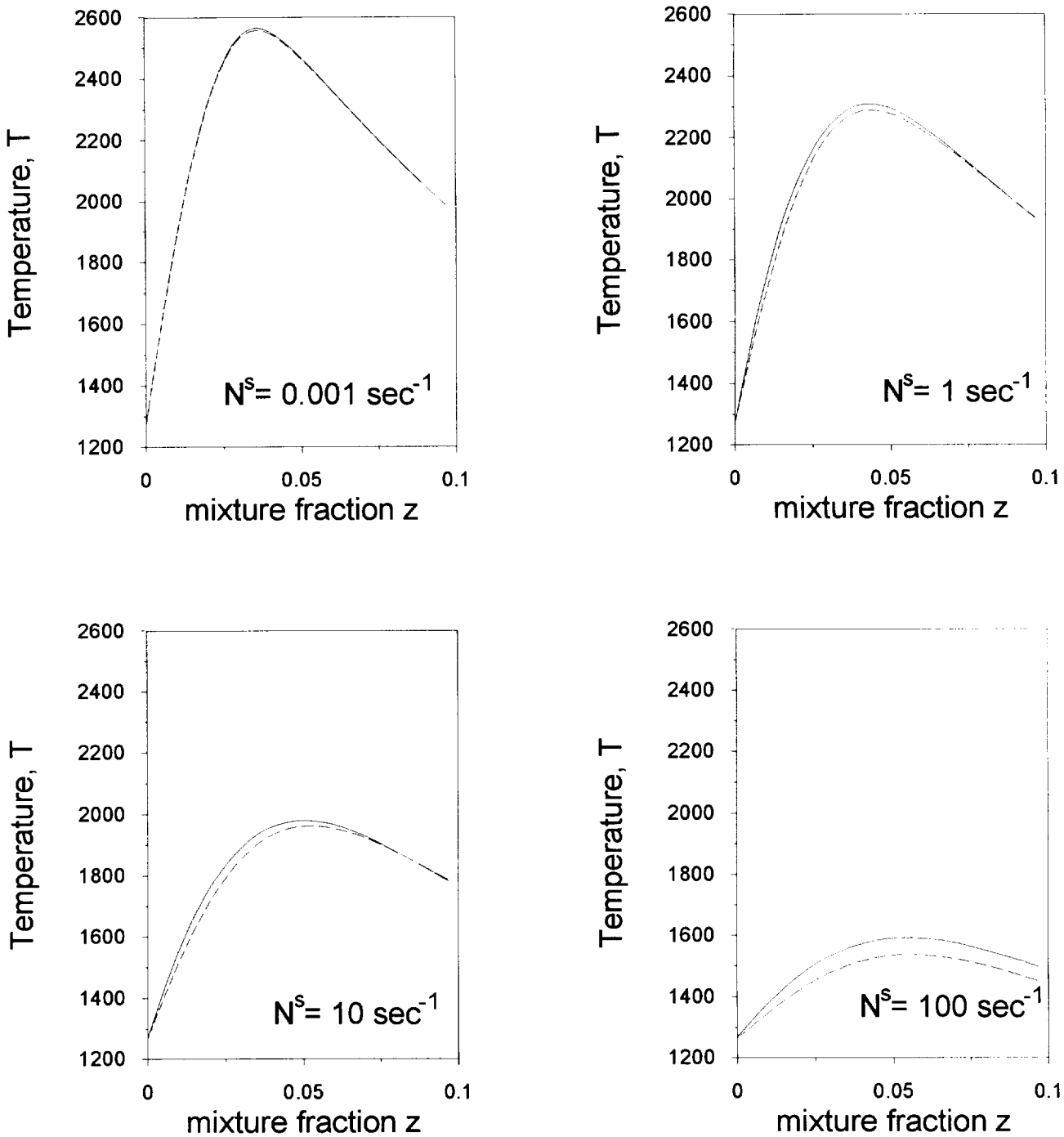

Fig.46a. Accuracy of simplified PEq method.

——— accurate FL solution

- - - - - simplified PEq method

Burrows—Kurkov test conditions.

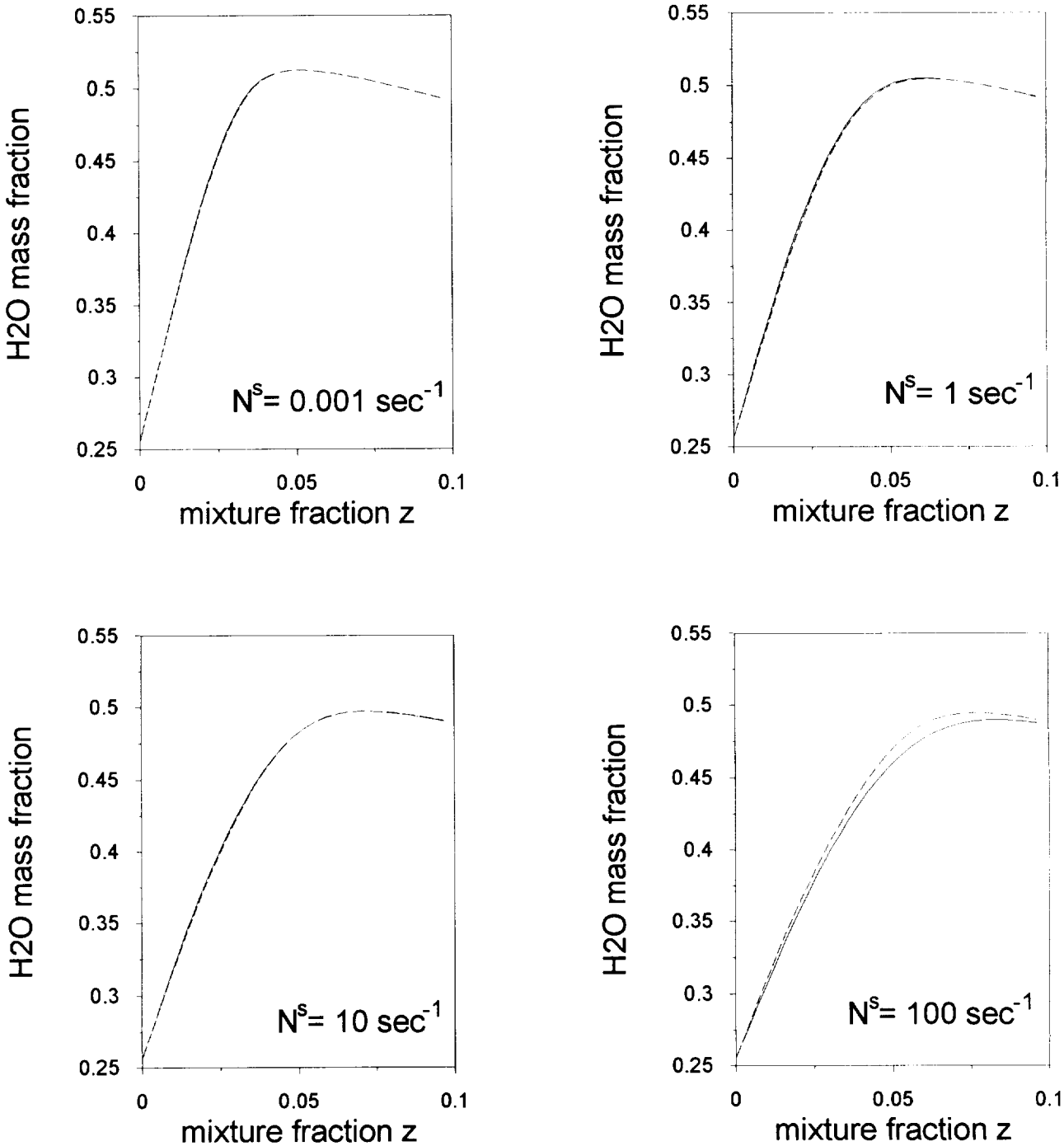

Fig.46b. Accuracy of simplified PEq method.

——— accurate FL solution

- - - - - - simplified PEq method

Burrows – Kurkov test conditions.

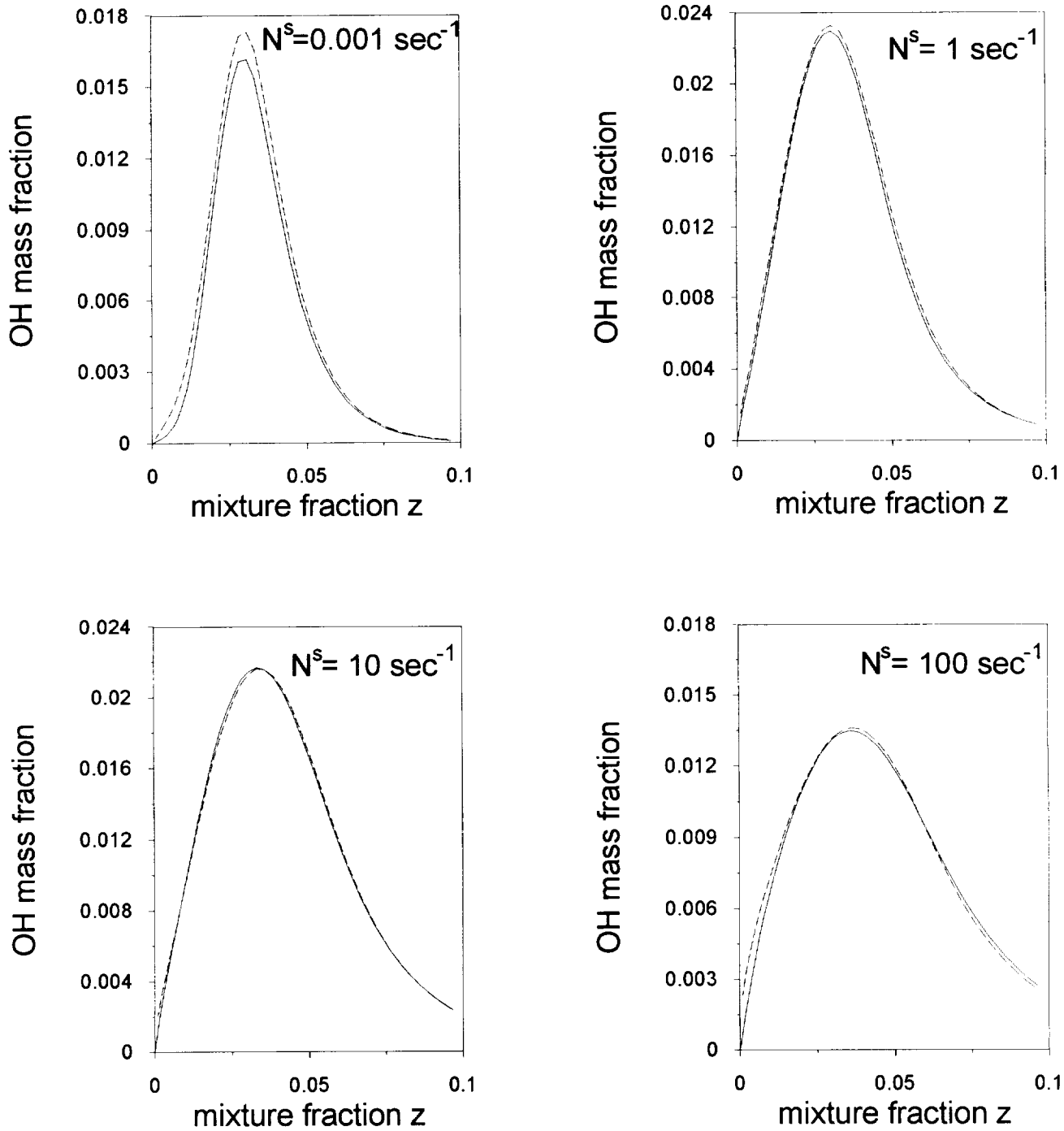

Fig.46c. Accuracy of simplified PEq method.

——— accurate FL solution

- - - - - simplified PEq method

Burrows – Kurkov test conditions.

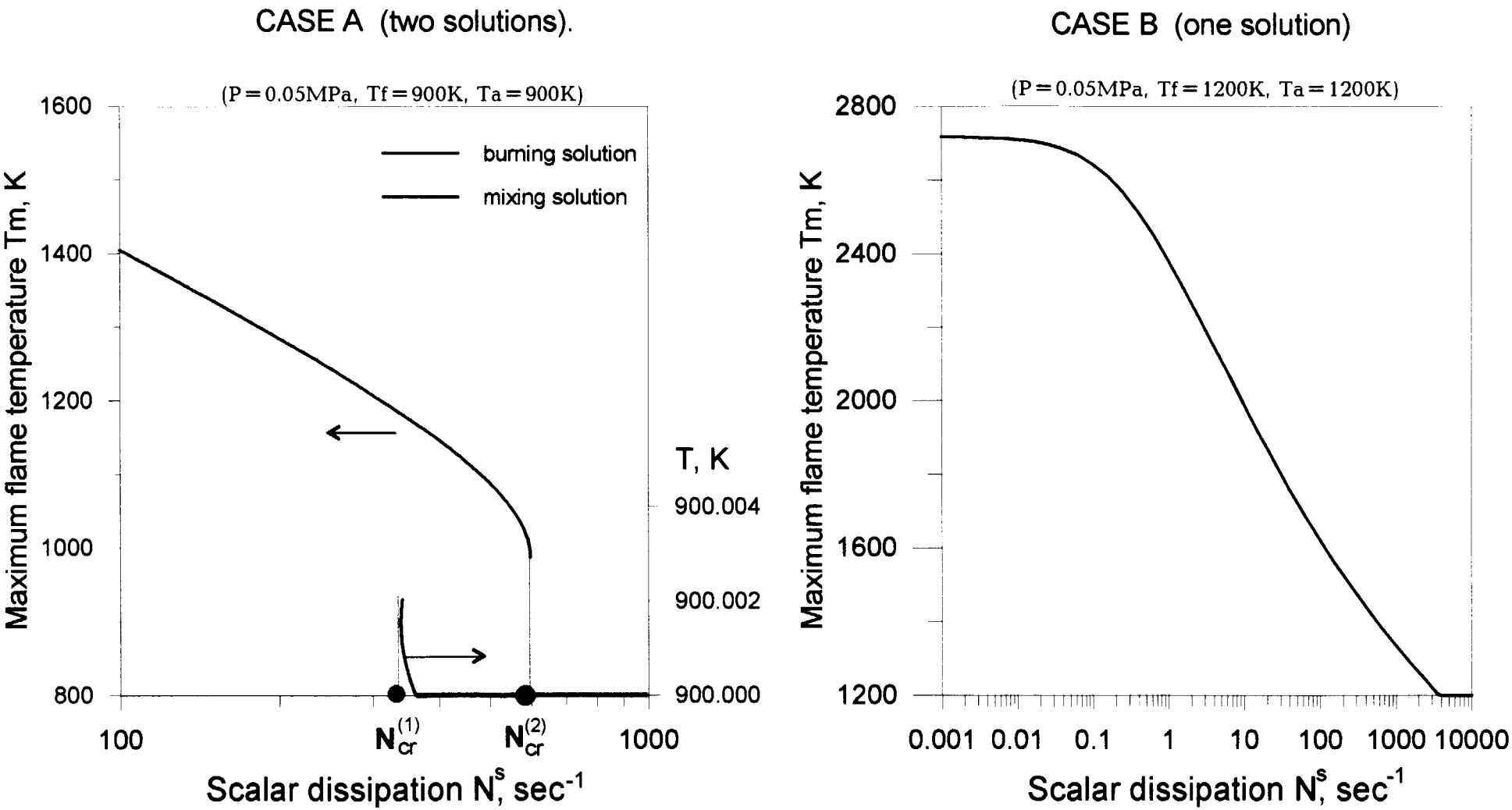

Fig.47. Different combustion modes predicted by flamelet model.

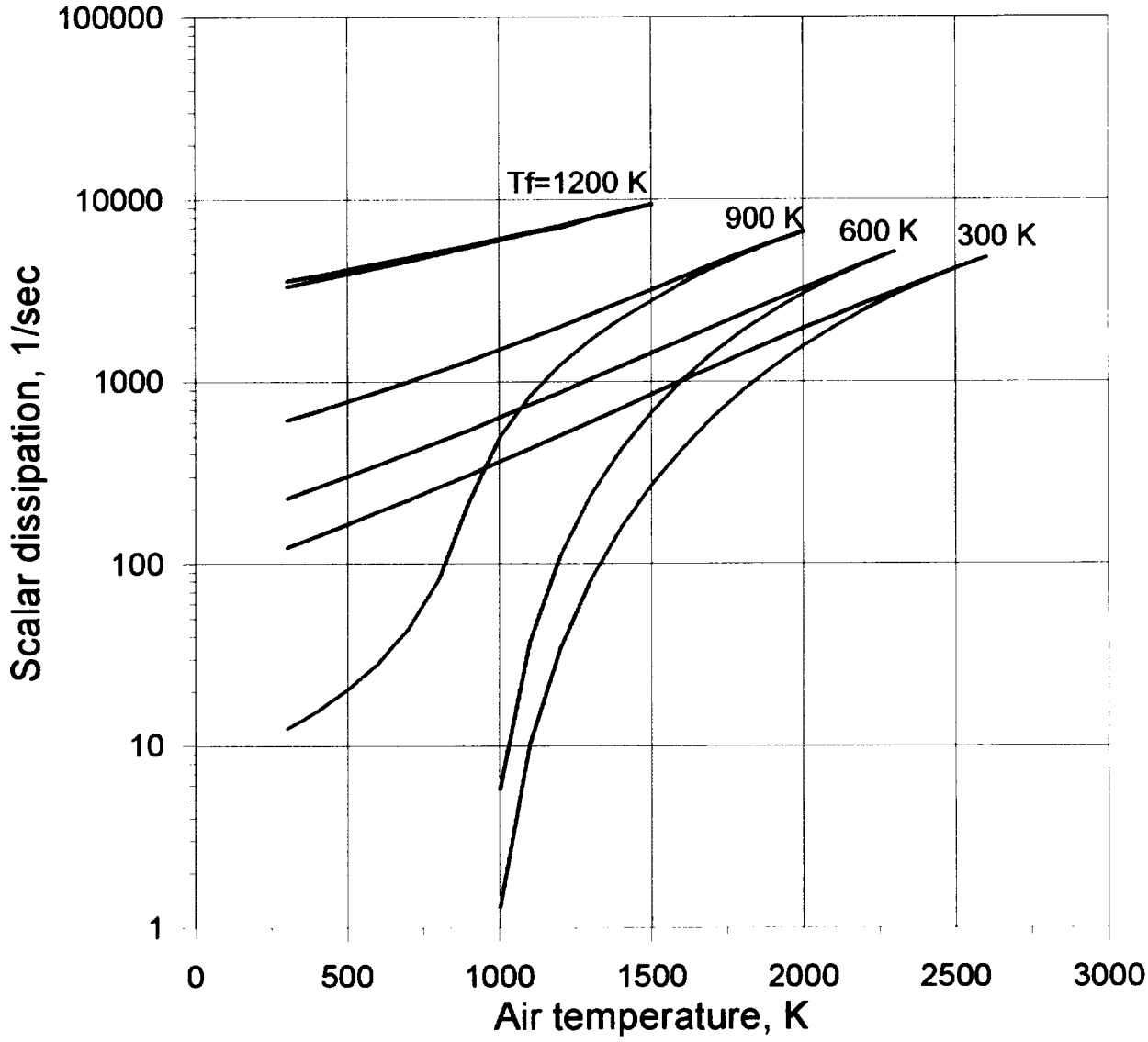

Fig.48a. Critical values of scalar dissipation vs air and fuel temperatures.
P=0.1 MPa

——— $N_{cr}^{(1)}$

——— $N_{cr}^{(2)}$

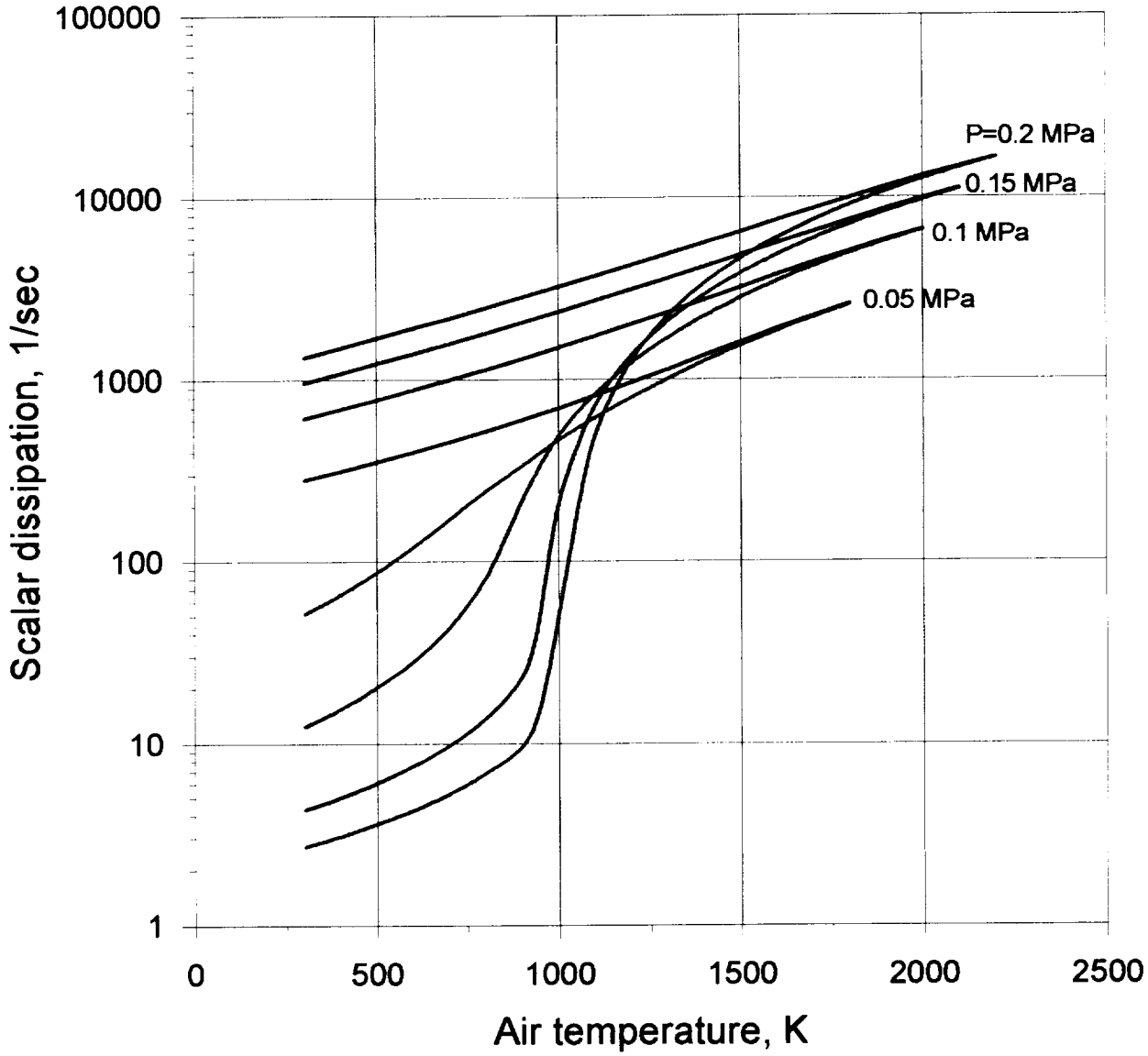

Fig.48b. Pressure influence on $N_{cr}^{(1)}$ and $N_{cr}^{(2)}$.
Tf = 900 K

——— $N_{cr}^{(1)}$

——— $N_{cr}^{(2)}$

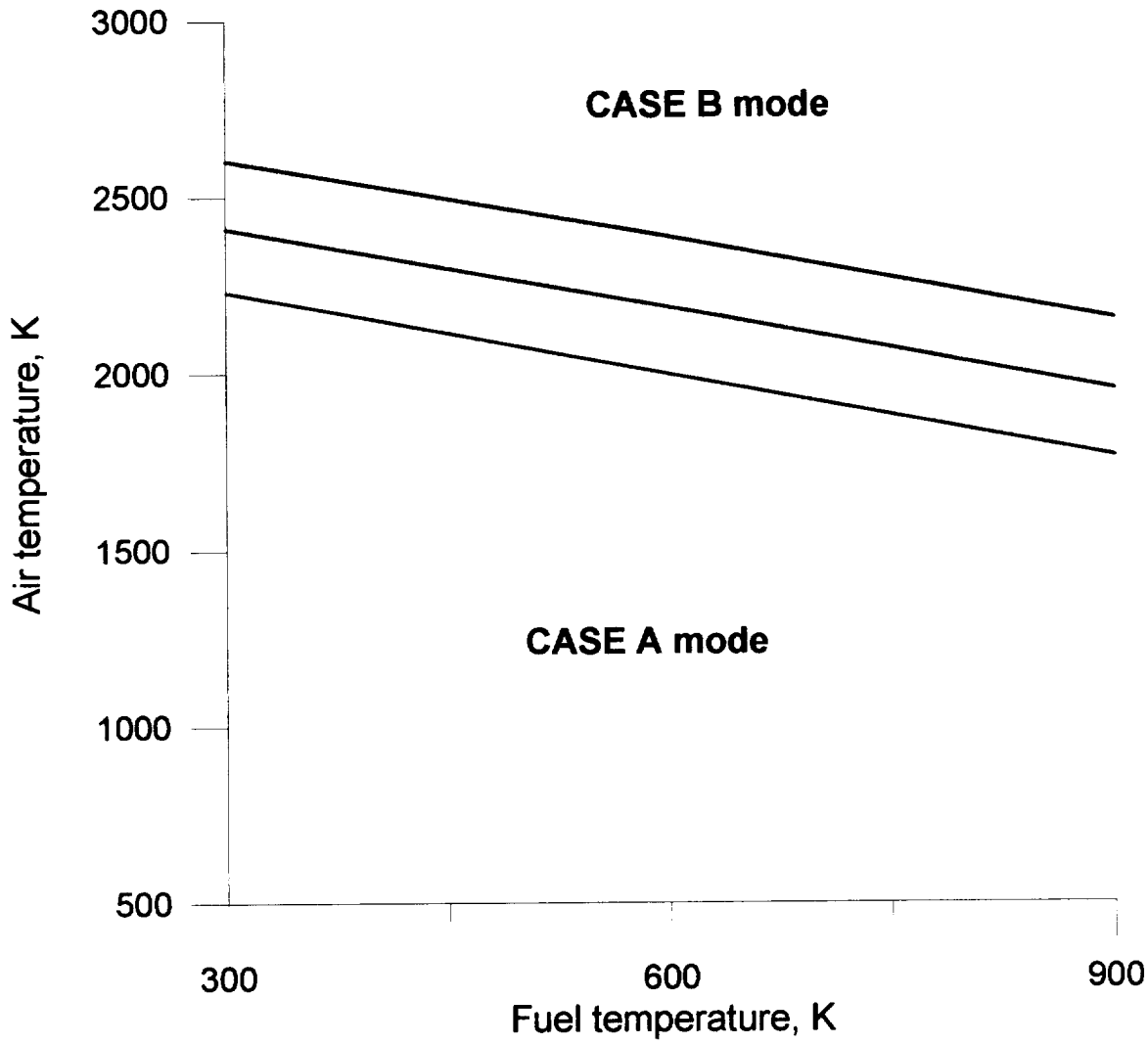

Fig.49. Boundary between combustion modes vs regime parameters.

——— P=0.05 MPa

——— P=0.1 MPa

——— P=0.2 MPa

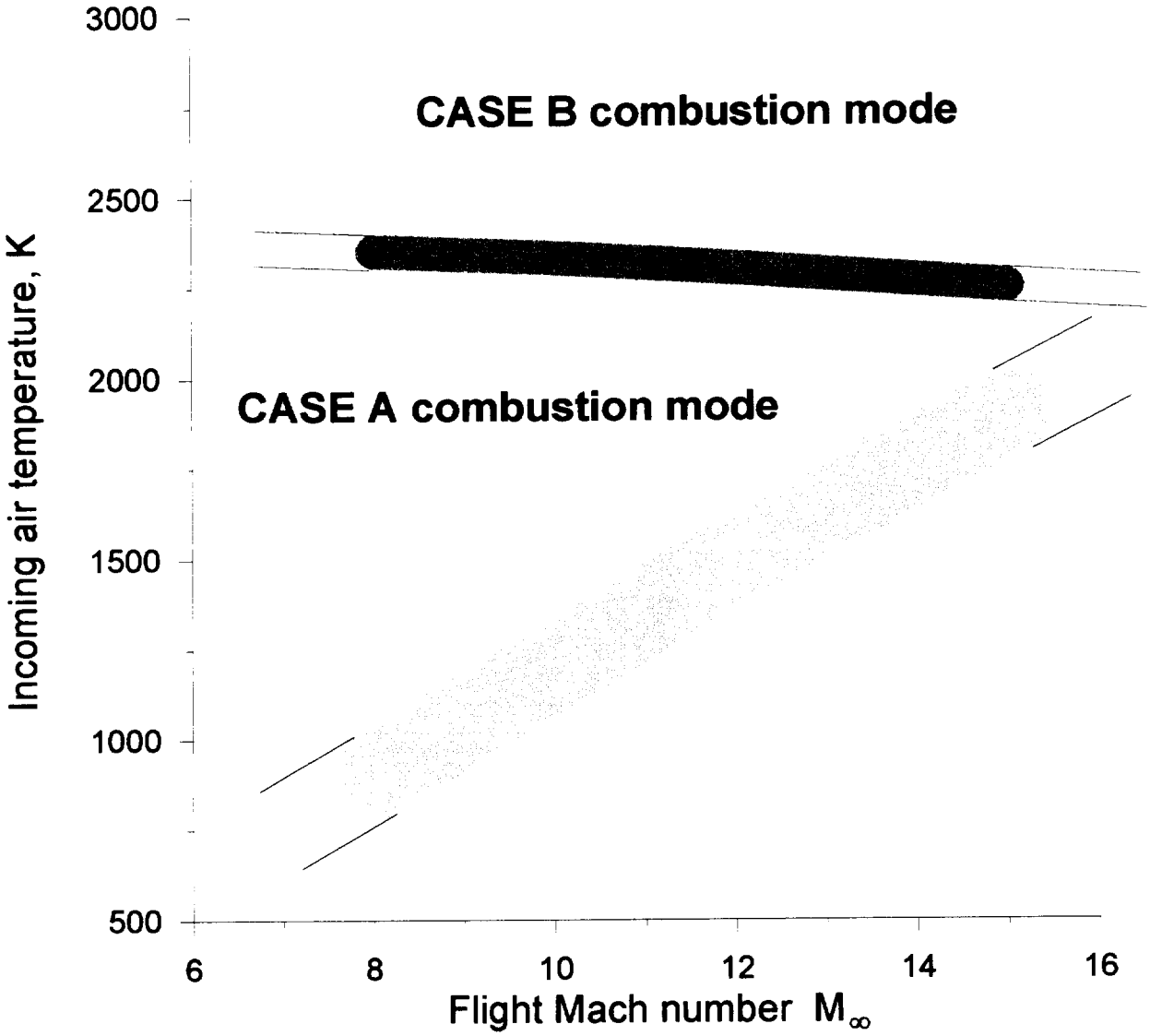

Fig.50. Comparison with typical scramjet operational conditions.

typical scramjet regimes

combustion modes transition boundary